Singlet oxygen and optical limiting applications of BODIPYs and other molecular dyes

A thesis submitted in fulfillment of the requirements for the degree of

DOCTOR OF PHILOSOPHY

Of

Rhodes University

by

Aviwe Khanya May

November 2021

Abstract

A series of structurally diverse novel and previously synthesized BODIPY core dyes are synthesized and characterized in this thesis. These BODIPYs were synthesized using 2-methylpyrrole, 2-ethylpyrrole, 2,4-dimethylpyrrole and 3-ethyl-2,4-dimethylpyrrole as the starting pyrroles. The combination of different pyrroles with the same aldehyde results in BODIPY core dyes that are structural analogues. These core dyes were used as precursors to synthesise halogenated BODIPYs and novel styrylBODIPY dyes, which were successfully characterized using FT-IR and ^{1}H NMR spectroscopy. The halogenated BODIPY core dyes and the styrylBODIPY dyes were also characterized using MALDI-TOF mass spectrometry.

The introduction of heavy atoms on the BODIPY core leads to a red shift of the main spectral. In the presence of styryl groups, the main spectral band red shifts to the far red end of the visible region. As expected, the halogenated BODIPY core dyes also had moderate singlet oxygen quantum yields. These halogenated core dyes were found to be suitable as photosensitizers as all the dyes reduced bacterial viability to below 50% during photodynamic antimicrobial chemotherapy (PACT) studies against *Staphylococcus aureus*. The structure-property relationships studied demonstrate that the presence of protons rather than methyls at the 1,7-positions or iodines at the 2,6-positions results in more favorable PACT activity. This is likely to be related to the greater ability of the *meso*-aryl to rotate into the plane of the dipyrromethene ligand and suggests that there should be a stronger focus on dyes of this type in future studies in this field.

During nonlinear optical (NLO) studies, all the styrylBODIPYs exhibited favorable reverse saturable absorption (RSA) responses. In the absence of methyl groups at the 1,7-positions,

the *meso*-aryl ring lies closer to the π-system of the BODIPY core, enhancing donor (D)–π–acceptor (A) properties and resulting in slightly enhanced optical limiting (OL) parameters. Additionally, there is no evidence that the introduction of heavy atoms at the 2,6-positions significantly enhances OL properties. In a similar manner, alkyl substituents at these positions also do not significantly enhance OL properties; this was studied for the first time using **15** with ethyl groups at the 2,6-positions. The combination of z-scan data and transient spectroscopy for **16** demonstrated that the main mechanism responsible for the NLO properties of nonhalogenated BODIPY dyes is one-photon absorption from the ground state followed by ESA in the singlet manifold. From the NLO studies of **25**, OL parameters of 1,3,5-tristyrylBODIPY dyes were found to be similar in magnitude to properties of distyrylBODIPY dyes, but to have less favorable optical properties for OL applications.

The OL properties of scandium phthalocyanines were assessed for the first time, since the Sc(III) ion, unusually for a first row transition metal ion, is known to readily form sandwich complexes. The presence of a Sc(III) ion does not significantly enhance the OL properties of phthalocyanines relative to those of rare earth metal ions that also form complexes of this type. Because BODIPYs and phthalocyanines typically absorb significantly in the visible region, transparent PBC polymer thin films of disilane-bridged compounds with minimal absorption in this region were studied and exhibited an excellent RSA response. These compounds may be useful in the design of OL materials that can protect the human eye.

The optimized geometries and spectroscopic properties of selected BODIPYs were studied. As expected, the presence of bromine, iodine, ethyl and styryl groups at different positions of the BODIPY core leads to a narrowing of the HOMO–LUMO band gap, which results in a red-shift of the main spectral band. Partial atomic charges have also been calculated for some of

the styrylBODIPY dyes studied for application in OL, and electrostatic potential energy maps were also visualized to better assess how the dipole moment of BODIPY dyes can be modulated since this can affect the OL properties. For all the BODIPYs studied, the electronegativity of the atoms present influences charge distribution on the BODIPY structure.

Acknowledgements

Firstly, I would like to thank my supervisor, Prof. Mack for the training, guidance and opportunities. To Prof. Nyokong, my co-supervisor, I remain grateful for the support and assistance. I would also like to thank Prof. Pitchou Ngoy who has also played a significant role in my training as a scientist, particularly in relation to synthesis and spectroscopy. A special thanks also goes to Ms Gail Cobus, Dr Jonathan Britton and Mr Francis Chindeka for all the work they do.

A special thanks also goes to past and current S22 members, particularly Dr Donovan Mafukidze and Dr Balaji Babu. I also acknowledge financial support from the Department of Science and Technology (DST) and National Research Foundation (NRF) of South Africa through DST/NRF South African Research Chairs Initiative for Professor of Medicinal Chemistry and Nanotechnology to TN (uid: 62620), and an NRF Extended support scholarship.

Finally, I would like to thank God almighty, my family and all my friends.

"*For I know the plans I have for you, declares the LORD, plans to prosper you and not to harm you, plans to give you hope and a future*." (Jeremiah 29:11)

Table of Contents

List of Symbols

A	Absorbance
α	Linear absorption coefficient
β	Nonlinear absorption coefficient
β_{eff}	Effective nonlinear absorption coefficient
ε	Molar extinction coefficient
f	Oscillator Strength
fs	Femtosecond
h	Hours
γ	Second-order hyperpolarizability
I_{lim}	Optical limiting threshold
$\mathrm{Im}[^{(3)}]$	Third-order nonlinear susceptibility
λ	Wavelength
min	Minutes
m/z	Mass to charge ratio
nm	Nanometer
ns	Nanosecond
ps	Picosecond
η	Refractive index
$^1O_2$	Singlet oxygen
Φ_Δ	Singlet oxygen quantum yield
Δ	Fluorescence quantum yield
S_n	n^{th} electronic excited state

S_0	Singlet ground state
S_1	First singlet excited state
S_2	Second excited state
T_1	First triplet excited state
τ_F	Fluorescence lifetime

List of Abbreviations

Abs	Absorption
B3LYP	Beck, three-Parameter, Lee-Yang-Parr
$BF_3{\cdot}OEt_2$	Boron trifluoride diethyl etherate
BODIPY	4,4'-difluoro-4-bora-3a,4a-diaza-*s*-indacene
CAM-B3LYP	Coulomb-attenuated B3LYP
CFU	Colony-forming units
DFT	Density-Functional Theory
DCM	Dichloromethane
DDQ	2,3-Dichloro-5,6-dicyano-1,4-benzoquinone
DMF	Dimethylformamide
DMSO	Dimethylsulfoxide
DPBF	1,3-Diphenylisobenzofuran
Em	Emission
EPR	Enhanced permeability and retention
ESA	Excited state absorption
Ex	Excitation
F	Fluorescence
FT-IR	Fourier-transform infrared spectroscopy
FWHM	Full width at half minimum
HF	Hartree-Fock
HpD	hematoporphyrin derivative
HOMO	Highest occupied molecular orbital

H_2Pc	Metal-free phthalocyanine
IC	Internal conversion
ICT	Intramolecular charge transfer
ISC	Intersystem-crossing
LUMO	Lowest unoccupied molecular orbital
MALDI-TOF	Matrix-assisted laser desorption/ionisation-time of flight
MS	Mass spectrometry
MPc	Metallophthalocyanine
NBS	*N*-bromosuccinimide
NIS	*N*-iodosuccinimide
Nd:YAG	Neodymium-doped yttrium aluminium garnet
NIR	Near-infrared region
NLA	Nonlinear absorption
NLO	Nonlinear optics
NLS	Nonlinear light scattering
NMR	Nuclear magnetic resonance spectroscopy
NR	Nonradiative decay
OL	Optical limiter/limiting
P	Phosphorescence
PACT	Photodynamic antimicrobial chemotherapy
PBC	Poly(bisphenol A carbonate)
PBS	Phosphate-buffered saline
PS	Photosensitizer

PDT	Photodynamic therapy
ROS	Reactive oxygen species
RSA	Reverse saturable absorption
SOMO	Single-occupied molecular orbital
TCSPC	Time-correlated single photon counting
TD-DFT	Time dependent Density-Functional Theory
TEA	Triethylamine
TFA	Trifluoroacetic acid
THF	Tetrahydrofuran
TLC	Thin layer chromatography
TPE	Tetraphenylethylene
2PA	Two-photon absorption
UV-Vis	Ultraviolet-visible
XRD	X-ray powder diffraction
ZnPc	Zinc phthalocyanine

List of Schemes

List of Figures

List of Tables

Chapter 1:

Introduction

1. Introduction

This thesis primarily examines the spectroscopic and photochemical properties of several series of novel boron dipyrromethene (BODIPY) dyes rationally selected to identify structure-property relationships and investigates their utility for applications in the photochemical inactivation of bacteria through a process referred to as photodynamic antimicrobial chemotherapy (PACT) and in nonlinear optics (NLO). The thesis also examines the NLO properties of monomeric and dimeric Sc(III) phthalocyanine complexes. The NLO studies conclude with an analysis of the properties of novel disilane-bridged tetraphenylethylene (TPE) dyes from which transparent polymer thin-film materials with optimal potential for practical applications can be prepared.

1.1. BODIPY dyes: discovery, structure and synthetic routes for BODIPY core dyes

BODIPY dyes are highly fluorescent dyes consisting of a dipyrromethene ligand complexed to a boron atom bonded to heteroatoms, typically forming a BF_2 moiety.[1–4] These dyes were first serendipitously synthesized and characterized by Treibs and Kreuzer in 1968.[5,6] More recently, atoms other than fluorine have been introduced at the boron center, and this has been shown to result in stable complexes.[5,7–10]

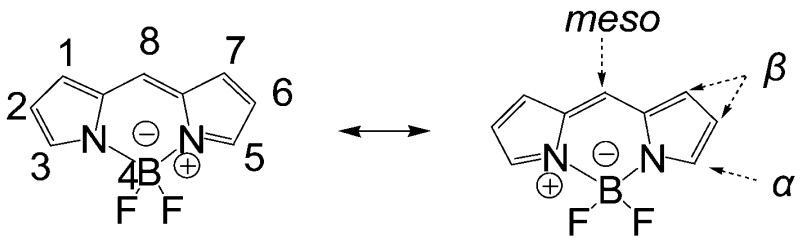

Figure 1.1. IUPAC numbering system for the BODIPY core. Reproduced with permission from Ref. 3; Copyright Royal Society of Chemistry, 2014.

The BODIPY core is structurally analogous to porphyrins, and the IUPAC numbering system is shown above; the carbon at the 8-position is typically termed the *meso*-carbon and those at the 3,5-positions the α-carbons, while those at the 2,6- and 1,7-positions are referred to as the β-carbons (**Figure 1.1**).[3,11] BODIPY core dyes are usually synthesized *via* an acid-catalyzed condensation reaction between a pyrrole and an electrophilic carbonyl compound, typically an aldehyde.[12] This leads to the formation of a relatively unstable dipyrromethane. The addition of an oxidizing agent such as 2,3-dichloro-5,6-dicyano-1,4-benzoquinone (DDQ) or *p*-chloranil to the reaction vessel results in the formation of a dipyrromethene which can then be complexed to a boron atom; the boron is added in the presence of a tertiary amine that provides basic conditions. To prevent polymerization and porphyrin formation during the reaction, a substituted pyrrole is typically used.[11] In this study, 2-ethylpyrrole, 2-methylpyrrole, 2,4-dimethylpyrrole and 3-ethyl-2,4-dimethylpyrrole were used to synthesize a series of novel BODIPY core dyes. Once formed, multiple post-synthetic structural modifications can be carried out on the BODIPY core at all the peripheral positions of the ligand. The structural modifications adopted in this work to enhance selected properties were as follows:

i. Modifications at the *meso*-position: Different functional groups can be introduced at the *meso*-position. These functional groups are selected to further facilitate the anticipated application of the dye or enhance selected properties. When there are methyl groups at the 1,7-positions, as is the case with the BODIPY dyes synthesized from 2,4-dimethylpyrrole and 3-ethyl-2,4-dimethylpyrrole in this study, there is typically a minimal mesomeric interaction between the *meso*-aryl substituent and the BODIPY core,[3,13] since the *meso*-aryl group lies orthogonal to the BODIPY core.

ii. Electrophilic substitution: The 2,6-positions of the 1,3,5,7-tetramethylBODIPY core and the 3,5-dimethylBODIPY core are susceptible to electrophilic attack. Typically, this substitution does not result in any additional changes to the BODIPY structure, especially with regards to the B-F bond.[11] Instead, the addition of specific substituents such as halogen atoms tends to enhance certain spectroscopic and physicochemical properties. Of interest here is the introduction of bromine and iodine atoms at the 2,6- and/or 1,7-positions of selected core dyes.

iii. Modification of methyl groups at the 3,5-positions: Styryl groups can be formed at the 3,5-positions due to the nucleophilic character of the methyl groups at these positions. These methyl groups are deprotonated to give intermediates that readily add to electron-rich aromatic aldehydes.[14] In contrast, the use of electron-deficient aldehydes to introduce substituents at the 3,5-positions is not favorable, and in some instances, the reaction does not yield styrylBODIPY dyes.[5,15,16] The resulting dyes typically have an extended degree of π-electron conjugation, and as such, they absorb and fluoresce at longer wavelengths, typically in the near-infrared region (NIR).[11] The most commonly used functional groups in this context are phenyl, vinyl, or thiophene groups.[11,17] Typically, the presence of electron-deficient substituents such as the pentafluorophenyl group at the *meso*-position enhances the acidity of the methyls at the 3,5-positions and leads to high yields.[16] Herein, carefully selected styryl groups are introduced to core dyes with specific *meso*-substituents suitable for application in NLO. Using a modified set of literature procedures,[15] attempts were made to use electron-deficient aldehydes to introduce substituents at the 3,5-positions and form styrylBODIPY dyes with anticipated excellent NLO properties. These dyes form donor (D)–π–acceptor (A) systems.[18–20]

1.2. BODIPY dye physicochemical properties

A Jabłoński diagram can be used to visualize the processes that a BODIPY dye can undergo upon interaction with electromagnetic radiation (**Figure 1.2**).

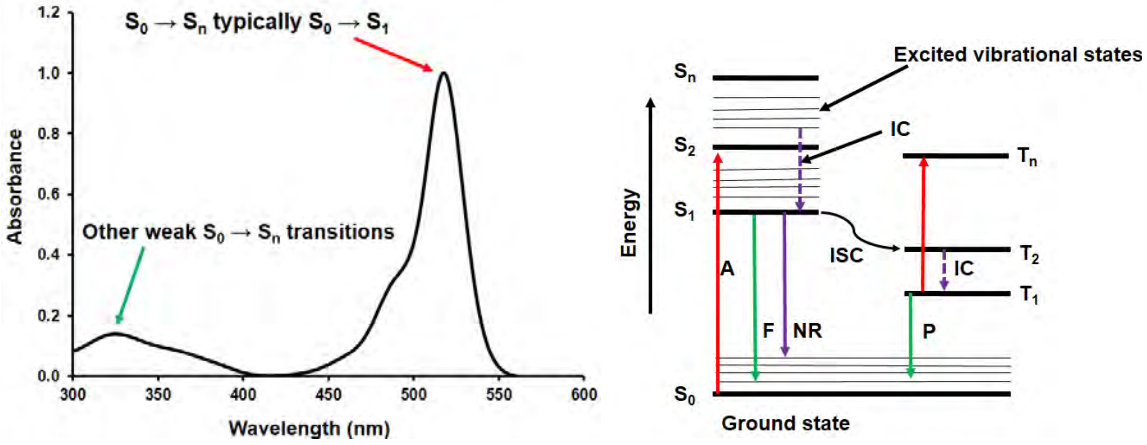

Figure 1.2. A typical BODIPY UV-visible absorption spectrum (LEFT) and a Jabłoński diagram (RIGHT) of possible electronic transitions upon photoexcitation. A = Absorption; F = Fluorescence; NR = Nonradiative decay; P = Phosphorescence; IC = Internal conversion; ISC = Intersystem crossing.

The absorption of a photon leads to photoexcitation to an excited singlet state (S_1–S_n), which then relaxes to the lowest vibrational level of the S_1 state through internal conversion (**Figure 1.2**). From this lowest vibrational level, the dye relaxes to the ground state by releasing a photon *via* fluorescence in accordance with Kasha's rule.[21,22] The presence of a heavy atom on the BODIPY structure enhances intersystem crossing to the T_1 state due to the heavy atom effect, which promotes spin-orbit coupling. A photon can be emitted by the T_1 state *via* phosphorescence, a process in competition with energy transfer from the T_1 state to ground state molecular oxygen. The latter results in the production of radicals and other reactive

oxygen species (ROS), including singlet oxygen ($^1O_2$). Singlet oxygen is utilized in biomedical applications of BODIPYs such as photodynamic therapy (PDT) and PACT.[11,23–25]

1.2.1. Absorption spectra of BODIPY dyes

The main absorption band of BODIPY core dyes lie in the 490–520 nm region (**Figure 1.2**), depending on the functional groups present on the ligand periphery. This absorption band arises from the $S_0 \rightarrow S_1$ transition.[3] Additionally, a shoulder band typically appears around 475–485 nm due to a vibrational overtone. This is followed by a weaker absorption band in the 300–400 nm region that can be attributed to the $S_0 \rightarrow S_2$ transition.[3] These absorption properties are usually retained over a wide pH range and at differing solvent polarity because the BODIPY core is zwitterionic.[26]

1.2.2. Photophysicochemical Properties of BODIPY dyes

A. Fluorescence properties of BODIPY dyes

The fluorescence properties of BODIPY dyes have been extensively researched for applications in different fields.[11] The fluorescence emission spectra are mirror images of the $S_0 \rightarrow S_1$ absorption band since fluorescence only occurs from the lowest vibrational level of the S_1 state to the S_0 state, according to Kasha's rule.[22] Because the BODIPY core absorbs in the 490–520 nm region, the narrow emission bands lie in the 500–550 nm region in the absence of extensive structural modification, with Stokes shift of approximately 10 nm.[11,22] One important fluorescence property is the fluorescence quantum yield (ϕ_F), a ratio of photons emitted relative to photons absorbed. This is typically very high for BODIPY dyes due to their rigid structures.[22,27] To determine the ϕ_F value, the fluorescence intensity of a BODIPY

dye is compared with that of a standard molecular dye with a known ϕ_F value.[28] In this work, the quantum yield is determined using Equation (1):

$$\Phi_F = \Phi_{F(Std)} \frac{F \cdot A_{Std} \cdot \eta^2}{F_{Std} \cdot A \cdot \eta^2_{Std}} \quad (1)$$

Where F and F_{Std} are the areas under the fluorescence curves for the sample and standard, respectively. A and A_{Std} are the absorbance values of the sample and standard at the excitation wavelength, while η and η_{std} are the respective refractive indices of the solvents in which the sample and standard solutions were prepared. Rhodamine 6G and zinc phthalocyanine (ZnPc) can be used as standards, with ϕ_F = 0.95 and 0.20 in ethanol and DMSO, respectively.[29,30]

In addition to the fluorescence quantum yield, the fluorescence lifetime (τ_F) can also be determined.[26,31–33] The τ_F value describes the average time the S_1 state exists before deactivating to the ground state *via* the radiative emission of a photon (fluorescence). Time-correlated single-photon counting (TCSPC) is a technique that can be used to determine the τ_F value.[33] A decay curve can be plotted and then deconvoluted to give the fluorescence lifetime as the time taken for the intensity to diminish to 1/e of its initial value. Both the ϕ_F and τ_F values are independent of the excitation wavelength because there is rapid deactivation from the populated S_n excited state to the fluorescent lowest excited state *via* internal conversion.[22,27] For the purposes of this study, τ_F values are often not included since they are difficult to measure for halogenated dyes with very low ϕ_F values.

B. Singlet oxygen quantum yield of BODIPY dyes

As stated above, energy transfer from a T_1 state to molecular oxygen leads to the production of ROS and in the context of this thesis, the main interest is in singlet oxygen. The generation of this ROS by a photosensitizer dye can be quantified using two methods, namely the physical/luminescence method and a comparative chemical method. In this work, the comparative method was used. This method uses a singlet oxygen quencher such as 1,3-diphenylisobenzofuran (DPBF), which reacts with the singlet oxygen generated. The stepwise decrease in the intensity of the main absorption peak of the DPBF quencher is followed using UV-visible absorption spectroscopy. Equation (2) shown below is used for calculating singlet oxygen quantum yields (Φ_Δ):[34,35]

$$\Phi_\Delta = {\Phi_\Delta}^{Std} \cdot \frac{R^{Sample} \cdot I^{Std}}{R^{Std} \cdot I^{Sample}} \qquad (2)$$

Where (${\phi_\Delta}^{std}$) is the singlet oxygen quantum yield for the standard (e.g. Rose Bengal or ZnPc). R^{Sample} and R^{Std} are the DPBF photobleaching rates in the presence of the sample under investigation and the standard, respectively. I^{Sample} and I^{Std} are the rates of light absorption by the sample and the standard, respectively.

1.3. Potential applications of BODIPY dyes synthesized.

The ideal properties of BODIPY dyes have led to research focusing on a diverse range of applications.[36] These properties include the high fluorescence quantum yields (0.6–1.0), insensitivity to solvent polarity and pH changes, large extinction coefficients (60 000–80 000 $M^{-1}cm^{-1}$), typically high solubility in most organic solvents, high photostability and stability under common physiological conditions.[3,13] BODIPY dyes have been studied for application in

chemosensing, laser dyes, cellular imaging, PDT, supramolecular polymers, biolabeling, nonlinear optical limiting and light-harvesting systems.[1,36–45] Recently, interest in these dyes for various other applications has increased enormously.[6,11,46] The applications of interest in the context of this thesis are described in more depth in the sections below.

1.3.1. Photodynamic therapy (PDT)

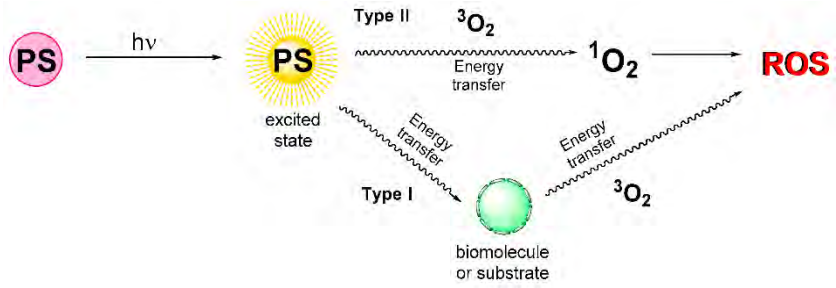

Figure 1.3. The PDT process and generation of ROS. Reproduced with permission from Ref. 50; Copyright MDPI, 2019.

Photosensitizer dyes can be used to generate singlet oxygen for biomedical applications such as PDT and PACT. Cancer, a disease that damages genetic material, is characterized by uncontrolled growth and spread of body cells, leading to the formation of tumors.[47] These tumors can be surgically removed, treated with drugs such as in chemotherapy or destroyed using defined sources of radiation (radiotherapy).[47] Both chemotherapy and radiotherapy have a series of drawbacks, much as they are successful.[47,48] These include their time-consuming procedures, the failure of surgery to remove deep-seated tumors and the damage of healthy cells close to the cancer cells by radiation beams. This necessitated extensive research into alternative therapeutic approaches such as PDT. PDT is based on the use of light, oxygen and a photosensitizer (PS) dye to generate reactive oxygen species (ROS), which kill cells *via* apoptosis or necrosis (**Figure 1.3**).[49–51] The absence of lymphatic drainage in cancer

cells ensures that the photosensitizer selectively localizes in tumors through what is termed the enhanced permeability and retention (EPR) effect.[50]

Red and infrared radiation are the most efficient forms of light because blue light fails to penetrate through tissue. It has been established that light in the 600−1200 nm region is optimal in this context. This spectral region is known as the optical window in biological tissue.[50] Light of the appropriate wavelength is generated from lasers and incandescent light sources. The photosensitizer used should be able to absorb this light.[50] Various photosensitizers have been clinically approved due to the absence of the drawbacks encountered with chemotherapy and radiotherapy.[50,52] The photosensitizer in this context is typically a delocalized aromatic molecule with an extensive conjugation of double bonds forming a central chromophore while containing side chains or auxochromes. The auxochromes lead to further electron delocalization leading to the alteration of the UV-visible absorption spectrum to give typically very intense absorption bands in the longer wavelength (red) spectral region.[53]

Tetrapyrrole based photosensitizers such as porphyrins, phthalocyanines, chlorins and bacteriochlorins are typically used. The initial photosensitizers such as hematoporphyrin derivative (HpD) and Photofrin® are termed first-generation photosensitizers since they were the first to be used in PDT. The second generation of photosensitizers was mainly based on the phthalocyanine structure. These photosensitizers are chemically pure and are relatively safe in relation to photosensitization of the patient after use in treatment,[54] since they can be used at lower concentrations. A majority of the second generation photosensitizers have intense absorption bands at longer wavelengths, allowing light to reach deep-seated tumors.[52,55] However, macrocyclic tetrapyrroles, such as porphyrins and phthalocyanines, can

be difficult to structurally modify in a manner that enhances their photophysical properties. Hence there is a need for structurally robust alternatives that provide facile structural modification.[52] Of interest here is the suitability of BODIPY dyes as photosensitizers as there has been a growing research focus in that regard.[1,43,49,52,56,57]

As mentioned previously, further structural modification of the BODIPY core dye can (i) promote intersystem crossing to the triplet state, hence facilitating the generation of singlet oxygen, and (ii) shift the main spectral band to longer wavelengths so that it absorbs light in the NIR region due to an extension of the π-conjugation system. The dyes synthesized for photosensitizer or singlet oxygen-dependent applications in this study are shown below (**Table 1.1**). Although PDT studies have not been carried out, the PACT studies reported demonstrate the suitability of BODIPY dyes as photosensitizer dyes in biomedical applications.

1.3.2. Photodynamic antimicrobial chemotherapy (PACT)

The emergence of antibiotic-resistant bacterial strains has somewhat reversed the breakthroughs that were initially made in treating bacterial infections after the discovery of antibiotics in the 20th century.[58,59] PACT has proven to be an alternative that can deal with antibiotic resistance.[60–63] To date, *in vitro* studies have demonstrated that this technique can be successfully applied against bacteria, viruses, and protozoa.[55,62,64] The PACT process is similar to PDT, i.e. it employs a photosensitizer and a light source of the appropriate wavelength to generate cytotoxic ROS such as singlet oxygen (**Figure 1.3**).[55,60,63] The death of the bacterial cells initiated by ROS begins by outer membrane damage, and given that the cell wall make-up is different in different bacterial strains, the properties of the photosensitizer

used are important. The cytoplasmic membrane of gram-positive bacteria is easily accessible because they contain a porous peptidoglycan layer and lipoteichoic acid, whereas, in gram-negative bacteria, the peptidoglycan layer is covered by a membrane on the outer and inner sides. [65,66] This means that for gram-negative bacteria, the cytoplasmic membrane is not easily accessible to photosensitizers.[67] Therefore, neutral, anionic or cationic photosensitizers inactivate gram-positive bacteria, whereas typically, only cationic photosensitizers inactivate gram-negative bacterial strains.[68–70] Because the BODIPY core can be easily modified, this enables easy functionalization, and the typically low dark toxicity make BODIPYs promising alternative photosensitizers for PACT. This is a growing research area.[71,72] In this work, non-cationic BODIPY core dyes are used as photosensitizers in the photodynamic inactivation of *Staphylococcus aureus* (**Table 1.1**).

1.3.3. Nonlinear optics (NLO)

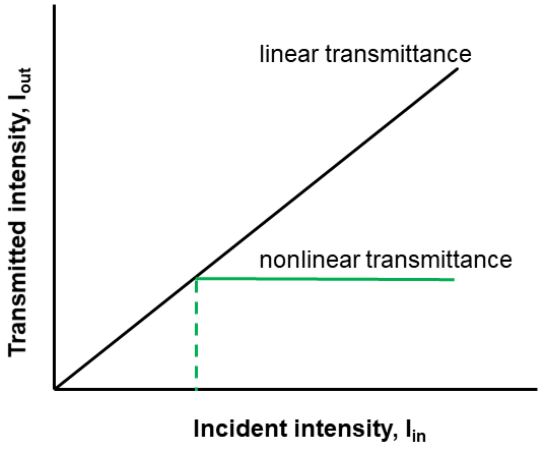

Figure 1.4. The ideal response of an optical limiter to high-intensity incident laser light.

NLO is the study of changes in the optical properties of materials when interacting with incident light of different intensities. Optical limiting (OL) is characterized by decreased transmittance by a sample at high incident laser intensity. Hence, optical limiting materials

must significantly decrease light transmittance at high incident intensities while remaining transparent under ambient light conditions (**Figure 1.4**). Research into optical limiter materials has gained momentum over the past few decades.[73]

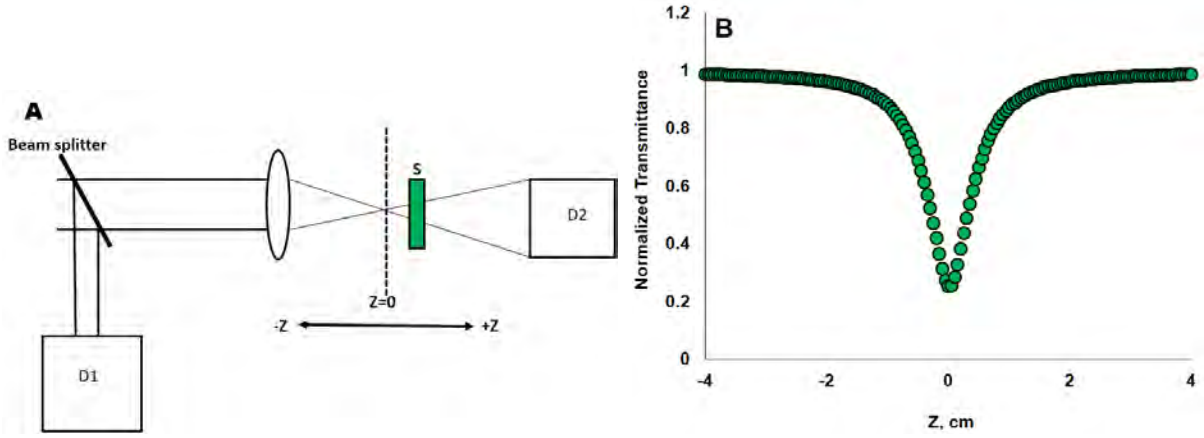

Figure 1.5. A schematic of the open-aperture z-scan instrument (A). D1 and D2 refer to photodetectors used to determine the intensity of the incident and transmitted light, while the sample is translated from –z and +z through the focal point of a lens. A typical reverse saturable absorption response obtained from the z-scan of an optical limiter (B).

There are multiple mechanisms involved in the optical limiting process.[74–76] Of particular interest to this thesis is nonlinear absorption (NLA). NLA can be studied using the single-beam z-scan technique (**Figure 1.5A**), wherein the sample is moved along the z-direction of a focused Gaussian beam; in the absence of an aperture in front of a photodetector (D2), the total transmitted energy is detected, and this gives the results for NLA by making use of a beam splitter to also determine the intensity of the incident beam through the use of a second photodetector (D1).[77] For the studies carried out in this thesis, the second harmonic of the Nd:YAG laser at 532 nm is used as the source of the beam. Research into OL materials is aimed at fabricating materials that can be used to protect light-sensitive objects such as the human

eye and optical sensors from intense incident laser beams.[78–80] This research has been necessitated by incidents of the irresponsible use of laser pointers in aviation, warfare and sometimes in sport.[19,81–83]

The response of an optical limiter to incident light of high intensity is characterized by a reverse saturable absorption (RSA) response (**Figure 1.5B**).[84,85] On the nanosecond timescale in the context of this study, RSA is characteristic of optical limiters, which undergo excited state absorption (ESA) that is more intense than the ground state absorption otherwise would have been.[19,79] ESA refers to the absorption of a photon from a lower excited state to a higher excited state and can occur in either the singlet or triplet manifold of a photosensitizer dye (**Figure 1.6A**).[86] Another important process in optical limiting is two-photon absorption (2PA), a third-order nonlinear process of materials wherein a molecule simultaneously absorbs two photons under high incident light intensity conditions (**Figure 1.6B**).

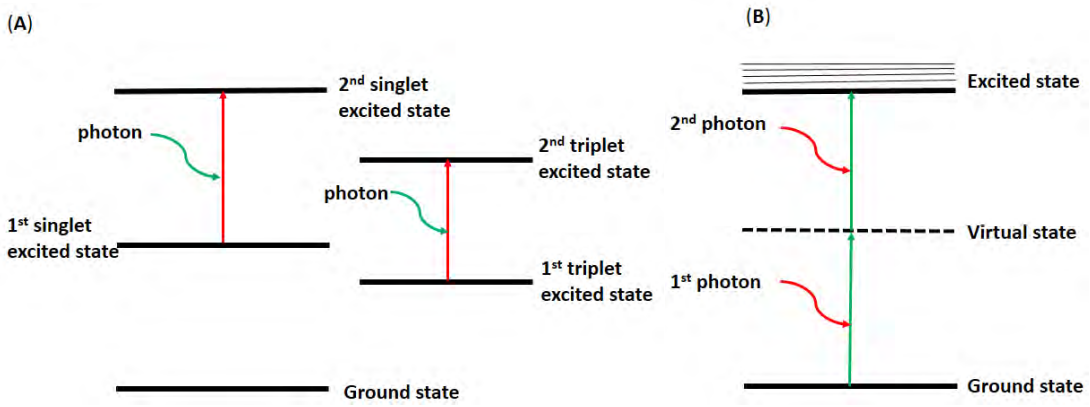

Figure 1.6. Jablonski diagrams showing the mechanism of excited state absorption (A) and two-photon absorption (B).

OL materials can be formed using various materials.[73] For NLA, organic dyes such as porphyrins and phthalocyanines have been demonstrated to possess excellent optical limiting

properties. These dyes typically have delocalized π-conjugation systems, which facilitate high polarizability when interacting with intense laser light.[76,85,87,88] As the dyes of interest, BODIPY dyes must be subjected to the structural modifications alluded to above before study using the second harmonic of the Nd:YAG at 532 nm. This is done to alter the optical properties and shift the main absorption band to a significantly longer wavelength relative to the main BODIPY spectral band that typically lies at ca. 500 nm. The introduction of styryl groups at the 3,5-positions red-shifts the main band and introduces an extended degree of π-conjugation, leading to higher polarizability.[11,14,17] The introduction of heavy atoms onto the BODIPY that enhance the rate of intersystem crossing may also play a role in modulating the optical limiting response if ESA from the T_1 state results in an enhanced or diminished RSA response. Heavy atoms typically significantly enhance the RSA response of phthalocyanines, whereas this effect has not been clearly observed for BODIPY dyes.[89–93] The work reported in this thesis focuses on studying a series of non-aggregated organic solutions of halogenated and non-halogenated mono- and distyrylBODIPY dyes in relation to their NLA properties at 532 nm by using the open aperture z-scan technique.

The data obtained from the z-scan measurements are analyzed using a procedure originally described by Sheik-Bahae and co-workers, Equation (3):[94]

$$T(z) = \frac{1}{\sqrt{\pi} q_0(z)} \int_{-\infty}^{\infty} ln\left[1 + q_0(z) e^{\tau^2}\right] d\tau \qquad (3)$$

Where $q_0(z)$ provides the magnitude of the nonlinear response, which can be described for a circular-shaped laser beam, by Equation (4):[20]

$$q_0(z) = \frac{2\beta_{eff} P_0 l_{eff}}{\pi \omega(z)^2} \qquad (4)$$

Where P_0 and l_{eff} are the peak power of the laser pulse and the effective pathlength, given by Equation (5):

$$l_{eff} = \frac{1-e^{-\alpha l}}{\alpha} \quad (5)$$

Where α and l are the linear absorption coefficient and the cuvette pathlength, respectively. The beam width as a function of sample position, ω(z) in Equation (4), can be obtained from Equation (6):

$$\omega(z) = \omega_0\sqrt{1+\left(\frac{z}{z_0}\right)^2} \quad (6)$$

Where z_0 and z are the Rayleigh length and the translation distance for the sample relative to the focus, respectively. z_0 is defined as $\pi\omega_0^2/\lambda$, with λ being the laser wavelength where ω_0 is the beam waist at the focus (z = 0), which is the distance from the center of the beam to a point where intensity decreases to $1/e^2$ of its axis value. The effective nonlinear absorption coefficient, β_{eff}, can be extracted from the experimentally measured transmittance using Equations (3–6). In this thesis, a numerical version of Equation (3) is used to derive $q_0(z)$ from the normalized transmittance values obtained experimentally:[95]

$$T(z) = 0.363e^{\left(\frac{-q_0(z)}{5.60}\right)} + 0.286e^{\left(\frac{-q_0(z)}{1.21}\right)} + 0.213e^{\left(\frac{-q_0(z)}{24.62}\right)} + 0.096e^{\left(\frac{-q_0(z)}{115.95}\right)} + 0.038e^{\left(\frac{-q_0(z)}{965.08}\right)} \quad (7)$$

On substituting Equation (6) into Equation (4), $q_0(z)$ can be defined by Equation (8):

$$q_0 = \frac{Q_0}{1+\left(\frac{z}{z_0}\right)^2} \quad (8)$$

where Q_0 is given as:

$$Q_0 = \frac{2\beta_{eff} P l_{eff}}{\pi\omega_0^2} \quad (9)$$

A Gaussian-shaped curve with Q_0 as the maximum value at z = 0 can be obtained from Equation (9). The full width at half minimum (FWHM) and peak values derived from the curve provide values for z_0 and Q_0, respectively. Equation (10) is used to obtain the value of β_{eff}, and this provides an important parameter for assessing the suitability of materials for OL applications:

$$\beta = \frac{\lambda Z_0 Q_0}{2P_0 l_{eff}} \quad (10)$$

The imaginary component of the third-order nonlinear susceptibility ($Im[\chi^{(3)}]$) is a measure of the speed of the response by an optical limiter to the perturbation induced by an incident laser pulse.[20] $Im[\chi^{(3)}]$ is directly proportional to the effective non-linear absorption coefficient, β_{eff}, and can be calculated using Equation (11):

$$Im[\chi^{(3)}] = \frac{\eta^2 \varepsilon_0 C \lambda \beta_{eff}}{2\pi} \quad (11)$$

Where η is the refractive index of the solvent, c is the speed of light, ε_0 is the permittivity of free space, and λ is the wavelength of the laser. The $Im[\chi^{(3)}]$ values have an optimal range of 10^{-9} to 10^{-15} in the context of OL applications.[20]

The intense laser radiation interacts with the permanent dipole of the dye molecule and leads to a bias in the average orientation of the molecules, which results in induced hyperpolarizability. The second-order hyperpolarizability (γ) quantifies this interaction per mole of the compound and can be determined using Equation (12):

$$\gamma = \frac{I_m[\chi^{(3)}]}{f^4 C_{mol} N_A} \quad (12)$$

Where C_{mol} is the molar concentration of the active species, f is the Lorentz local field enhancement factor defined as $f = (\eta^2 + 2)/3$ (where η is the refractive index of the sample),

and N_A is Avogadro's constant. The γ values have an optimal range of 10^{-29} to 10^{-34} in the context of OL applications.[20]

The limiting threshold intensity (I_{lim}) is defined as the input fluence at which the nonlinear transmittance is reduced to 50% of the linear transmittance value. The guidelines provided by the International Commission on Non-Ionizing Radiation Protection help to determine suitable exposure limits to a variety of lasers.[96] Equation (13) can then be used to determine that the use of 10 ns laser pulses at 532 nm results in as an exposure limit:

$$\text{Exposure Limit} = 2.7 C_A t^{0.75}\ \text{J.cm}^{-2} \quad (13)$$

Where C_A is a correction factor (= 1 for 400–700 nm), and t is the exposure time. This equation provides a limit of 0.95 J.cm^{-2} for a 0.25 s exposure time corresponding to the normal blink reflex for the human eye.[97]

The BODIPY dyes studied here are rationally selected to analyze the effect of various structural modifications on the optical limiting properties. The presence of electron-donating and electron-withdrawing groups (either at the *meso*-position or the 3,5-positions) is expected to create a donor (D)–π–acceptor (A) or D–π–A system due to the presence of the BODIPY core π-conjugation system separating the groups. The D–π–A systems of these dyes are known as push-pull systems and have previously been shown to enhance the optical limiting properties of BODIPY dyes and other compounds.[19,20,98–100] This is mainly because the asymmetrical nature of the system results in a dipole moment, which induces hyperpolarizability upon interaction with laser radiation.[92,98] Photoexcitation by the incident laser light results in a shift of electrons from donor to acceptor groups and the formation of a dipole moment.[98,99] The introduction of heavy atoms in the form of bromine onto the 2,6-

positions of some of the dyes being studied will be used to assess the optical limiting response in the triplet excited state relative to the response in the singlet excited state.

1.4. Phthalocyanines

Phthalocyanines are a type of tetrapyrrolic macrocycle that was initially discovered in 1907.[101] Following the initial discovery of the metal-free phthalocyanine (H_2Pc) (**Figure 1.7A**), the central cavity of phthalocyanines has been shown to accommodate more than 70 different elemental ions. For most phthalocyanine structures successfully synthesized to date, the central cavity accommodates a metal ion, and a metallophthalocyanine (MPc) is formed (**Figure 1.7B**).[80,85,102] These phthalocyanines can be used in a wide range of applications including, but not limited to catalysis, PDT, photonics and NLO. Most of these applications are based on electron transfer reactions which are favored by the 18 π-electron conjugated ring system of PCs.[102] In this work, two scandium complexes, a monomeric phthalocyanine and a bis(phthalocyanine), are studied in organic media for application in NLO.

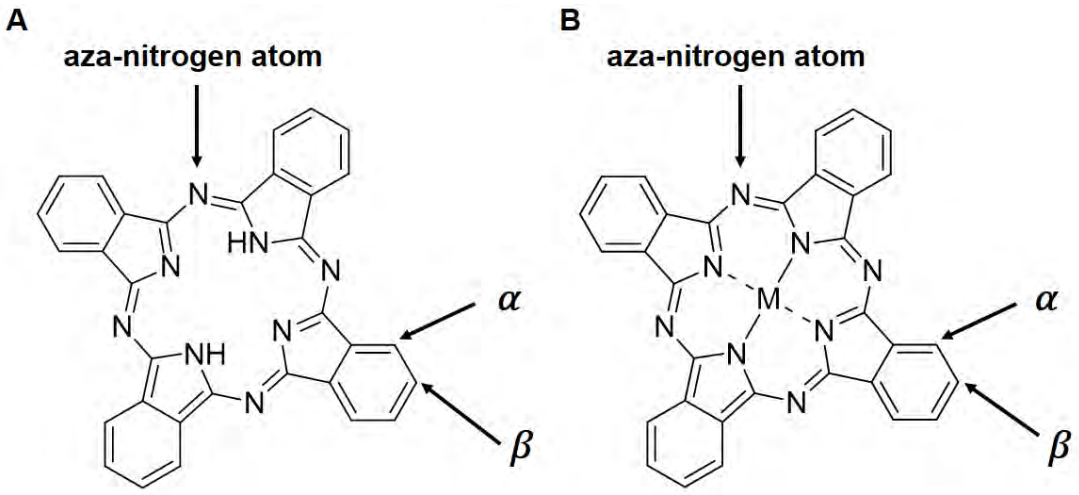

Figure 1.7. General structures of free base phthalocyanine (H_2Pc) (A) and a metal phthalocyanine (MPc) complex (B).

1.4.1. Synthesis

Phthalocyanines are synthesized directly from a precursor, typically a substituted phthalonitrile which is refluxed at the boiling point of a selected organic solvent. If the reaction is carried out in the absence of a metal salt, an H_2Pc is formed, whereas in the presence of a metal salt, an MPc forms.[103–105] Similarly, a bis(phthalocyanine), commonly referred to as a sandwich complex, can be synthesized directly from phthalonitrile precursors by controlling the ratio of phthalonitrile to a salt of a trivalent metal ion. Alternatively, the H_2Pc may be synthesized initially and used as a precursor to be refluxed with the metal salt of interest to enable metal insertion. By controlling the ratio of H_2Pc to metal salt, either or both the monomeric phthalocyanine and bis(phthalocyanine) will form, and the products can be carefully purified by chromatography.[106,107]

1.4.2. UV-visible absorption spectra of metallophthalocyanines

Both monomeric phthalocyanines and bis(phthalocyanines) have characteristic absorption spectra resulting from different electronic transitions.

1.4.2.1. Monomeric phthalocyanine UV-visible absorption spectra

The electronic transitions associated with the UV-visible spectra of phthalocyanines are shown in **Figure 1.8A**. The two main absorption bands of phthalocyanines are referred to as the Q and B bands in ascending energy (**Figure 1.8B**).[108] Overlapping B_1 and B_2 bands arise from transitions from a_{2u} and b_{2u} molecular orbitals (MOs) to the e_g lowest unoccupied molecular orbital (LUMO) (**Figure 1.8A**). The Q band, on the other hand, is representative of a transition from the a_{1u} highest occupied molecular orbital (HOMO) to a degenerate e_g orbital

(LUMO) (**Figure 1.8A**). It is the most intense band in the visible region of the phthalocyanine spectrum.[108]

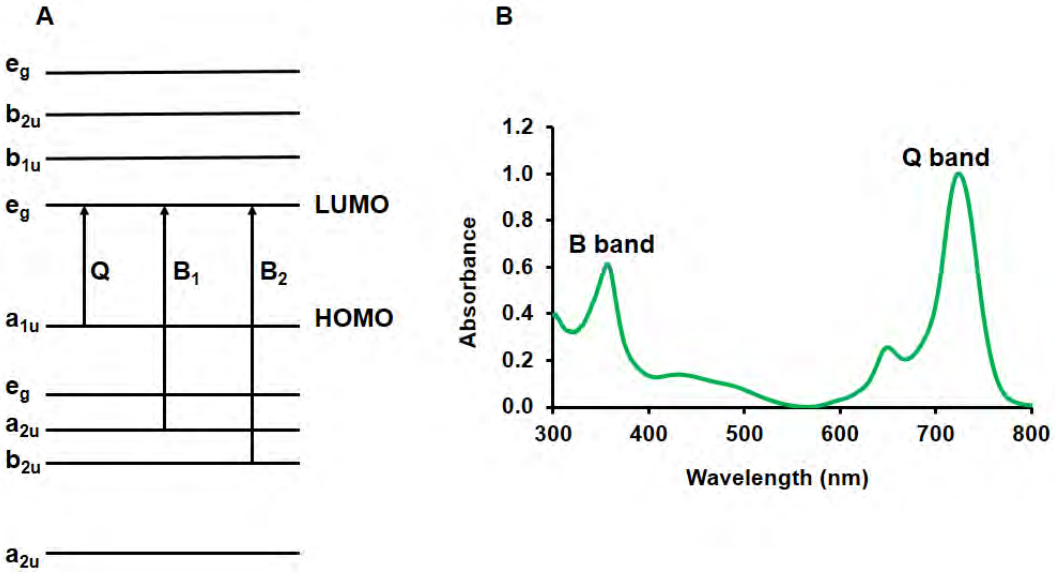

Figure 1.8. The electronic transitions (A) that are responsible for the major spectral bands observed in a typical phthalocyanine monomer spectra (B).

1.4.2.2. Bis(phthalocyanine) absorption spectra

The UV-visible spectra of bis(phthalocyanines) are more complex than those of phthalocyanine monomers, since there are two phthalocyanine ligands and a trivalent central metal ion. In the context of the anionic blue form $[M^{III}(Pc)_2]^-$, both phthalocyanine ligands are neutral dianions, and the observed spectral bands are broadly similar to those of monomer complexes with split Q_1 and Q_2 bands being observed due to exciton coupling effects.[109,110] In the spectra of the green form of metal bis(phthalocyanines) $[M^{III}(Pc)_2]$, there are characteristic bands associated with the presence of a cationic phthalocyanine ligand (**Figure 1.9A**). These bands are referred to in descending energy terms as the B-band, blue valence (BV) band, Q-band and the red valence (RV) band (**Figure 1.9B**).[74,109–111] The initial predictions of the

electronic transitions associated with the absorption spectra of $M^{III}Pc_2$ complexes were performed using valence effective Hamiltonian (VEH) calculations.[112]

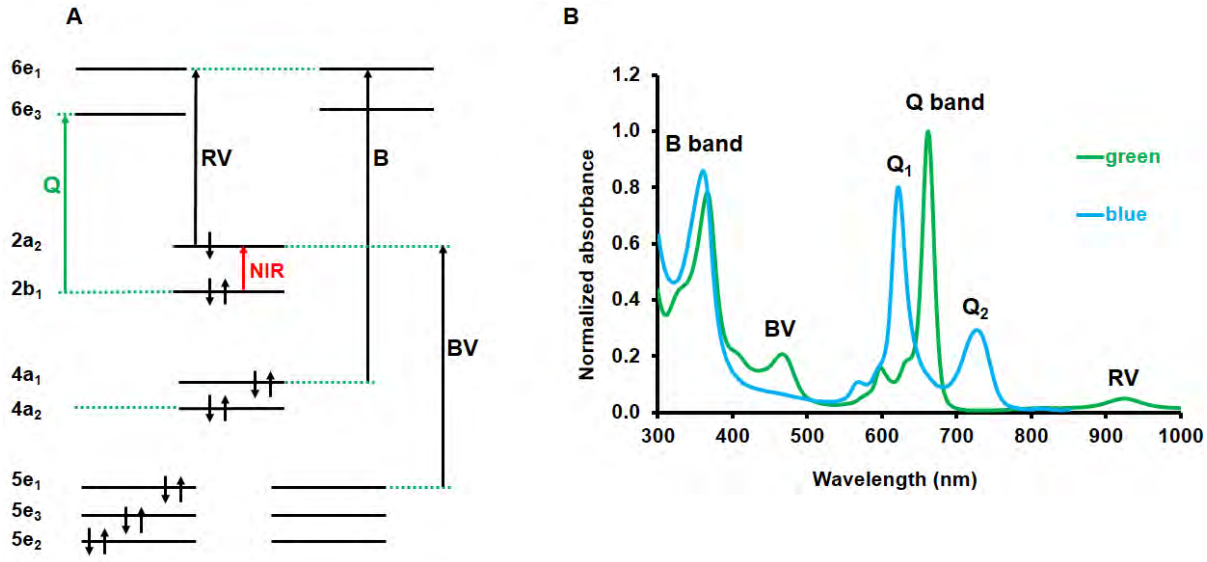

Figure 1.9. Electronic transitions (A) which lead to the characteristic UV-visible absorption spectrum of the green *vs* the blue forms of bis(phthalocyanines) (B).[106,113]

Each of the absorption bands associated with neutral $[M^{III}Pc_2]$ complexes can be related to a dominant electronic transition (**Figure 1.9**):[109,111,112,114–116]

I. The B-band is associated with the allowed $4a_1(\pi) \rightarrow 6e_1(\pi^*)$ transition.

II. The BV band, which lies in the 400–500 nm region, is a result of the $5e_1(\pi) \rightarrow 2a_2(\pi^*)$ transition.

III. The Q-band arises from the $2b_1(\pi) \rightarrow 6e_3(\pi^*)$ transition.

IV. The RV band is a result of a forbidden vibronic $2a_2(\pi) \rightarrow 6e_1(\pi^*)$ transition that involves a singly occupied molecular orbital (SOMO).

The introduction of an electron onto the Pc ring leads to the formation of the reduced or blue form, and in the UV-visible absorption spectrum, the Q-band becomes split, and the BV band disappears (**Figure 1.9B**).[109,111]

1.5. Summary of aims.

In this thesis, a series of structurally diverse BODIPY dyes are synthesized and characterized. The structural modifications were rationally selected to enhance the singlet oxygen generation of the dyes and shift the main BODIPY spectral band to longer wavelengths to minimize absorbance across the visible region under ambient light conditions. The aims can be summarized as follows:

1. Synthesis and photophysical study of a series of structurally modified BODIPY dyes. BODIPY dye structures are designed to facilitate an assessment of the structure-property relationships related to the use of a series of different alkyl-substituted pyrroles as precursors.

2. Study the antimicrobial activity or bacterial inactivation ability of the heavy atom-substituted core dyes that are synthesized to study the effects of using different pyrrole precursors and halogen heavy atoms.

3. Study the nonlinear optical behavior of a series of mono-, di- and tristyrylBODIPY dyes in organic media to identify structure-property relationships in the context of their optical limiting properties.

4. Study, for the first time, the nonlinear optical behavior of scandium phthalocyanine monomer and dimer complexes at 532 nm in organic solvents.

5. Report on the nonlinear optical behavior of transparent polymer thin films fabricated from novel disilane-bridged tetraphenylethylene (TPE) dyes.

6. Perform molecular modelling for a representative set of BODIPY dyes from the synthesized series to identify trends in the electronic structures and optical properties.

The PACT and NLO properties of the following BODIPY dyes were studied in this thesis:

Table 1.1. **Applications of the synthesized BODIPY dyes**.

Dye	Intended application
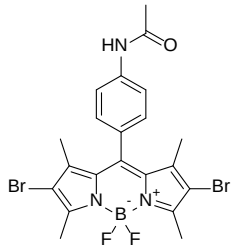	PACT
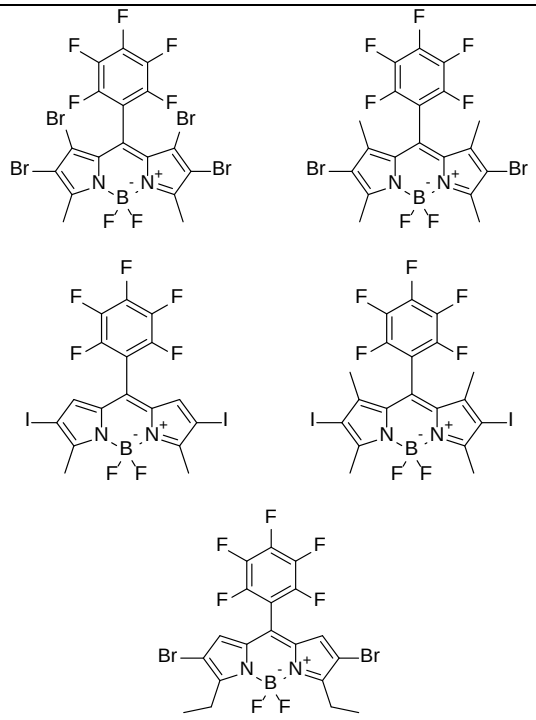	PACT

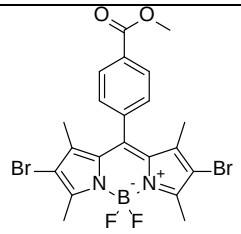	PACT
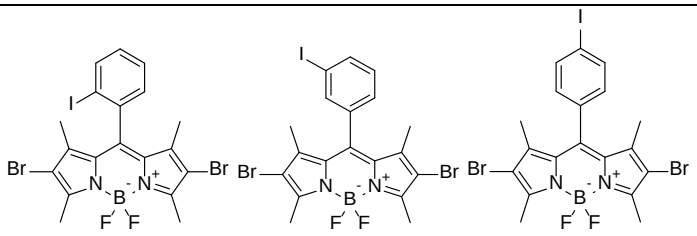	PACT
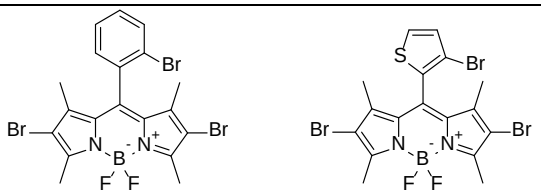	PACT
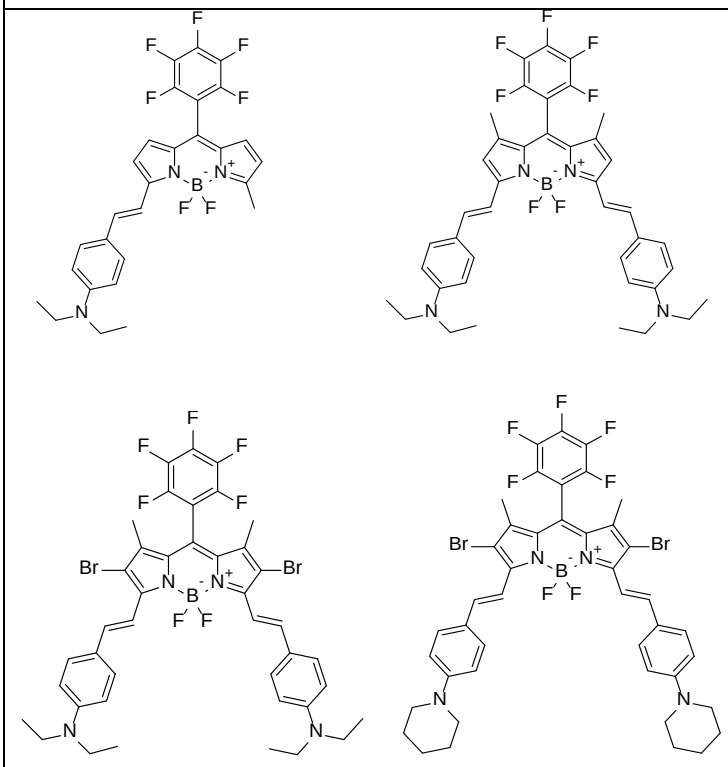	NLO

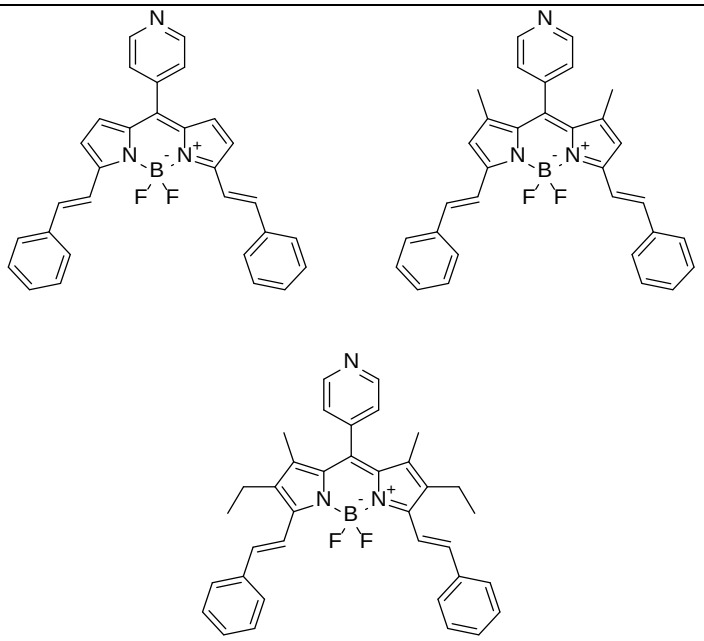	NLO
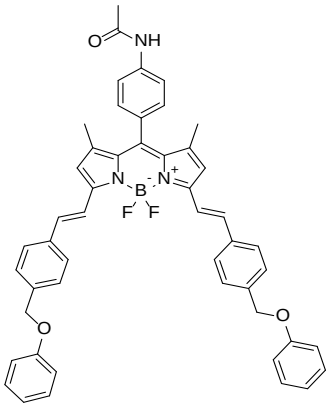	NLO
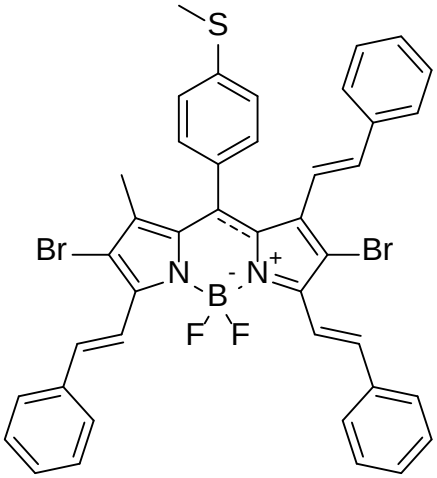	NLO

To date, the following publications contain results to be discussed in this thesis:

1. Ngoy, B. P.; **May, A. K**.; Mack, J.; Nyokong, T., *Frontiers in Chemistry* **2019**, **7:740** [doi: 10.3389/fchem.2019.00740]

2. **May, A. K**.; Majumdar, P.; Martynov, A. G.; Lapkina, L. A.; Troyanov, S. I.; Gorbunova, Y. G.; Tsivadze, A. Y.; Mack, J.; Nyokong, T., *Journal of Porphyrins and Phthalocyanines* **2020**, **24(4): 589–601** [doi: 10.1142/S108842462050011X]

3. **May, A. K**.; Mack, J.; Nyokong, T., *Journal of Porphyrins and Phthalocyanines* **2020**, **24(9): 1129–1137** [doi: 10.1142/S1088424620500315]

4. Harris, J.; **May, A. K**.; Ngoy, B. P.; Mack, J. and Nyokong, T., *Journal of Porphyrins and Phthalocyanines* **2019**, **23(01n02): 63–75** [doi: 10.1142/S1088424619500019]

The following additional publications also contain work conducted during the doctoral studies that are described in this thesis:

1. Martynov, A. G.; Mack, J.; **May, A. K**.; Nyokong, T.; Gorbunova, Y. G; Tsivadze, A. Y., *ACS Omega* **2019**, **4(4): 7265–7284** [doi: 10.1021/acsomega.8b03500]

2. Feng, H.; Zhou, Z.; **May, A. K**; Chen, J.; Mack, J.; Nyokong, T.; Gai, L.; Lu, H., *Journal of Materials Chemistry C* **2021**,**9**, **6470**–**6476** [doi: 10.1039/d1tc01488a]

Chapter 2:

Experimental

2.1. Materials

Trifluoroacetic acid (TFA), 2,4-dimethylpyrrole, 2-ethylpyrrole, 3-ethyl-2,4-dimethylpyrrole, 2,3,4,5,6-pentafluorobenzaldehyde, 2-bromobenzaldehyde, benzaldehyde, 4-acetamidobenzaldehyde, 5-bromothiophene-2-carboxaldehyde, 4-diethylaminobenzaldehyde, 2-iodobenzaldehyde, 3-iodobenzaldehyde, 4-iodobenzaldehyde, methyl 4-formylbenzoate**,** 4-(1-piperidinyl)benzaldehyde, 4-pyridinecarboxaldehyde, tetrachloro-1,4-benzoquinone (*p*-chloranil), triethylamine (TEA), boron trifluoride diethyl etherate ($BF_3{\cdot}OEt_2$), acetic acid (glacial), sodium sulfate, piperidine, Rhodamine 6G, 1,3-diphenylisobenzofuran (DBPF), *N*-bromosuccinimide (NBS), *N*-iodosuccinimide (NIS) and zinc phthalocyanine (ZnPc) were purchased from Sigma-Aldrich, while hydrochloric acid (32%) was purchased from Merck. Rose Bengal was purchased from Fluka. 2-Methylpyrrole was purchased from Achemo Chemicals. Silica gel 60 for flash column chromatography was purchased from Merck. Spectroscopic grade solvents were used for the z-scan and photophysical studies. All solvents were dried using molecular sieves before use in synthesis. Phosphate-buffered saline (PBS) solution (pH 6.8) was prepared with appropriate amounts of Na_2HPO_4 and NaOH in ultra-pure water from a Milli-Q water system (Millipore Corp, Bedford, MA, USA). Nutrient agar and agar bacteriological BBL Muller Hinton broth were purchased from Merck. *Staphylococcus aureus* (ATCC 25923) was purchased from Davies Diagnostics.

2.2. Instrumentation

- Ultraviolet-visible (UV–Vis) absorption spectra were measured at room temperature on a Shimadzu UV-2550 spectrophotometer. A 1 cm pathlength quartz cuvette was used.

- Proton nuclear magnetic resonance (^{1}H-NMR) spectra were recorded at room temperature on a Bruker AMX 600 NMR spectrometer in $CDCl_3$ unless stated otherwise.
- Fluorescence emission and excitation spectra were obtained using a Varian Cary Eclipse spectrofluorimeter, while fluorescence lifetimes were calculated by using a Picoquant FluoTime 200 time-correlated single-photon counting instrument.
- Mass spectral data were collected with a Bruker AutoFLEX III Smart beam TOF/TOF mass spectrometer. The spectra were acquired using α-cyano-4-hydroxycinnamic acid as the MALDI matrix and a positive mode of operation.
- Fourier-transform infrared spectra (FT-IR) were recorded on a Perkin Elmer Spectrum 100 spectrometer.
- The singlet oxygen experiments were conducted using an Ekspla NT342B-20-AW–Nd:YAG laser (max output–1J, pulse duration 3–6 ns) with parametric generation (max output–50 mJ, pulse duration 3–5 ns, wavelength 400–2400 nm), as the light source.
- An RAU-530D autoclave was used for autoclaving nutrient broth, nutrient agar, and phosphate buffer and for the sterilization of the apparatus used for PACT studies.
- A vortex mixer was used to mix the bacterial suspensions, and a HERMLE Z233M-2 centrifuge was used to harvest bacterial cells.
- The optical densities of bacterial cultures were determined using an LEDETECT 96 from LABXIM Products.
- A Scan® 500 automatic color colony counter was used to determine colony-forming units (CFU)/mL values.

- The open aperture z-scan measurements were performed using a frequency-doubled Nd:YAG laser (Quanta-Ray, 1.5 J/7 or 10 ns FWHM pulse duration) as the excitation source. The laser was operated in a near Gaussian transverse mode with a low pulse repetition rate of 10 Hz and an energy range of 0.1–0.1 mJ, at 532 nm. This low repetition rate prevents cumulative thermal nonlinearities. The beam was spatially filtered during measurements to remove the higher-order modes and tightly focused with a 15 cm focal length lens. The z-scan data of the organic solutions were collected using a 2 mm quartz cuvette. UV-visible absorption spectra were recorded before and after measurement to ensure that the dyes were not aggregated in solution since aggregation could lead to significant nonlinear scattering (NLS) and, as such, interfere with the NLA results being studied here.

- Femtosecond transient absorption measurements were carried out by Prof. Bokolombe Ngoy of Kinshasa University in the laboratory of Prof. Petr Klan of Masaryk University in Brno, Czech Republic with a Clark MXR CPA2001 775 nm laser with a pulse energy of 0.9 mJ, and a full width at half-maximum of 150 fs, and an operating frequency of 426 Hz as has been reported previously by Klícova et al.[37,117] with slight modifications. The pump-supercontinuum probe technique was implemented with a titanium-sapphire (Ti/Sa) laser system. The output at 775 nm was directly frequency-doubled by a β-barium borate (BBO) crystal to 387.5 nm with output pulses of 1 μJ energy and below 150 fs pulse width. Generation of the probe beam was carried out by focusing a 2 mm CaF_2 plate in front of the 775 nm beam in order to produce a 270–690 nm supercontinuum span. The nanosecond laser flash photolysis kinetics were studied at Rhodes University with an

Ekspla NT 342B-20-AW laser with pulses of 7 ns duration. Samples were deoxygenated with inert nitrogen gas.

- Geometry optimizations of the synthesized dyes were performed by using the B3LYP functional of the Gaussian software package, with SDD basis sets.[118] TD-DFT calculations were also performed using the CAM-B3LYP functional with SDD basis sets. Avogadro, an advanced molecular editor and visualizer program, was used for all visualizations of molecular orbitals**.**[119]

2.3. Synthesis

A series of BODIPY dyes, **1-17**, were synthesized, as described below along with the attempted syntheses of target distyrylBODIPY structures, **18-24**. Novel BODIPY core dyes, **1a**,[100] **1b**, **1c**, **1j**, **1k**, **3d**, **3e**, **3g** and **3l** and brominated core dyes, **5a**, **6a**, **7c**, **7d**, **7e**, **7g**, **7h** and **8a**, were synthesized, along with previously synthesized core dyes **1l**,[120] **1m**,[121] **2a**,[122] **3a-c**,[123–125] **3f**,[126] **3h-i**,[19,127] **3j-k**,[128,129] **4b**,[130] and halogenated analogues, **7a**,[131] **7f**,[126] **7i**,[132] **9a**,[130] following procedures described below. The appropriate BODIPY core dyes or brominated BODIPY core dyes were used as precursors in the synthesis of novel monostyrylBODIPY dye **10** and novel distyrylBODIPY dyes **11-17**. A 1,3,5-tristyrylBODIPY dye, **25**, was previously synthesized by Jessica Harris, a former MSc student at Rhodes University,[133] and no characterization was carried out in this work as the dye was only studied in context of Chapter 4.

2.3.1. BODIPY core dye synthesis (Scheme 1.1)

2-Ethylpyrrole, 2-methylpyrrole, 2,4-dimethylpyrrole or 3-ethyl-2,4-dimethylpyrrole (2.0 mol eq) and the corresponding aldehyde (1.0 mol eq) were dissolved in dry dichloromethane (CH_2Cl_2) (50 ml) under argon. TFA (2–3 drops) was added, and the reaction mixture was stirred

at room temperature. When the aldehyde was consumed (monitored by TLC), a solution of *p*-chloranil (1.2 mol eq) in dry CH_2Cl_2 (10 ml) was added at 0 °C. The solution was allowed to warm up to room temperature while stirring for 30 min under argon. A deep purple color was observed, and TLC confirmed the synthesis of the dipyrromethene. TEA (7 mol eq) and $BF_3{\cdot}Et_2O$ (11 mol eq) were added dropwise at 0 °C, and the mixture was left to stir at room temperature overnight. The mixture was then filtered and washed with water (100 ml), dried over anhydrous sodium sulfate and the residue purified by flash column chromatography. The characterization data for the pure fractions of the novel and previously synthesized dyes, as mentioned above,[19,100,120–132] are detailed below for each dye.

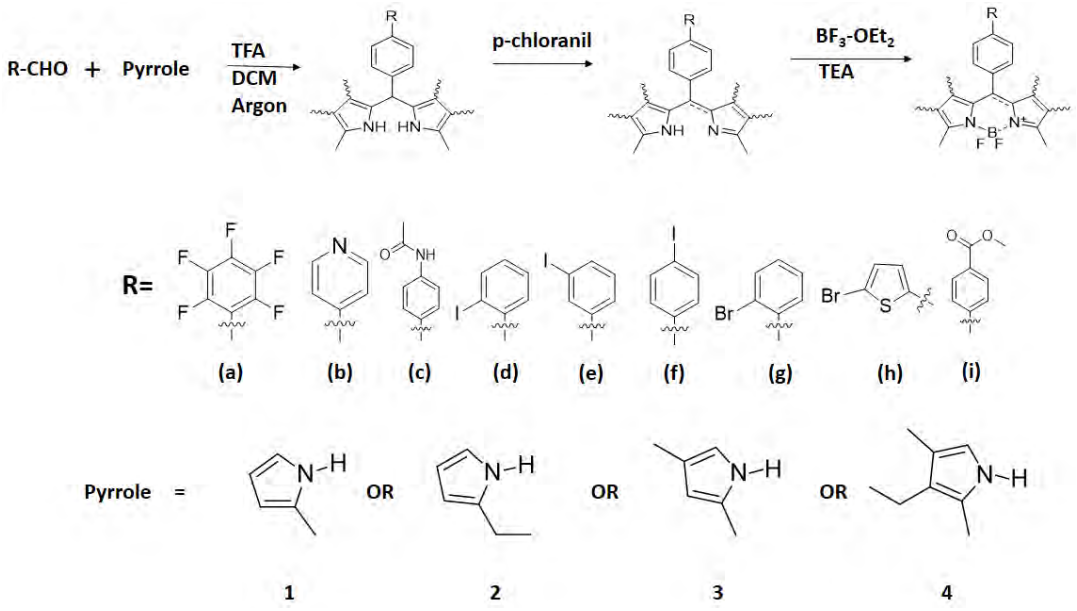

Scheme 2.1. Synthesis of BODIPYs **1**-**4(a**-**i)**.

1a was obtained in 36% yield after silica-gel chromatography by using 2-methylpyrrole and 2,3,4,5,6-pentafluorobenzaldehyde as the precursors. Eluent: petroleum ether/ethyl acetate (9:1). UV-vis (DMSO) λ, nm 525. ^{1}H NMR (600 MHz, THF-d_8) δ_H, ppm 6.79–6.78 (d, J = 4.1 Hz, 2H), 6.38–6.35 (d, J = 4.2 Hz, 2H), 2.60 (s, 6H). FT-IR (cm^{-1}): 2921, 2851 (C-H), 1569 (C=C), 1488, 1443 (C-N), 1128 (C-F), 425 (C-H).

1b was obtained in 28% yield after silica-gel chromatography by using 2-methylpyrrole and 4-pyridinecarboxaldehyde as the precursors. Eluent: petroleum ether/ethyl acetate (1:3). UV-vis (DMSO) λ, nm 518. ^{1}H NMR (600 MHz, $CDCl_3$) δ_H, ppm 8.78 (s, 2H), 7.43 (s, 2H), 6.66 (s, 2H), 6.32 (s, 2H), 2.68 (s, 6H). FT-IR (cm^{-1}): [1] 2918 (C-H), 1563 (C=C), 1487, 1454 (C-N), 430 (C-H).

1c was obtained in 32% yield after silica-gel chromatography by using 2-methylpyrrole and 4-acetamidobenzaldehyde as the precursors. Eluent: petroleum ether/ethyl acetate (1:4). ^{1}H NMR (600 MHz, $CDCl_3$) δ_H, ppm 7.66–7.62 (d, *J* = 8.2 Hz, 2H), 7.49–7.46 (d, *J* = 8.4 Hz, 2H), 7.43 (s, 1H), 6.75–6.72 (d, *J* = 3.9 Hz, 2H), 6.30–6.28 (d, *J* = 4.0 Hz, 2H), 2.67 (s, 6H), 2.25 (s, 3H). FT-IR (cm^{-1}): 3242 (N-H amide stretch), 2921, 2852 (C-H stretch), 1519 (N-H amide bend), 1448, 1398 (C-N stretch), 1136 (C-N stretch), 994 (=C-H bend), 430 (C-H).

2a was obtained in 28% yield after silica-gel chromatography by using 2-ethylpyrrole and 2,3,4,5,6-pentafluorobenzaldehyde as the precursors. Eluent: petroleum ether/ethyl acetate (9:1). UV-vis (DMSO) λ, nm 527. ^{1}H NMR (400 MHz, $CDCl_3$) δ_H, ppm 6.55–6.52 (d, *J* = 4.1 Hz, 2H), 6.32–6.29 (d, *J* = 4.2 Hz, 2H), 3.04–2.97 (m, *J* = 7.6 Hz, 4H), 1.29–1.26 (t, *J* = 7.6 Hz, 6H). FT-IR (cm^{-1}): 2921, 2853 (C-H), 1568 (C=C), 1491, 1460 (C-N), 1120 (C-F), 461 (C-H).

3a was obtained in 37% yield after silica-gel chromatography by using 2,4-dimethylpyrrole and 2,3,4,5,6-pentafluorobenzaldehyde as the precursors. Eluent: petroleum ether/ethyl acetate (9:1). UV-vis (DMSO) λ, nm 517. ^{1}H NMR (600 MHz, $CDCl_3$) δ_H, ppm 6.04 (s, 2H), 2.55 (s, 6H), 1.60 (s, 6H). FT-IR (cm^{-1}): 2923, 2851 (C-H), 1551 (C=C), 1493, 1451 (C-N), 1146 (C-F), 468 (C-H).

3b was obtained in 32% yield after silica-gel chromatography by using 2,4-dimethylpyrrole and 4-pyridinecarboxaldehyde as the precursors. Eluent: petroleum ether/ethyl acetate (1:3). UV-vis (DMSO) λ, nm 505. ^{1}H NMR (600 MHz, $CDCl_3$) δ_H, ppm 8.79–8.78 (d, *J* = 5.8 Hz, 2H),

7.32–7.30 (d, *J* = 5.8 Hz, 2H), 6.01 (s, 2H), 2.56 (s, 6H), 1.41 (s, 6H). FT-IR (cm^{-1}): 2912 (C-H), 1544 (C=C), 1423, 1386 (C-N), 471 (C-H).

3c was obtained in 33% yield after silica-gel chromatography by using 2,4-dimethylpyrrole and 4-acetamidobenzaldehyde as the precursors.[37] Eluent: petroleum ether/ethyl acetate (1:8). UV-vis (DMSO) λ, nm 501. ^{1}H NMR (600 MHz, $CDCl_3$) δ_H, ppm 7.75–7.65 (d, J = 7.9 Hz, 2H), 7.47 (s, 1H), 7.27–7.19 (d, J = 7.9 Hz, 2H), 6.00 (s, 2H), 2.57 (s, 6H), 2.25 (s, 3H), 1.44 (s, 6H). FT-IR (cm^{-1}): 3368 (N-H amide stretch), 2920 (C-H stretch), 2852 (C-H stretch), 1529 (N-H amide bend), 1459, 1399 (C-N stretch), 1186 (C-N stretch), 967 (=C-H bend), 470 (C-H).

3d was obtained in 23% yield after silica-gel chromatography by using 2,4-dimethylpyrrole and 2-iodobenzaldehyde as the precursors. Eluent: petroleum ether/ethyl acetate (9:1). UV-vis (DMSO) λ, nm 509. ^{1}H NMR (400 MHz, $CDCl_3$) δ_H, ppm 7.98–7.94 (d, J = 7.9 Hz, 1H), 7.52–7.47 (m, 1H), 7.32–7.29 (m, J = 7.4, 1.4 Hz, 1H), 7.19–7.14 (m, 1H), 5.99 (s, 2H), 2.57 (s, 6H), 1.40 (s, 6H). FT-IR (cm^{-1}): 2921, 2853 (C-H), 1540 (C=C), 1504, 1459 (C-N), 633 (C-I), 470 (C-H).

3e was obtained in 17% yield after silica-gel chromatography by using 2,4-dimethylpyrrole and 3-iodobenzaldehyde as the precursors. Eluent: petroleum ether/ethyl acetate (9:1). UV-vis (DMSO) λ, nm 504. ^{1}H NMR (400 MHz, $CDCl_3$) δ_H, ppm 7.85–7.80 (d, J = 7.7 Hz, 1H), 7.68 (s, 1H), 7.30–7.21 (m, 2H), 5.99 (s, 2H), 2.55 (s, 6H), 1.43 (s, 6H). FT-IR (cm^{-1}): 2920, 2852 (C-H), 1538 (C=C), 1504, 1461 (C-N), 530 (C-I), 471 (C-H).

3f was obtained in 19% yield after silica-gel chromatography by using 2,4-dimethylpyrrole and 4-iodobenzaldehyde as the precursors. Eluent: petroleum ether/ethyl acetate (9:1). UV-vis (DMSO) λ, nm 503. ^{1}H NMR (600 MHz, $CDCl_3$) δ_H, ppm 7.79–7.75 (d, J = 8.2 Hz, 2H), 6.99–6.95 (d, J = 8.3 Hz, 2H), 5.92 (s, 2H), 2.48 (s, 6H), 1.34 (s, 6H). FT-IR (cm^{-1}): 2920, 2852 (C-H), 1584 (C=C), 1504, 1461 (C-N), 578 (C-I), 469 (C-H).

3g was obtained in 55% yield after silica-gel chromatography by using 2,4-dimethylpyrrole and 2-bromobenzaldehyde as the precursors. Eluent: petroleum ether/ethyl acetate (4:1). UV-vis (DMSO) λ, nm 509. ^{1}H NMR (600 MHz, $CDCl_3$) δ_H, ppm 7.71–7.68 (d, *J* = 8.0 Hz, 1H), 7.48–7.44 (t, *J* = 7.5 Hz, 1H), 7.37–7.32 (m, *J* = 8.0, 1.2 Hz, 1H), 7.31–7.28 (d, *J* = 7.5 Hz, 1H), 5.99 (s, 2H), 2.56 (s, 6H), 1.42 (s, 6H).

3h was obtained in 30% yield after silica-gel chromatography by using 2,4-dimethylpyrrole and 5-bromothiophene-2-carboxaldehyde as the precursors. Eluent: petroleum ether/ethyl acetate (4:1). UV-vis (DMSO) λ, nm 517. ^{1}H NMR (600 MHz, Acetone-d_6) δ_H, ppm 7.35–7.33 (d, J = 3.7 Hz, 1H), 7.08–7.06 (d, J = 3.7 Hz, 1H), 6.19 (s, 2H), 2.51 (s, 6H), 1.74 (s, 6H). FT-IR (cm^{-1}): 2918, 2851 (C-H stretch), 1536, 1499 (C-N stretch), 1181 (C-N stretch), 469 (C-H).

3i was obtained in 60% yield after silica-gel chromatography by using 2,4-dimethylpyrrole and methyl 4-formylbenzoate as the precursors. Eluent: petroleum ether/ethyl acetate (4:1). UV-vis (DMSO) λ, nm 503. ^{1}H NMR (600 MHz, Acetone-d_6) δ_H, ppm 8.25–8.22 (d, J = 7.9 Hz, 2H), 7.62–7.59 (d, J = 7.9 Hz, 2H), 6.15 (s, 2H), 3.97 (s, 3H), 2.53 (s, 6H), 1.40 (s, 6H). FT-IR (cm^{-1}): 2953 (C-H stretch), 2914 (C-H stretch), 1712 (C=O), 1277, 1062 (C-O), 1459, 1410 (C-N stretch), 1188, 1062 (C-N stretch), 1277, 1062 (C-O), 965 (=C-H bend), 465 (C-H).

4b was obtained in 26% yield after silica-gel chromatography by using 3-ethyl-2,4-dimethylpyrrole and 4-pyridinecarboxaldehyde as the precursors. Eluent: petroleum ether/ethyl acetate (1:1). UV-vis (DMSO) λ, nm 528.^{1}H NMR (600 MHz, $CDCl_3$) δ_H, ppm 8.82–8.79 (d, J = 5.6 Hz, 2H), 7.39–7.36 (d, J = 5.7 Hz, 2H), 2.56 (s, 6H), 2.35–2.30 (m, J = 7.5 Hz, 4H), 1.32 (s, 6H), 1.02–0.98 (m, J = 7.6 Hz, 6H). FT-IR (cm^{-1}): 2920 (C-H), 1536 (C=C), 1468, 1403 (C-N).

2.3.2. Brominated BODIPY core dye synthesis (Scheme 2.2–2.4)

BODIPYs **1-3** (1 mol eq) and NBS (3 mol eq) were dissolved in CH_2Cl_2 (20 mL). NBS was added in excess to the reaction vessels containing **1a** and **2a**. The mixture was left to stir under Ar/N_2 at room temperature; the reaction was followed by thin-layer chromatography to completion. The product was washed with water and the organic phase dried over sodium sulfate. Finally, purification was achieved *via* flash column chromatography.

2.3.2.1. Synthesis of **5a**

BODIPY **5a** was synthesized from **1a** using the procedure described above (**Scheme 2**).

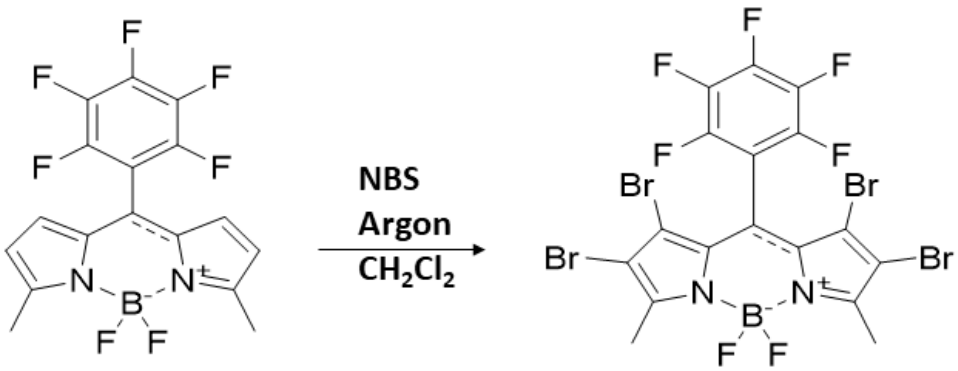

Scheme 2.2. Bromination of BODIPY **1a** to form **5a**.

5a was obtained in 32% yield. Eluent: petroleum ether/ethyl acetate (9:1). UV-vis (DMSO) λ, nm 561. ^{1}H NMR (600 MHz, $CDCl_3$) δ_H, ppm 2.63 (s, 3H), 1.62 (s, 3H). FT-IR (cm^{-1}): 2919, 2854 (C-H), 1568 (C=C), 1501, 1450 (C-N), 1116 (C-F), 619 (C-Br); MALDI-TOF Anal. calcd m/z 701.72; Found: $[M + H]^+$ 703.11.

2.3.2.2. Synthesis of **6a**

BODIPY **6a** was synthesized from **2a** using the procedure described above (**Scheme 2.3**). **6a** was obtained in 65% yield after silica-gel chromatography. Eluent: petroleum ether/ethyl

acetate (9:1). UV-vis (DMSO) λ, nm 562. ^{1}H NMR (400 MHz, $CDCl_3$) δ_H, ppm 6.69 (s, 2H), 3.08–2.98 (m, J = 7.5 Hz, 4H), 1.38–1.33 (t, J = 7.5 Hz, 6H). FT-IR (cm^{-1}): 2985, 2943 (C-H), 1565 (C=C), 1484, 1424 (C-N), 1118 (C-F), 613 (C-Br). MALDI-TOF Anal. calcd m/z 571.93; Found: $[M]^+$ 571.68.

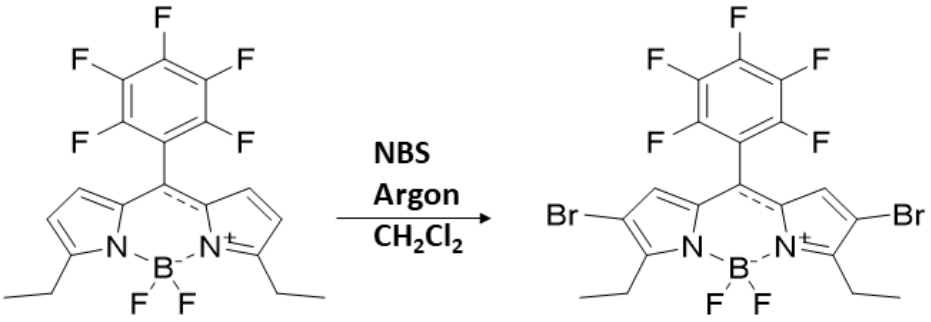

Scheme 2.3. Bromination of BODIPY **2a** to form **6a**.

2.3.2.3. Synthesis of **7a-i**

Novel and previously synthesized BODIPYs **7a-i** were synthesized from **3a-i** using the procedure described above (**Scheme 2.4**).[126,130–132]

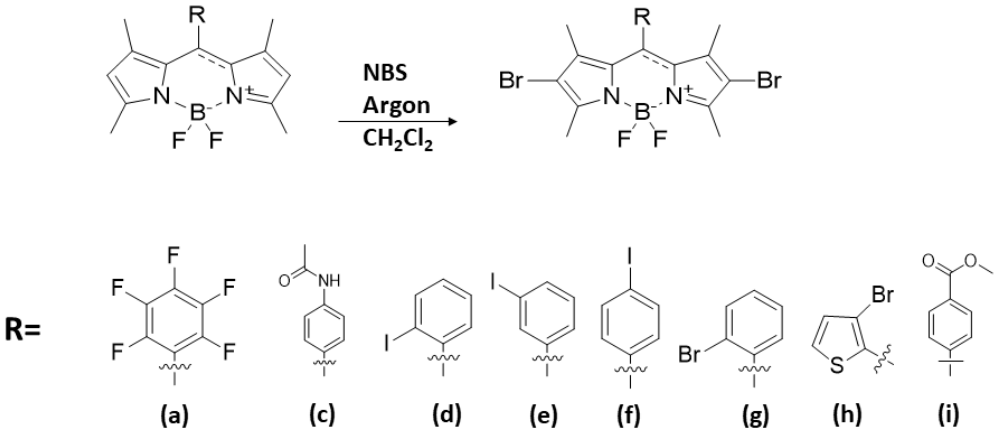

Scheme 2.4. Bromination of BODIPY **3a**-**i** to form **7a**-**i**.

7a was obtained in 70% yield after silica-gel chromatography. Eluent: petroleum ether/ethyl acetate (9:1). UV-vis (DMSO) λ, nm 549. ^{1}H NMR (600 MHz, $CDCl_3$) δ_H, ppm 2.58 (s, 6H), 1.58

(s, 6H). FT-IR (cm^{-1}): 2920, 2850 (C-H), 1529 (C=C), 1495, 1455 (C-N), 1170 (C-F), 525 (C-Br). MALDI-TOF Anal. calcd m/z 571.93; Found: $[M]^+$ 572.40.

7c was obtained in 30% yield after silica-gel chromatography. Eluent: petroleum ether/ethyl acetate (1:8). UV-vis (DMSO) λ, nm 527. ^1H NMR (600 MHz, $CDCl_3$) δ_H, ppm 7.78–7.72 (d, J = 8.2 Hz, 2H), 7.55 (s, 1H), 7.24–7.19 (d, J = 8.2 Hz, 2H), 2.62 (s, 6H), 2.27 (s, 3H), 1.44 (s, 6H). FT-IR (cm^{-1}): 3287 (N-H), 2919, 2855 (C-H), 1527 (N-H), 1463, 1392 (C-N), 1162 (C-N), 521 (C-Br). MALDI-TOF Anal. calcd m/z 539.27; Found: $[M]^+$ 539.02.

7d was obtained in 73% yield after silica-gel chromatography. Eluent: petroleum ether/ethyl acetate (9:1). UV-vis (DMSO) λ, nm 536. ^1H NMR (400 MHz, $CDCl_3$) δ_H, ppm 7.92–7.88 (m, *J* = 8.1 Hz, 1H), 7.47–7.40 (m, *J* = 12.7, 7.5, 6.7 Hz, 1H), 7.20–7.13 (m, 2H), 2.55 (s, 6H), 1.32 (s, 6H). FT-IR (cm^{-1}): 2943, 2866 (C-H), 1535 (C=C), 1460 (C-N), 642 (C-I), 509 (C-Br). MALDI-TOF Anal. calcd m/z 607.88; Found: $[M]^+$ 607.77.

7e was obtained in 50% yield after silica-gel chromatography. Eluent: petroleum ether/ethyl acetate (9:1). UV-vis (DMSO) λ, nm 531. ^1H NMR (400 MHz, $CDCl_3$) δ_H, ppm 7.82–7.78 (m, 1H), 7.59 (s, 1H), 7.21–7.18 (m, 2H), 2.53 (s, 6H), 1.35 (s, 6H). FT-IR (cm^{-1}): 2928, 2864 (C-H), 1532 (C=C), 1457 (C-N), 592 (C-I), 524 (C-Br). MALDI-TOF Anal. calcd m/z 607.88; Found: $[M]^+$ 607.79.

7f was obtained in 68% yield after silica-gel chromatography. Eluent: petroleum ether/ethyl acetate (9:1). UV-vis (DMSO) λ, nm 530. ^1H NMR (400 MHz, $CDCl_3$) δ_H, ppm 7.90–7.87 (d, *J* = 8.3 Hz, 2H), 7.05–6.99 (d, *J* = 8.3 Hz, 2H), 2.60 (s, 6H), 1.41 (s, 6H). FT-IR (cm^{-1}): 2922, 2867 (C-H), 1538 (C=C), 1460 (C-N), 587 (C-I), 527 (C-Br). MALDI-TOF Anal. calcd m/z 607.88; Found: $[M]^+$ 607.79.

7g was obtained in 36% yield after silica-gel chromatography. Eluent: petroleum ether/ethyl acetate (4:1). UV-vis (DMSO) λ, nm 535. ^{1}H NMR (600 MHz, $CDCl_3$) δ_H, ppm 7.75–7.72 (d, *J* = 8.1 Hz, 1H), 7.51–7.48 (m, *J* = 7.5 Hz, 1H), 7.43–7.38 (m, *J* = 11.1, 4.3 Hz, 1H), 7.28 (s, 1H), 2.61 (s, 6H), 1.41 (s, 6H). FT-IR (cm^{-1}): 2966, 2900 (C-H), 1536, 1457 (C-N), 1181 (C-N), 533 (C-Br). MALDI-TOF Anal. calcd m/z 559.89; Found: $[M]^+$ 560.20.

7h was obtained in 29% yield after silica-gel chromatography. Eluent: petroleum ether/ethyl acetate (4:1). UV-vis (DMSO) λ, nm 545. ^{1}H NMR (600 MHz, Acetone-d_6) δ_H, ppm 7.40–7.38 (d, *J* = 3.7 Hz, 1H), 7.18–7.16 (d, *J* = 3.7 Hz, 1H), 2.56 (s, 6H), 1.73 (s, 6H). FT-IR (cm^{-1}): 2919, 2851 (C-H stretch), 1535, 1453 (C-N stretch), 1178 (C-N stretch), 528 (C-Br). MALDI-TOF Anal. calcd m/z 568.85; Found: $[M]^+$ 568.16.

7i was obtained in 92% yield after silica-gel chromatography. Eluent: petroleum ether/ethyl acetate (4:1). UV-vis (DMSO) λ, nm 530. ^{1}H NMR (300 MHz, DMSO-d_6) δ_H, ppm 8.16–8.14 (d, J = 8.5 Hz, 2H), 7.64–7.61 (d, J = 8.5 Hz, 2H), 3.91 (s, 3H), 2.52 (s, 6H), 1.31 (s, 6H). FT-IR (cm^{-1}): 2995 (C-H stretch), 2951 (C-H stretch), 1724 (C=O), 1268, 1091 (C-O), 1458, 1399 (C-N stretch), 1188, 1091 (C-N stretch), 1268, 1091 (C-O), 998 (=C-H bend), 532 (C-Br stretch). MALDI-TOF Anal. calcd m/z 539.99; Found: $[M + H]^+$ 541.27.

2.3.3. Iodinated BODIPY core dye synthesis (Scheme 2.5–2.6)

2.3.3.1. Synthesis of **8a** (**Scheme 2.5**)

BODIPY **1a** (1 mol eq) and excess NIS were dissolved in CH_2Cl_2 (20 mL). The mixture was left to stir under Ar/N_2 at room temperature; the reaction was followed by thin-layer chromatography to completion. The product was washed with water and the organic phase dried over sodium sulfate. Finally, purification was achieved *via* flash column chromatography

eluting with petroleum ether:ethyl acetate (9:1), and **8a** was obtained in 57 % yield. UV-vis (DMSO) λ, nm 573. ^{1}H NMR (600 MHz, $CDCl_3$) δ_H, ppm 6.84 (s, 2H), 2.67 (s, 6H). FT-IR (cm^{-1}): 2918 (C-H), 1559 (C=C), 1496 (C-N), 1107 (C-F), 616 (C-I); MALDI-TOF Anal. calcd m/z 637.88; Found: $[M + H]^+$ 638.87.

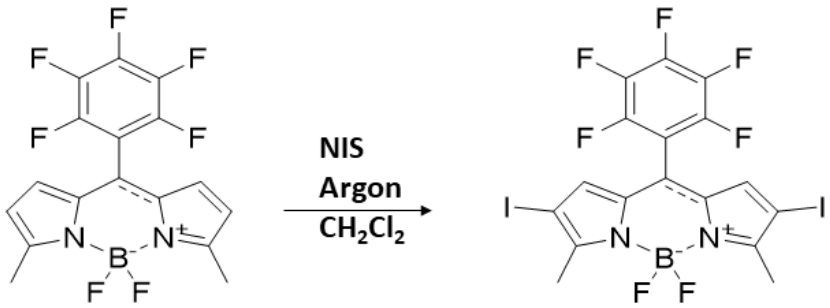

Scheme 2.5. Iodination of BODIPY **1a** to form **8a**.

2.3.3.2. Synthesis of **9a** (**Scheme 2.6**)

BODIPY **9a** was synthesized following the procedure described for **8a** and was obtained in 61 % yield. UV-vis (DMSO) λ, nm 558. ^{1}H NMR (600 MHz, $CDCl_3$) δ_H, ppm 2.67 (s, 6H), 1.64 (s, 6H) ppm. FT-IR ($cm^{-1)}$: 2920, 2855 (C-H), 1532 (C=C), 1455 (C-N), 1167 (C-F), 522(C-I). MALDI-TOF Anal. calcd m/z 665.91; Found: $[M]^+$ 665.95.

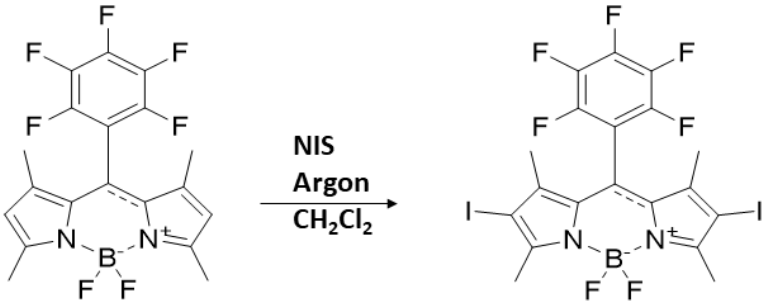

Scheme 2.6. Iodination of BODIPY **3a** to form **9a**.

2.3.4. Synthesis of mono and distyrylBODIPY dyes (Scheme 2.7–2.14)

2.3.4.1. BODIPY 10 (Scheme 2.7)

BODIPY **1a** (1 mol eq) and 4-diethylaminobenzaldehyde (1.4 mol eq) were dissolved in dry benzene (20 mL) under Ar with stirring, followed by the drop-wise addition of glacial acetic acid (0.4 mL).[100] Thereafter, piperidine (0.4 mL) was added slowly, followed by heating and reflux in the presence of a Dean-Stark trap for the azeotropic removal of water formed during the condensation reaction. The reaction was monitored by TLC to completion and quenched with water. The organic phase was then dried over sodium sulfate. Separation was achieved by flash column chromatography with petroleum ether:ethyl acetate (9:1). **10** was obtained in 25% yield. UV-vis (DMSO) λ, nm 681. ^{1}H NMR (600 MHz, $CDCl_3$) δ_H, ppm 7.47–7.44 (d, J = 6.3 Hz, 4H), 7.31–7.27 (d, J = 16.0 Hz, 2H), 6.87–6.85 (d, J = 4.7 Hz, 2H), 6.57–6.55 (d, J = 4.5 Hz, 2H), 3.37–3.35 (d, J = 6.7 Hz, 4H), 2.59 (s, 3H), 1.15–1.13 (t, J = 7.1 Hz, 6H). FT-IR (cm^{-1}): 2920, 2873 (C-H), 1587 (C=C), 1555, 1524 (C-N), 1478 (C-H), 1185 (C-F), 430 (C-H). MALDI-TOF Anal. calcd m/z 545.31; Found: $[M]^+$ 545.53.

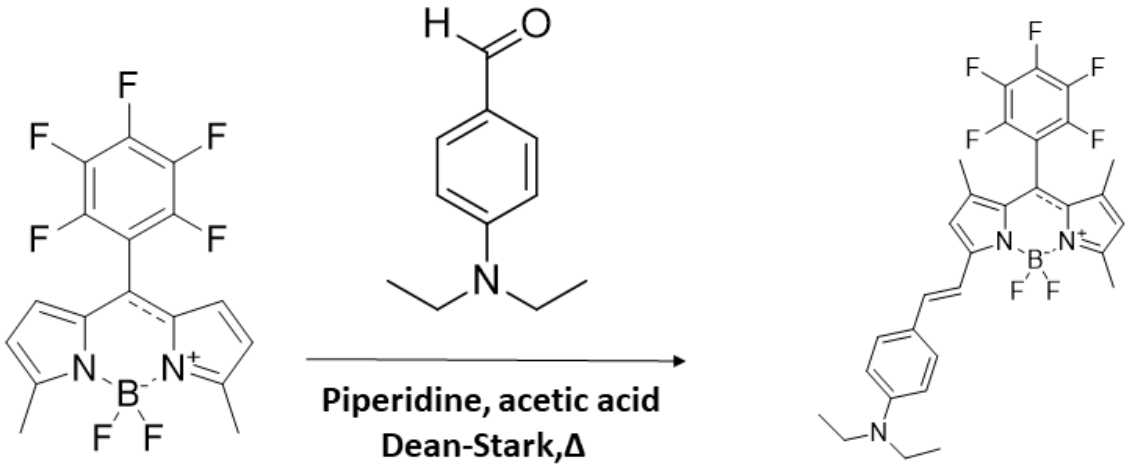

Scheme 2.7. Synthesis of BODIPY **10**.

2.3.4.2. BODIPY 11 (Scheme 2.8)

BODIPY **11** was synthesized from BODIPY **3a** using the procedure described for BODIPY **10** and was obtained in 23% yield after silica-gel chromatography.[100] Eluent: petroleum ether/ethyl acetate (9:1). UV-vis (DMSO) λ, nm 661. ^{1}H NMR (600 MHz, $CDCl_3$) δ_H, ppm 7.50–7.47 (d, J = 8.5 Hz, 4H), 6.68–6.65 (d, J = 6.7 Hz, 4H), 6.64–6.61 (d, J = 8.3 Hz, 4H), 5.99 (s, 2H), 3.43–3.39 (m, 8H), 1.64 (s, 3H), 1.59 (s, 3H), 1.20–1.18 (t, J = 7.1 Hz, 12H). FT-IR (cm^{-1}): 2966, 2920 (C-H), 1586 (C=C), 1548 (C-N), 1490 (C-H), 1149 (C-F), 441(C-H). MALDI-TOF Anal. calcd m/z 733.01; Found: $[M]^+$ 732.60.

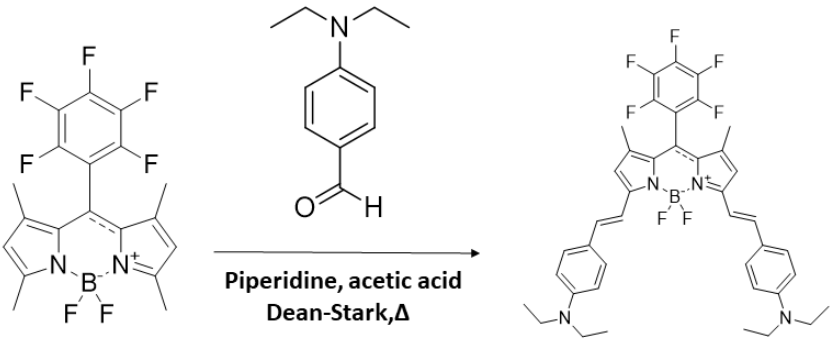

Scheme 2.8. Synthesis of BODIPY **11**.

2.3.4.3. BODIPY 12 (Scheme 2.9)

BODIPY **12** was synthesized from BODIPY **7a** using the procedure described for BODIPY **10** and was obtained in 30% yield after silica-gel chromatography.[100] Eluent: petroleum ether/ethyl acetate (9:1). UV-vis (DMSO) λ, nm 718. ^{1}H NMR (600 MHz, $CDCl_3$) δ_H, ppm 8.34–3.43 (d, J = 16.3 Hz, 2H), 7.60–7.57 (d, J = 8.9 Hz, 6H), 6.73–6.68 (d, J = 8.4 Hz, 4H), 3.49–8.14 (m, J = 7.0 Hz, 8H), 2.67 (s, 6H), 1.26–1.22 (t, J = 7.1 Hz, 12H). FT-IR (cm^{-1}): 2920, 2851 (C-H), 1586 (C=C),

1525, 1489 (C-N), 1346, 1301 (C-H), 1169 (C-F), 508(C-Br). MALDI-TOF Anal. calcd m/z 890.39; Found: $[M]^+$ 891.06.

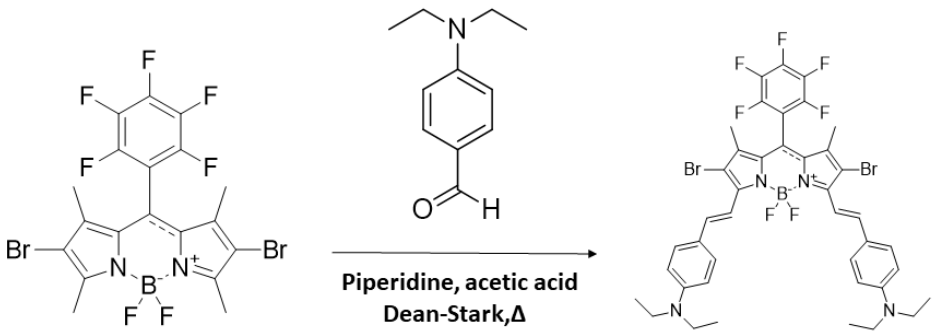

Scheme 2.9. Synthesis of BODIPY **12**.

2.3.4.4. BODIPY 13 (Scheme 2.10)

BODIPY **13** was synthesized from BODIPY **1b** and benzaldehyde using the procedure described for BODIPY **10** and was obtained in 18% yield after silica-gel chromatography. Eluent: petroleum ether/ethyl acetate (1:3). UV-vis (DMSO) λ, nm 648. ^{1}H NMR (600 MHz, $CDCl_3$) δ_H, ppm 8.80–8.73 (d, *J* = 3.4 Hz, 2H), 7.79–7.74 (d, *J* = 16.3 Hz, 2H), 7.66–7.63 (d, *J* = 7.5 Hz, 4H), 7.45–7.43 (d, *J* = 5.2 Hz, 2H), 7.42–7.39 (t, *J* = 7.6 Hz, 4H), 7.38–7.32 (m, 4H), 6.96–6.93 (d, *J* = 4.5 Hz, 2H), 6.73–6.71 (d, *J* = 4.4 Hz, 2H). FT-IR (cm^{-1}): 2903 (C-H), 1552 (C=C), 1472, 1428 (C-N), 496 (C-H). MALDI-TOF Anal. calcd m/z 473.19; Found: $[M - F + Na]^+$ 477.80 (Calcd m/z 477.18).

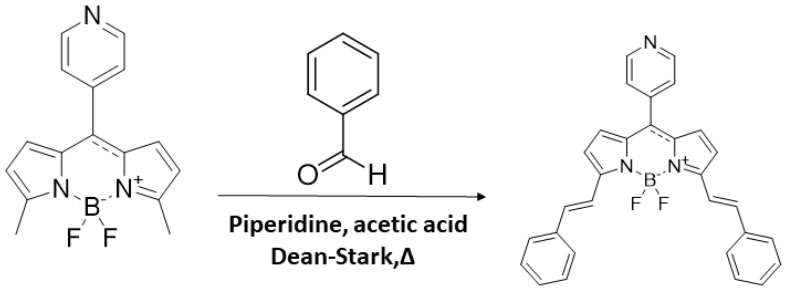

Scheme 2.10. Synthesis of BODIPY **13**.

2.3.4.5. BODIPY 14 (Scheme 2.11)

BODIPY **14** was synthesized from BODIPY **3b** and benzaldehyde using the procedure described for BODIPY **10** and was obtained in 26% yield after silica-gel chromatography. Eluent: petroleum ether/ethyl acetate (1:3). UV-vis (DMSO) λ, nm 634. ^{1}H NMR (600 MHz, $CDCl_3$) δ_H, ppm 7.82–7.75 (d, *J* = 16.3 Hz, 2H), 7.69–7.65 (d, *J* = 7.6 Hz, 6H), 7.46–7.42 (t, 4H), 7.38–7.35 (t, 2H), 7.34–7.29 (d, *J* = 16.2 Hz, 4H), 6.70 (s, 2H), 1.51 (s, 6H). FT-IR (cm^{-1}): 2916 (C-H), 1536 (C=C), 1489, 1441 (C-N), 468 (C-H). MALDI-TOF Anal. calcd m/z 501.22; Found: $[M + H]^+$ 502.23.

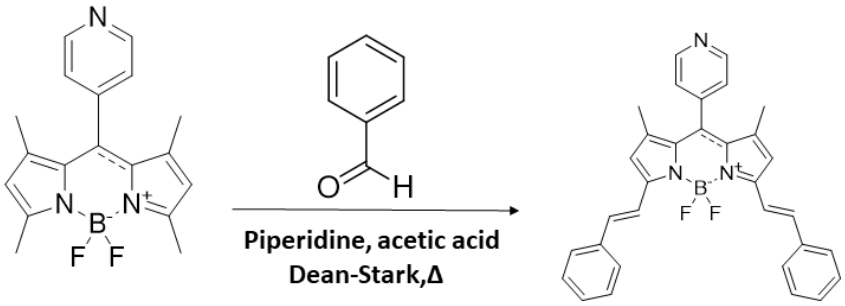

Scheme 2.11. Synthesis of BODIPY **14**.

2.3.4.6. BODIPY 15 (Scheme 2.12)

BODIPY **15** was synthesized from BODIPY **4b** and benzaldehyde using the procedure described for BODIPY **10** and was obtained in 22% yield after silica-gel chromatography. Eluent: hexane/CH_2Cl_2 (1:3). UV-vis (DMSO) λ, nm 643. ^{1}H NMR (600 MHz, $CDCl_3$) δ_H, ppm 8.84–8.81 (d, J = 5.7 Hz, 2H), 7.83–7.78 (d, J = 16.8 Hz, 2H), 7.68–7.64 (d, J = 7.5 Hz, 4H), 7.45–7.42 (m, J = 7.6 Hz, 4H), 7.39–7.38 (m, J = 4.5, 1.3 Hz, 2H), 7.37–7.35 (d, J = 7.4 Hz, 2H), 7.33–7.31 (d, J = 5.5 Hz, 2H), 2.67–2.62 (m, J = 7.5 Hz, 4H), 1.39 (s, 6H), 1.21–1.18 (t, J = 7.5 Hz, 6H). FT-IR (cm^{-1}): 2969 (C-H), 1523 (C=C), 1438, 1400 (C-N). MALDI-TOF Anal. calcd m/z 557.28; Found: $[M]^+$ 557.20.

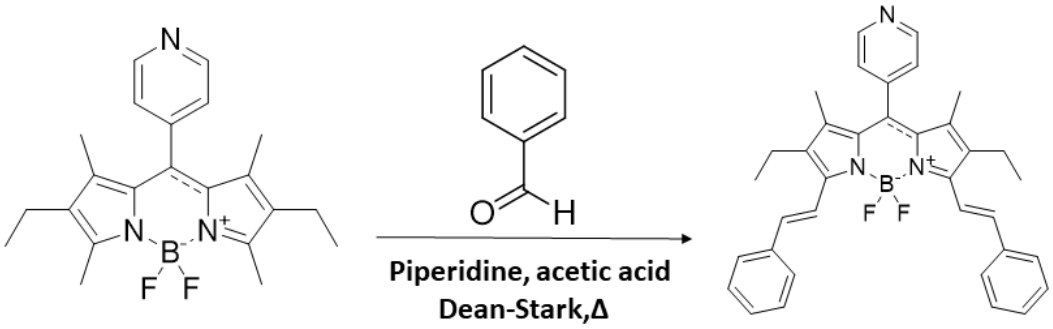

Scheme 2.12. Synthesis of BODIPY **15**.

2.3.4.7. BODIPY 16 (Scheme 2.13)

BODIPY **16** was synthesized from BODIPY **3c** and 4-(benzyloxy)benzaldehyde using the procedure described for BODIPY **10** and was obtained in 32% yield.[37] UV-vis (DMSO) λ, nm 647. ^{1}H NMR (600 MHz, $CDCl_3$) δ, ppm 7.72–7.67 (d, J = 7.9 Hz, 2H), 7.64–7.58 (m, 6H), 7.51–7.46 (m, 5H), 7.46–7.42 (m, 4H), 7.39–7.35 (m, 2H), 7.27–7.21 (m, 4H), 7.04–7.00 (d, J = 8.2 Hz, 4H), 6.62 (s, 2H), 5.13 (s, 4H), 2.24 (s, 3H), 1.48 (s, 6H). FT-IR (cm^{-1}): 3377 (N-H amide stretch), 2916 (C-H stretch), 2853 (C-H stretch), 1471 (N-H amide bend), 1368 (C-N stretch), 1103 (C-N stretch), 1154 (C-O-C), 979 (=C-H bend). MALDI-TOF Anal. calcd m/z 769.86; Found: $[M]^+$ 769.30.

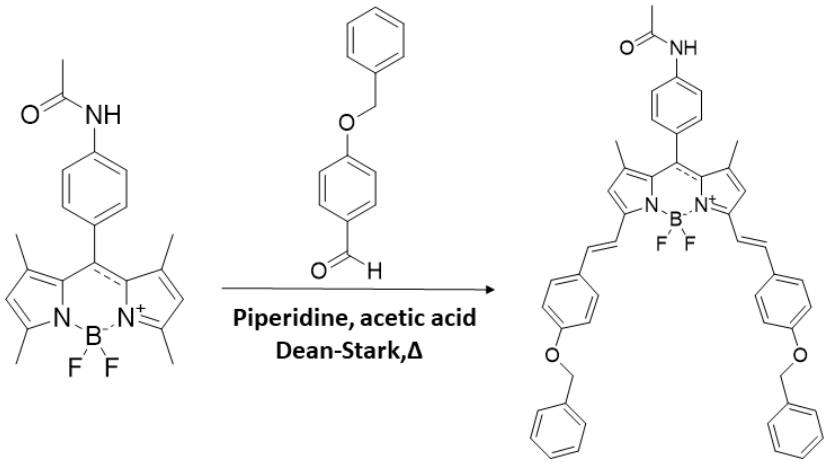

Scheme 2.13. Synthesis of BODIPY **16**.

2.3.4.8. BODIPY 17 (Scheme 2.14)

BODIPY **17** was synthesized from BODIPY **7a** and 4-(1-piperidinyl)benzaldehyde using the procedure described for BODIPY **10** and was obtained in 30% yield. UV-vis (DMSO) λ, nm 686. ^{1}H NMR (600 MHz, $CDCl_3$) δ, ppm 9.76 (s, 4H), 7.76–7.73 (d, *J* = 8.9 Hz, 4H), 6.92–6.90 (d, *J* = 9.0 Hz, 4H), 3.44–3.42 (m, *J* = 5.2 Hz, 8H), 1.69 (s, 12H), 1.27 (s, 6H). FT-IR (cm^{-1}): 2919, 2852 (C-H), 1530 (C=C), 1489, 1446 (C-N), 1161 (C-F), 523 (C-Br). MALDI-TOF Anal. calcd m/z 914.14; Found: $[M]^+$ 914.34.

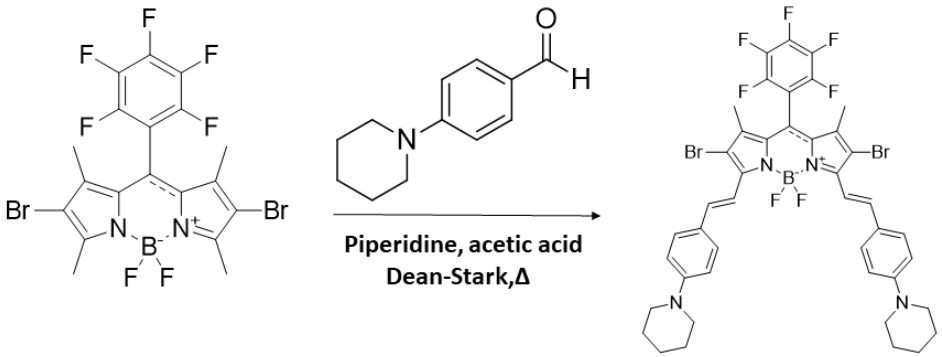

Scheme 2.14. Synthesis of BODIPY **17**.

2.3.5. Challenges encountered during synthesis

In a similar manner to the synthesis of the BODIPY core dyes described above, other BODIPY core dyes were synthesized during this work, and these were used as precursors for the synthesis of styrylBODIPY dyes.

2.3.5.1. BODIPY core synthesis (Scheme 2.15)

In a similar manner to the synthesis of BODIPYs **1-4(a-i)**, BODIPY core dyes **1j-m** and **3j-l** were synthesized (**Scheme 2.15**). Only the structural characterization by ^{1}H NMR is included for

these precursor dyes. This is because no further characterization was carried out as the dyes were not studied in a detailed manner in subsequent chapters.

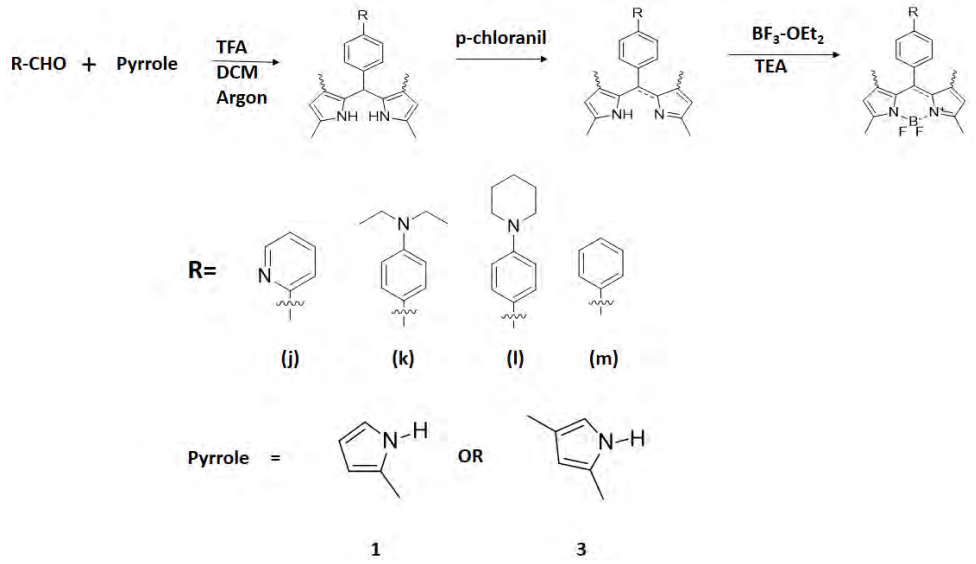

Scheme 2.15. Synthesis of BODIPYs **1j**-**m** and **3j**-**l**.

1j was obtained in 26% yield after silica-gel chromatography by using 2-methylpyrrole and 2-pyridinecarboxaldehyde as the precursors. Eluent: petroleum ether/ethyl acetate (1:1). ^{1}H NMR (600 MHz, $CDCl_3$) δ_H, ppm 8.80–8.82 (d, *J* = 4.6 Hz, 1H), 7.89–7.86 (m, *J* = 7.7, 1.6 Hz, 1H), 7.61–7.58 (d, *J* = 7.8 Hz, 1H), 7.50–7.47 (m, *J* = 7.2, 5.1 Hz, 1H), 6.81–6.78 (d, *J* = 4.1 Hz, 2H), 6.31–6.29 (d, *J* = 4.1 Hz, 2H), 2.67 (s, 6H).

1k was obtained in 33% yield after silica-gel chromatography by using 2-methylpyrrole and 4-diethylaminobenzaldehyde as the precursors. Eluent: petroleum ether/ethyl acetate (5:1). ^{1}H NMR (600 MHz, $CDCl_3$) δ_H, ppm 7.27 (s, 4H), 6.40–6.38 (d, J = 4.4 Hz, 4H), 2.67 (s, 18H).

1l was obtained in 23% yield after silica-gel chromatography by using 2-methylpyrrole and 4-(1-piperidinyl)benzaldehyde as the precursors. Eluent: petroleum ether/ethyl acetate (4:2). ^{1}H NMR (600 MHz, $CDCl_3$) δ_H, ppm 7.21 (s, 2H), 7.07–7.04 (d, *J* = 8.4 Hz, 2H), 7.01 (s, 2H), 5.91 (s, 2H), 3.2 –3.18 (m, 4H), 2.49 (s, 6H), 1.41 (s, 6H).

1m was obtained in 36% yield after silica-gel chromatography by using 2-methylpyrrole and benzaldehyde as the precursors. Eluent: petroleum ether/ethyl acetate (4:1). ^{1}H NMR (600 MHz, $CDCl_3$) δ_H, ppm 7.56–7.48 (m, 5H), 6.75–6.72 (d, *J* = 3.5 Hz, 2H), 6.31–6.27 (d, *J* = 3.7 Hz, 2H), 2.68 (s, 6H).

3j was obtained in 28% yield after silica-gel chromatography by using 2,4-dimethylpyrrole and 2-pyridinecarboxaldehyde as the precursors. Eluent: petroleum ether/ethyl acetate (1:1). ^{1}H NMR (600 MHz, $CDCl_3$) δ_H, ppm 8.82–8.80 (d, *J* = 4.8 Hz, 1H), 7.89–7.86 (m, *J* = 7.7, 3.9 Hz, 1H), 7.49–7.47 (t, 1H), 7.46–7.44 (d, *J* = 6.2 Hz, 1H), 5.99 (s, 2H), 2.56 (s, 6H), 1.33 (s, 6H).

3k was obtained in 38**%** yield after silica-gel chromatography by using 2-methylpyrrole and 4-diethylaminobenzaldehyde as the precursors. Eluent: petroleum ether/ethyl acetate (5:1). ^{1}H NMR (600 MHz, $CDCl_3$) δ_H, ppm 6.95–6.93 (d, *J* = 8.7 Hz, 2H), 6.67–6.65 (d, *J* = 8.8 Hz, 2H), 5.90 (s, 2H), 3.35–3.31 (m, *J* = 7.1 Hz, 4H), 2.48 (s, 6H), 1.44 (s, 6H), 1.14–1.11 (t, *J* = 7.1 Hz, 6H).

3l was obtained in 25% yield after silica-gel chromatography by using 2,4-dimethylpyrrole and 4-(1-piperidinyl)benzaldehyde as the precursors. Eluent: petroleum ether/ethyl acetate (4:2). ^{1}H NMR (600 MHz, $CDCl_3$) δ_H, ppm 7.39–7.36 (d, *J* = 8.5 Hz, 2H), 6.74–6.71 (d, *J* = 3.8 Hz, 2H), 6.20–6.18 (d, *J* = 4.1 Hz, 2H), 3.31–3.25 (m, 4H), 2.57 (s, 6H), 1.73 (s, 3H), 1.63–1.58 (d, *J* = 5.3 Hz, 3H), 1.19 (s, 6H).

2.3.5.2. Attempted synthesis of distyrylBODIPY dyes 18–24 (Scheme 2.16)

The BODIPY core dyes **1j-m** and **3j-l** described above were used for the attempted synthesis of a series of distyrylBODIPY dyes *via* Knoevenagel condensation reactions, in a similar manner to the syntheses described for **10-17** (**Scheme 2.16**). During the reactions, the starting

BODIPY remained unreacted for up to 72 h and in some instances, a dark brown or black substance with no distinct UV-visible absorption bands formed.

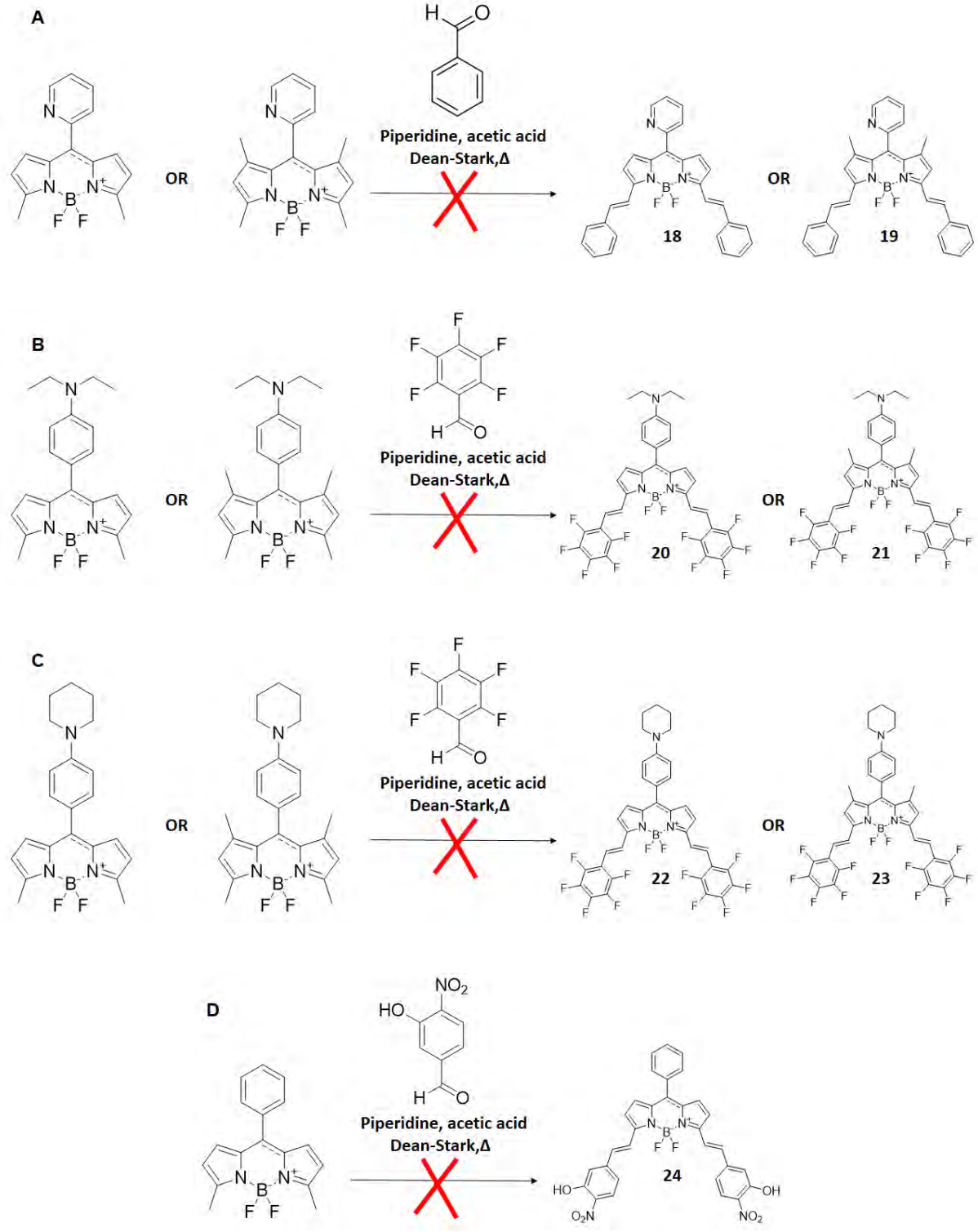

Scheme 2.16. Synthesis of BODIPYs **18**-**24**.

Chapter 3:

Structural and spectroscopic characterization of BODIPY dyes

This chapter details the synthesis of the target BODIPY structures and outlines the results obtained from the techniques used to characterize the BODIPYs. The first part looks at the synthesis and characterization of BODIPY core dyes, followed by the properties of halogenated core dyes and finally, the π-extended or styrylBODIPYs. Spectra obtained during the characterization are not included for all the dyes synthesized, but a few selected ones are used as a representative set. The spectroscopic and physicochemical properties of the BODIPYs are also discussed. Initially, an acid-catalyzed condensation reaction was used to synthesize BODIPY core dyes. Some of these dyes were then brominated and iodinated at the 1,7- and 2,6-positions. Subsequently, some of the core and brominated dyes were used in a Knoevenagel condensation reaction to extend the π-system of the dyes at the 3,5-positions, hence forming red-shifted π-extended BODIPYs. The halogenated core dyes were used in PACT, whereas the π-extended styrylBODIPYs were studied for application in NLO. The synthesis procedures used in this thesis are well-established in the literature, so only minor modifications were performed.[3,4,9,11,43,92,134]

BODIPY cores **1**–**4** (**Scheme 2.1**) were synthesized from the appropriate aldehydes and a corresponding pyrrole. BODIPYs **1a**–**c** were synthesized from 2-methylpyrrole, **2a** was synthesized from 2-ethylpyrrole, **3a**–**i** were synthesized from 2,4-dimethylpyrrole, and **4b** was synthesized from 3-ethyl-2,4-dimethylpyrrole. The core dyes **1a**, **2a**, **3a**–**i** were brominated to introduce bromine heavy atoms onto the BODIPY core and form **5a**, **6a** and **7a**–**i**, respectively (**Scheme 2.2**–**2.4**). To introduce the heavier iodine atoms onto the BODIPY core, **1a** and **3a** were reacted with NIS to form **8a** and **9a** (**Scheme 2.5**–**2.6**). Heavy atom-containing BODIPYs **5**-**9** were studied for application in PACT studies. A series of styrylBODIPY dyes were also synthesized for NLO studies from the core and brominated BODIPY dyes (**Scheme 2.7**–**2.14**).

BODIPYs **1a**, **3a**, and **7a** were respectively reacted with 4-diethylaminobenzaldehyde through a Knoevenagel condensation reaction to form **10**, **11** and **12** (**Scheme 2.7**–**2.9**). Similarly, BODIPYs **1b**, **3b**, and **4b** were reacted with benzaldehyde to form **13**, **14** and **15** (**Scheme 2.10**–**2.12**). BODIPY **3c** was reacted with 4-benzyloxybenzaldehyde to form **16** (**Scheme 2.13**). Finally, **7a** was reacted with 4-(1-piperidinyl)benzaldehyde to form **17** (**Scheme 2.14**). As mentioned in Chapter 2, some of the BODIPY dyes synthesized and characterized are novel, while some have been previously synthesized.[19,100,120–132]

3A – Synthesis and characterization of BODIPY core dyes

3.1. *Meso*-pentafluorophenylBODIPY core synthesis and characterization (**1a**, **2a** and **3a**)

3.17.1. Synthesis (**Scheme 3.1**)

Following established literature methods, 2-methylpyrrole, 2-ethylpyrrole or 2,4-dimethylpyrrole (2.0 mol eq), and 2,3,4,5,6-pentafluorobenzaldehyde (1.0 mol eq) were reacted in dry CH_2Cl_2 using the typical one-pot trifluoroacetic acid-catalyzed condensation reaction.[11–13,100]

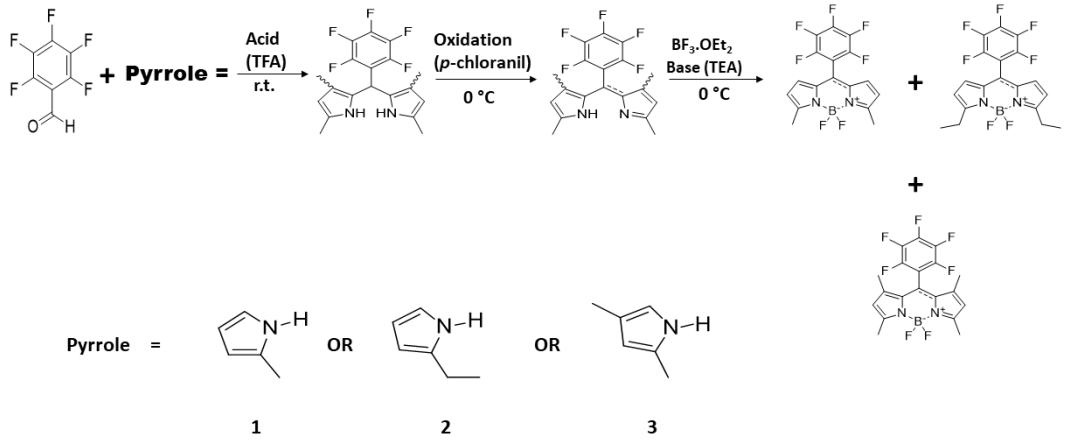

Scheme 3.1. Synthesis of core dyes **1a**, **2a** and **3a** using a typical one-pot acid-catalyzed reaction.

3.17.2. Structural characterization of **1a**, **2a** and **3a**

BODIPY **1a** has ten protons. The signals for all ten can be identified in the ^{1}H NMR spectrum (**Figure 3.1**). The doublets at 6.79–6.78 and 6.38–6.35 ppm each integrate to two protons and can be assigned to the four protons at the 1-, 2-, 6- and 7-positions of the BODIPY core. The six singlet proton signals at 2.60 ppm can be attributed to the six methyl protons attached to the 3- and 5-positions.

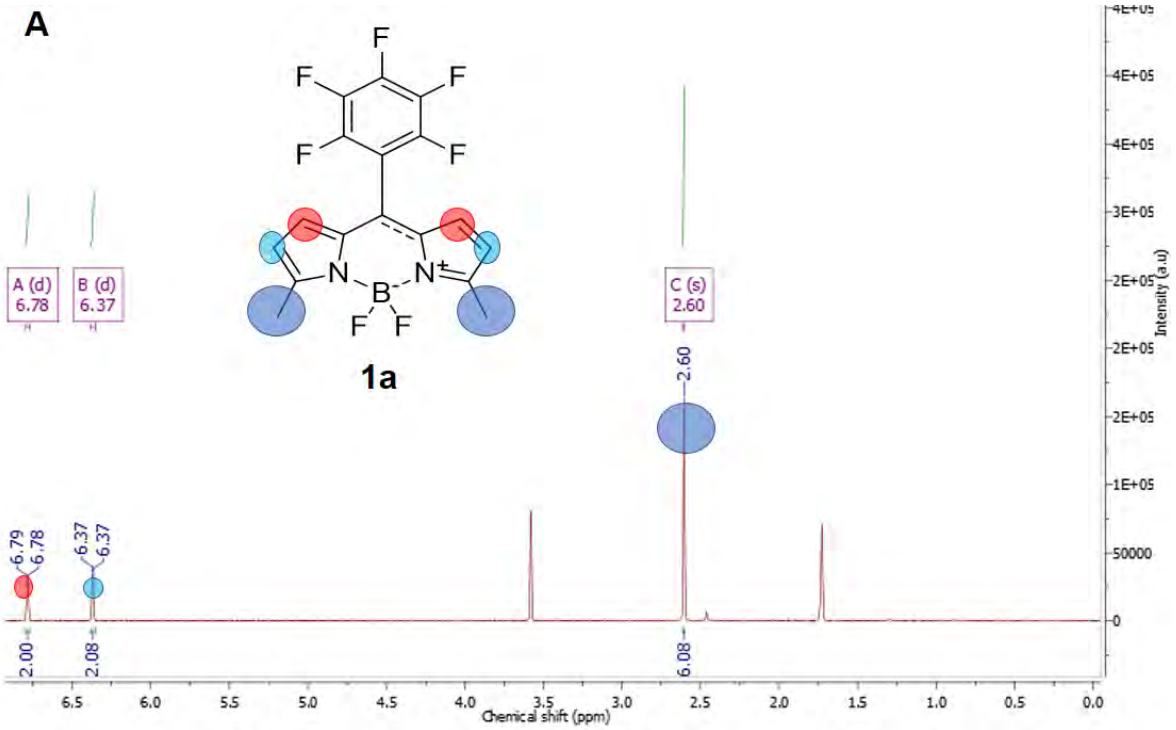

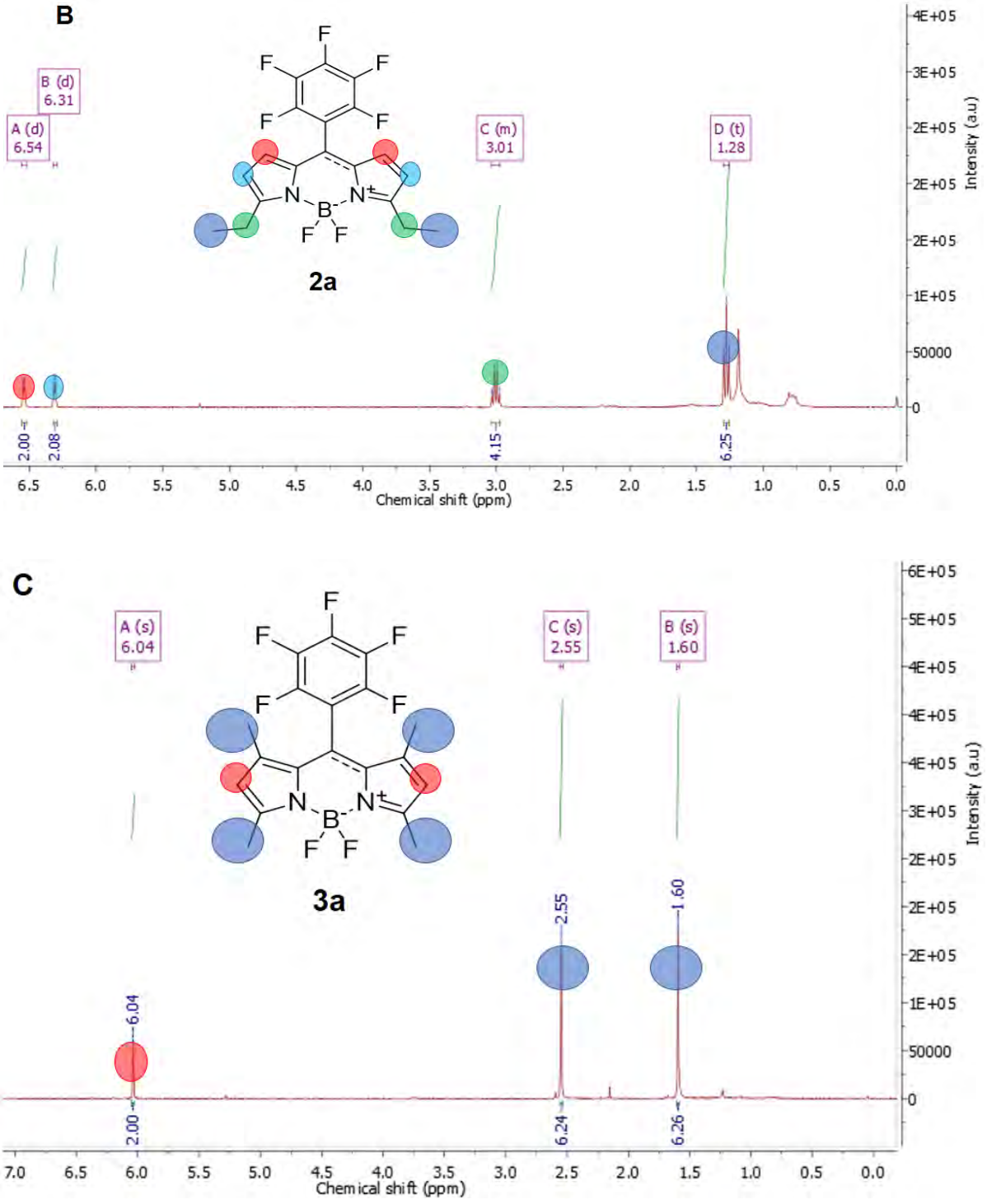

Figure 3.1. ^{1}H NMR spectra of BODIPY core dyes.

Similarly, the ^{1}H NMR spectrum of **2a** displays the four protons at the 1-, 2-, 6- and 7-positions of the BODIPY core as doublets that appear at 6.55–6.52 and 6.32–6.29 ppm (**Figure 3.1**).

Because of ethyl groups at the 3- and 5-positions, the total number of protons increases to fourteen. The protons associated with the ethyl groups appear as a multiplet signal that integrates to four protons at 3.04–2.97 ppm, and as a triplet signal that integrates to six protons at 2.60 ppm. In the ^{1}H NMR spectrum of **3a**, all the peaks are singlets since there are no neighboring protons. The first of these signals appears at 6.04 ppm, integrates to two protons, and can be assigned to the 2,6-positions of the BODIPY core. The peaks for the twelve methyl protons at the 1-, 3-, 5- and 7-positions of **3a** lie at 2.55 and 1.60 ppm. These signals each integrate as six protons.

The FT-IR spectra of all three core dyes contained the peaks anticipated for the BODIPY core. Of interest are the C-F stretches found at 1128, 1120 and 1146 cm^{-1} for **1a**, **2a** and **3a**, and the C-H stretches observed at 425, 461 and 468 cm^{-1} for the bonds at the 2,6-positions.

3.17.3. Spectroscopic and physicochemical properties of **1a**, **2a** and **3a**

The UV-visible absorption spectra of **1a**, **2a** and **3a** in DMSO shown below are typical of *meso*-substituted BODIPY core dyes, with no signs of aggregation (**Figure 3.2A**). The absorption maxima lie at 525, 527 and 517 nm, respectively. Typically, the absorption maximum of a *meso*-aryl-substituted 1,3,5,7-tetramethyl BODIPY dyes lies *ca.* 500 nm, but the maximum for **3a** lies at 517 nm.[3,13] This is attributed to the presence of the strongly electron-withdrawing pentafluorophenyl *meso*-group. There are no significant differences in the spectra of **1a** and **2a**. The major spectral bands are slightly red-shifted relative to that of **3a**. This red-shift is thought to be due to the absence of methyl groups at the 1,7-positions, enabling greater rotation of the *meso*-aryl substituents; this will be explored further in Chapter 6.

The fluorescence excitation and emission spectra for all the dyes displayed the expected trends. Representative spectra are shown below (**Figure 3.2B**). As expected based on Kasha's rule, the excitation spectrum is identical to the UV-visible absorption spectrum, whereas the emission is a mirror image.[21,22] The fluorescence spectrum and quantum yield values (**Table 3.1**) show that all three dyes are highly fluorescent, with **3a** having a higher quantum yield than **1a** and **2a**. This results from the presence of methyl groups at the 1,7-positions of **3a** inhibiting rotation of the *meso*-substituent, which leads to nonradiative decay for **1a** and **2a**.

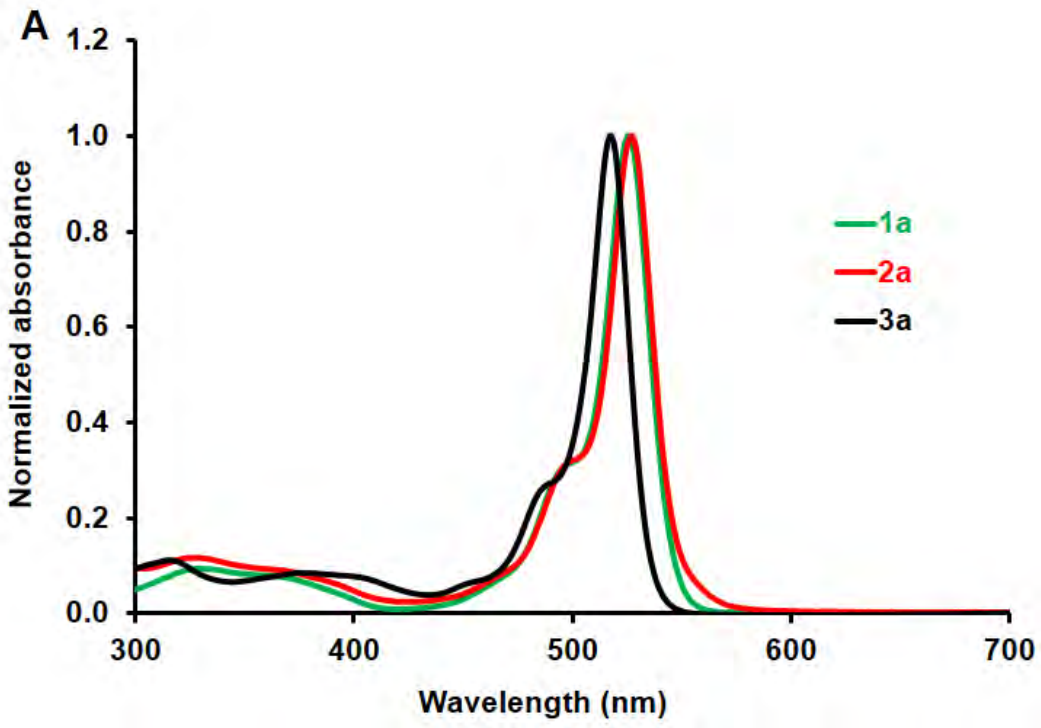

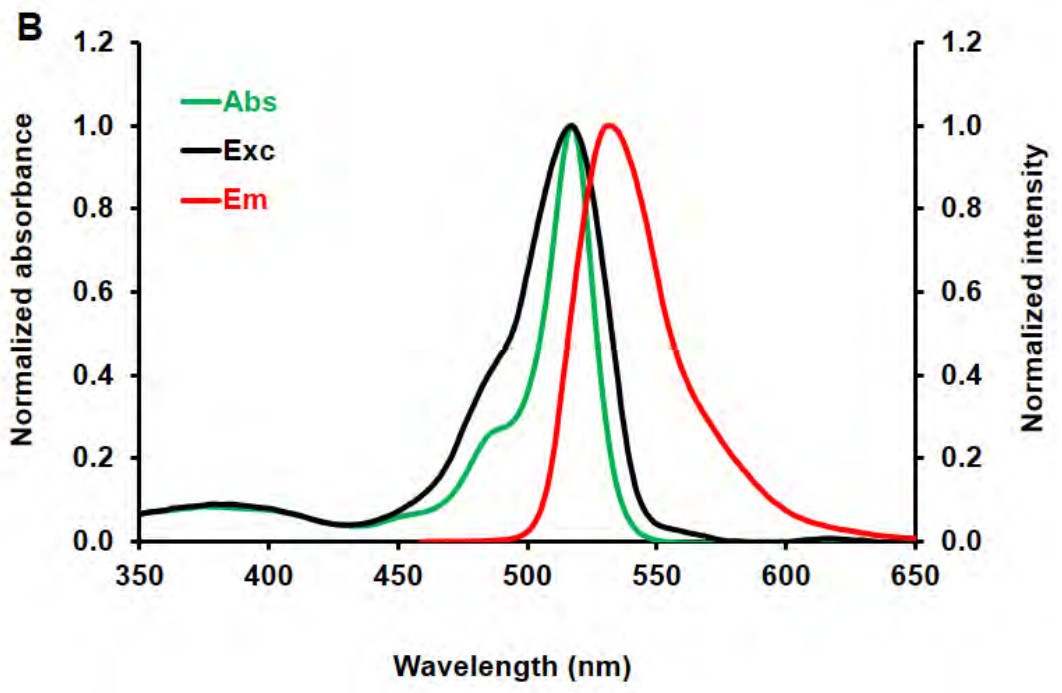

Figure 3.2. Normalized absorption spectra of core dyes **1a**, **2a** and **3a** (A), and excitation (black) and emission (red) spectra of **3a** (B) in DMSO.

Table 3.1. Photophysical data for BODIPYs **1a**, **2a** and **3a** in DMSO.

	λ_{Abs} (nm)	λ_{Ex} (nm)	λ_{Em} (nm)	Stokes shift (cm^{-1})	Φ_F	log ε
1a	525	524	542	597	0.80	4.50
2a	527	529	540	457	0.86	4.40
3a	517	517	531	510	0.94	4.48

3.2. *Meso*-pyridylBODIPY core dye synthesis and characterization (**1b**, **3b** and **4b**)

3.17.1. Synthesis (**Scheme 3.2**)

2-Methylpyrrole, 2,4-dimethylpyrrole and 3-ethyl-2,4-dimethylpyrrole (2.0 mol eq) and 4-pyridinecarboxaldehyde (1.0 mol eq) were reacted in dry CH_2Cl_2 following the typical one-pot trifluoroacetic acid-catalyzed reaction.

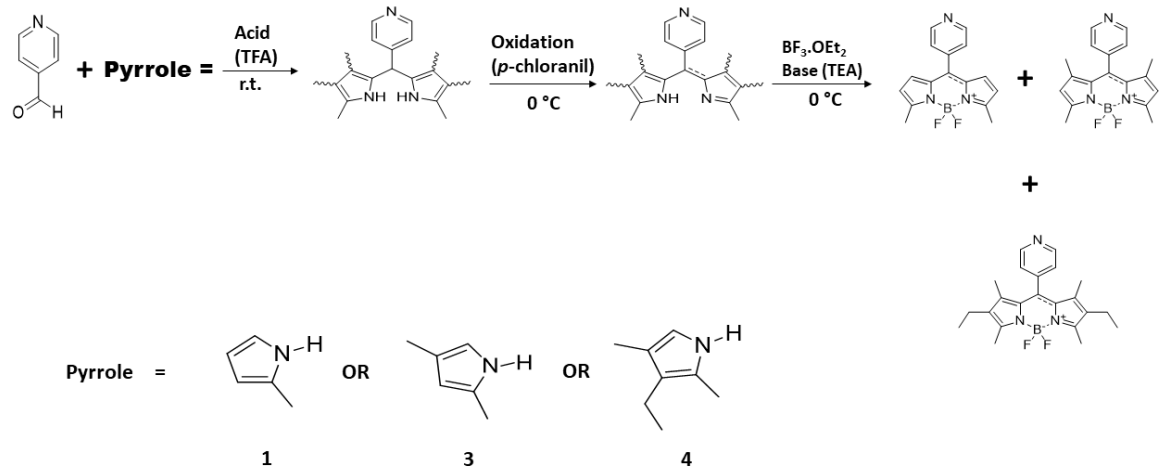

Scheme 3.2. Synthesis of core dyes **1b**, **3b** and **4b** using a typical one-pot acid-catalyzed reaction.

3.17.2. Structural characterization of **1b**, **3b** and **4b**

BODIPY **1b** has fourteen protons, and signals for these can be readily assigned in the ^{1}H NMR spectrum. Surprisingly, the four phenyl protons appear as singlet signals at 8.78 and 7.43 ppm, each integrating as two protons. Similarly, the four protons at the 1-, 2-, 6- and 7-positions of the BODIPY core appear as singlet signals at 6.66 and 6.32 ppm. The six singlet proton signals at 2.68 ppm belong to the six methyl protons attached to the BODIPY core. In the spectrum of **3b**, the four phenyl protons appear as doublets at 8.79–8.78 and 7.32–7.30 ppm, each integrating to two protons. The two protons at the 2,6-positions give rise to a singlet at 6.03

ppm. This is followed by the singlet signals for the twelve methyl protons found at the 1-, 3-, 5- and 7-positions, at 2.59 and 1.43 ppm. Similarly, in the ^{1}H NMR spectrum of **4b**, the four phenyl protons appear as doublets at 8.82–8.79 and 7.39–7.36 ppm. The twelve methyl protons at the 1-, 3-, 5- and 7-positions appear at 2.56 and 1.32 ppm. The signals for the protons associated with the ethyl groups at the 2,6-positions of **4b** appear as multiplet signals at 2.35–2.30, integrating to four protons and 1.02–0.98 ppm integrating to six protons. The FT-IR spectra of all three core dyes contained the peaks anticipated for the BODIPY core.

3.17.3. Spectroscopic and physicochemical properties of **1b**, **3b** and **4b**

The UV-visible absorption spectra of **1b**, **3b** and **4b** in DMSO are shown below (**Figure 3.3**). No signs of aggregation are observed. The absorption maxima lie at 518, 505 and 528 nm, respectively. The absorption maximum of **3b** lies close to 500 nm, as expected for a *meso*-aryl substituted 1,3,5,7-tetramethyl BODIPY dye. The maximum for **1b** is red-shifted by *ca.* 13 nm relative to that of **3b** due to the absence of methyl groups at the 1,7-positions enabling greater rotation of the *meso*-aryl substituent. A further red-shift of *ca.* 23 nm is observed in the UV-visible absorption spectrum of **4b**, and this is due to the presence of the ethyl groups at the 2,6-positions relative to **3b**, which contains protons in these positions. The fluorescence quantum yield values (**Table 3.2**) show that **3b** and **4b** are moderately fluorescent, whereas **1b** is more weakly fluorescent. This is due to the absence of methyl groups at the 1,7-positions of **1b**, which allows rotation of the *meso*-substituent, leading to nonradiative decay.

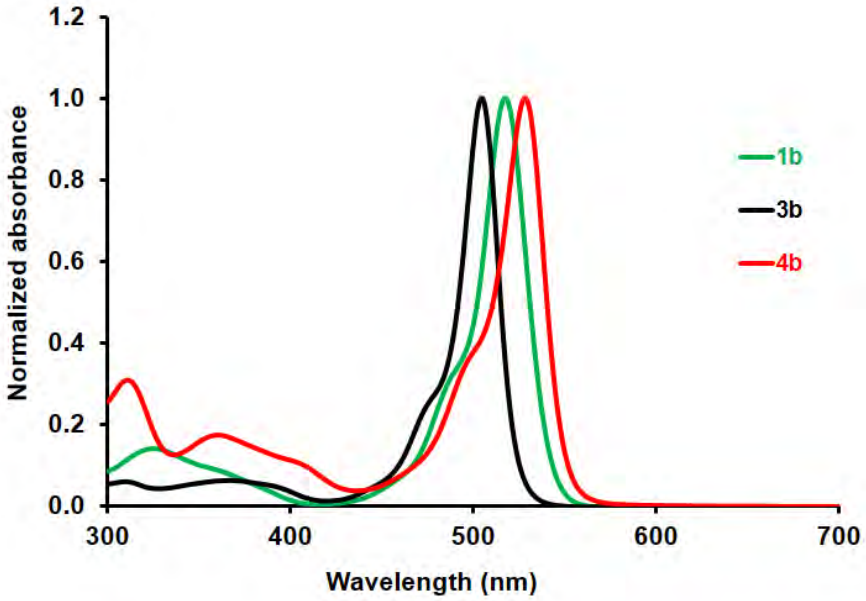

Figure 3.3. Normalized absorption spectra of core dyes **1b**, **3b** and **4b** in DMSO.

Table 3.2. Photophysical data for BODIPYs **1b**, **3b** and **4b** in DMSO.

	λ_{Abs} (nm)	λ_{Ex} (nm)	λ_{Em} (nm)	Stokes shift (cm^{-1})	Φ_F	log ε
1b	518	519	542	855	0.19	4.50
3b	505	504	519	534	0.60	4.37
4b	528	527	545	591	0.66	4.40

3.3. *Meso*-acetamidophenylBODIPY core dye synthesis and characterization (**1c** and **3c**)

3.17.1. Synthesis (**Scheme 3.3**)

2-Methylpyrrole and 2,4-dimethylpyrrole (2.0 mol eq) and 4-pyridinecarboxaldehyde (1.0 mol eq) were reacted in dry CH_2Cl_2 following the typical one-pot trifluoroacetic acid-catalyzed reaction.[37]

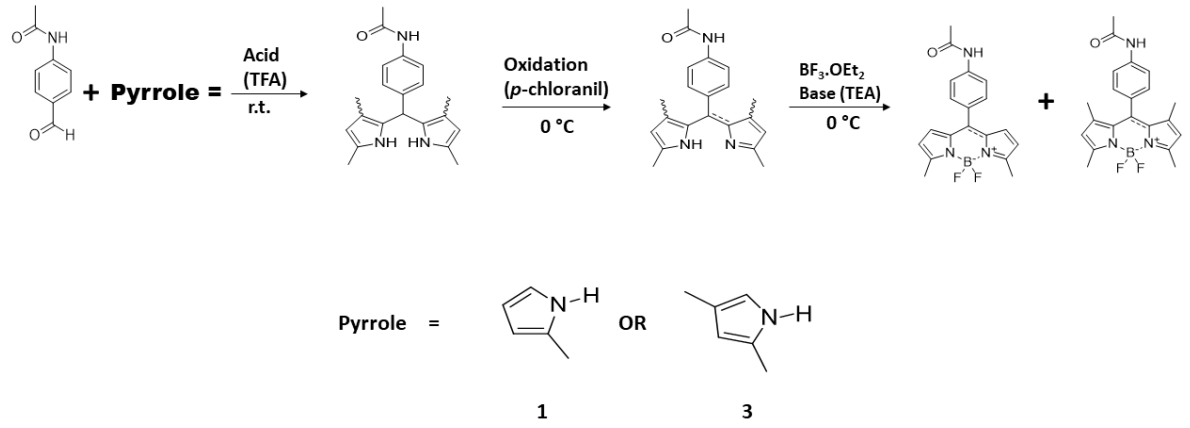

Scheme 3.3. Synthesis of core dyes **1c** and **3c** using a typical one-pot acid-catalyzed reaction.

3.17.2. Structural characterization of **1c** and **3c**

BODIPY **1c** contains a total of eighteen protons, and the combined signals from the ^{1}H NMR spectrum integrate to a total of eighteen protons. Four phenyl protons appear as doublets at 7.66–7.62 and 7.49–7.46 ppm, followed by a singlet integrating to one proton, for the amide proton, at 7.43 ppm. The four protons at the 1-, 2-, 6- and 7-positions of the BODIPY core appear as doublets at 6.75–6.72 and 6.30–6.28 ppm, each integrating to two protons. These are followed by the singlet signal at 2.67 ppm, which is attributed to the six methyl protons attached to the BODIPY core, and finally, the singlet signal for the three methyl protons of the *meso*-acetamido group appear at 2.25 ppm. Differences attributed to the presence of methyl groups at the 1,7-positions are observed in the ^{1}H NMR spectrum of **3c**. Four phenyl protons still appear as doublets at 7.75–7.65 and 7.27–7.19 ppm and the amide proton also still appears as a singlet at 7.47 ppm. The two protons at the 2,6-positions give rise to a singlet at 6.00 ppm. Due to the additional two methyl groups, twelve methyl proton signals appear at 2.57 and 1.44 ppm. The singlet signal for the three methyl protons of the *meso*-acetamido group still appears at 2.25 ppm. The FT-IR spectra of both dyes contained the peaks

anticipated for the BODIPY core. Of interest is the C-H stretch observed at 470 cm^{-1} for the bonds at the 2,6-positions of **3c**.

3.17.3. Spectroscopic and physicochemical properties of **3c**

The UV-visible absorption spectrum of **3c** in DMSO is typical of a *meso*-substituted BODIPY core dye with no aggregation observed (**Figure 3.4**). The absorption maximum lies at 501 nm, close to the 500 nm maximum typical of 1,3,5,7-tetramethyl BODIPY dyes.[3,13] The fluorescence quantum yield value shows that the dye is highly fluorescent (**Table 3.3**).

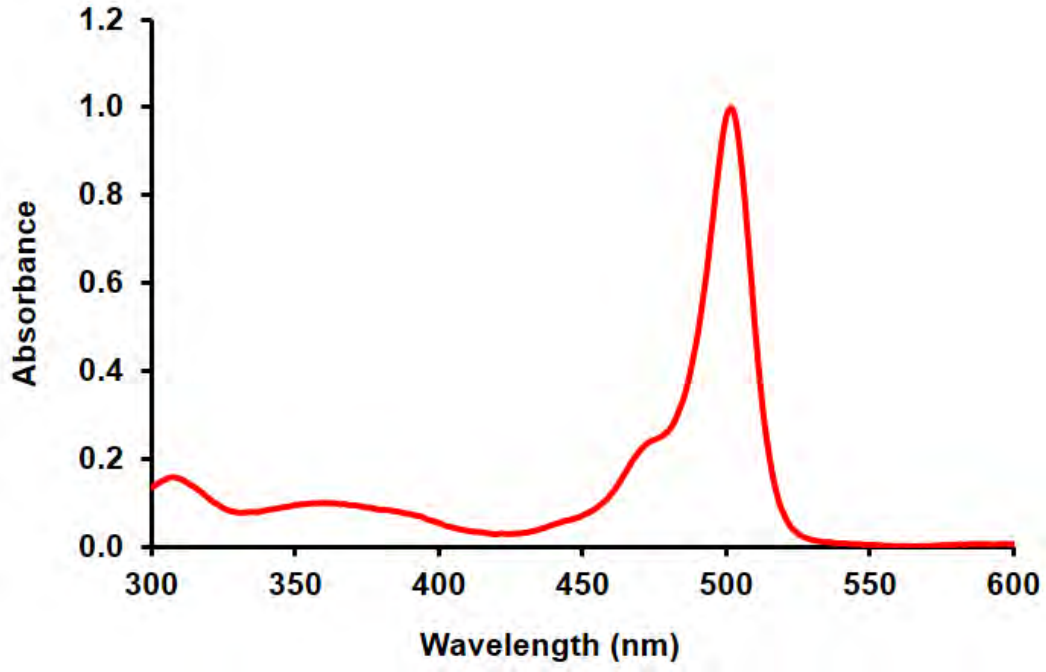

Figure 3.4. The UV-visible absorption spectrum of **3c** in DMSO.

Table 3.3. Photophysical data for BODIPY **3c** in DMSO.

λ_{Abs} (nm)	λ_{Ex} (nm)	λ_{Em} (nm)	Stokes shift (cm^{-1})	Φ_F	log ε
501	501	514	505	0.85	5.58

3.4. *Meso*-iodophenylBODIPY core dye synthesis and characterization (**3d**, **3e** and **3f**)

3.17.1. Synthesis (**Scheme 3.4**)

2,4-Dimethylpyrrole (2.0 mol eq) and 2-iodobenzaldehyde, 3-iodobenzaldehyde or 4-iodobenzaldehyde (1.0 mol eq) were reacted in dry CH_2Cl_2 following the typical one-pot trifluoroacetic acid-catalyzed reaction.

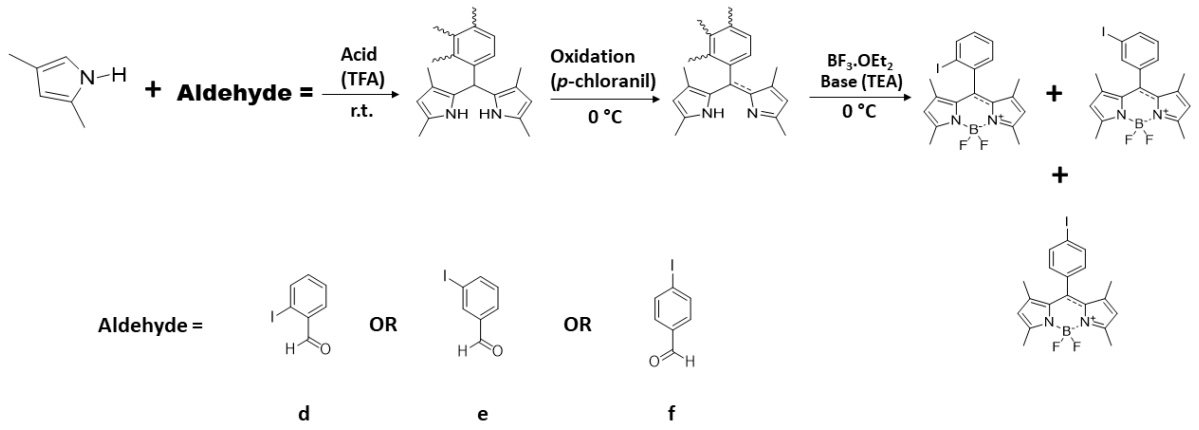

Scheme 3.4. Synthesis of core dyes **3d**, **3e** and **3f** using a typical one-pot acid-catalyzed reaction.

3.17.2. Structural characterization of **3d**, **3e** and **3f**

Because **3d**, **3e** and **3f** are analogous and only differ by the position of the iodine atom on the *meso*-ring, they all contain a total of eighteen protons. The four phenyl protons in the ^{1}H NMR spectrum of **3d** appear as one doublet signal at 7.98–7.94 ppm and three multiplet signals at 7.52–7.47, 7.32–7.29 and 7.19–7.14 ppm, each integrating to one proton. The signal for the two protons at the 2,6-positions appears as a singlet at 5.99 ppm, followed by the twelve methyl protons on the BODIPY core at 2.57 and 1.40 ppm. The spectrum of **3e** is slightly different in the aromatic region, with the four phenyl protons appearing as one doublet which integrates to one proton at 7.85–7.80 ppm, a singlet signal integrating to one proton at 7.68

ppm and a multiplet signal at 7.30–7.21 ppm, integrating to two protons. The rest of the ^{1}H NMR spectrum of **3e** is similar to that of **3d**. The two protons at the 2,6-positions appear as a singlet at 5.99 ppm, and the twelve methyl protons on the BODIPY core are at 2.55 and 1.43 ppm.

The aromatic region of the ^{1}H NMR spectrum of **3f** is also different to the previous two dyes. The signals for the four phenyl protons appear as two doublets at 7.79–7.75 and 6.99–6.95 ppm, each integrating to two protons. The rest of the ^{1}H NMR spectrum is, however, similar. The two protons at the 2,6-positions appear as a singlet at 5.92 ppm, and the twelve methyl protons on the BODIPY core also appear as singlet signals, with each integrating to six protons as previously observed, at 2.48 and 1.34 ppm. The FT-IR spectra of all three dyes contained the peaks anticipated for the BODIPY core. Of interest are the C-H stretches observed at 470, 471 and 469 cm^{-1} for the bonds at the 2,6-positions of **3d**, **3e** and **3f**, respectively.

3.17.3. Spectroscopic and physicochemical properties of **3d**, **3e** and **3f**

The UV-visible absorption spectra of **3d**, **3e** and **3f** in DMSO are typical spectra observed for *meso*-substituted BODIPY core dyes with no aggregation observed (**Figure 3.5**). The absorption maxima lie close to the 500 nm maximum typical of 1,3,5,7-tetramethyl BODIPY dyes.[3,13] The main spectral band of **3d** is slightly red-shifted by *ca.* 5 nm relative to those of the other two dyes, and this may be due to the iodine atom being close to the π-system of the BODIPY core as it is on the 2-position of the *meso* phenyl ring. The fluorescence quantum yield value shows that the dyes are highly fluorescent (**Table 3.4**).

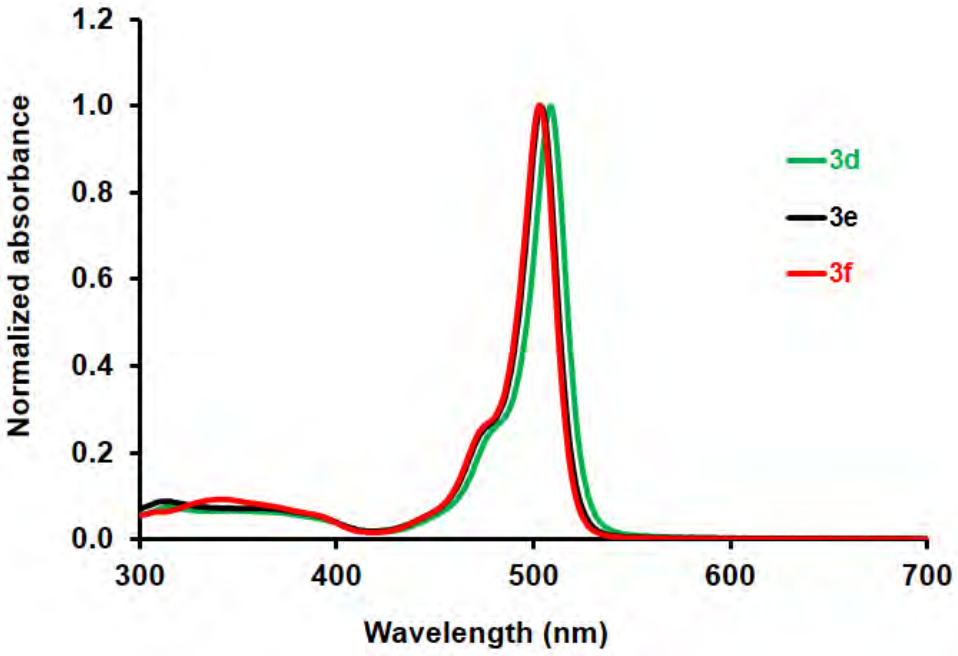

Figure 3.5. Normalized absorption spectra of core dyes **3d**, **3e** and **3f** in DMSO.

Table 3.4. Photophysical data for BODIPYs **3d**, **3e** and **3f** in DMSO.

	λ_{Abs} (nm)	λ_{Ex} (nm)	λ_{Em} (nm)	Stokes shift (cm^{-1})	Φ_F	log ε
3d	509	508	521	453	0.75	4.49
3e	504	503	517	499	0.81	4.49
3f	503	503	516	501	0.71	4.47

3.5. *Meso*-bromophenylBODIPY core dye synthesis and characterization (3g)

3.17.1. Synthesis (**Scheme 3.5**)

2,4-Dimethylpyrrole (2.0 mol eq) and 2-bromobenzaldehyde (1.0 mol eq) were reacted in dry CH_2Cl_2 following the typical one-pot trifluoroacetic acid-catalyzed reaction.

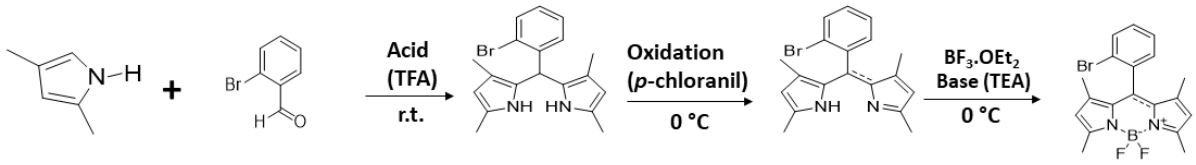

Scheme 3.5. Synthesis of core dye **3g** using a typical one-pot acid-catalyzed reaction.

3.17.2. Structural characterization of **3g**

In the ^{1}H NMR spectrum of **3g**, the four phenyl protons each appear as singlets integrating to one proton. These are two doublets at 7.71–7.68 and 7.31–7.28 ppm, a triplet at 7.48–7.44 and a multiplet at 7.37–7.32 ppm. A signal at 5.99 ppm is assigned to the two protons at the 2,6-positions, and this is followed by the twelve methyl protons on the BODIPY core at 2.56 and 1.42 ppm.

3.17.3. Spectroscopic and physicochemical properties of **3g**

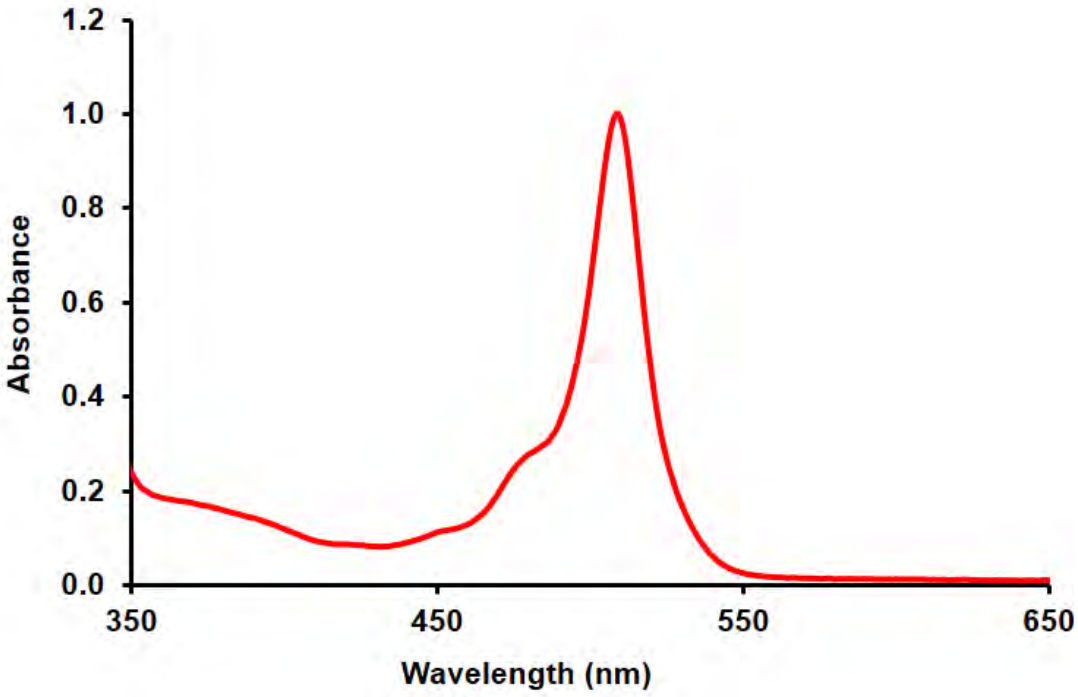

Figure 3.6. The UV-visible absorption spectrum of core dye **3g** in DMSO.

The UV-visible absorption spectrum of **3g** in DMSO is typical of a *meso*-substituted BODIPY core dye, with the absorption maximum at 508 nm, close to the 500 nm maximum typical of 1,3,5,7-tetramethyl BODIPY dyes (**Figure 3.6**).[3,13] The fluorescence quantum yield value shows that the dye is fairly fluorescent (**Table 3.5**).

Table 3.5. Photophysical data for BODIPY **3g** in DMSO.

λ_{Abs} (nm)	λ_{Ex} (nm)	λ_{Em} (nm)	Stokes shift (cm^{-1})	Φ_F	log ε
509	508	522	489	0.70	4.45

3.6. *Meso*-bromothienylBODIPY core dye synthesis and characterization (**3h**)

3.17.1. Synthesis (**Scheme 3.6**)

2,4-Dimethylpyrrole (2.0 mol eq) and 5-bromo-2-thiophenecarboxaldehyde (1.0 mol eq) were reacted in dry CH_2Cl_2 following the typical one-pot trifluoroacetic acid-catalyzed reaction.

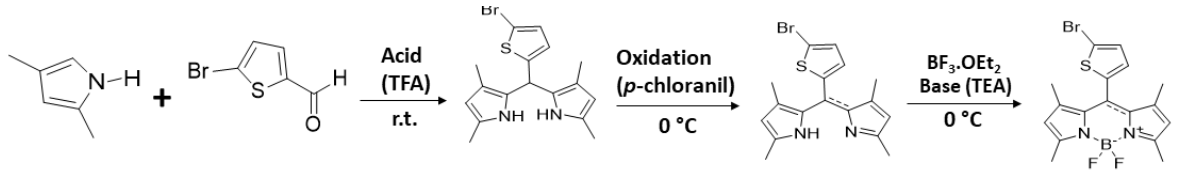

Scheme 3.6. Synthesis of core dye **3h** using a typical one-pot acid-catalyzed reaction.

3.17.2. Structural characterization of **3h**

The ^{1}H NMR spectrum of **3h** shows a total of sixteen protons, as expected. The two protons in the aromatic region appear as doublets at 7.35–7.33 and 7.08–7.06 ppm. The two protons at the 2,6-positions appear as a singlet at 6.19 ppm, and the twelve methyl protons on the BODIPY core appear as singlet signals at 2.51 and 1.74 ppm. The FT-IR spectrum contains the

peaks anticipated for the BODIPY core, and of interest is the C-H stretch at 469 cm^{-1} for the bonds at the 2,6-positions.

3.17.3. Spectroscopic and physicochemical properties of **3h**

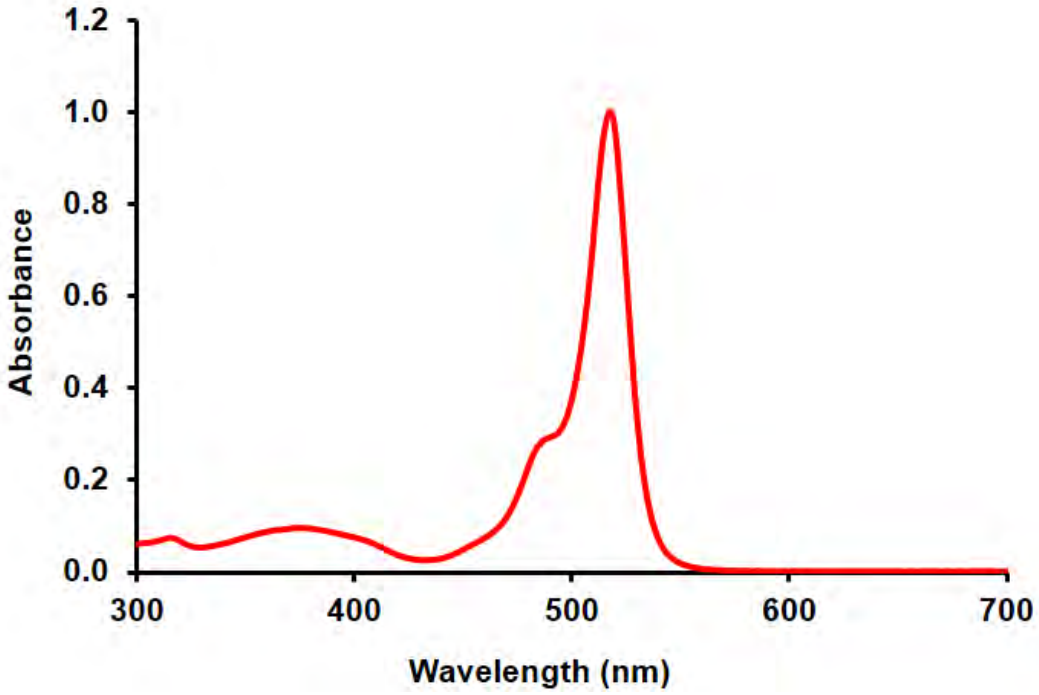

Figure 3.7. The UV-visible absorption spectrum of core dye **3h** in DMSO.

The UV-visible absorption spectrum of **3h** in DMSO is typical of a *meso*-substituted BODIPY core dye with no aggregation observed; the absorption maximum lies at 517 nm (**Figure 3.7**). The low fluorescence quantum yield value shows that the dye is less fluorescent than the other 1,3,5,7-tetramethyl BODIPY dyes (**Table 3.6**). The low fluorescence and relative red-shift from the typical absorption maximum of *ca.* 500 nm for 1,3,5,7-tetramethyl BODIPY dyes are due to the presence of the thiophene group.[134]

Table 3.6. Photophysical data for BODIPY **3h** in DMSO.

λ_{Abs} (nm)	λ_{Ex} (nm)	λ_{Em} (nm)	Stokes shift (cm^{-1})	Φ_F	log ε
517	519	528	403	0.16	4.48

3.7. *Meso*-methyl 4-formylphenylBODIPY core dye synthesis and characterization (**3i**)

3.17.1. Synthesis (**Scheme 3.7**)

2,4-Dimethylpyrrole (2.0 mol eq) and methyl 4-formylbenzoate (1.0 mol eq) were reacted in dry CH_2Cl_2 following the typical one-pot trifluoroacetic acid-catalyzed reaction.

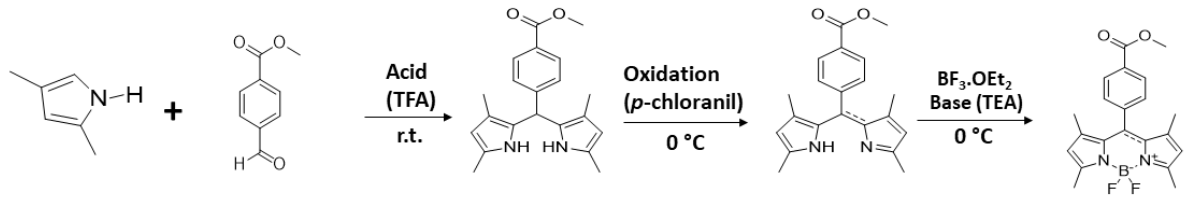

Scheme 3.7 Synthesis of core dye **3i** using a typical one-pot acid-catalyzed reaction.

3.17.2. Structural characterization of **3i**

The ^{1}H NMR spectrum shows all twenty-one protons expected from the structure of **3i**. Two doublets at 8.25–8.22 and 7.62–7.59 ppm can be assigned to the four phenyl protons, and they each integrate to two protons. At 6.15 ppm, a singlet signal that integrates to two protons can be assigned to the protons at the 2,6-positions. At 3.97 ppm, a singlet signal for the methyl protons of the ester group can be found, followed by the twelve methyl protons on the BODIPY core, which appear as singlet signals at 2.53 and 1.40 ppm. The FT-IR spectrum

contains the peaks anticipated for the BODIPY core, and of interest is the C-H stretch for the bonds at the 2,6-positions observed at 465 cm^{-1}.

3.17.3. Spectroscopic and physicochemical properties of **3i**

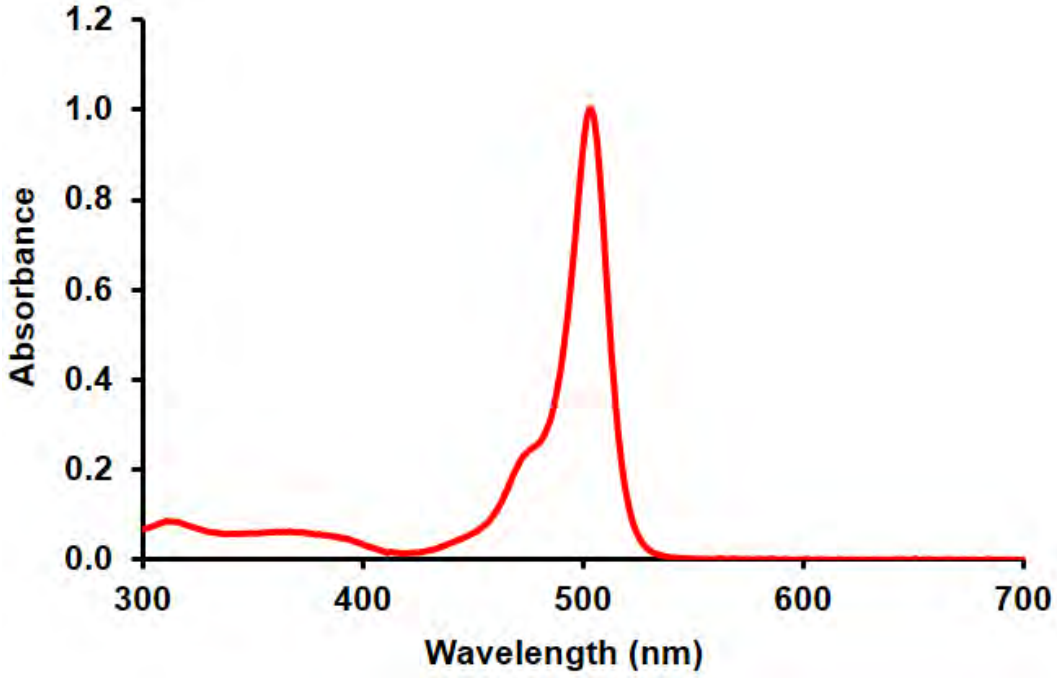

Figure 3.8. The UV-visible absorption spectrum of core dye **3i** in DMSO.

The UV-visible absorption spectrum of **3i** in DMSO is typical of a *meso*-substituted BODIPY core dye, and the absorption maximum lies at 503 nm, close to the 500 nm maximum typical of 1,3,5,7-tetramethyl BODIPY dyes (**Figure 3.8**).[3,13] The fluorescence quantum yield value shows that the dye is fairly fluorescent (**Table 3.7**).

Table 3.7. Photophysical data for BODIPY **3i** in DMSO.

λ_{Abs} (nm)	λ_{Ex} (nm)	λ_{Em} (nm)	Stokes shift (cm^{-1})	Φ_F	log ε
503	503	518	576	0.59	4.42

3B – Synthesis and characterization of halogenated BODIPY core dyes

This section details the synthesis and characterization of heavy atom-containing BODIPYs from some of the core dyes detailed above. The reactions were carried out using established literature methods.[11–13]

3.8. Halogenated *meso*-pentafluorophenylBODIPY core dyes (**5a**, **6a**, **7a**, **8a** and **9a**)

3.17.1. Synthesis (**Scheme 3.8**)

BODIPY core dyes **1a**, **2a** and **3a** (1 mol eq) and NBS or NIS (3 mol eq) were dissolved in CH_2Cl_2 (20 mL). NBS and NIS were added in excess to the reaction vessels containing **1a** and **2a** to exploit the absence of methyl groups at the 1,7-positions. These positions were expected to be able to accommodate bromine and iodine heavy atoms. The reaction was carried out in an inert atmosphere, and the flask was left to stir at room temperature while the reaction was followed by thin-layer chromatography to completion.[100]

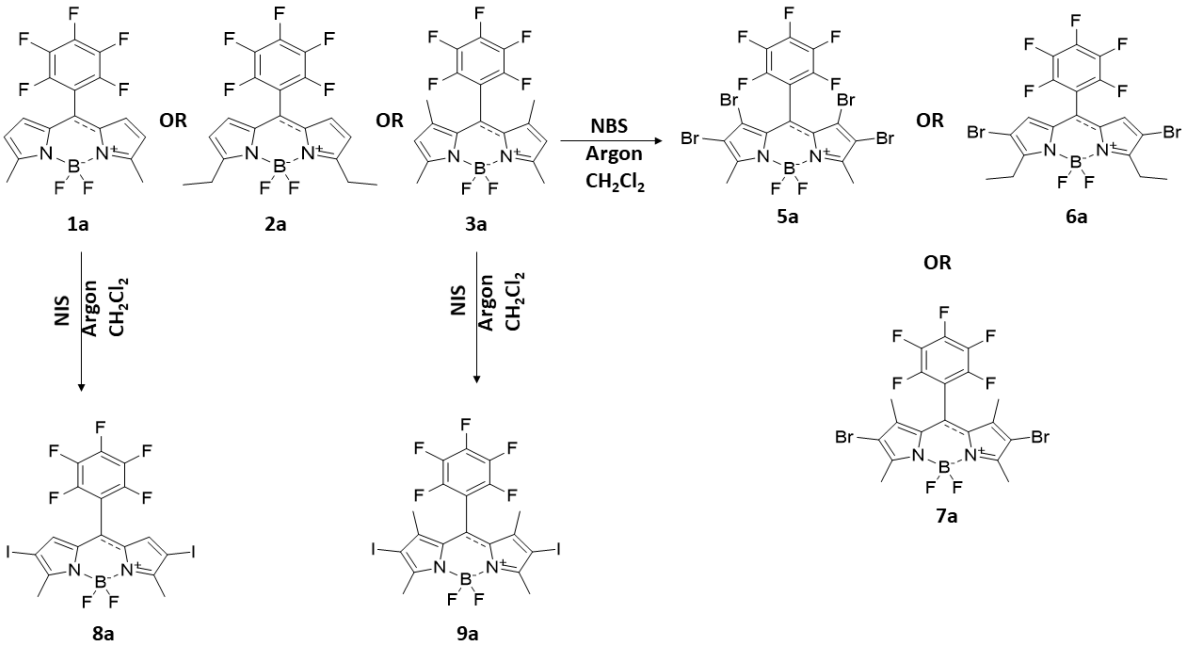

Scheme 3.8. Synthesis of halogenated core dyes **5a**, **6a 7a**, **8a** and **9a**.

3.17.2. Structural characterization of **5a**, **6a**, **7a**, **8a** and **9a**

BODIPY **1a** was used to synthesize **5a** and **8a**, and there are noticeable changes in the ^{1}H NMR spectrum obtained for the halogenated **5a** and **8a** (**Figure 3.9**). For **5a**, the four protons at the 1-, 2-, 6- and 7-positions of the BODIPY core are no longer present as the positions are now occupied by bromine atoms. Only the singlet proton signal at 2.63 ppm attributed to the six methyl protons attached to the 3- and 5-positions is maintained. On the other hand, in the ^{1}H NMR spectrum **8a**, the two protons at the 1,7-positions appear as a singlet at 6.84 ppm while those at 2,6-positions disappear due to the presence of iodine atoms at these positions. The signal for the six protons at the 3,5-positions appears as a singlet at 2.67 ppm.

BODIPY **6a** was synthesized from **2a**. In the ^{1}H NMR spectrum, the signal for the protons at the 2,6-positions disappears due to the presence of bromine atoms at these positions. The two protons at the 1,7-positions appear as a singlet at 6.69 ppm, whereas the protons assigned to the ethyl groups at the 3- and 5-positions appear as a multiplet integrating to four protons at 3.08–2.98 and as a triplet which integrates to six protons at 1.38–1.33 ppm.

BODIPY **3a** was used to synthesize **7a** and **9a**. In the ^{1}H NMR spectra of **7a** and **9a**, the signals for the protons at the 2,6-positions disappear due to the presence of bromine and iodine atoms at these positions. The twelve protons assigned to the 1-, 3-, 5- and 7-positions of **7a** and **9a** appear as singlet signals, each integrating to six protons, at 2.58 and 1.58 ppm, and 2.67 and 1.64 ppm, respectively.

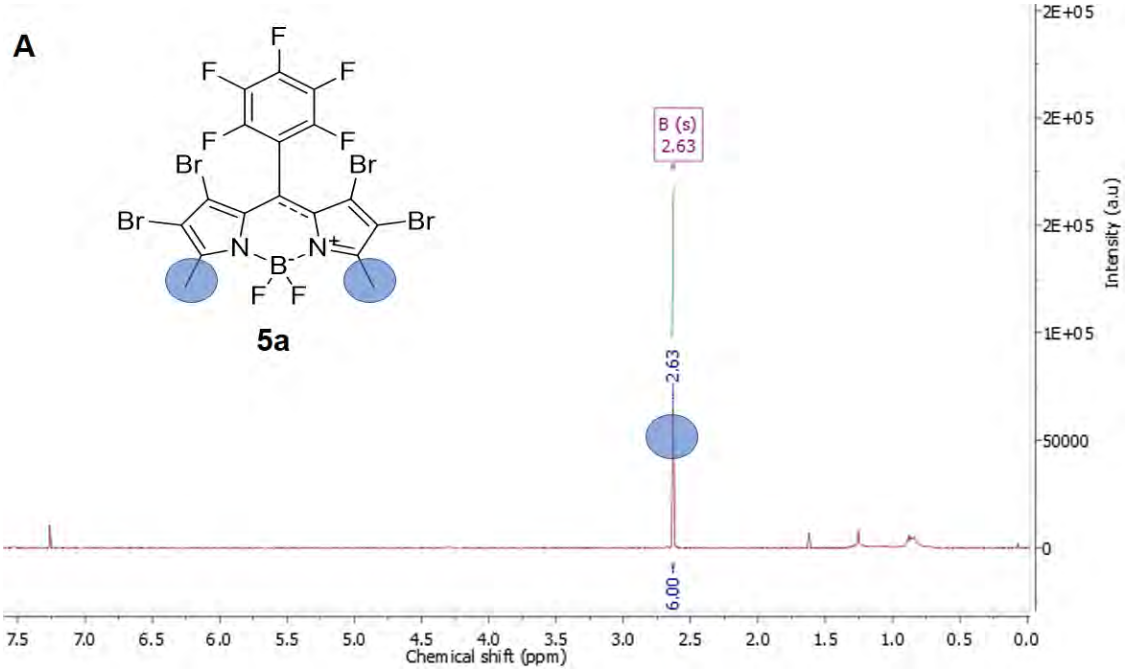
A
F
F
F
F
F
Br
Br
Br
N
B
N+
F
F
5a
B (s)
2.63
2.63
6.00
2E+05
2E+05
2E+05
1E+05
50000
0
Intensity (a.u)
7.5
7.0
6.5
6.0
5.5
5.0
4.5
4.0
3.5
3.0
2.5
2.0
1.5
1.0
0.5
0.0
Chemical shift (ppm)

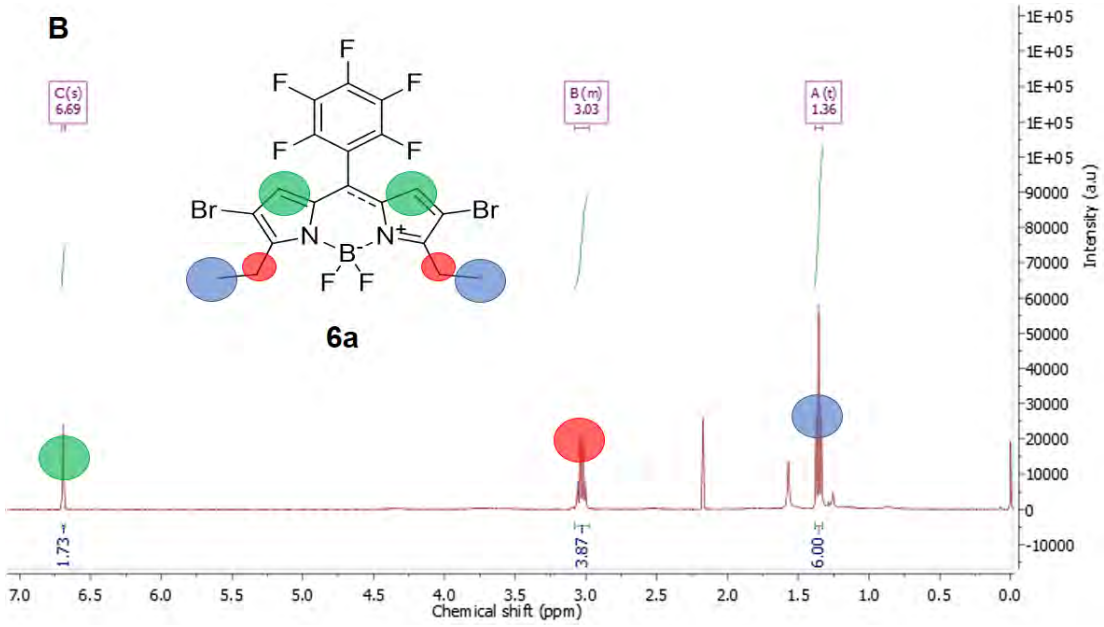
B
C(s)
6.69
B(m)
3.03
A(t)
1.36
F
F
F
F
F
Br
Br
N
B
N+
F
F
6a
1.73
3.87
6.00
1E+05
1E+05
1E+05
1E+05
1E+05
90000
80000
70000
60000
50000
40000
30000
20000
10000
0
-10000
Intensity (a.u)
7.0
6.5
6.0
5.5
5.0
4.5
4.0
3.5
3.0
2.5
2.0
1.5
1.0
0.5
0.0
Chemical shift (ppm)

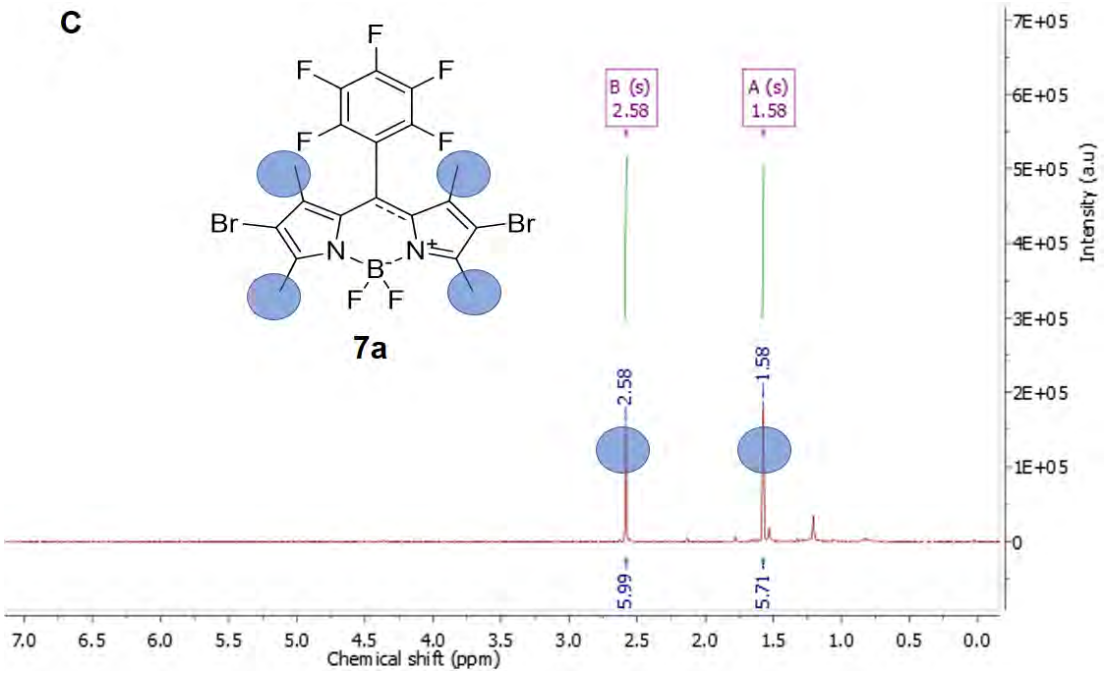
C
F
F
F
F
F
Br
Br
N
B
N+
F
F
7a
B (s)
2.58
A (s)
1.58
2.58
1.58
5.99
5.71
7E+05
6E+05
5E+05
4E+05
3E+05
2E+05
1E+05
0
Intensity (a.u)
7.0
6.5
6.0
5.5
5.0
4.5
4.0
3.5
3.0
2.5
2.0
1.5
1.0
0.5
0.0
Chemical shift (ppm)

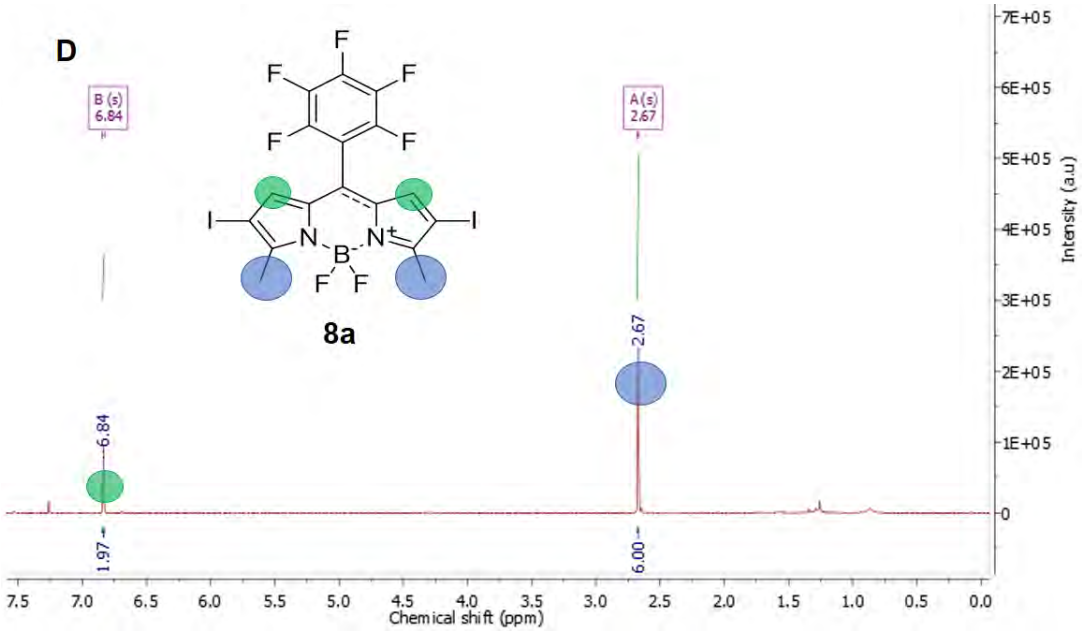
D
F
F
F
F
F
I
I
N
B
N+
F
F
8a
B (s)
6.84
A(s)
2.67
6.84
2.67
1.97
6.00
7E+05
6E+05
5E+05
4E+05
3E+05
2E+05
1E+05
0
Intensity (a.u)
7.5
7.0
6.5
6.0
5.5
5.0
4.5
4.0
3.5
3.0
2.5
2.0
1.5
1.0
0.5
0.0
Chemical shift (ppm)

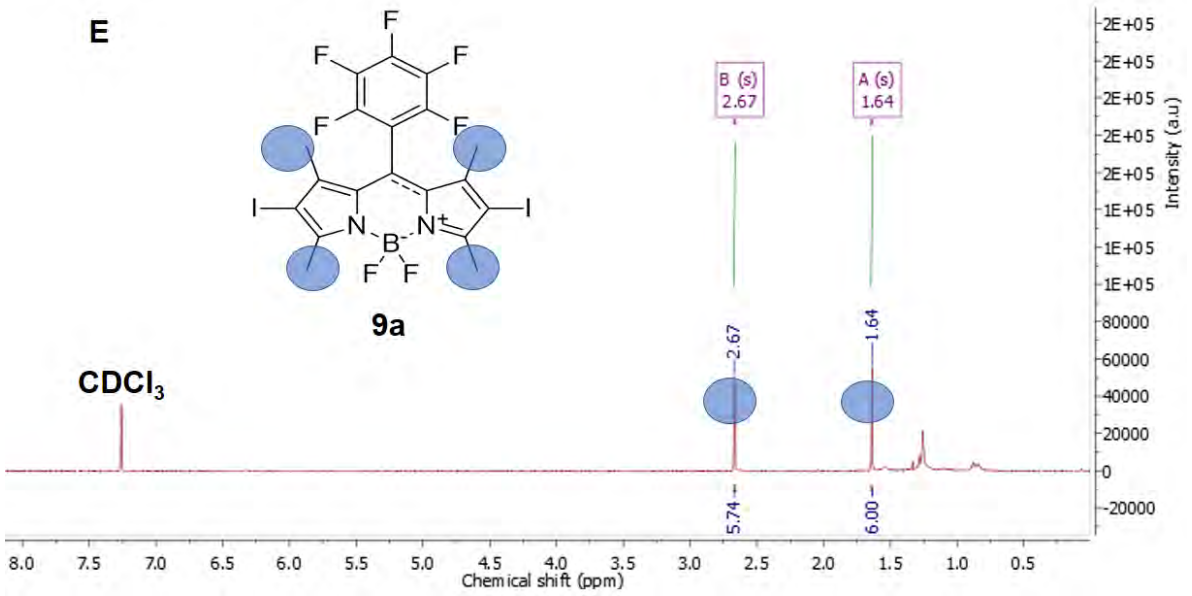

Figure 3.9. ^{1}H NMR spectra of halogenated BODIPY core dyes.

In the FT-IR spectra of all the halogenated core dyes **5a**, **6a 7a**, **8a** and **9a**, the C-H stretches of the bonds at the 2,6-positions of the cores disappear, and C-Br and C-I stretches are observed instead. These appear at 619, 613, 525, 616 and 522 cm^{-1}, respectively. The halogenated core dyes **5a**, **6a 7a**, **8a** and **9a**, were confirmed by MALDI-TOF mass spectrometry as the parent peaks respectively were observed at 703.11 amu (calc: 701.72; M + H^+), 571.68 amu (calc: 571.93; M^+), 572.40 amu (calc: 571.93; M + H^+), 638.87 amu (calc: 637.88; M + H^+) and 665.95 amu (calc: 665.91; M^+).

3.17.3. Spectroscopic and physicochemical properties of **5a**, **6a 7a**, **8a** and **9a**

The UV-visible absorption spectra of **5a**, **6a 7a**, **8a** and **9a** in DMSO are shown below, with no signs of aggregation (**Figure 3.10**). The spectra are typical of halogenated BODIPY cores, and the maxima lie at 561, 562, 549, 573 and 558 nm, respectively. The red-shift relative to the spectra of the BODIPY core dyes is expected, and this will be explained in detail in Chapter 6. [3,13] There are no significant differences in the spectra of **5a** and **6a**, and they are slightly red-

shifted relative to **7a**. For **5a**, this red-shift is attributed to the presence of additional bromine heavy atoms on the core relative to **7a**, whereas for **6a**, the absence of methyl groups at the 1,7-positions still enables greater rotation of the *meso*-aryl substituent as was the case with the BODIPY core dye.

The fluorescence quantum yield values of the iodinated dyes **8a** and **9a** (**Table 3.8**) are negligible relative to the brominated analogues, and this is expected as iodine quenches fluorescence in BODIPY dyes. BODIPYs **5a**, **6a** and **7a** are fairly fluorescent, but the quantum yields are lower than those obtained for the core dyes **1a** and **2a**. This decrease is also expected because of the presence of bromine heavy atoms on the BODIPY core. The decreases in fluorescence quantum yields obtained for all five dyes are consistent with the results obtained during the singlet oxygen studies (**Table 3.8**). The iodinated dyes have higher singlet oxygen quantum yields than the brominated analogues, and this is because iodine is heavier than bromine. A representative ground state absorption spectrum obtained from the photodegradation of DPBF by **7c** is shown below, and the singlet oxygen quantum yields for the other halogenated dyes were obtained in a similar manner (**Figure 3.11B**).

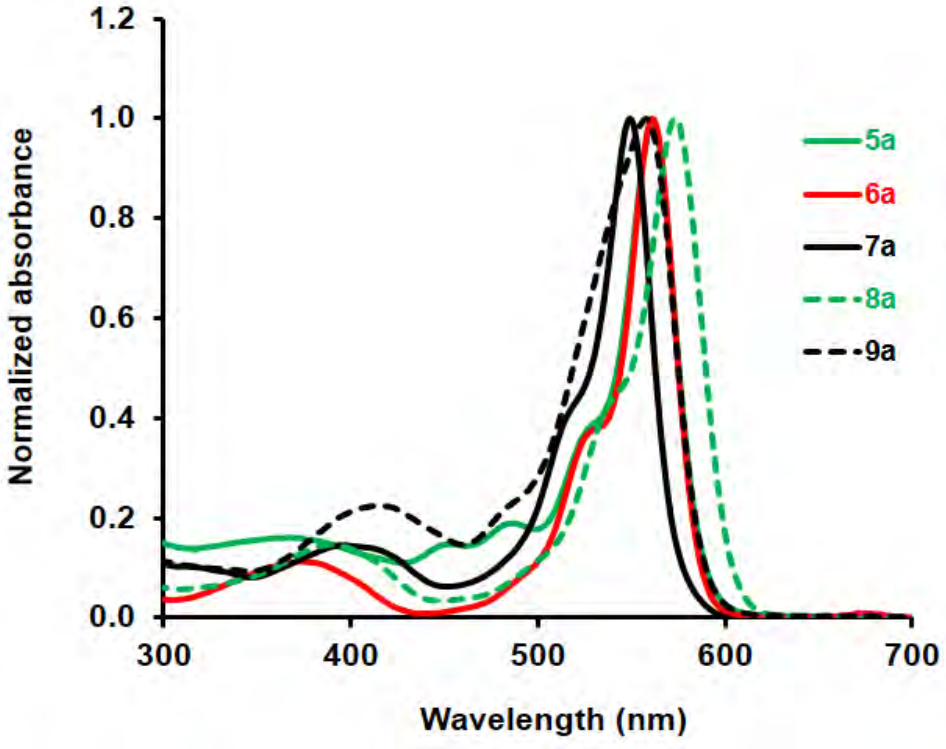

Figure 3.10. Normalized absorption spectra of halogenated core dyes **5a**, **6a 7a**, **8a** and **9a** in DMSO.

Table 3.8. Photophysical data for BODIPYs **5a**, **6a 7a**, **8a** and **9a** in DMSO.

	λ_{Abs} (nm)	λ_{Ex} (nm)	λ_{Em} (nm)	Stokes shift (cm^{-1})	Φ_F	log ε	Φ_Δ
5a	561	561	583	673	0.16	4.47	0.27
6a	562	562	582	612	0.31	4.44	0.57
7a	549	548	570	671	0.12	4.47	0.67
8a	573	-	-	-	0.04	4.44	0.76
9a	558	-	-	-	0.03	4.47	0.95

3.9. Brominated *meso*-acetamidophenylBODIPY core dye (**7c**)

3.17.1. Synthesis (**Scheme 3.9**)

BODIPY **7c** was synthesized following the procedure described above (**Scheme 3.8**).

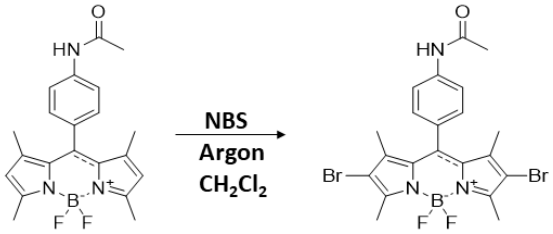

Scheme 3.9. Synthesis of brominated core dye **7c**.

3.17.2. Structural characterization of **7c**

BODIPY **1c** was used to synthesize **7c**. In the ^{1}H NMR spectrum, only the signal for the protons at the 2,6-positions disappears on moving from **1c** to **7c**. The four phenyl protons still appear as doublets at 7.78–7.72 and 7.24–7.19 ppm. The singlet signal integrating to one proton at 7.55 ppm can be assigned to the amide proton. The twelve methyl proton signals for the two methyl groups at the 1,7- and 3,5-positions appear at 2.62 and 1.44 ppm. The singlet signal for the three methyl protons of the *meso*-acetamido group lies at 2.27 ppm. In the FT-IR spectrum, the C-H stretch previously observed at 470 cm^{-1} for the bonds at the 2,6-positions of **3c** disappears, and a C-Br stretch appears 521 cm^{-1}. The structure of BODIPY **7c** was further confirmed by MALDI-TOF mass spectrometry as the parent peak was observed at 539.02 amu (calc: 539.27; $[M]^+$).

3.17.3. Spectroscopic and physicochemical properties of **7c**

The UV-visible absorption spectrum of **7c** in DMSO together with the spectra for the photodegradation of DPBF by **7c** in the presence of laser light is shown below (**Figure 3.11**).

The absorbance maximum lies at 527 nm, and there was no aggregation observed. As expected, a red-shift of *ca.* 26 nm is observed relative to the spectra of the BODIPY core dye **3c** due to the presence of bromine heavy atoms at the 2,6-positions. These heavy atoms also lead to a significantly lower fluorescence quantum yield and a fairly high quantum yield, Φ_Δ (**Table 3.9**). Sample and standard solutions were combined with the singlet oxygen quencher DPBF in DMSO to obtain the Φ_Δ value by comparing the rate of the decrease in the absorbance of DPBF at 416 nm to that of the standard (**Figure 3.11B**). These Φ_Δ values were only determined for the dyes used as photosensitizers in PACT, as discussed in Chapter 5.

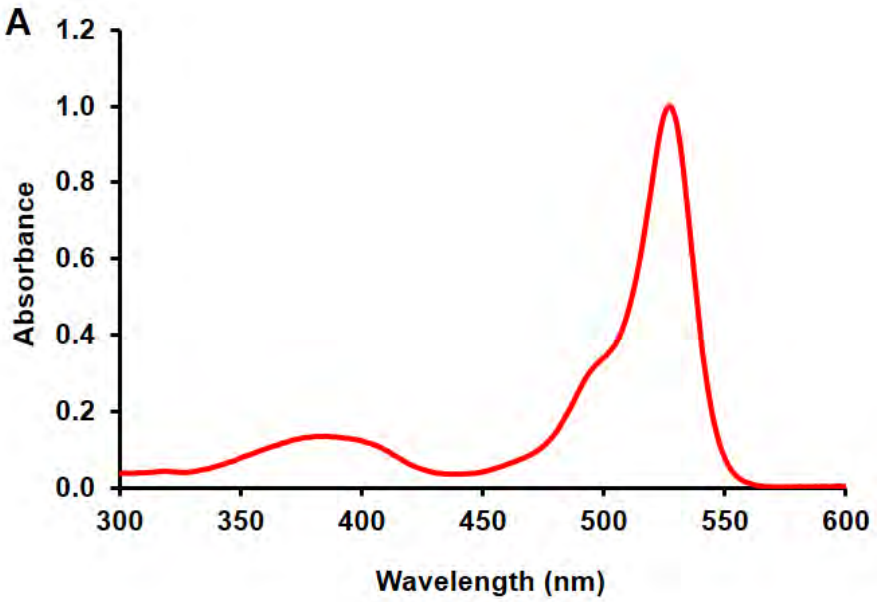

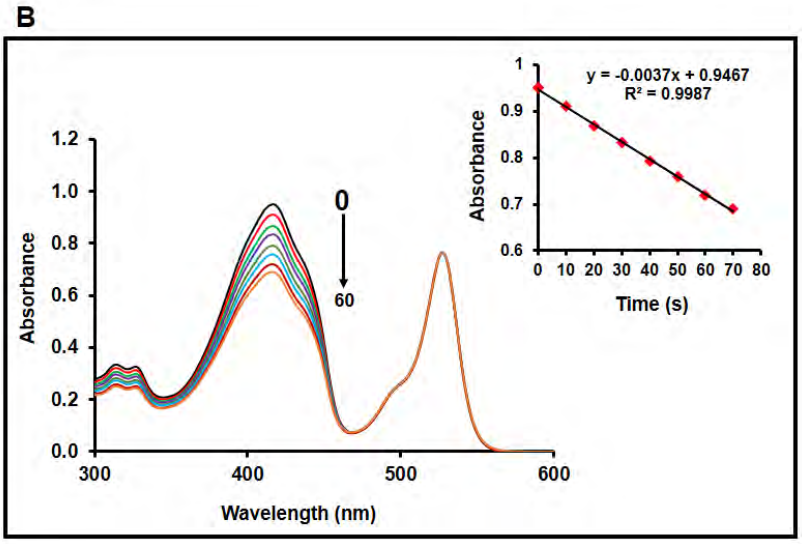

Figure 3.11. The normalized UV-visible absorption spectrum of **7c** in DMSO (A), and absorption spectra showing the photodegradation of DPBF by **7c** at 10 s intervals (B).

Table 3.9. Photophysical data for BODIPY **7c** in DMSO.

λ_{Abs} (nm)	λ_{Ex} (nm)	λ_{Em} (nm)	Stokes shift (cm^{-1})	Φ_F	log ε	Φ_Δ
527	526	544	593	0.16	4.46	0.82

3.10. Halogenated *meso*-iodophenylBODIPY core dyes (**7d**, **7e** and **7f**)

3.17.1. Synthesis (**Scheme 3.10**)

Halogenated BODIPY core dyes **7d**, **7e** and **7f**, were synthesized following the procedure described above (**Scheme 3.8**).

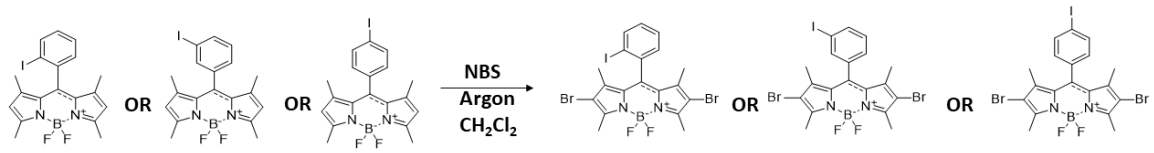

Scheme 3.10. Synthesis of brominated core dyes **7d**, **7e** and **7f**.

3.17.2. Structural characterization of **7d**, **7e** and **7f**

BODIPYs **3d**, **3e** and **3f** were used in the synthesis of **7d**, **7e** and **7f**. A noticeable and noteworthy change in the ^{1}H NMR spectra obtained for the halogenated dyes is the disappearance of the signal for the protons at the 2,6-positions, which was previously observed in the 5.90–6.00 ppm range. The four phenyl protons in the ^{1}H NMR spectrum of **7d** appear as two multiplets that each integrate to one proton at 7.92–7.88 and 7.47–7.40 ppm, and another multiplet which integrates to two protons at 7.20–7.13 ppm. The twelve methyl protons on the BODIPY core appear at 2.55 and 1.32 ppm, with each peak integrating to six protons. In the ^{1}H NMR spectrum of **7e**, the four phenyl protons can be assigned to a multiplet at 7.82–7.78 ppm, a singlet 7.59 ppm and another multiplet at 7.21–7.18 ppm. The first two peaks integrate to one proton each, and the second one integrates to two protons. These are followed by the singlet signals for the twelve methyl protons on the BODIPY core at 2.53 and 1.35 ppm, each integrating to six protons. Finally, in the ^{1}H NMR spectrum of **7f**, the four phenyl protons appear as two doublets integrating to two protons each, at 7.90–7.87 and 7.05–6.99 ppm. The twelve methyl protons on the BODIPY core of **7f** appear as two singlet signals at 2.60 and 1.41 ppm, each integrating to six protons.

The only noteworthy change in the FT-IR spectra is the disappearance of the peaks for the C-H stretches observed around 470 cm^{-1} for the bonds at the 2,6-positions, and the appearance of C-Br stretches for the new bonds at these positions. These appear at 509, 524 and 527 cm^{-1} for **7d**, **7e** and **7f**, respectively. The halogenated core dyes **7d**, **7e** and **7f**, were confirmed by MALDI-TOF mass spectrometry as the parent $[M]^{+}$ peaks respectively were observed at 607.77 amu, 607.79 amu and 607.79 amu, while the predicted m/z value for **7d**, **7e**, and **7f** is 607.88 amu.

3.17.3. Spectroscopic and physicochemical properties of **7d**, **7e** and **7f**

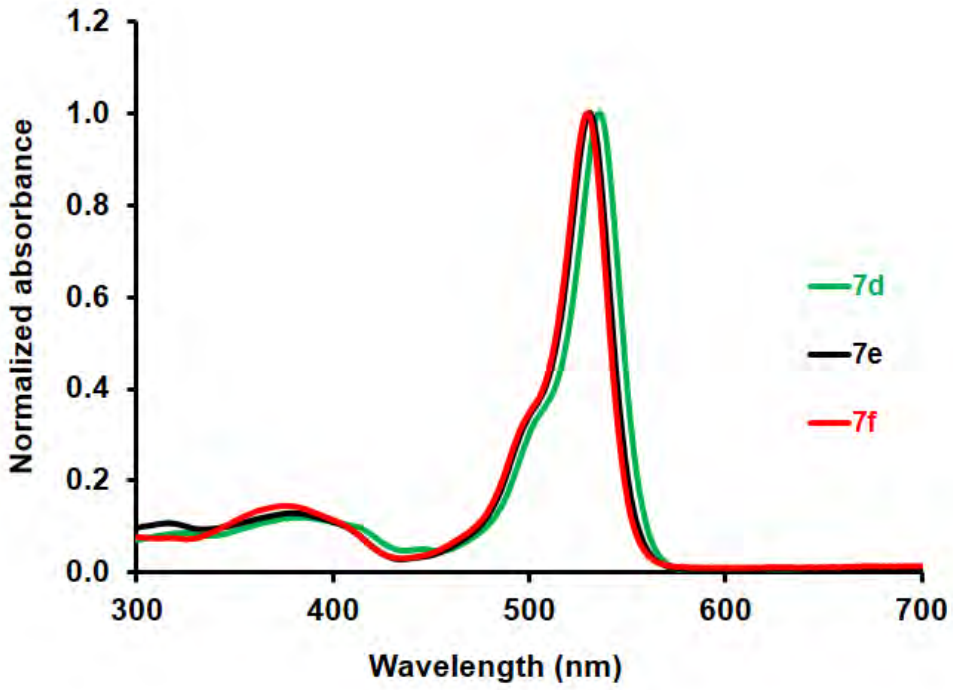

Figure 3.12. Normalized absorption spectra of halogenated core dyes **7d**, **7e** and **7f** in DMSO.

The UV-visible absorption spectra of **7d**, **7e** and **7f** in DMSO are shown below (**Figure 3.12**). The spectra are typical of halogenated BODIPY core dyes, and the maxima lie at 536, 531 and 530 nm, respectively, with no sign of aggregation. This red-shift relative to the spectra of the BODIPY core dyes is expected. [3,13] There are no significant differences in the spectra of **7d**, **7e** and **7f** except the red-shift of *ca.* 5 nm observed for **7d** relative to **7e** and **7f**. This is similar to the observation made above for **3d** relative to **3e** and **3f**. The fluorescence quantum yield values are not significantly different, and they have decreased significantly relative to the values obtained for **3d**, **3e** and **3f**, due to the presence of bromine heavy atoms on the BODIPY core (**Table 3.10**). As expected, the heavy bromine atoms also result in high singlet oxygen quantum yields.

Table 3.10. Photophysical data for BODIPYs **7d**, **7e** and **7f** in DMSO.

	λ_{Abs} (nm)	λ_{Ex} (nm)	λ_{Em} (nm)	Stokes shift (cm^{-1})	Φ_F	log ε	Φ_Δ
7d	536	534	553	574	0.23	4.41	0.75
7e	531	530	550	651	0.28	4.46	0.68
7f	530	530	548	620	0.30	4.47	0.62

3.11. Halogenated *meso*-bromophenylBODIPY core dye (**7g**)

3.17.1. Synthesis (**Scheme 3.11**)

Halogenated BODIPY core dye **7g** was synthesized following the procedure described above (**Scheme 3.8**).

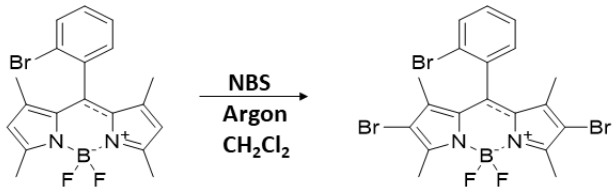

Scheme 3.11. Synthesis of brominated core dye **7g**.

3.17.2. Structural characterization of **7g**

BODIPY **3g** was used to synthesize **7g**. The main difference in the ^{1}H NMR spectrum of the core and the brominated core is the disappearance of the signal assigned to the protons at the 2,6-positions. The four phenyl protons of **7g** appear as a doublet at 7.75–7.72 ppm, a multiplet at 7.51–7.48, a multiplet at 7.43–7.38 and a singlet at 7.28 ppm. All peaks integrate to one proton each. The twelve methyl proton signals for the two methyl groups at the 1,7-

and 3,5-positions are assigned to the peaks at 2.61 and 1.41 ppm. In the FT-IR spectrum, a C-Br stretch appears 533 cm^{-1} and can be assigned to the bonds at the 2,6-positions. The structure of BODIPY **7g** was further confirmed by MALDI-TOF mass spectrometry as the parent peak was observed at 560.20 amu (calc: 559.89; $[M]^+$).

3.17.3. Spectroscopic and physicochemical properties of **7g**

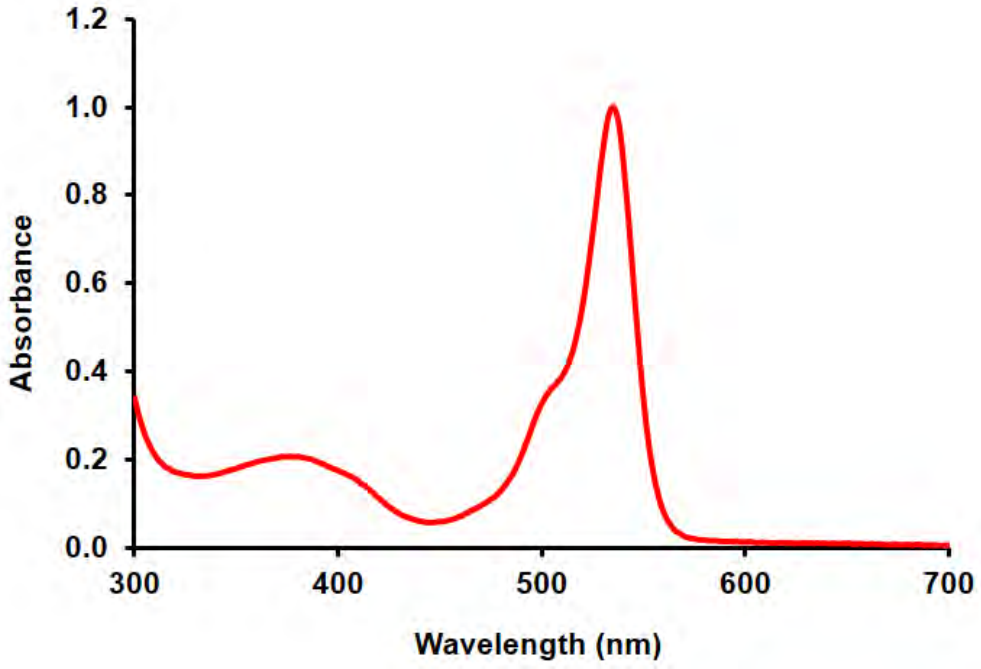

Figure 3.13. The UV-visible absorption spectrum of halogenated core dye **7g** in DMSO.

The UV-visible absorption spectrum of **7g** in DMSO is shown above (**Figure 3.13**). The absorbance maximum lies at 535 nm, and there was no aggregation observed. As expected, the presence of bromine heavy atoms at the 2,6-positions leads to a significant decrease in the fluorescence quantum yield and a moderately high singlet oxygen quantum yield, Φ_Δ (**Table 3.9**).

Table 3.11. Photophysical data for BODIPYs **7g** in DMSO.

λ_{Abs} (nm)	λ_{Ex} (nm)	λ_{Em} (nm)	Stokes shift (cm^{-1})	Φ_F	log ε	Φ_Δ
535	534	553	608	0.19	4.44	0.48

3.12. Halogenated *meso*-bromothienylBODIPY core dye (**7h**)

3.17.1. Synthesis (**Scheme 3.12**)

Halogenated BODIPY core dye **7h** was synthesized following the procedure described above (**Scheme 3.8**).

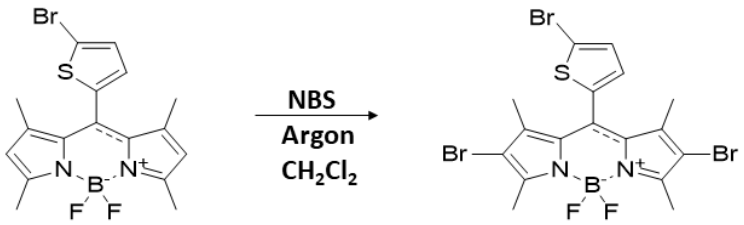

Scheme 3.12. Synthesis of brominated core dye **7h**.

3.17.2. Structural characterization of **7h**

The ^{1}H NMR spectrum of **7h** has two protons in the aromatic region, as expected. These appear as doublets, each integrating to one proton at 7.40–7.38 and 7.18–7.16 ppm. These are followed by the twelve methyl protons on the BODIPY core assigned to the singlet signals at 2.56 and 1.73 ppm. As expected, the signal for the protons at the 2,6-positions disappears on moving from **3h** to **7h**, due to the presence of bromine atoms at these positions. The FT-IR spectrum contains a C-Br stretch peak at 528 cm^{-1}, and this replaces the peak observed at 469 cm^{-1} in the spectrum of the core for the bonds at the 2,6-positions. The structure of

BODIPY **7h** was further confirmed by MALDI-TOF mass spectrometry as the parent peak was observed at 568.16 amu (calc: 568.85; $[M]^+$).

3.17.3. Spectroscopic and physicochemical properties of **7h**

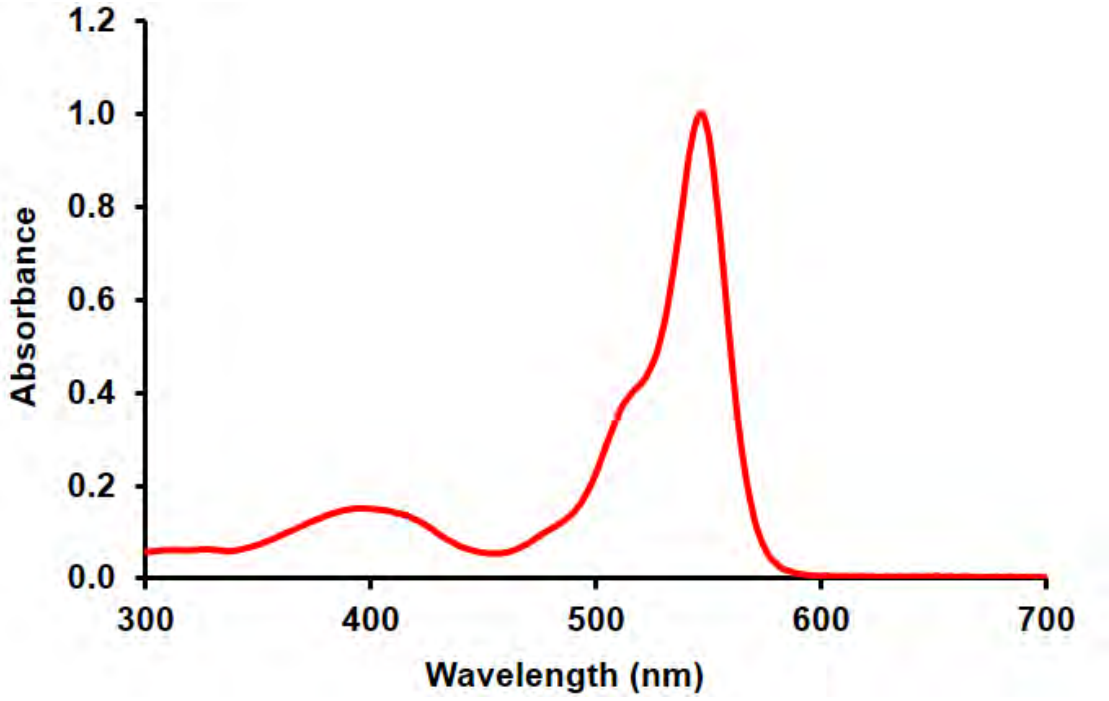

Figure 3.14. The UV-visible absorption spectrum of halogenated core dye **7h** in DMSO.

Table 3.12. Photophysical data for BODIPYs **7h** in DMSO.

λ_{Abs} (nm)	λ_{Ex} (nm)	λ_{Em} (nm)	Stokes shift (cm^{-1})	Φ_F	log ε	Φ_Δ
545	545	563	587	0.09	4.39	0.52

3.13. Halogenated *meso*-methyl 4-formylphenylBODIPY core dye (**7i**)

3.17.1. Synthesis (**Scheme 3.13**)

Halogenated BODIPY core dye **7h** was synthesized following the procedure described above (**Scheme 3.8**).

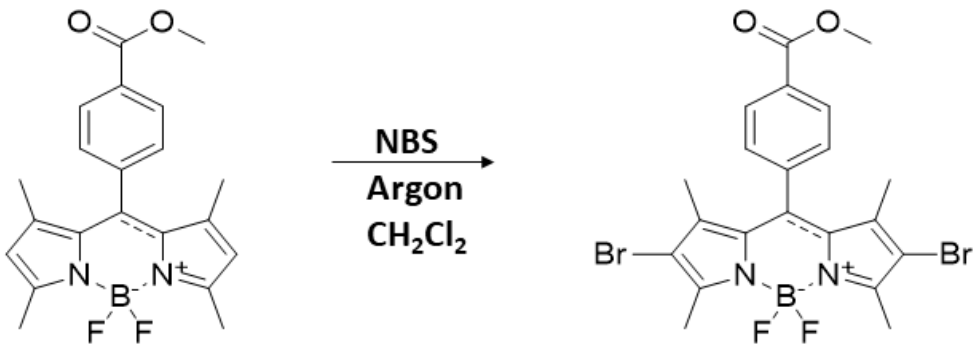

Scheme 3.13. Synthesis of brominated core dye **7i**.

3.17.2. Structural characterization of **7i**

The ^{1}H NMR spectrum of **7i** shows two doublets at 8.16–8.14 and 7.64–7.61 ppm, which can be assigned to the four phenyl protons. A singlet signal at 3.91 ppm is assigned to the methyl protons of the ester group, and this is followed by the twelve methyl protons on the BODIPY core, which appear as singlet signals at 2.52 and 1.31 ppm. In the FT-IR spectrum, the C-H stretch peak for the bonds at the 2,6-positions observed at 465 cm^{-1} for the core is replaced by a C-Br stretch peak at 532 cm^{-1}. The structure of BODIPY **7i** was further confirmed by MALDI-TOF mass spectrometry as the parent peak was observed at 541.27 amu (calc: 539.99; $[M + H]^+$).

3.17.3. Spectroscopic and physicochemical properties of **7i**

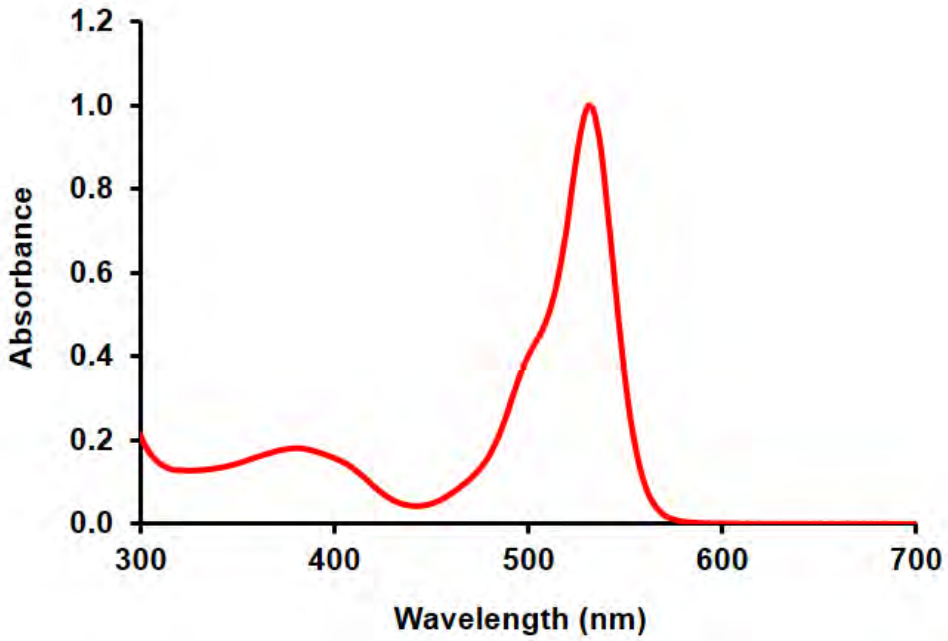

Figure 3.15. The UV-visible absorption spectrum of halogenated core dye **7i** in DMSO.

Table 3.13. Photophysical data for BODIPYs **7i** in DMSO.

λ_{Abs} (nm)	λ_{Ex} (nm)	λ_{Em} (nm)	Stokes shift (cm^{-1})	Φ_F	log ε	Φ_Δ
530	530	549	653	0.20	5.0	0.40

3C – Synthesis and characterization of styrylBODIPY dyes

This section details the synthesis and characterization of BODIPY dyes with extended π-systems. These dyes were synthesized using the known Knoevenagel condensation reaction from some of the core dyes and halogenated core dyes detailed above.[11–13]

3.14. 3-mono and 3,5-diethylaminostyrylBODIPY dyes (**10**, **11** and **12**)

3.17.1. Synthesis (**Scheme 3.14**)

BODIPYs **10**, **11** and **12** were synthesized using modified Knoevenagel condensation reactions, in which **1a**, **2a** and **7a** were used as precursors, respectively.[100] The corresponding starting BODIPY dye was mixed with 4-diethylaminobenzaldehyde in dry benzene. The reactions were carried out at reflux temperatures in the presence of a few drops of piperidine and acetic acid. During the reaction, a Dean-Stark trap was used for the azeotropic removal of water formed from the condensation reaction.

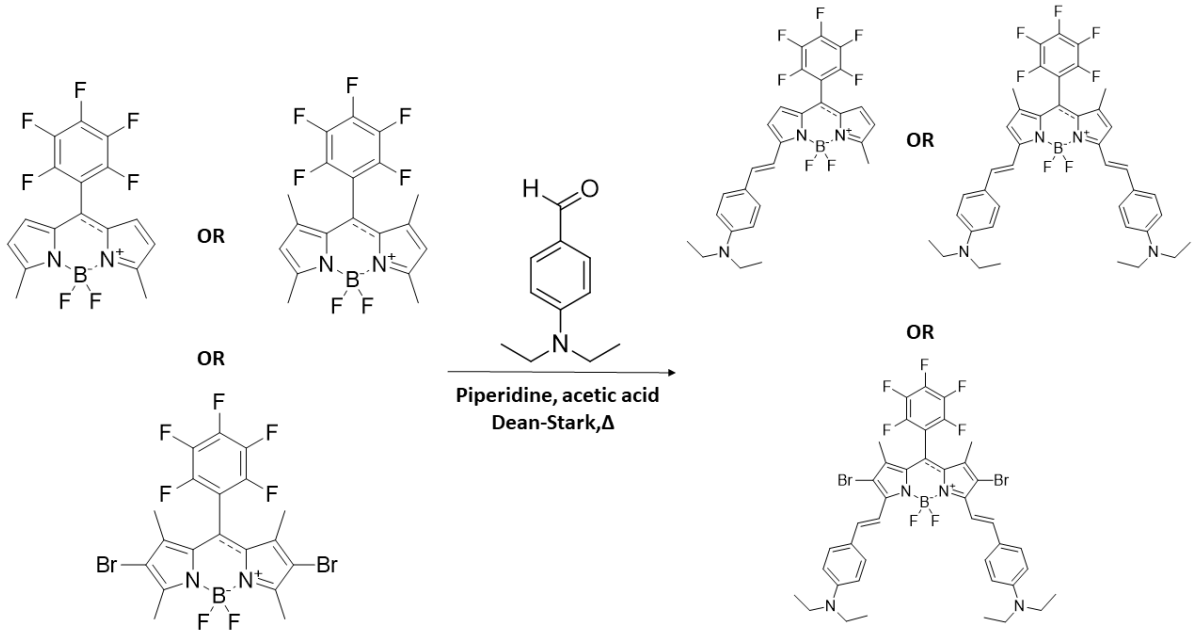

Scheme 3.14. Synthesis of styrylBODIPY dyes **10**, **11** and **12**.

3.17.2. Structural characterization of **10**, **11** and **12**

BODIPYs **1a**, **2a** and **7a** were used to synthesize **10**, **11** and **12**, respectively. In the ^{1}H NMR spectrum of **10**, one doublet which integrates to four protons can be assigned to the phenyl ring on the styryl group, at 7.47–7.44 ppm (**Figure 3.16**). The doublet at 7.31–7.27 ppm integrates to two protons and can be attributed to the bridging vinyl bond of the styryl group. The peaks for the four protons on the 1-, 2-, 6- and 7-positions of the BODIPY core appear as two doublets integrating to two protons at 6.87–6.85 and 6.57–6.55 ppm. Because of the ethyl groups of diethylamino group on the styryl, a doublet that integrates to four protons at 3.37–3.35 ppm can be assigned to the CH_2 groups, whereas the triplet signal at 1.15–1.13 ppm can be assigned to the methyls of the ethyl groups as it integrates to six protons.

For **11**, the ^{1}H NMR spectrum has two doublets at 7.50–7.47 and 6.68–6.65 ppm, which each integrate to four protons and can be assigned to the phenyl rings on the styryl groups. The doublet at 6.64–6.61 ppm, which integrates to four protons, can be assigned to the bridging alkenes between the styryl groups and the core. The two protons at the 2,6-positions of the BODIPY core appear as a singlet that integrates to two protons at 5.99 ppm. This is followed by a multiplet assigned to the eight protons of the CH_2 groups of the ethyl groups of diethylamino groups, at 3.43–3.39 ppm. Two singlet signals at 1.64 and 1.59 ppm, each integrating to three protons, can be assigned to the methyl groups at the 1,7-positions. The last peak in the ^{1}H NMR spectrum of **11** is a triplet at 1.20–1.18 ppm, which integrates to the twelve protons on the methyls of the ethyl groups.

The third and final ^{1}H NMR spectrum for this set of compounds is that of **12**. In this spectrum, the protons on the phenyl rings of the styryl groups appear as two doublets at 8.34–8.23 and

7.60–7.57 ppm, integrating to two and six protons, respectively. The doublet at 6.73–6.68 ppm, which integrates to four protons, can be assigned to the bridging alkenes between the styryl groups and the core. This is followed by a multiplet assigned to the eight protons of the CH_2 groups of the ethyl groups of diethylamino groups, at 3.49–8.14 ppm. The methyl groups at the 1,7-positions are assigned to the singlet signal at 2.67 ppm, which integrates to six protons. Finally, the triplet at 1.26–1.22 ppm is assigned to the twelve protons on the methyls of the ethyl groups.

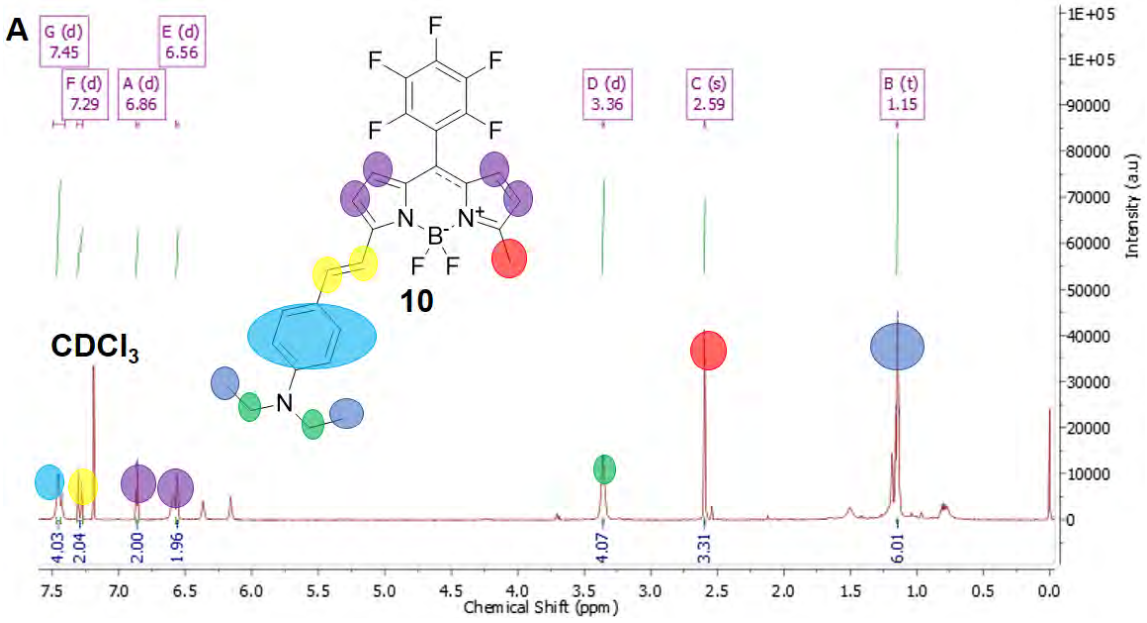

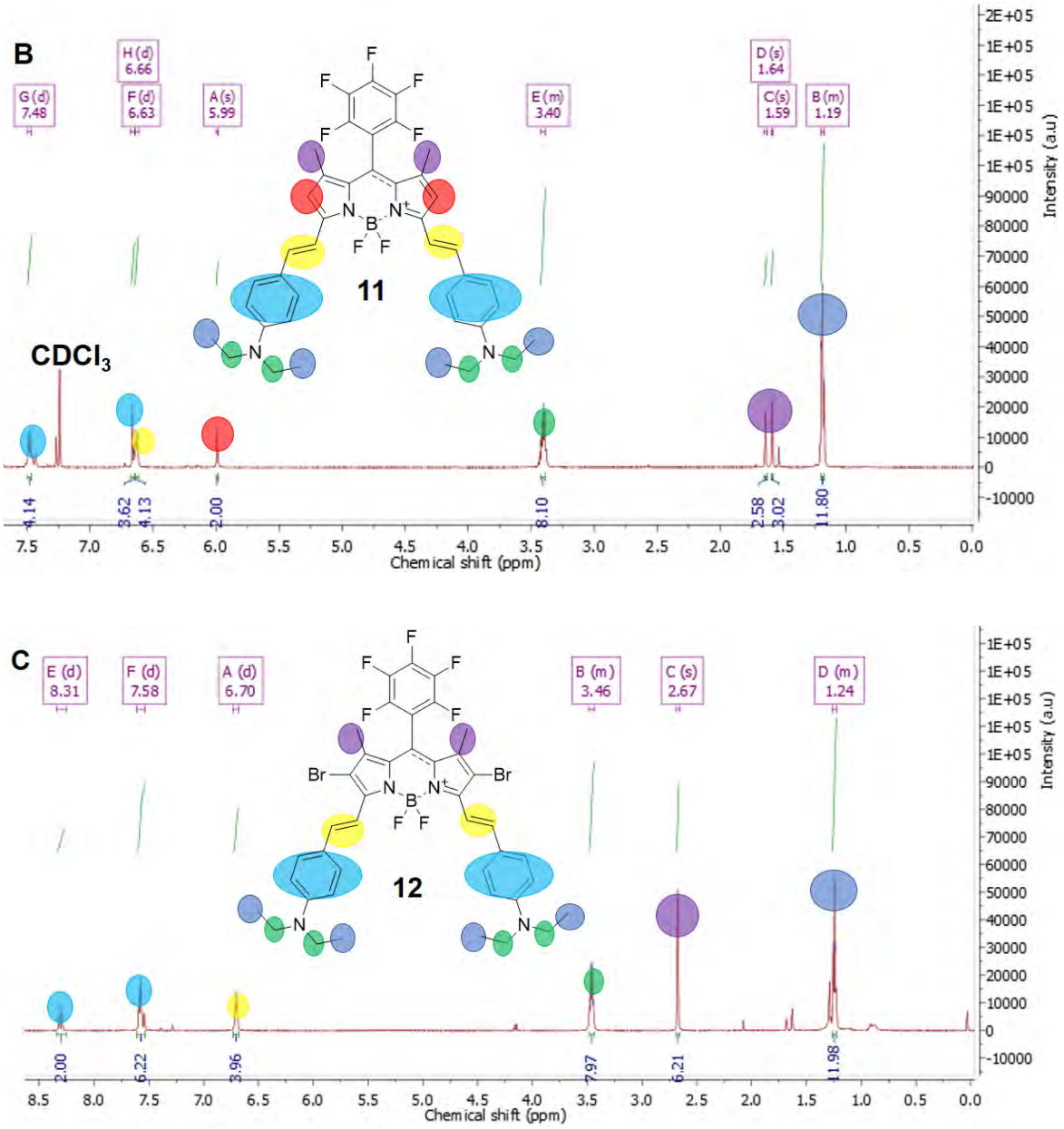

Figure 3.16. ^{1}H NMR spectra of styrylBODIPY dyes.

All three dyes were confirmed by MALDI-TOF mass spectrometry, and the parent peaks were observed at 545.53 amu (calc: 545.31; $[M]^{+}$), 732.60 amu (calc: 733.01; $[M]^{+}$) and 891.06 amu (calc: 890.39; $[M]^{+}$) for **10**, **11** and **12**, respectively.

3.17.3. Spectroscopic and physicochemical properties **10**, **11** and **12**

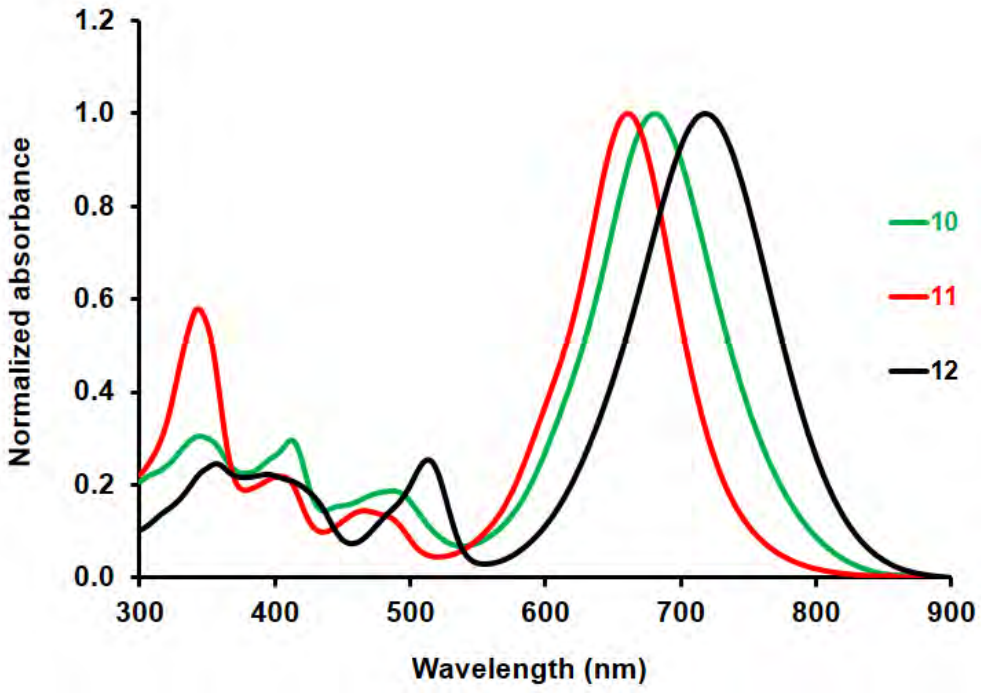

Figure 3.17. Normalized absorption spectra of styrylBODIPY dyes **10**, **11** and **12** in DMSO.

The UV-visible absorption spectra obtained for BODIPYs **10**, **11** and **12** in DMSO and CH_2Cl_2 are typical of spectra usually obtained for a distyrylBODIPY. BODIPYs **10** and **12** are significantly red-shifted relative to 11. For **10**, this is due to the absence of the methyl groups on at the 1,7-positions. This has an effect on the D–π–A properties associated with the diethylaminostyryl and pentafluorophenyl groups. For **12**, it is due to the presence of bromine heavy atoms at the 2,6-positions. This will be discussed in detail in Chapter 6. The fluorescence properties of the dyes were not detected in organic solutions due to intramolecular charge transfer (ICT) introduced by the lone pairs of electrons on the nitrogen atoms on the styryl groups. Usually, this ICT can be eliminated by coordinating a cation onto the nitrogen atoms or by dissolving the dye in acidic media to protonate the nitrogen atoms.[135,136] However, the fluorescence properties in acidic media were not studied in this

work as they have no significant bearing on the optical limiting applications these dyes were studied for.

Table 3.14. Photophysical data in CH_2Cl_2 and DMSO for **10**, **11** and **12** and benzene for **12**.

Solvent	BODIPY	λ_{Abs} (nm)	λ_{Ex} (nm)	λ_{Em} (nm)	Stokes shift (cm^{-1})	Φ_F	log ε
DMSO	**10**	681	-	-	-	-	4.33
CH_2Cl_2		667	-	-	-	-	5.48
DMSO	**11**	661	-	-	-	-	5.15
CH_2Cl_2		649	-	-	-	-	5.04
DMSO	**12**	718	-	-	-	-	4.63
CH_2Cl_2		700	-	-	-	-	4.61
Benzene		709	-	-	-	-	4.64

3.15. 3,5-DistyrylBODIPY dyes (**13**, **14** and **15**)

3.17.1. Synthesis (**Scheme 3.15**)

BODIPYs **13**, **14** and **15** were synthesized following the procedure described above for **10**, **11** and **12** (**Scheme 3.14**).

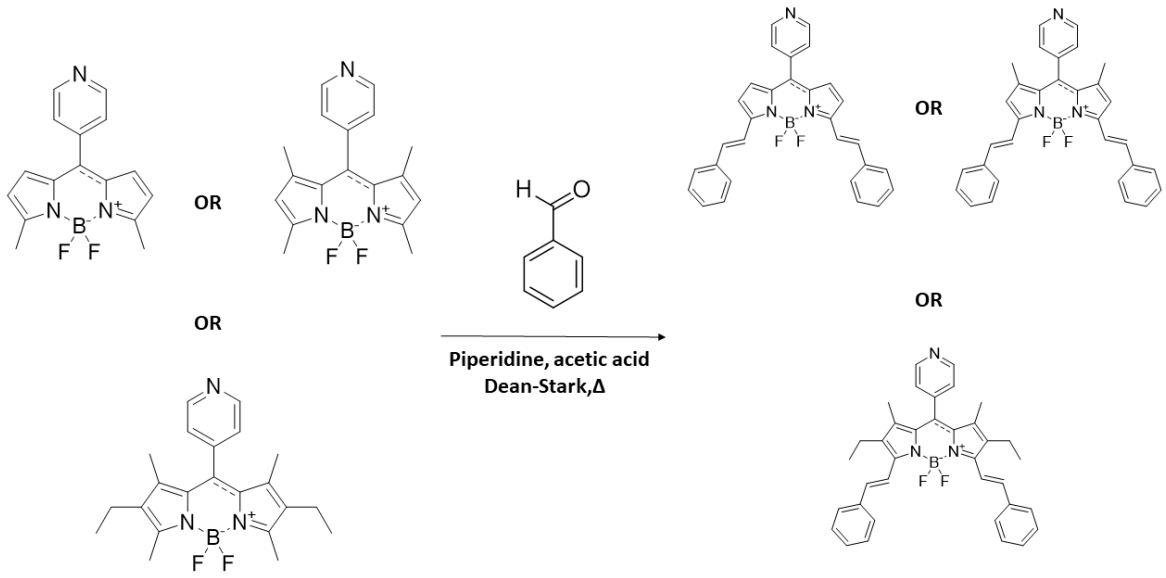

Scheme 3.15. Synthesis of styrylBODIPY dyes **13**, **14** and **15**.

3.17.2. Structural characterization of **13**, **14** and **15**

BODIPYs **13**, **14** and **15** were synthesized from **1b**, **3b** and **4b**, respectively. The ^{1}H NMR spectrum of **13**, the four protons on the *meso* phenyl ring, can be assigned to the two doublets, individually integrating to two protons, at 8.80–8.73 and 7.79–7.74 ppm. The doublet at 7.66–7.63 ppm, which integrates to four protons, can be attributed to the bridging alkenes between the styryl groups and the core. The signals for the protons of the phenyl rings on the styryl groups appear as three signals. These are a doublet that integrates to two protons at 7.45–7.43 ppm, a triplet that integrates to four protons at 7.42–7.39 ppm and a multiplet which integrates to four protons at 7.38–7.32 ppm. The four protons on the 1-, 2-, 6- and 7-positions of the BODIPY core appear as two doublets, individually integrating to two protons, at 6.96–6.93 and 6.73–6.71 ppm.

For **14**, the triplet peaks at 7.46–7.42 and 7.38–7.35 ppm, which integrate to four and two protons, respectively, can be assigned to the three neighboring protons on each phenyl ring

of the styryls. They are assigned in this manner because each has two neighbors and this, therefore, results in a triplet signal. The remainder of the protons on the phenyl rings of the styryls combine with the peaks from the *meso*-phenyl ring. This results in two doublets that integrate two and six protons at 7.82–7.75 and 7.69–7.65 ppm, respectively. The doublet at 7.34–7.29 ppm, which integrates to four protons, can be attributed to the bridging alkenes between the styryl groups and the core. The two protons at the 2,6-positions of the BODIPY core appear as a singlet at 6.70 ppm, whereas the singlet at 1.51 ppm integrating to six protons can be assigned to the methyl groups at the 1,7-positions.

In the ^{1}H NMR spectrum of **15**, two doublets that lie at 8.84–8.81 and 7.83–7.78 ppm and integrate to two protons each can be assigned to the *meso*-phenyl ring. The signals for the protons of the phenyl rings on the styryl groups appear as three peaks. These are a doublet that integrates to four protons at 7.68–7.64 ppm, a multiplet that integrates to four protons at 7.45–7.42 ppm and a multiplet that integrates to two protons at 7.39–7.38 ppm. The bridging alkenes between the styryl groups and the core are assigned to the two doublets at 7.37–7.35 and 7.33–7.31 ppm. The CH_2 groups of the ethyl groups at the 2,6-positions are assigned to the multiplet peak, which integrates to four protons at 2.67–2.62 ppm. Finally, the methyl groups at the 1,7-positions are assigned to the singlet signal at 1.39 ppm, which integrates to six protons. The six protons at 1.21–1.18 ppm are assigned to the methyls of the ethyl groups.

The structures of the three dyes were confirmed by MALDI-TOF mass spectrometry, and the parent peaks were observed at 477.80 amu (calc: 473.19; $[M - F + Na]^+$), 502.23 (calc: 501.22; $[M + H]^+$) amu and 557.20 amu (calc: 557.28; $[M]^+$) for **13**, **14**, **15**, respectively. Typically, molecules with low molecular weights such as **13** are not ideal candidates for analysis by

MALDI-TOF mass spectrometry, mainly due to interferences from peaks associated with most of the common matrices used.[138,139] The unusual parent peak obtained for **13** relative to the spectra of **14** and **15** can be attributed to this.

3.17.3. Spectroscopic and physicochemical properties **13**, **14** and **15**

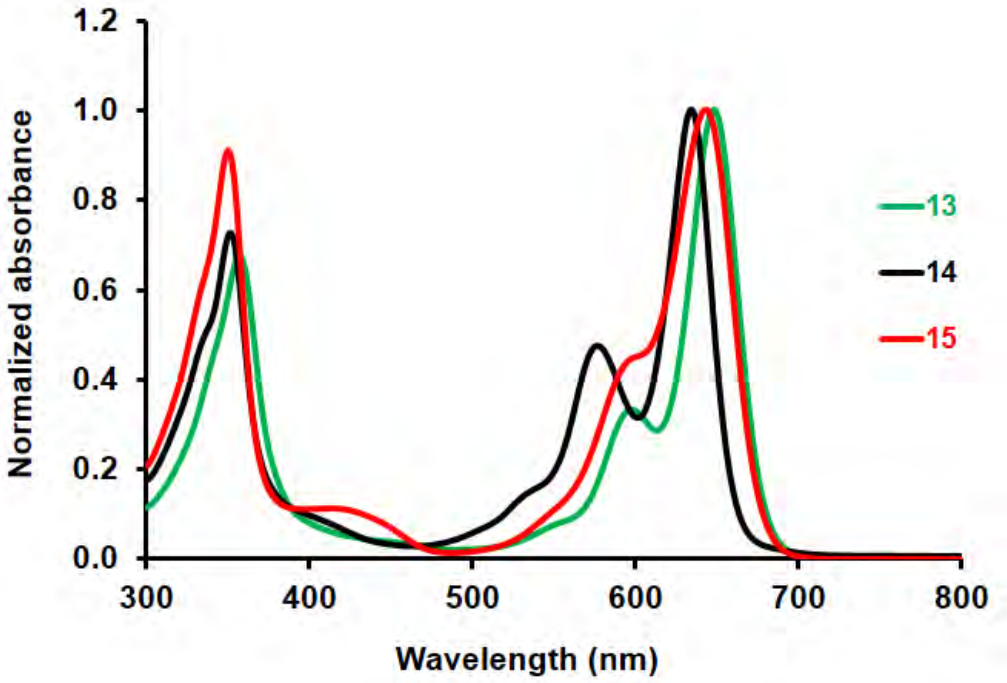

Figure 3.18. Normalized absorption spectra of styrylBODIPY dyes **13**, **14** and **15** in DMSO.

The UV-visible absorption spectra of BODIPYs **13**, **14** and **15** in DMSO are typical of spectra usually obtained for distyryl substituted BODIPY dyes (**Figure 3.18**). BODIPY **14** is highly fluorescent relative to **13** and **15**, and this can be attributed to the absence of methyl groups at the 1,7-positions for **13**. This allows rotation of the *meso*-substituent, leading to nonradiative decay, whereas **15** is less fluorescent because of the presence of ethyl groups at the 2,6-positions.

Table 3.15. Photophysical data for BODIPYs **13**, **14** and **15** in DMSO.

	Solvent	λ_{Abs} (nm)	λ_{Ex} (nm)	λ_{Em} (nm)	Stokes shift (cm^{-1})	Φ_F	log ε
13	DMSO	648	649	667	440	0.53	4.42
	Benzene	647	648	665	418	0.61	4.43
14	DMSO	634	633	645	269	0.71	4.45
	Benzene	634	634	647	317	0.28	4.44
15	DMSO	643	643	661	424	0.52	4.43
	Benzene	643	645	662	446	0.29	4.49

3.16. 3,5-DibenzyloxystyrylBODIPY (**16**)

3.17.1. Synthesis (**Scheme 3.16**)

BODIPY **16** was synthesized following the procedure described above for **10**, **11** and **12** (**Scheme 3.14**).[37]

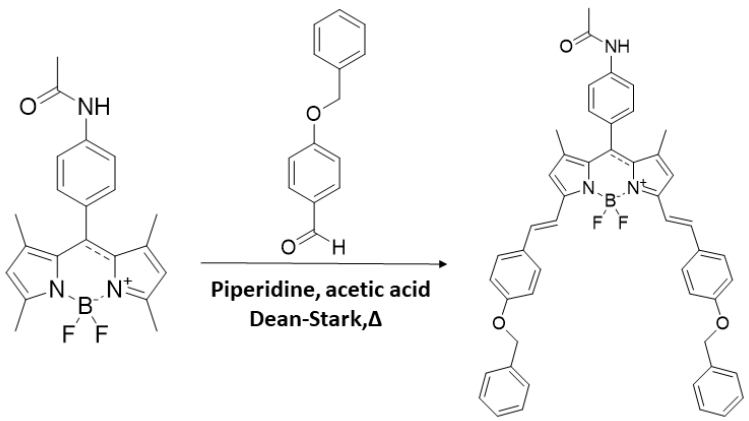

Scheme 3.16. Synthesis of styrylBODIPY **16**.

3.17.2. Structural characterization of **16**

The ^{1}H NMR spectrum of **16** has a complicated spectrum that cannot be easily assigned in the aromatic region. The spectrum does, however, integrate to the forty-two total protons expected. In the aromatic region, there is a doublet that integrates to two protons at 7.72–7.67 ppm, a multiplet that integrates to six protons at 7.64–7.58 ppm, a multiplet that integrates to five protons at 7.51–7.46 ppm, a multiplet that integrates to four protons at 7.46–7.42 ppm, another multiplet which integrates to two protons at 7.39–7.35 ppm and a final multiplet which integrates to four protons at 7.27–7.21 ppm. After the complex peaks in the aromatic region, a doublet that integrates to four protons at 7.04–7.00 ppm can be assigned to the bridging alkenes between the styryl groups. The protons at the 2,6-positions can be assigned to the singlet peak, which integrates to two protons at 6.62 ppm. The doublet signal at 5.13 ppm, which integrates to four protons, is assigned to the CH_2 protons adjacent to the oxygen atoms of the benzyloxy groups on the styryls. The singlet signal for the three methyl protons of the *meso*-acetamido group lies at 2.24 ppm. Finally, the methyl groups at the 1,7-positions are assigned to the singlet signal at 1.48 ppm, which integrates to six protons.

The structure of the dye was further confirmed by MALDI-TOF mass spectrometry. The parent peak was observed at 769.30 amu (calc: 769.86; $[M]^{+}$).

3.17.3. Spectroscopic and physicochemical properties **16**

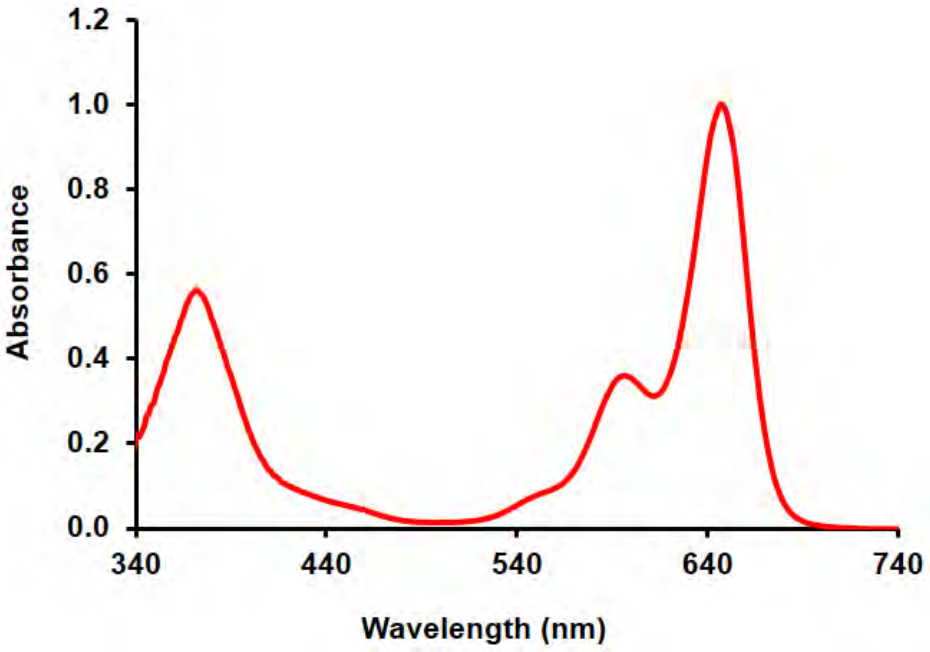

Figure 3.19. The UV-visible absorption spectrum of styrylBODIPY **16** in DMSO.

The UV-visible absorption spectra of BODIPY **16** is typical of spectra usually obtained for a distyryl substituted BODIPY. BODIPY **16** is highly fluorescent in both organic solvents studied, and this can be attributed to the presence of protons at the 2,6-positions.

Table 3.16. Photophysical data for BODIPY **16** in DMSO and CH_2Cl_2.

Solvent	λ_{Abs} (nm)	λ_{Ex} (nm)	λ_{Em} (nm)	Stokes shift (cm^{-1})	Φ_F	log ε
DMSO	647	648	664	396	0.47	5.84
CH_2Cl_2	644	644	660	376	0.40	5.56

3.17. 3,5-DipiperidinylstyrylBODIPY (**17**)

3.17.1. Synthesis (**Scheme 3.17**)

BODIPY **17** was synthesized following the procedure described above for **10**, **11** and **12** (**Scheme 3.14**).

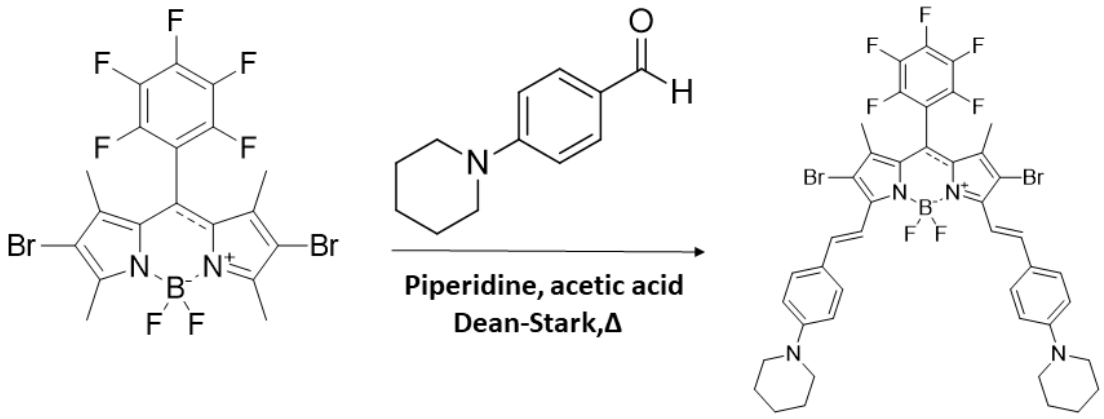

Scheme 3.17. Synthesis of styrylBODIPY **17**.

3.17.2. Structural characterization of **17**

The ^{1}H NMR spectrum of **17** has singlet and doublet signals that integrate to four protons each at 9.76 and 7.76–7.73 ppm, respectively. These can be assigned to the protons on the phenyl rings. The four protons from the bridging alkenes between the styryl groups are assigned to a doublet peak at 6.92–6.90 ppm. The multiplet peak, which integrates to eight protons at 3.44–3.42 ppm, is assigned to the four CH_2 groups of the piperidinyl closest to the nitrogen atom, whereas the six that are furthest from the nitrogen atom can be assigned to the singlet peak at 1.69 ppm, which integrates to twelve protons. Finally, the methyl groups at the 1,7-positions can be assigned to the singlet signal at 1.27 ppm, which integrates to six

protons. The structure of the dye was further confirmed by MALDI-TOF mass spectrometry, and the parent peak was observed at 914.34 amu (calc: 914.14; $[M]^+$).

3.17.3. Spectroscopic and physicochemical properties **17**

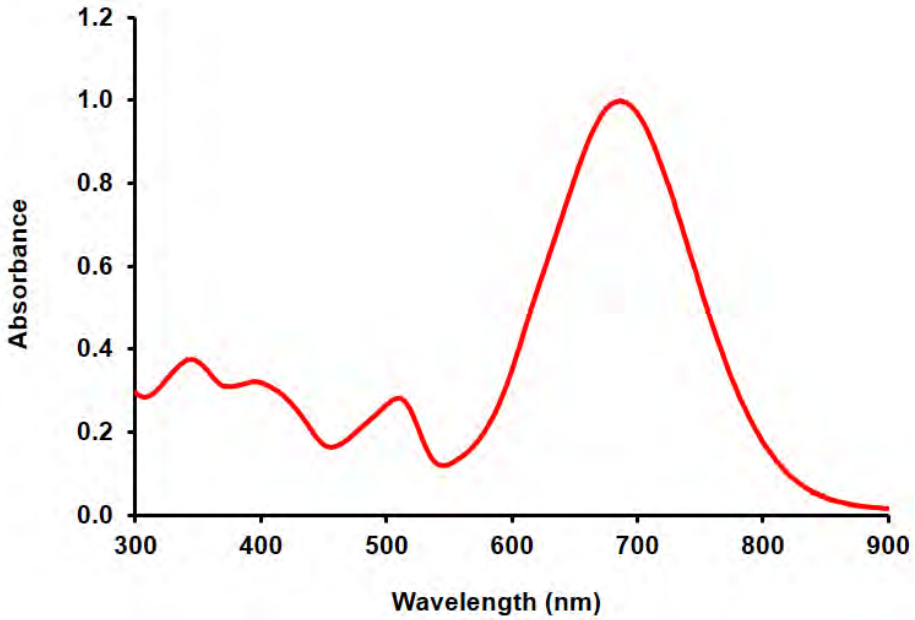

Figure 3.20. The UV-visible absorption spectrum of styrylBODIPY **17** in DMSO.

The UV-visible absorption spectra obtained for BODIPY **17** in DMSO is slightly red-shifted relative to a typical di-styrylBODIPY dye. This red-shift and the absence of fluorescence in organic media is attributed to intramolecular charge transfer (ICT) introduced by the lone pairs of electrons on the nitrogen atoms on the styryl groups.

Table 3.17. Photophysical data for BODIPY **17** in DMSO and benzene.

Solvent	λ_{Abs} (nm)	λ_{Ex} (nm)	λ_{Em} (nm)	Stokes shift (cm^{-1})	Φ_F	log ε
DMSO	686	-	-	-	-	4.44
Benzene	680	-	-	-	-	4.48

3.18. Failed syntheses of BODIPYs 18–24

BODIPYs **18-24** were synthesized following the procedure described above for **10**, **11** and **12**, from BODIPYs **1j-m** and **3j-l** and the corresponding benzaldehyde (**Scheme 3.18**).

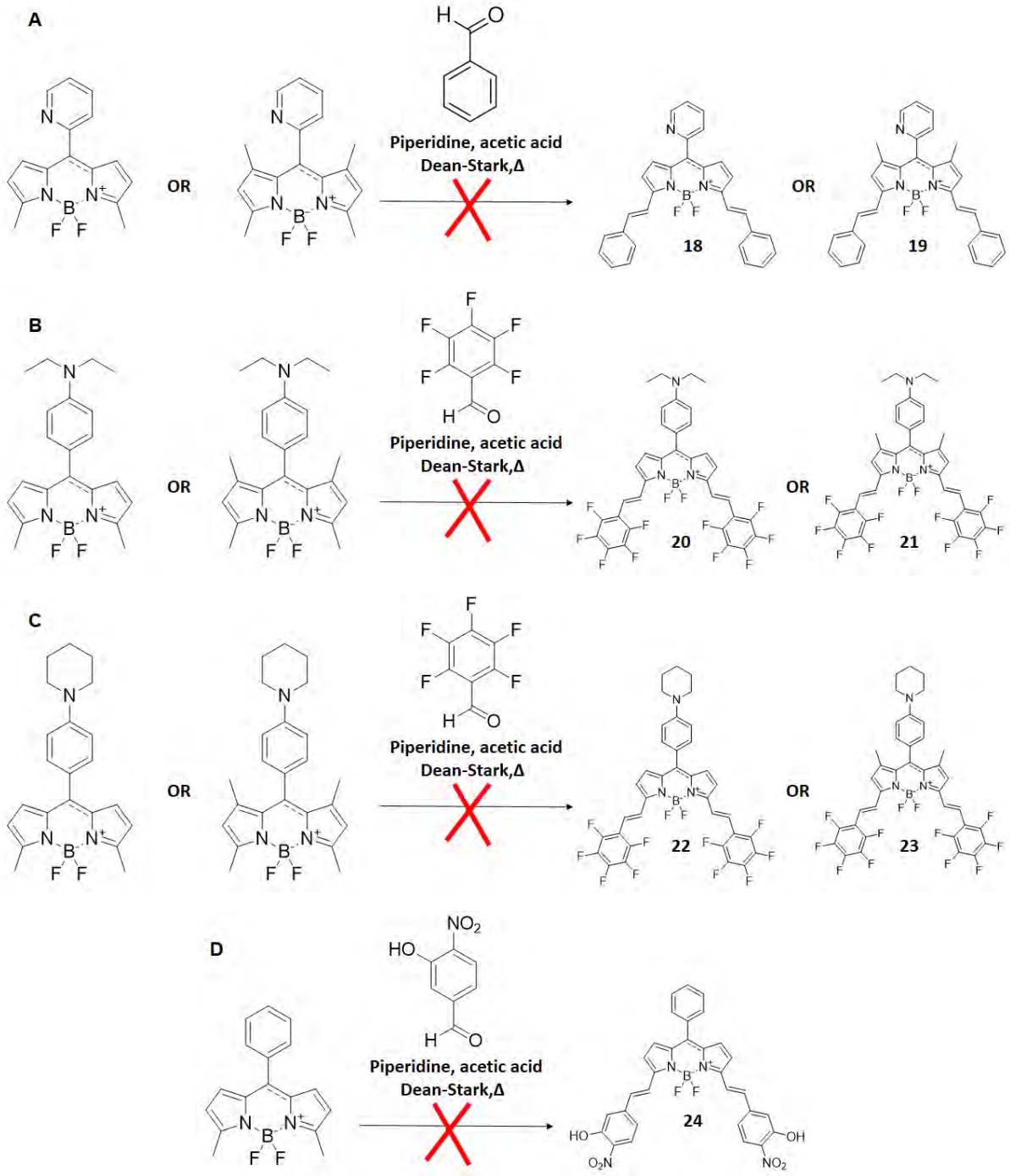

Scheme 3.18. Synthesis of styrylBODIPYs **18**-**24**.

During the synthesis of styrylBODIPY dyes *via* the Knoevenagel condensation reaction, the color of the reaction mixture is expected to form a blue or green color depending on the nature of the functional groups present on the BODIPY. This is because the Knoevenagel condensation reaction is known to yield either monostyryl or distyrylBODIPY dyes, preferably at the 3,5-positions.[15] This color change was not observed during the synthesis of target BODIPYs **18-24** as the mixture maintained the color of the starting BODIPY, or in some instances, a dark brown or black substance with no distinct UV-visible absorption bands formed. This was observed when either benzene or toluene was used as the solvent, and no characteristic absorption bands could be identified. It has been previously shown that electron-rich substituents readily give styrylBODIPY dyes at significant yields, but in some rare instances, styrylBODIPY dyes have been formed using electron-deficient aldehydes as substituents at the 3,5-positions.[15]

The challenges encountered in the synthesis of **20-24** in this work can be explained using the nature of the substituents on the aldehydes used. The aldehydes contain electron-withdrawing groups, and aldehydes of this nature, together with other electron-deficient aldehydes, have been found to be unreactive during Knoevenagel condensation reactions.[5,15,16] Following the work by Galangau *et al*. on Knoevenagel condensation reactions using aldehydes with electron-withdrawing groups was also unsuccessful.[15] BODIPY dyes **20-23** were targeted as D-π-A analogues of **10-12** and **17**, while **18** and **19** were targeted as analogues of **13** and **14**.

Chapter 4:

Nonlinear optical (NLO) limiting properties of BODIPY dyes and other molecular dyes

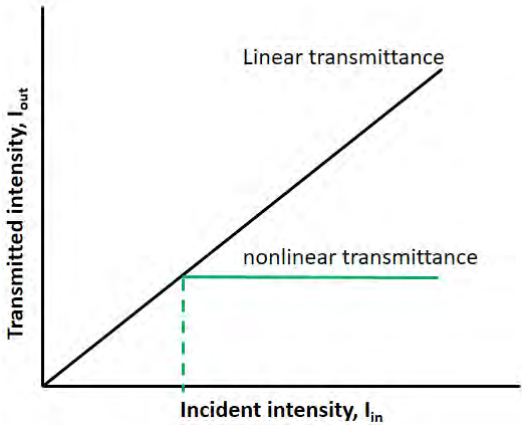

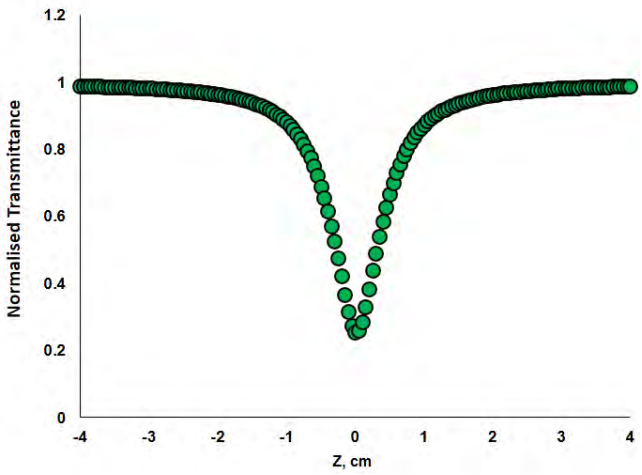

This chapter covers the nonlinear optical (NLO) limiting properties of BODIPY dyes in organic solutions and briefly looks at the NLO properties of other complexes, namely a monomeric phthalocyanine and a bis(phthalocyanine) and novel disilane-bridged tetraphenylethylene (TPE) architectures.[140,141]

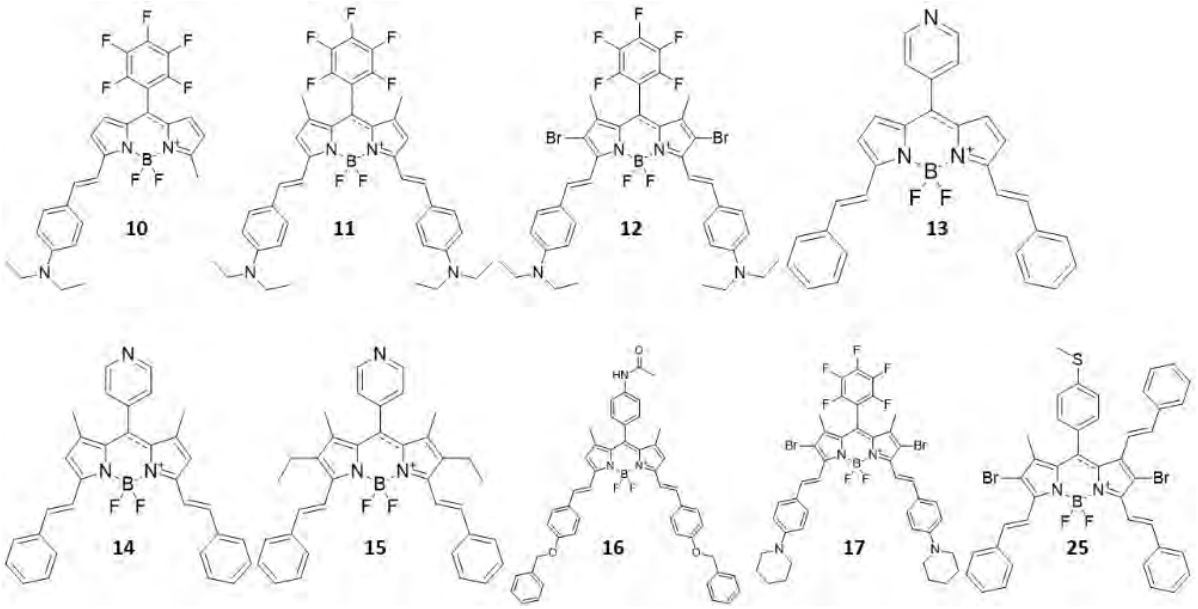

Figure 4.1. Structural differences in the styrylBODIPY dyes used for NLO studies.

The BODIPY dyes were rationally selected to investigate the effect of structure on optical limiting properties. The presence of electron-donating and electron-withdrawing groups or a D–π–A system that creates a push-pull system is expected to enhance the NLO properties, as has been shown previously with BODIPYs and other compounds.[19,20,98–100] In this work, the effect of this push-pull system and the presence of electron-donating substituents at the 3,5-positions on the hyperpolarizability and NLO properties is examined, in general terms, by using seven novel distyrylBODIPY dyes. These are BODIPYs **10-15** and **17** (**Figure 4.1**). BODIPY **16** was used to better understand the mechanism responsible for the typically favorable NLO responses observed for nonhalogenated BODIPY dyes.[37] Complementary results from

transient absorption spectroscopy studies will also be discussed and related to the NLO properties obtained for **16**. The NLO properties of a 1,3,5-tristyrylBODIPY dye **25** are also studied to examine whether further styrylation offers any advantages for OL applications.[142]

Some of the novel dyes shown in **Figure 4.1** are structural analogues, with minor modifications rationally introduced to analyze the effect of structure on the properties being studied. The dyes were selected to study of the effect of the presence of methyl groups rather than protons at the 1,7-positions of the BODIPY core and the presence of bromine heavy atoms at the 2,6-positions on the NLO properties. The first set of these analogous dyes is comprised of **10**, **11** and **12**, and the second set is **13**, **14** and **15**. In the first set, **10** has protons at the 1,7-positions, whereas **11** has methyl groups at these positions. For **10**, this is expected to enable rotation of the *meso*-aryl substituent due to the absence of the steric strain introduced by the methyl groups in the case of **12**. Secondly, **12** is analogous to **11** but contains heavy atoms at the 2,6-positions, and this was used to assess the difference in the optical limiting properties obtained in the singlet manifold for **11** to those of **12** obtained in the triplet manifold due to the intersystem crossing linked to the bromine heavy atoms. In the second set, **13** contains protons at the 1,7-positions, whereas **14** and **15** have methyl groups at these positions. Secondly, **14** and **15** only differ with the substituents present at the 2,6-positions; **14** has protons, whereas **15** has ethyl groups. The ethyl groups were incorporated on the BODIPY core to explore the effect that alkyl substituents have on the NLO properties. Finally, **17** is analogous to **12**, but a piperidinyl group is added to the styryl groups.

The two final sections of this chapter detail the NLO properties of molecular dyes other than BODIPYs, namely two scandium phthalocyanines synthesized at the Russian Academy of

Sciences and novel disilane-bridged TPE architectures synthesized at the Hangzhou Normal University (**Figure 4.2**).[106,140]

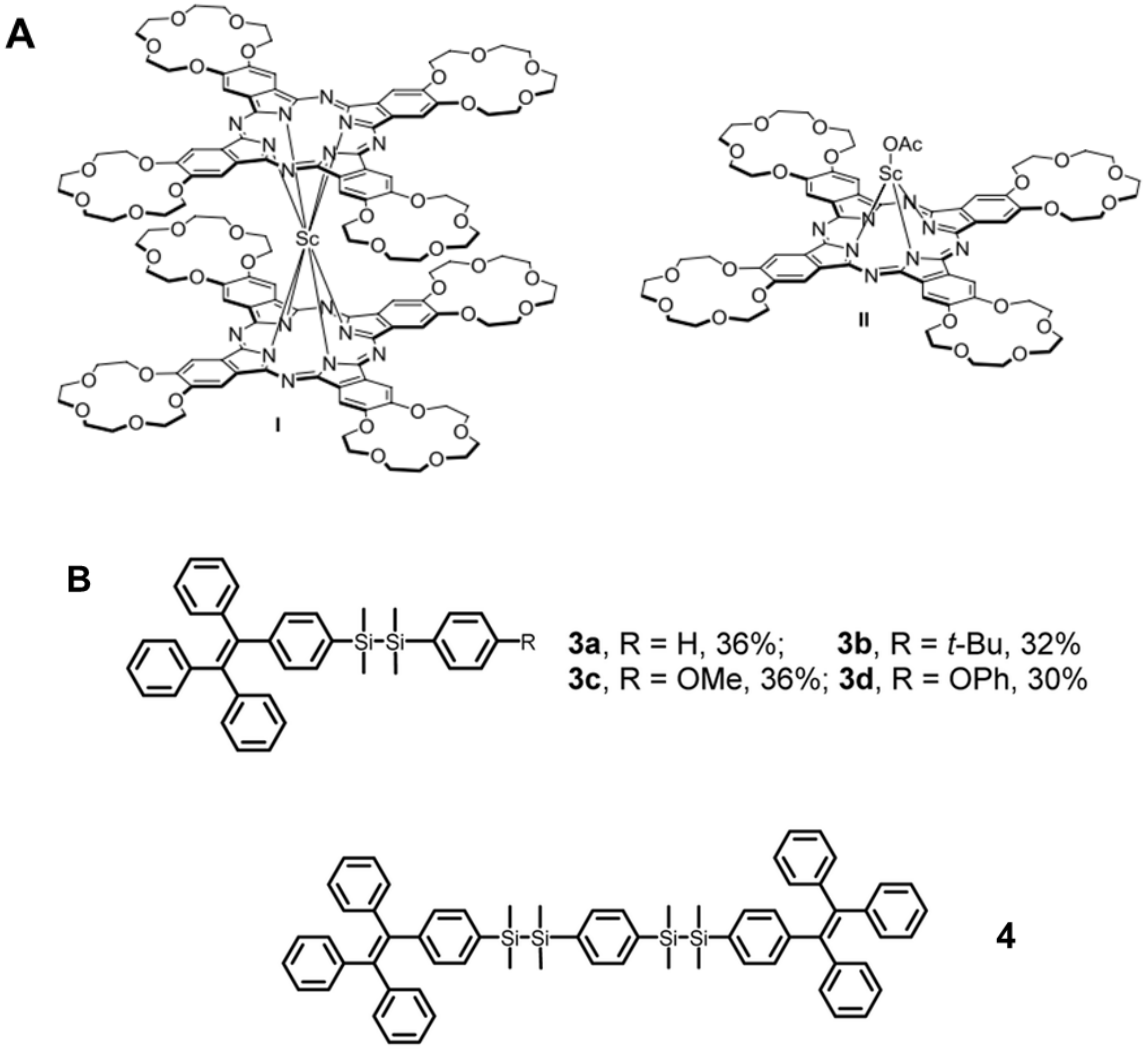

Figure 4.2. Molecular dyes used for NLO studies in addition to styrylBODIPY dyes.

The optical limiting (OL) properties of the compounds studied here were carried out with non-aggregated organic solutions of the compounds using the z-scan setup with 7 or 10 ns laser pulses at an input intensity of *ca.* 35 μJ, except for the scandium complexes which were studied at an input intensity of *ca.* 58 μJ. The studies were carried out in different organic solvents for each set of compounds, and this was carried out after optimizing for solubility

and eliminating aggregation of the samples. The NLO responses of the novel disilane-bridged TPE architectures were also assessed using poly(bisphenol A carbonate) (PBC) polymer thin films. Because of the use of nanosecond laser pulses, the RSA responses observed are expected not to be strictly due to 2PA. Hence, the 2PA intrinsic β value cannot be measured, as would be the case if femtosecond laser pulses were used. Instead, the effective nonlinear absorption coefficient (β_{eff}) is obtained.[76,143]

4.1. Optical limiting properties of 10, 11 and 12 in CH_2Cl_2

The optical limiting properties of **10**, **11** and **12** were assessed in CH_2Cl_2.[100] For all three dyes, an extension of the π-system shifts the main absorption band to longer wavelengths relative to the 532 nm wavelength used to carry out the z-scan measurements (**Figure 4.3**). Due to the degree of ground state absorption at this wavelength, all dyes have non-zero linear absorption coefficients (α) (**Table 4.1**). Therefore, linear single-photon absorption populates the excited states enabling ESA from the S_1 state for **10** and **11** and from the T_1 state for the heavy atom-containing **12** since the bromine heavy atoms promote intersystem crossing to the triplet manifold. Hence, the RSA responses observed are due to a combination of 2PA and ESA (**Figure 4.4A**). For any material to be considered a good optical limiter, there must be a significant decrease in transmittance at increased input fluence values. All the dyes studied in this work exhibit this property. A representative plot is shown for **10** (**Figure 4.4B**).

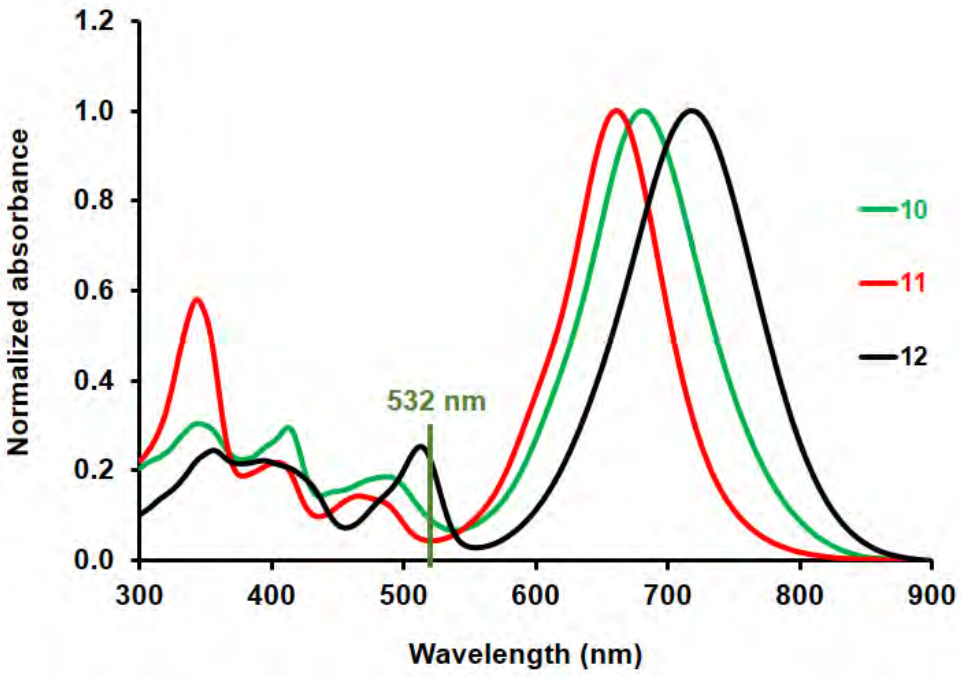

Figure 4.3. Normalized absorption spectra of **10**, **11** and **12** with the 532 nm wavelength used for the NLO studies highlighted.

Another plot of interest in OL studies is the plot of transmittance *vs* input fluence, which can be used in determining the limiting threshold intensity (I_{lim}) or the input fluence value at which nonlinear transmittance is reduced by 50% relative to the linear transmittance value (**Figure 4.4C**). It has been determined from a guideline published by the International Commission on Non-Ionizing Radiation Protection that for an exposure of 0.25 s, equal to the time for the normal human blink reflex, an exposure limit of 0.95 J.cm^{-2} is required to prevent significant damage to the human eye from the second harmonic of Nd:YAG lasers used in this work.[19,96] In other words, the I_{lim} values for a good optical limiter should be preferably below 0.95 J.cm^{-2} (**Table 4.1**). All the calculated parameters lie in the expected range as previously observed for BODIPY dyes and other organic dyes, except for the I_{lim} values, which are above 0.95 J.cm^{-2} for some of the dyes (**Table 4.1**).[20,79,95,142,144,145]

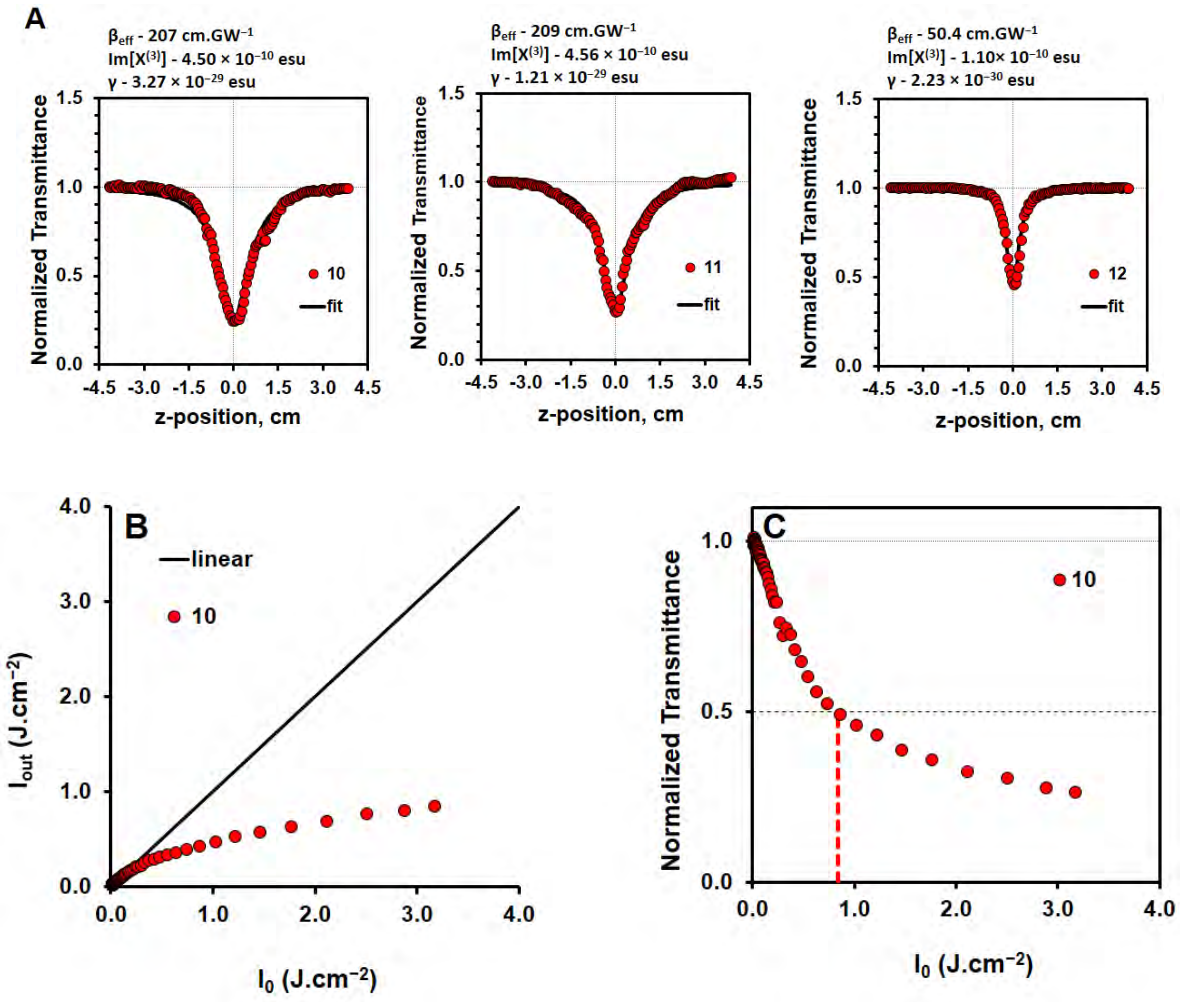

Figure 4.4. Open-aperture z-scan data for **10**, **11** and **12**; calculated parameters displayed on top of the RSA curves (A). Representative plot of output fluence (I_{0out}) *vs* input fluence (I_0) (B) and normalized transmittance *vs* input fluence curve (B); similar plots were obtained for all the other dyes studied in this work. Adapted from Ref. 100.

Two conclusions can be drawn from the differences in the parameters calculated in this work for **10**, **11** and **12**. Firstly, due to the slightly higher ϒ values obtained for **10**, which was studied at a significantly lower concentration than the other two dyes, there is evidence that BODIPY dyes of this type may possess slightly enhanced OL properties relative to other dyes. The absence of methyl groups at the 1,7-positions for **10** allows the *meso*-aryl ring to lie closer to

the π-system of the BODIPY core, enhancing the D-π-A properties that are associated with favorable OL properties. Secondly, the significantly lower values of the parameters calculated for **12** relative to those for **11** leads to the conclusion that there is no evidence that halogenation (introduction of heavy atoms) of BODIPY dyes significantly enhances OL properties, in contrast to what has been reported for other organic dyes such as metallophthalocyanines and porphyrins.[79,146]

4.2. Optical limiting properties of 13, 14 and 15 in benzene

The optical limiting properties of **13**, **14** and **15** were assessed in benzene and DMSO. It is noteworthy in this context that unlike in the previous set of compounds discussed above, **13**, **14** and **15** contain no heavy atoms. This means that the RSA responses observed (**Figure 4.6**) are expected to be due to a combination of 2PA and ESA in the singlet manifold, with no triplet states involved. Of interest in this work was comparing the effect of protons and methyl groups at the 1,7-positions for **13** and **14**, and the presence of protons for **13** and **14** and ethyl groups at the 2,6-positions for **15**. To date, there is limited information on the OL properties of 2,6-diethyl-3,5-distyrylBODIPY dyes in the literature.[95]

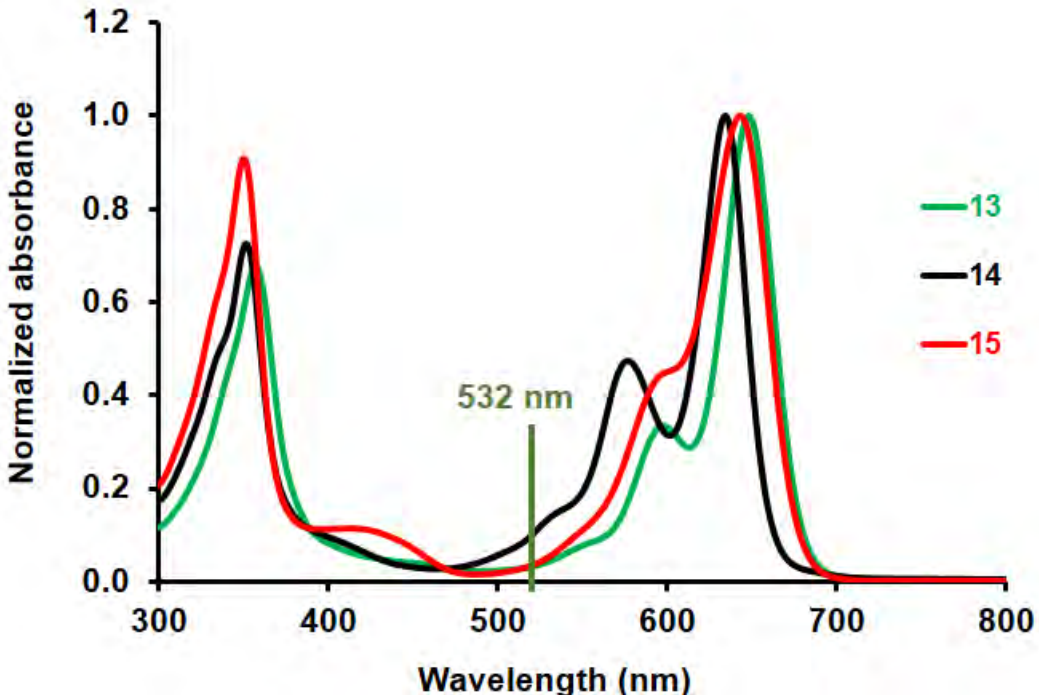

Figure 4.5. Normalized absorption spectra of **13**, **14** and **15**.

All the calculated parameters lie in the expected range, and **13** with no methyl groups at the 1,7-positions also possesses slightly enhanced OL parameters in this set of compounds (**Table 4.1**). The OL parameters of 2,6-diethyl-3,5-distyrylBODIPY dye **15** are not significantly different from those of **13**.

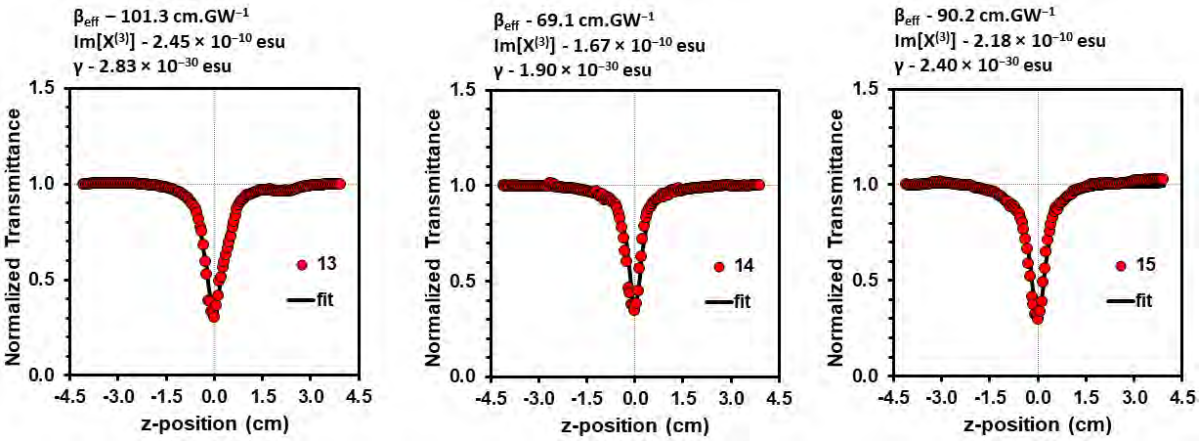

Figure 4.6. Open-aperture z-scan data for **13**, **14** and **15**.

4.3. Optical limiting properties of 16 in CH_2Cl_2

The OL properties of **16** were studied in CH_2Cl_2 to explore the mechanism responsible for the OL properties of 3,5-distyrylBODIPY dyes. The dye exhibits a favorable RSA response, and the OL parameters are highly favorable and are similar in magnitude to values previously observed for BODIPY dyes (**Figure 4.7** and **Table 4.1**).[95]

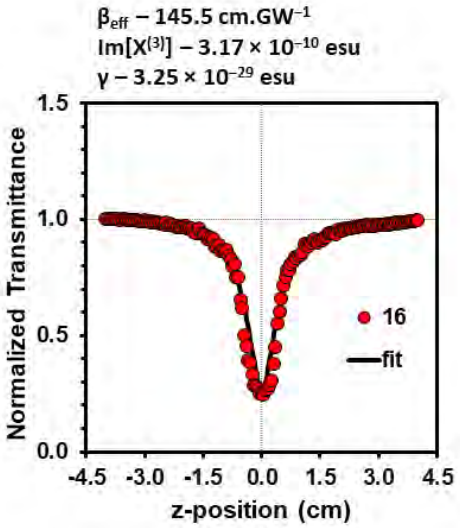

Figure 4.7. Open-aperture z-scan data for **16**. Adapted from Ref. 37.

As mentioned above, ESA in nonhalogenated BODIPY dyes is expected to occur in the singlet manifold due to the absence of intersystem crossing into the triplet manifold. Herein, the OL properties of **16** are combined with pump-probe transient absorption spectroscopy, which was carried out using femtosecond laser pulses. This study was undertaken to clearly demonstrate that ESA in nonhalogenated BODIPY dyes involves singlet excited states with no involvement of the triplet excited states. In other words, the aim was to better understand what happens during z-scan measurements when the S_1 state is populated upon electronic excitation. During the transient spectroscopic study, 5.0×10^{-3} M solutions of **16** in CH_2Cl_2 were subjected to a femtosecond laser pulse at 387.5 nm. From the transient absorption

spectrum, three intense ground state depletion peaks are observed at 371, 596 and 645 nm, and they correspond to the main absorption bands of **16** (**Figure 4.8** and **Figure 4.9A**).

Additionally, an intense broad peak is observed in the transient absorption spectrum between 400−580 nm with a maximum at 481 nm (**Figure 4.9**). In this region, **16** has minimal ground-state absorption. Hence this peak can be attributed to ESA. This ESA occurs from the S_1 state because **16** contains no heavy atoms to promote intersystem crossing into the triplet state. The decay curve observed for the transient absorption spectrum was found to be consistent with the fluorescence lifetime of **16** of 4.6 ns (**Figure 4.9B**).[37] Attempts to further confirm this were made by measuring decay curves for the triplet states of **16** using degassed CH_2Cl_2 solutions and a nanosecond laser pulse. No decay curve was observed in contrast with brominated core dye **7c**. It can therefore be concluded that the T_1 state is unlikely to play a significant role in the OL properties of the nonhalogenated **16**.

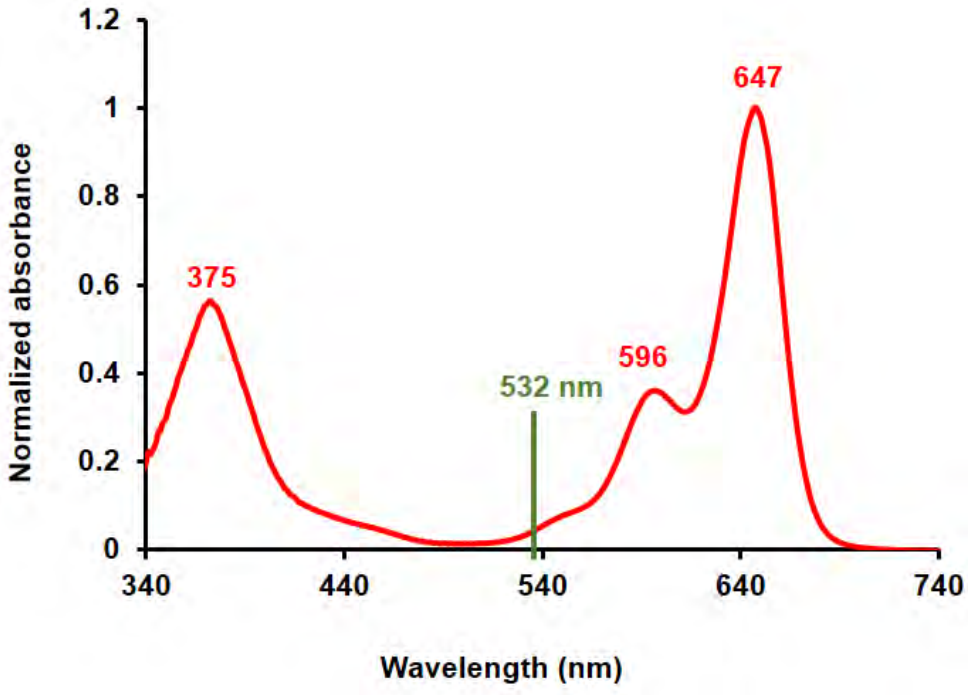

Figure 4.8. The UV-visible absorption spectrum of **16**. Adapted from Ref. 37.

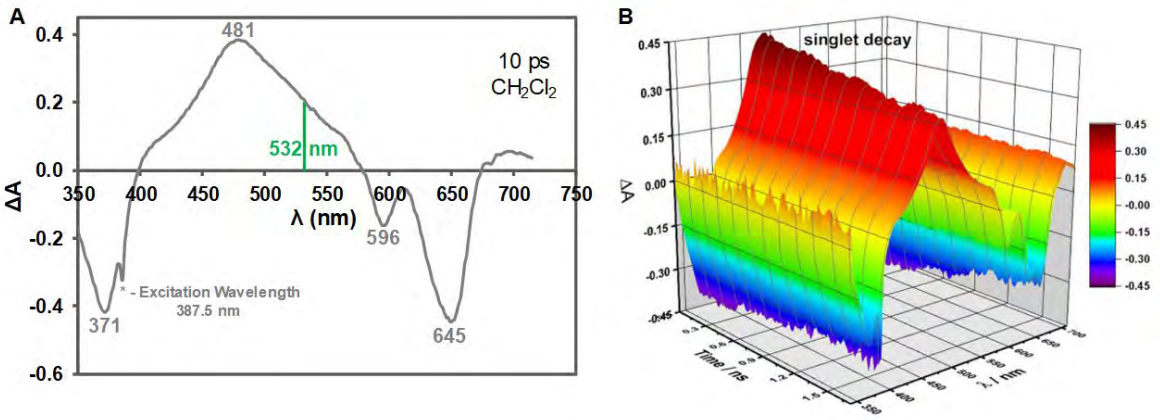

Figure 4.9. The transient absorption spectrum of **16** at 10 ps after a 150 fs laser pulse at 387.5 nm in CH_2Cl_2 (A). The 532 nm wavelength used for the open-aperture z-scan measurement is highlighted with a green vertical line. Time-resolved transient absorption spectra of **16** in CH_2Cl_2 after a 150 fs laser pulse at an excitation wavelength of 387.5 nm (B). Reproduced from Ref. 37.

4.4. Optical limiting properties of 12 and 17 in benzene and CH_2Cl_2

Structurally, **12** and **17** are analogous and differ only with respect to the electron-donating piperidinyl and diethylamino groups present on the styryl groups. The OL properties of these two dyes were studied in benzene and CH_2Cl_2, and favorable RSA responses were observed for both dyes (**Figure 4.11**). The OL properties obtained (**Table 4.1**) were similar in magnitude to those typically obtained for BODIPY dyes and other organic compounds. Additionally, there are no significant differences in the values of the OL parameters obtained for **12** and **17**. Hence, it can be concluded that from the two functional groups studied here, that there is no evidence that the nature of the nitrogen electron-donating group present on the styryl groups significantly influences the OL properties of D-π-A type BODIPY dyes.

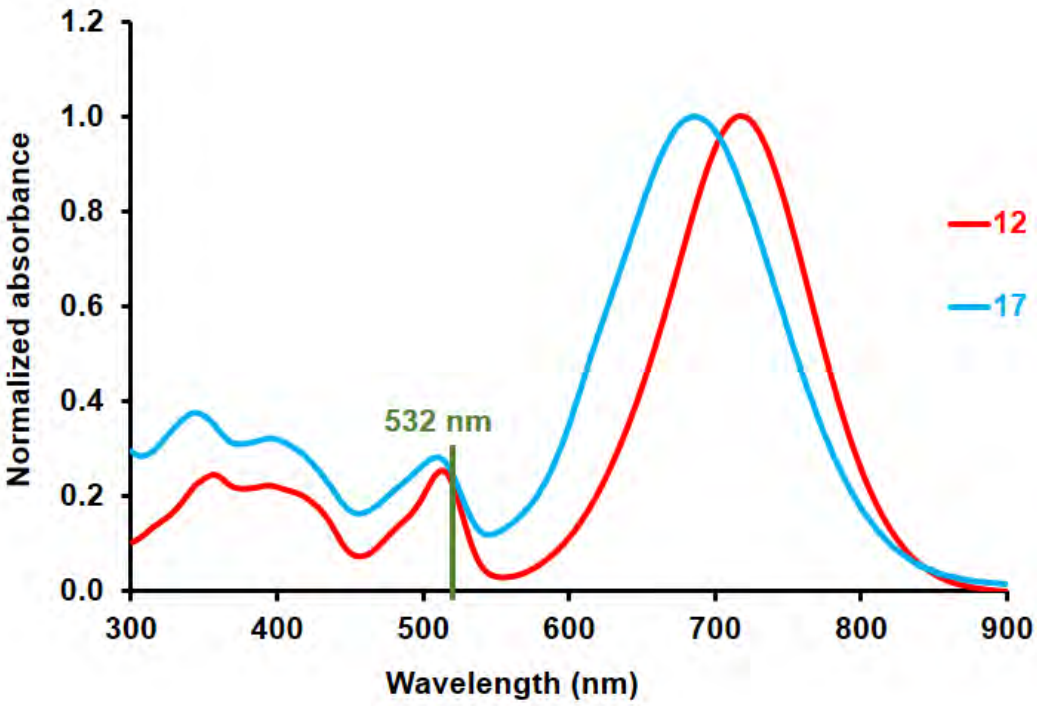

Figure 4.10. Normalized absorption spectra of **12** and **17**.

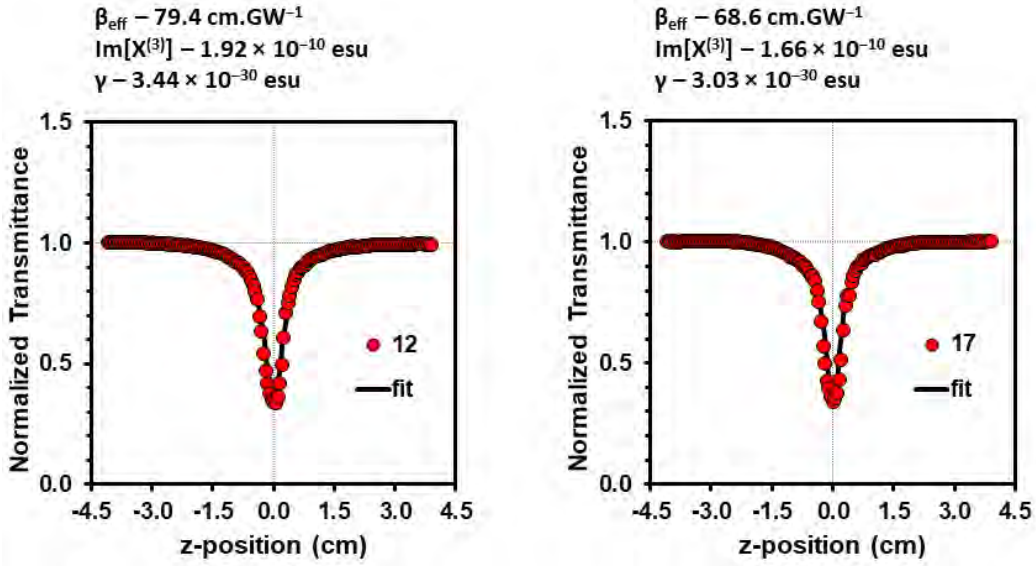

Figure 4.11. Open-aperture z-scan data for **12** and **17** in benzene.

4.5. Optical limiting properties of a 1,3,5-tristyrylBODIPY dye (25) in DMF

The NLO properties are discussed above for a monostyrylBODIPY and several distyrylBODIPY dyes. In this section, the NLO properties derived from a study carried out using organic solutions of a 1,3,5-tristyrylBODIPY dye, **25** are discussed.[142] This study provides data that provide a basis for comparing the NLO properties of tristyrylBODIPY dyes with the NLO properties of other styrylBODIPY dyes. BODIPY **25** was previously synthesized by an MSc student at Rhodes University,[133] and no structural and photophysical characterization is carried out in this work as the interest is on assessing NLO properties.

From the UV-visible absorption spectrum, it is evident that **25** absorbs significantly at 532 nm (**Figure 4.12**), in a similar manner to the distyrylBODIPY dyes discussed above. This leads to large α values, especially at the higher concentration of 2.1×10^{-4} M (**Table 4.1**). In a similar manner to the dyes discussed above, the RSA responses observed are due to a combination of 2PA and ESA (**Figure 4.13A**). This is because the presence of linear single-photon absorption, which leads to the population of the excited states, enables ESA from the S_1 and T_1 states. The triplet manifold is involved because the bromine heavy atoms at the 2,6-positions of **25** promote intersystem crossing to the triplet manifold. This intersystem crossing to the triplet manifold is confirmed by the singlet oxygen quantum yield of 0.17 in ethanol, previously reported for **25**.[133] It is evident that as is often observed for styrylBODIPY dyes, the organic solvent solutions of **25** lead to a significant decrease in transmittance at increased input fluence values (**Figure 4.13B**). The OL parameters of **25** obtained at concentrations of 1.1×10^{-4} and 2.1×10^{-4} M, and input pulse energies of 30 and 45 μJ are not significantly different from those reported for other styrylBODIPY dyes (**Table 4.1**).[95] However, it is significant that the α value related to linear absorption is significantly higher. The reasons for

this and the implications for the utility of these dyes for OL applications will be described in detail in Chapter 6.

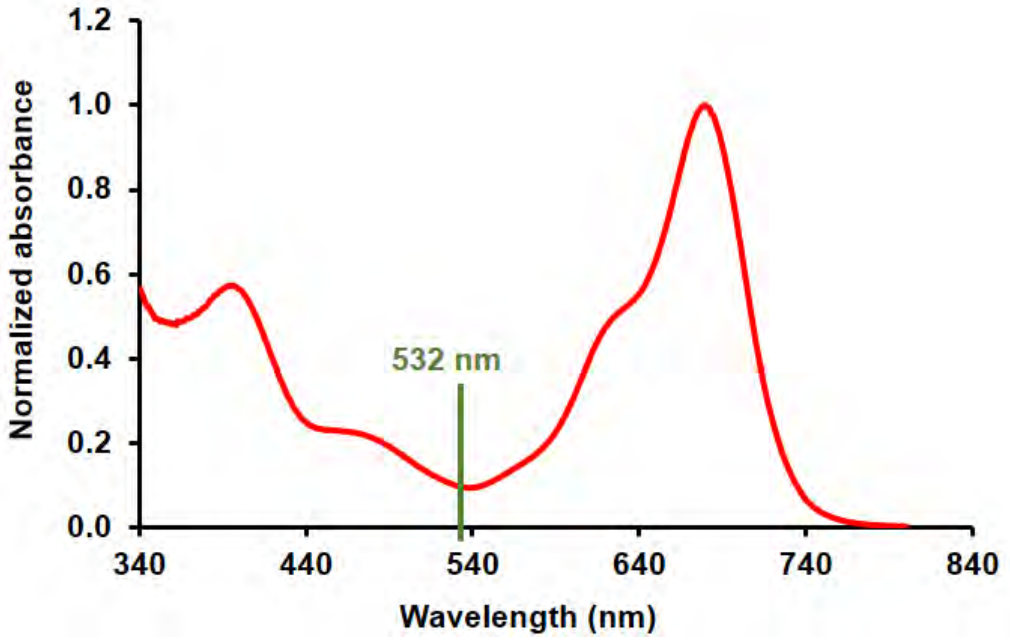

Figure 4.12. The UV-visible absorption spectrum of **25**.

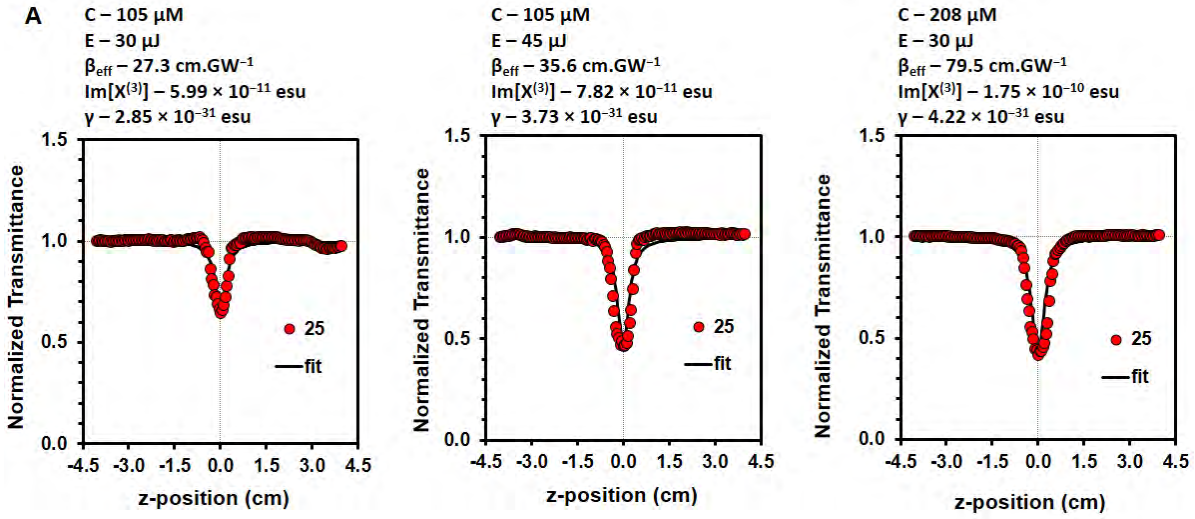

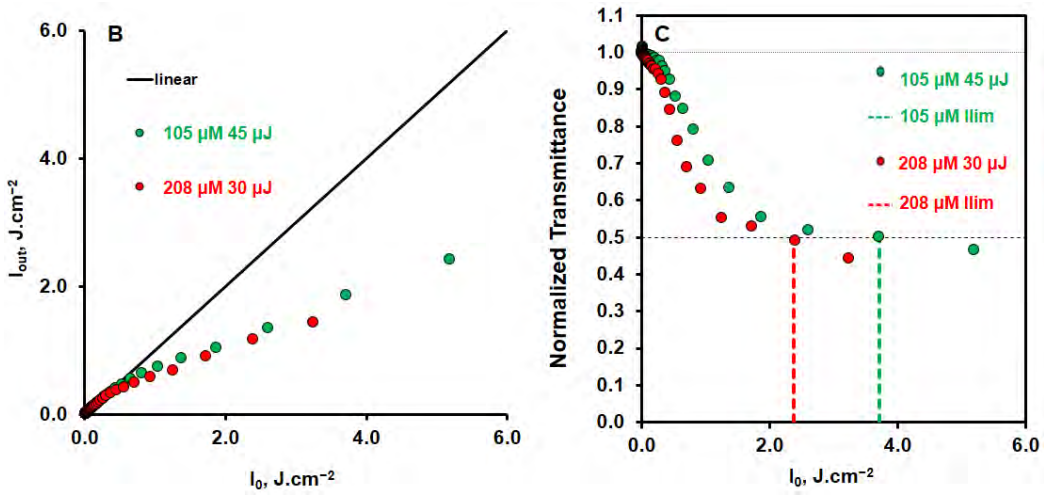

Figure 4.13. Open-aperture z-scan data for **25**; concentration, input pulse energy and calculated parameters displayed on top of the RSA curves (A). A plot of output fluence (I_{0out}) *vs* input fluence (I_0) (B) and normalized transmittance *vs* input fluence curve (B). Adapted from Ref. 142.

4.6. Summary of BODIPY NLO properties

Table 4.1. Nonlinear optical limiting parameters of BODIPY dyes **10**–**17** and **25**.

	Solvent	Conc. (M)	α (cm^{-1})	β_{eff} ($cm.GW^{-1}$)	Im[$\chi^{(3)}$] (esu)	γ (esu)	I_{lim} ($J.cm^{-2}$)
10		7.0×10^{-6}	0.71	206.8	4.50×10^{-10}	3.27×10^{-29}	0.8
11	CH_2Cl_2	1.9×10^{-5}	1.51	209.3	4.56×10^{-10}	1.21×10^{-29}	0.9
12		2.3×10^{-5}	0.68	50.4	1.10×10^{-10}	2.23×10^{-30}	4.3
13	Benzene	3.6×10^{-5}	0.28	101.3	2.45×10^{-10}	2.83×10^{-30}	1.5
	DMSO	2.2×10^{-5}	0.30	103.0	2.42×10^{-10}	4.87×10^{-30}	2.3

14	Benzene	3.6×10^{-5}	0.99	69.1	1.67×10^{-10}	1.90×10^{-30}	1.5
	DMSO	2.2×10^{-5}	0.76	5.8	1.37×10^{-11}	2.80×10^{-31}	N/A
15	Benzene	3.6×10^{-5}	0.53	90.2	2.18×10^{-10}	2.40×10^{-30}	1.6
	DMSO	2.2×10^{-5}	0.32	22.3	5.23×10^{-11}	1.06×10^{-30}	N/A
16	CH_2Cl_2	4.9×10^{-6}	0.78	145.5	3.17×10^{-10}	3.25×10^{-29}	0.8
17	Benzene	2.3×10^{-5}	0.45	68.6	1.66×10^{-10}	3.03×10^{-30}	2.0
	CH_2Cl_2	2.3×10^{-5}	0.54	36.6	7.96×10^{-11}	1.74×10^{-30}	5.0
12	Benzene	2.3×10^{-5}	0.45	79.4	1.92×10^{-10}	3.44×10^{-30}	2.0
25	DMF	1.1×10^{-4}	1.11	27.3	5.99×10^{-11}	2.85×10^{-31}	N/A
				35.6	7.82×10^{-11}	3.73×10^{-31}	3.7
		2.1×10^{-4}	2.26	79.5	1.75×10^{-10}	4.22×10^{-31}	2.4

4.7. Optical limiting properties of scandium phthalocyanine complexes in $CHCl_3$

Phthalocyanines have been shown to possess favorable OL properties. This is true for monophthalocyaninates, bisphthalocyaninates, trisphthalocyaninates and other multidecker sandwiches.[111,147–151] From these studies, it has been demonstrated that the presence of rare earth metals in the central cavity of these phthalocyanine complexes promotes π-π interaction between macrocycles, hence enhancing the OL properties of multidecker phthalocyanines.[111,148,150] In this work, the OL properties of scandium phthalocyanine complexes were investigated for the first time using the second harmonic of the Nd:YAG laser

at 532 nm. Of the trivalent metal cations with strong Lewis acidity, scandium has the smallest ionic radius, enabling it to form exotic coordination compounds.[152,153] Like other trivalent central metal ions, scandium can also form double-decker complexes existing as radical species and nonradical anions.[106,141]

The scandium phthalocyanines used contain peripheral benzo-fused 15-crown-5 (15C5) crown ether moieties (**Figure 4.2A**).[106,141] The first complex is a bisphthalocyaninate, and both the radical/green (**I**) and anionic/blue (**Ia**) forms of the complex were studied. The second complex is a monophthalocyaninate (**II**). To correct for the differences observed in the spectral properties of the monomeric **II** and the dimeric **I** and its anionic form, **Ia**, the z-scan measurements were carried out using a fixed concentration and incident laser pulse energy. The dyes had minimal ground state absorption at 532 nm (**Figure 4.14**), and this is also evident from the relatively low values for the linear absorption coefficients, α (**Table 4.2**).

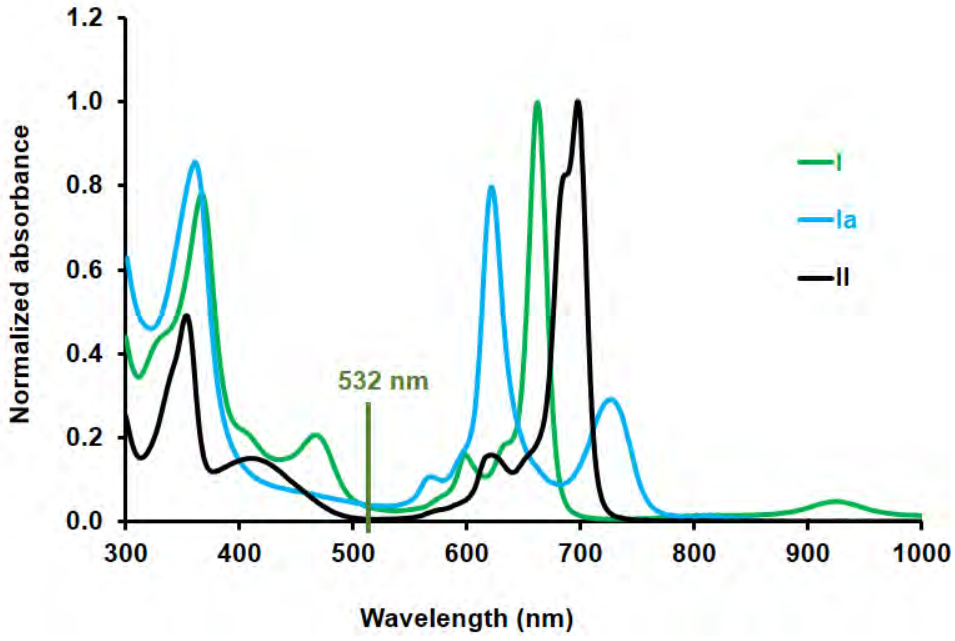

Figure 4.14. Normalized absorption spectra of scandium phthalocyanine complexes **I**, **Ia** and **II** in $CHCl_3$. Adapted from Ref. 141.

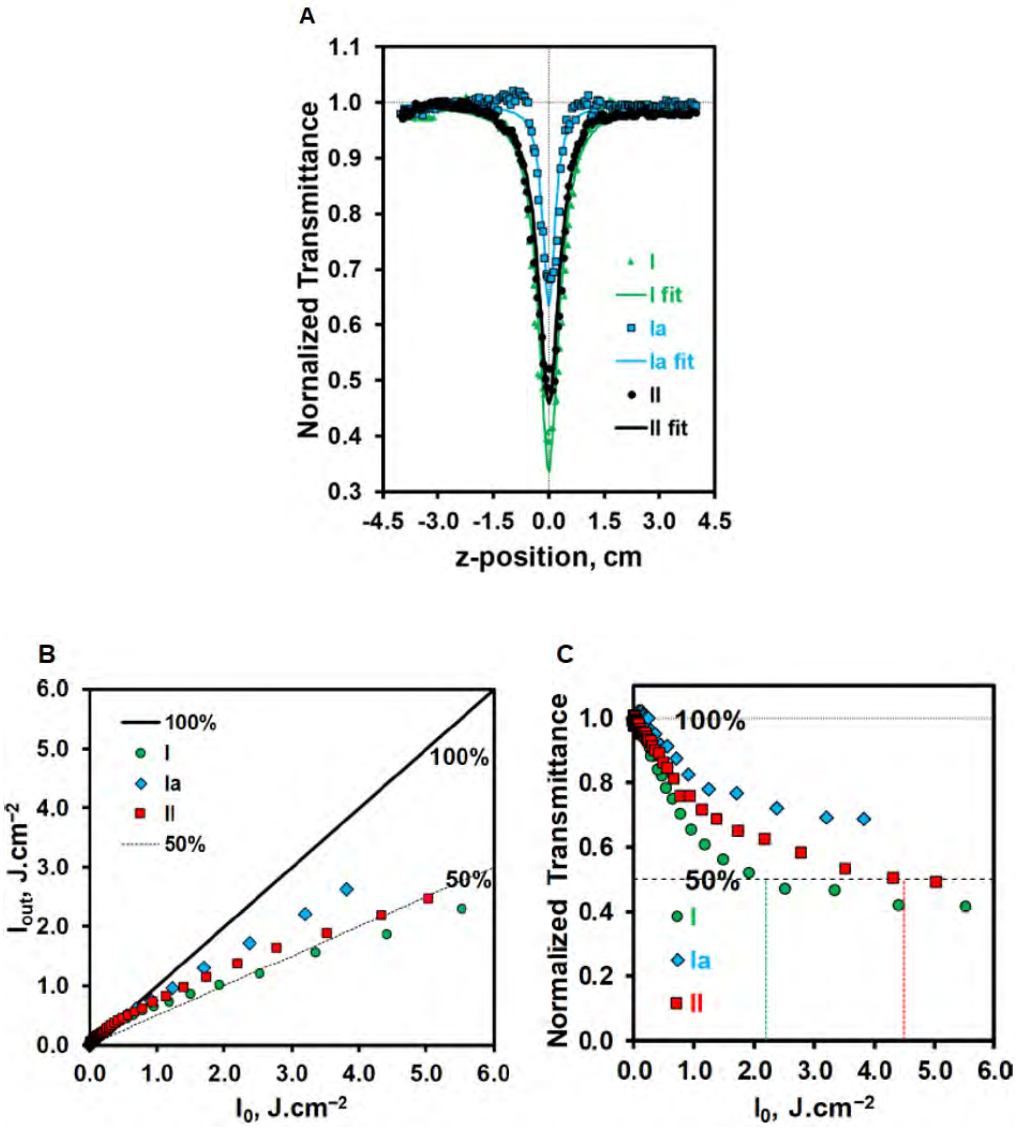

Figure 4.15. Open-aperture z-scan data for **I**, **Ia** and **II** (A). Plots of output fluence (I_{0ut}) *vs* input fluence (I_0) (B) and normalized transmittance *vs* input fluence curve (B). Reproduced from Ref. 141; Copyright World Scientific Publishing, 2020.

Strong RSA responses can be observed in the data obtained during the z-scan measurements using $CHCl_3$ solutions of **I**, **Ia** and **II** (**Figure 4.15A**). These RSA responses probably arise from multiple processes, as explained with halogenated and nonhalogenated BODIPY dyes above. Because there is scope for linear absorption due to the non-zero α values, one photon absorption from the ground state is likely to be followed by ESA from the S_1 and T_1 excited

states. From the plot of output fluence *vs* input fluence (**Figure 4.15B**), it is evident that the Sc(III) complexes do not lead to a significantly attenuated transmittance at high incident fluence values. This is known to be a requirement for a material to be considered as an optical limiter, as is the case for many metallophthalocyanines and the BODIPY dyes studied in this work and elsewhere. All the OL parameters obtained for **I**, **Ia** and **II** lie in the expected range except the I_{lim} values, which are all above 0.95 J.cm^{-2} (**Figure 4.15C** and **Table 4.2**). It can therefore be concluded that from the results obtained in this work, the presence of the Sc(III) ion is unlikely to significantly improve OL properties of double-decker phthalocyanines to magnitudes more favorable than what has been previously reported for rare earth metal phthalocyanine complexes.

Table 4.2. Nonlinear optical limiting parameters of **I**, **Ia** and **II** at a concentration of *ca.* 5.8 × 10^{-6} M and an input pulse energy of 58 μJ.

Dye	**α (cm^{-1})**	**β_{eff} (cm.GW^{-1})**	**Im[$\chi^{(3)}$] (esu)**	**γ (esu)**	**I_{lim} (J.cm^{-2})**
I	0.13	62	1.3 × 10^{-10}	1.3 × 10^{-29}	2.2
Ia	0.82	27	5.6 × 10^{-11}	5.3 × 10^{-30}	-
II	0.12	41	8.8 × 10^{-11}	8.0 × 10^{-30}	4.5

4.8. Reverse saturable absorption curves of disilane-bridged architectures in PBC polymer thin films

A series of novel σ-bridged molecules connected *via* disilane linkers were synthesized and characterized at the Hangzhou Normal University, and the optical limiting properties of these were studied in THF and PBC polymer thin films at Rhodes University during the course of this PhD work.[139] The transparent thin films were prepared using 9.0 x 10^{-5} M solutions (2.5 mL) of **3a-d** and **4** mixed with PBC (100 mg) in THF. The mixture was sonicated for 15 min and then left to stir at room temperature, and subsequently, using a drop and dry method, a fraction of the solution was transferred onto a glass slide placed on a Petri dish. The film thicknesses were measured using the knife-edge attachment of a Bruker D8 Discover X-ray diffraction (XRD) system. The curves obtained during the study are displayed below (**Figure 4.16**).[140]

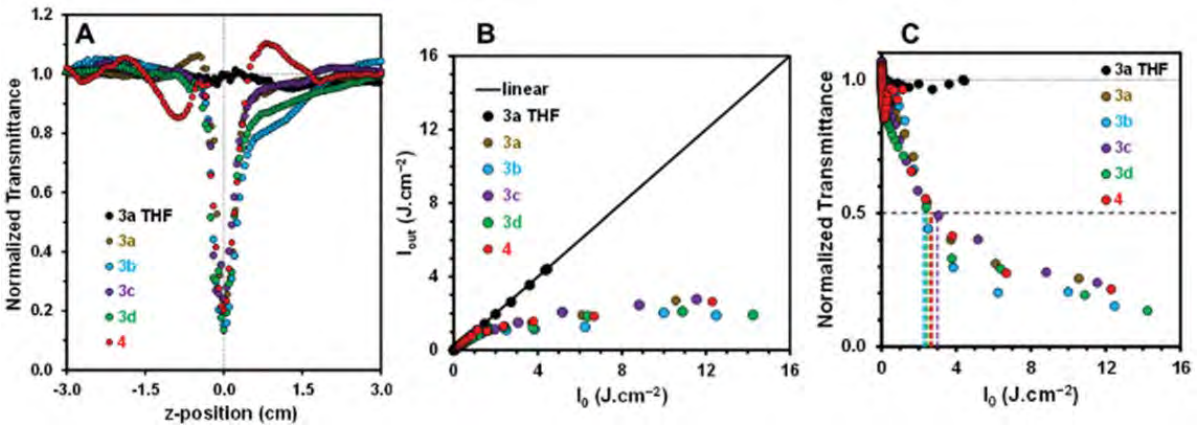

Figure 4.16. Open-aperture z-scan curves (A), plots of output fluence (I_{0ut}) *vs* input fluence (I_0) (B) and normalized transmittance *vs* input fluence curve (C) of **3a-d** and **4** in PBC thin films and in THF for **3a**. Reproduced with permission from Ref. 140; Copyright Royal Society of Chemistry, 2021.

During the z-scan measurements, negligible OL properties were observed in THF solutions since there was no significant RSA response for **3a-d** and **4**. The RSA curve and plots obtained for the THF solution of **3a** are shown above as an example (**Figure 4.16**). When the z-scan measurements were carried out using the PBC polymer thin films, strong RSA responses were observed (**Figure 4.16A**). The β_{eff} values from the fitted RSA curves of **3a-d** and **4** PBC polymer thin films were calculated to be 51, 110, 61, 91 and 48 cm·GW^{-1}, respectively. The I_{lim} values were determined to be 2.6, 2.3, 3.0, 2.4 and 2.7 J.cm^{-2} for the **3a-d** and **4** PBC polymer thin films, respectively (**Figure 4.16C**). As mentioned above, the I_{lim} values for a good optical limiter at 532 nm should be below 0.95 J.cm^{-2}. Therefore, the values obtained in this work are not low enough. However, they could easily be further lowered by increasing the concentration of **3a-d** and **4** used to prepare the thin films.

4.9. Concluding remarks

The OL studies undertaken here using non-aggregated solutions of BODIPY dyes in organic solvents further demonstrate the potential suitability of these dyes in the fabrication of OL materials with real-life applications such as in aviation safety. All the BODIPYs exhibited favorable reverse saturable absorption responses characterized by a significant decrease in transmittance at high laser light intensity and as the focal point of the z-scan instrument is approached. The main purpose of the NLO studies undertaken in this thesis was to investigate the effect of specific structural modifications within series of BODIPYs on their optical limiting properties.

The properties obtained for **15** are not significantly different to those of **13**. Hence it can be concluded that there is scope for research into 2,6-diethyl-3,5-distyrylBODIPY dyes as this is

the first report on the OL properties of BODIPY dyes of this type. Since the presence of heavy atoms on the BODIPY core does not significantly enhance BODIPY OL properties,[93] **16** was used to better understand the mechanism responsible for the typically favorable NLO responses observed for nonhalogenated BODIPY dyes.[37] This was done using transient spectroscopy with a femtosecond laser system wherein a broad band in the visible region attributed to ESA from the S_1 state was observed since the associated decay curve was consistent with the fluorescence lifetime of **16**. This ESA is therefore associated with the S_1 rather than the T_1 state because **16** contains no heavy atoms to promote intersystem crossing. This was further confirmed by triplet state decay curve measurements in which no signal was observed for **16** in contrast with brominated core dye **7c**.[37] The favorable NLO responses observed for nonhalogenated BODIPY dyes can therefore be attributed to one-photon absorption from the ground state followed by ESA in the singlet manifold.

From the comparative study of the OL properties of the structurally analogous **12** and **17** dyes, there are no significant differences observed in the OL parameters obtained for these two dyes. This leads to the conclusion that the nature of the nitrogen electron-donating group present on the styryl groups does not significantly influence the OL properties of D-π-A type BODIPY dyes. The OL parameters obtained for the 1,3,5-tristyrylBODIPY dye **25** are not significantly different to those of **10-17** and other 3,5-distyrylBODIPY dyes which have been previously reported.[95,141] This means that 1,3,5-tristyrylBODIPY dyes do not possess more favorable properties than other styrylBODIPY dyes. Therefore, monostyrylBODIPY, distyrylBODIPY, and tristyrylBODIPY dyes all possess OL parameters with values similar in magnitude and in the anticipated ranges that have been reported for other molecular dyes that are viewed as favorable for this application.

The OL properties of a monomeric scandium phthalocyanine and those of the green and blue forms of a dimeric scandium phthalocyanine were also investigated in this work.[141] Although similar in magnitude to what has been observed for other phthalocyanines of this type, the results obtained are not exceptional. Since this was the first report of the OL properties of a scandium phthalocyanine, it can be concluded based on these results that the Sc(III) ion does not significantly enhance OL properties of phthalocyanines to better magnitudes than what has been observed for other metallophthalocyanines, especially rare earth metal phthalocyanine complexes.[109,111,147–151]

The promising OL properties of the BODIPY dyes studied above are broadly comparable to the properties previously reported for other types of organic dye, such as porphyrins and phthalocyanines.[85,88,89] They can be further enhanced in two ways. Firstly, by embedding the dyes in polymer thin films and secondly by conjugation to nanomaterials, as both have been used to enhance the OL properties of BODIPY dyes and other types of organic dyes.[19,147,154–157] The other challenge that may arise when using BODIPY dyes to fabricate protective OL materials is their significant absorption in the visible region. This is problematic because OL materials should ideally remain transparent under ambient light conditions when protection of the human eye is involved. This can be addressed by modifying the BODIPY structure and shifting the main spectral band of the BODIPY chromophore to the red so that there is minimal absorbance across the entire visible region.

Alternatively, research into compounds known to not absorb significantly in the visible region may help alleviate this challenge. The OL properties of the optically transparent disilane-bridged compounds from collaborative work that do not absorb significantly in the visible region (*ca.* 400–700 nm) are reported above.[140] These dyes exhibit excellent RSA responses

when embedded in PBC to create transparent polymer this films. These transparent films are a step towards the creation of OL materials for potential real-life applications. A possible drawback with the results obtained using these PBC polymer thin films is that the I_{lim} values were above 0.95 $J.cm^{-2}$. However, these values could be further lowered by increasing the concentration of the dye used to prepare the thin films and/or their pathlength.

Chapter 5:

Photodynamic Antimicrobial Chemotherapy (PACT) properties of neutral BODIPY dyes against *Staphylococcus aureus*

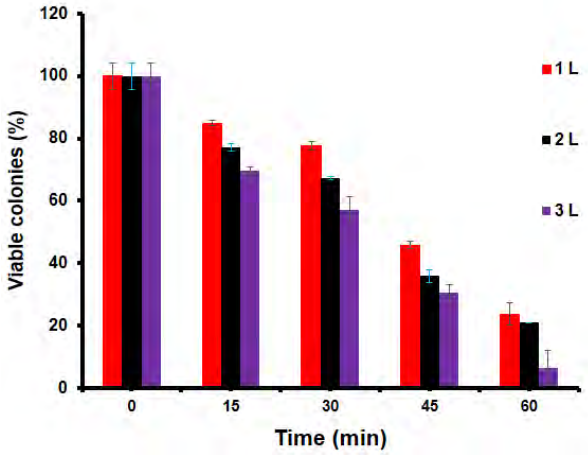

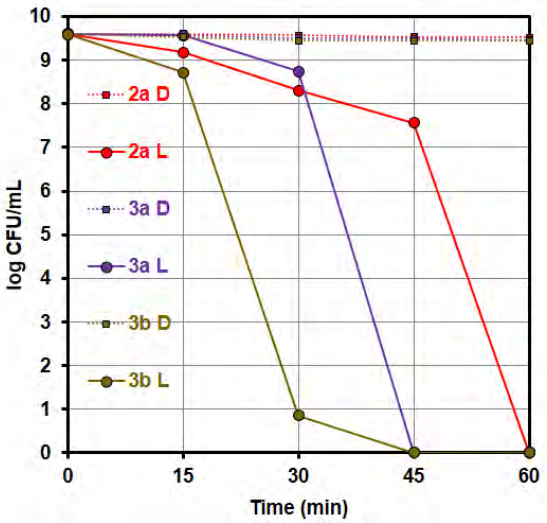

This chapter covers the results obtained from the photodynamic antimicrobial chemotherapy (PACT) studies conducted using neutral brominated and iodinated BODIPY dyes (**Figure 5.1**). PACT has been shown to be an effective alternative to antibiotics for targeting both gram-negative and gram-positive bacteria, yeasts and fungi. This becomes important in the context of antibiotic-resistant microorganisms.[158] Gram-positive bacteria have a porous peptidoglycan layer which allows drugs such as antibiotics and photosensitizers to bypass the cytoplasmic membrane and localize in the cytoplasm.[159] Gram-negative bacteria, on the other hand, contain a cell wall with an inner and an outer membrane on either side of the peptidoglycan layer. This cell wall makes it impossible for neutral and anionic photosensitizers to localize in the cytoplasm.[59,159] In this work, the suitability of BODIPY dyes as photosensitizers in the photoinactivation of the gram-positive *Staphylococcus aureus* is being assessed. BODIPY dyes are known to be small zwitterionic molecules that can be taken up by gram-positive bacteria.[72,160,161] The singlet oxygen quantum yields of these dyes were quantified in Chapter 3.

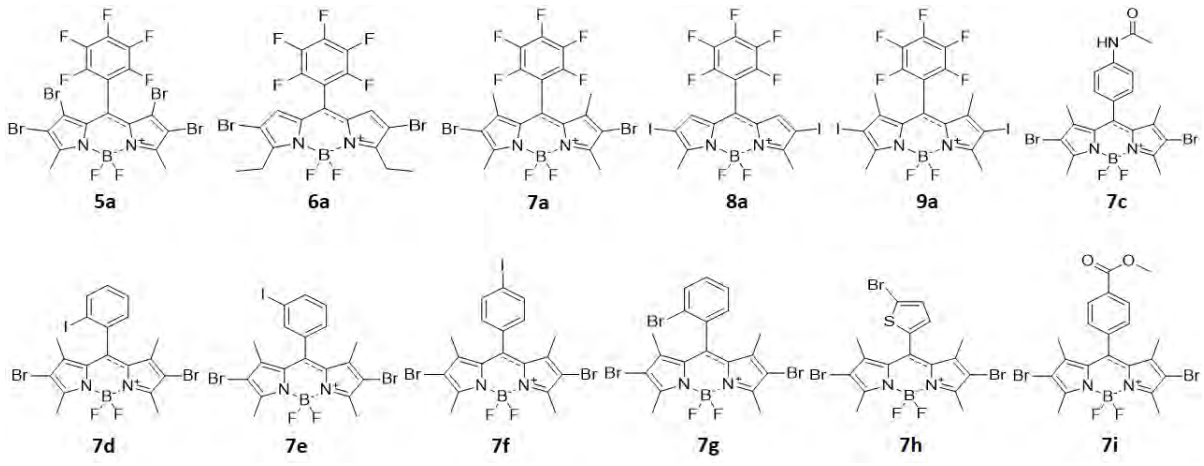

Figure 5.1. Halogenated BODIPY dyes used for PACT studies.

BODIPY dyes **5a**, **6a**, **7a**, **8a** and **9a**, are structurally analogous with minor differences on the BODIPY core. The main differences are the absence and presence of methyl groups at the 1,7-positions, the presence of ethyl or methyl groups at the 3,5-positions, and the presence of bromine or iodine heavy atoms at the 2,6-positions. The other analogous dyes are **7d**, **7e** and **7f**, which contain iodine atoms at different positions of the *meso*-aryl ring.

5.1. PACT Studies of *Staphylococcus aureus* in solution

The PACT studies were carried out in 2% DMSO-PBS due to the insolubility of the dyes being studied in PBS. In a similar manner to what has been previously reported,[18,61,161] the bacterial cells were also studied in 2% DMSO-PBS in the absence of BODIPY dyes as a control experiment, and the bacterial cells remained viable. Initially, the dyes were studied at different concentrations, and the lowest concentration of 1 μM could eliminate viable bacteria after irradiation for some of the dyes (**Figure 5.2A**). In instances where the dyes did not completely eliminate viable bacteria, the bacterial viability was reduced to values significantly less than 50% (**Figure 5.2A**), except for **5a**, as will be discussed below. Because of this, the photodynamic inactivation studies were carried out using 1 μM dye solutions for all the BODIPYs to maintain consistency.

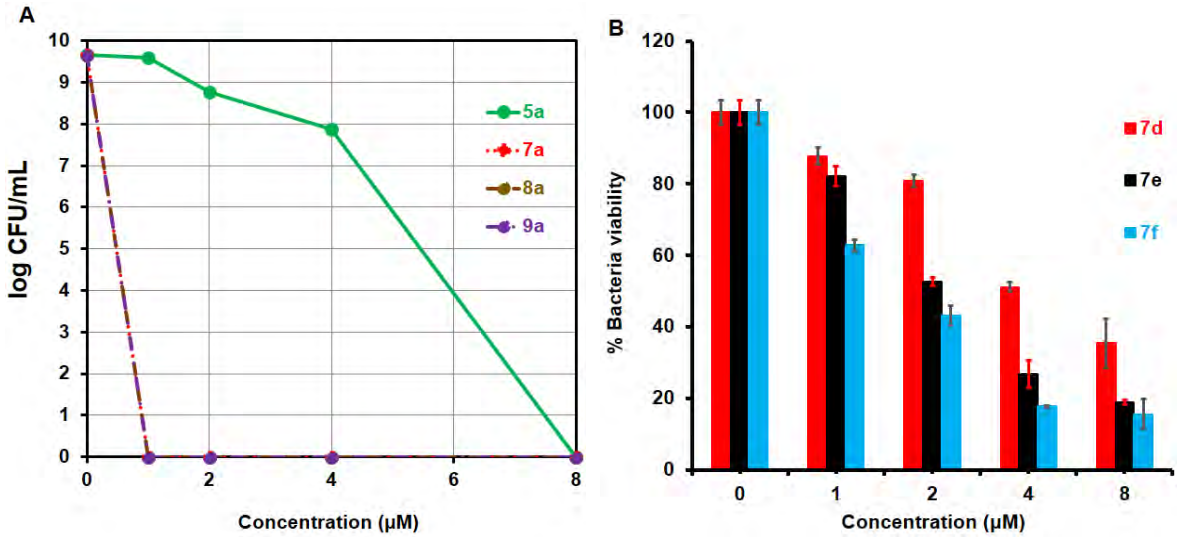

Figure 5.2. Representative plots for the photodynamic inactivation of *Staphylococcus aureus* by different concentrations of **5a**, **7a**, **8a** and **9a** after 60 min irradiation (A) and **7d**, **7e** and **7f** after 30 min irradiation (B).

The *Staphylococcus aureus* was grown on agar plates by following the manufacturer's specifications. An individual colony was subsequently inoculated into the nutrient broth and agitated on a rotary shaker (*ca.* 200 rpm) overnight at 37°C to obtain the bacterial culture used for the study. Aliquots of this culture were then transferred to 6 mL of fresh broth and incubated at 37°C to obtain a mid-logarithmic phase (OD 620 nm ≈ 0.6). The optical density of the culture was determined using the Ledetect 96 from Labxim Products so that log reduction values could be calculated in units of colony-forming units per millilitre ($CFU.mL^{-1}$). The broth was removed by centrifugation at 3000 rpm for 15 min followed by washing with PBS three times. The culture was diluted to 1/1000 in PBS to give the working stock solution. The photodynamic antimicrobial studies were then performed following previously reported methods.[161–163]

During the experiments, suspensions of the bacteria were incubated in an oven equipped with a shaker for 30 min in the dark at 37°C. Then, half (3 mL) of the incubated bacterial suspensions were irradiated close to the absorption maxima of the dyes in a 24 well plate. The irradiations were carried out using a Thorlabs M530L3 light emitting diode (LED) mounted onto the housing of a Modulight 7710-680 medical laser system. An irradiance value of 110 $mW.cm^{-2}$ was measured with a Coherent FieldmaxII TOP energy/power meter fitted with a Coherent Powermax PM10 sensor. The other half of the suspension was kept in the dark. After irradiation, 100 µL samples were inoculated in triplicates, and the plates were incubated inverted at 37°C overnight.

5.2. Results and discussion

5.2.1. PACT activity

The BODIPY dyes used as photosensitizers in this work were only able to significantly reduce the viability of *Staphylococcus aureus* in the presence of light, i.e. there was minimal dark toxicity as a significant number of cells remained viable when stored in the dark (**Figure 5.3** and **Figure 5.4**). This shows that, as expected, when BODIPY dyes are used as photosensitizers, it is indeed cytotoxic oxygen species that inactivates the *Staphylococcus aureus*.[72,160,161]

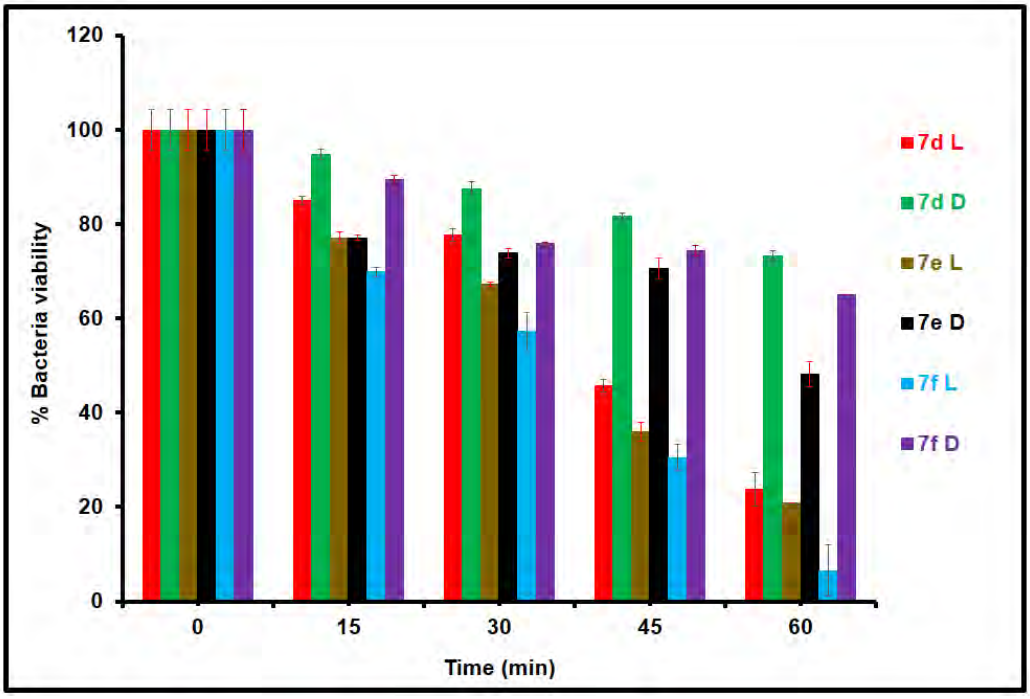

Figure 5.3. PACT inactivation of *Staphylococcus aureus* after 60 min irradiation. Studies were carried out using 1 µM BODIPY solutions.

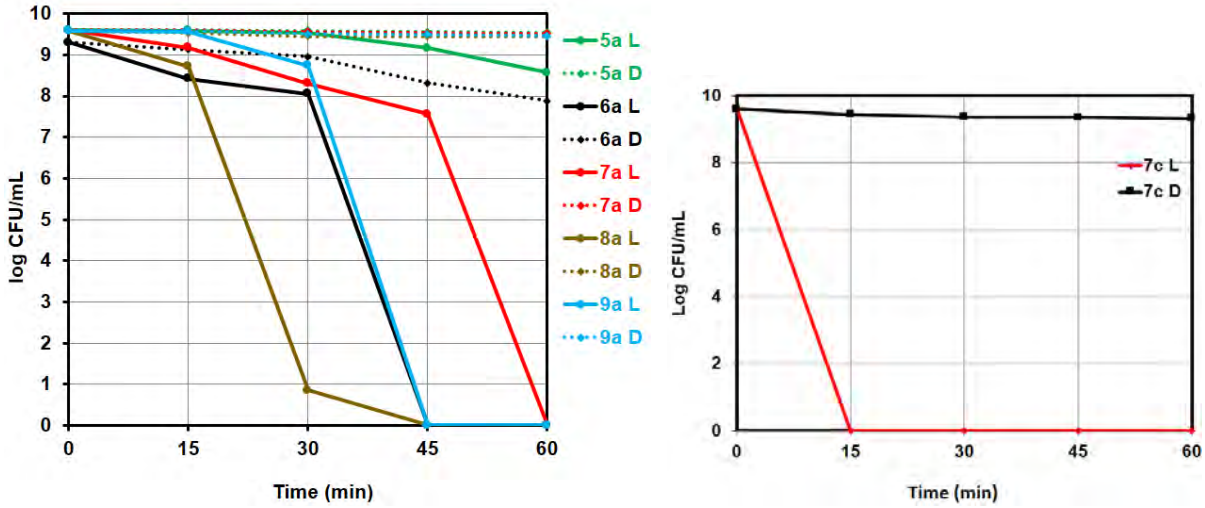

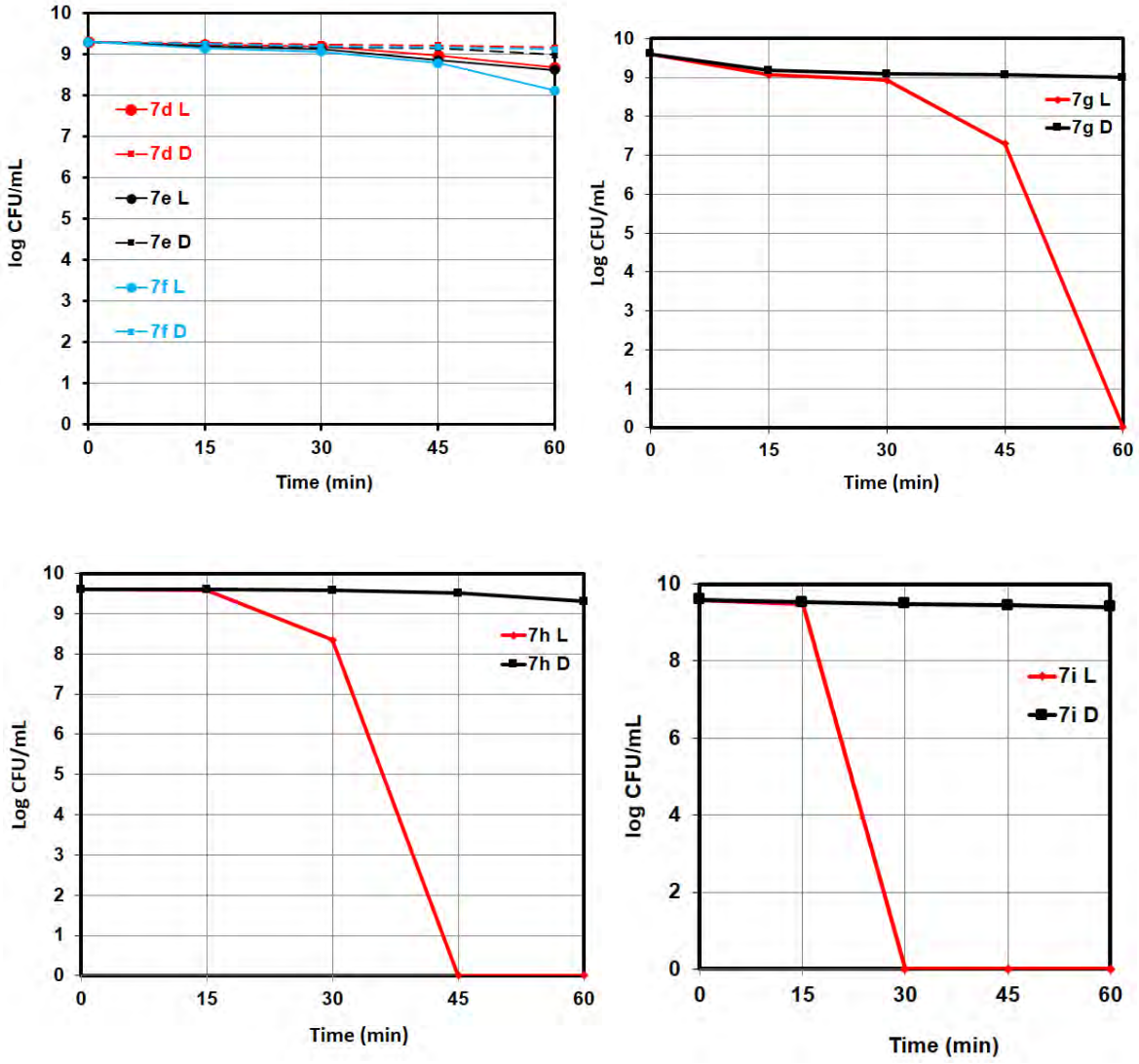

Figure 5.4. Log reduction curves for *Staphylococcus aureus* during the PACT inactivation studies. Studies were carried out using 1 µM BODIPY solutions.

The dyes used in this work were mainly used to assess the effects of structural differences on the PACT activity of BODIPY dyes. There is no significant difference in PACT activity among the analogous BODIPYs **7d**, **7e** and **7f**, with **7f** displaying slightly higher PACT activity (**Figure 5.4**). For **5a**, **6a**, **7a**, **8a** and **9a**, the presence of iodines on the BODIPY core enhances antimicrobial activity relative to the activity of bromine-containing dyes except for **6a**. This can be attributed to the heavy atom effect as iodine is heavier and is expected to significantly

enhance intersystem crossing to the triplet state and singlet oxygen generation. On the other hand, the activity of **6a**, which is comparable to the iodinated **8a** and **9a** (**Figure 5.4**), can be attributed to the absence of methyl groups at the 1,7-positions. Similar observations can be made for **8a** relative to **9a**, where **8a** shows higher activity within the first thirty min of irradiation. Both **6a** and **8a** do not contain methyl groups at the 1,7-positions. This is likely to eliminate steric strain and allow the *meso*-aryl ring to lie closer to the plane of the π-system of the BODIPY core. This will be demonstrated in Chapter 6. At this point, it is not clear whether this plays a role in the cellular uptake and activity of BODIPYs of this type. Related to this point is how the lowest activity was observed for **5a**, which has four bromine atoms at the 1,7- and 2,6-positions. It is unclear whether the steric strain introduced by the bromine atoms at the 1,7-positions plays a role in the low PACT activity observed for **5a**, in addition to the significantly lower singlet oxygen quantum yield.

5.2.2. Photostability of 5a, 7a, 8a and 9a

During the irradiation of photosensitizers, the singlet oxygen produced can degrade the photosensitizer through a process known as photobleaching.[164,165] To assess this, the stability of **5a**, **7a**, **8a** and **9a** was studied. DMSO solutions of the BODIPYs were irradiated with the Thorlabs M530L3 LED (110 $mW.cm^{-2}$) used to carry out the bacterial inactivation studies detailed above. The irradiations were carried out for 60 min with the LED mounted onto the housing of a Modulight 7710-680 medical laser system in a similar manner to the PACT activity studies. The samples were subsequently stored in the dark for a further 48h, and UV-visible absorption spectra were recorded at 24 h intervals (**Figure 5.5**). A control study was carried out wherein the spectra of dyes stored in the dark.

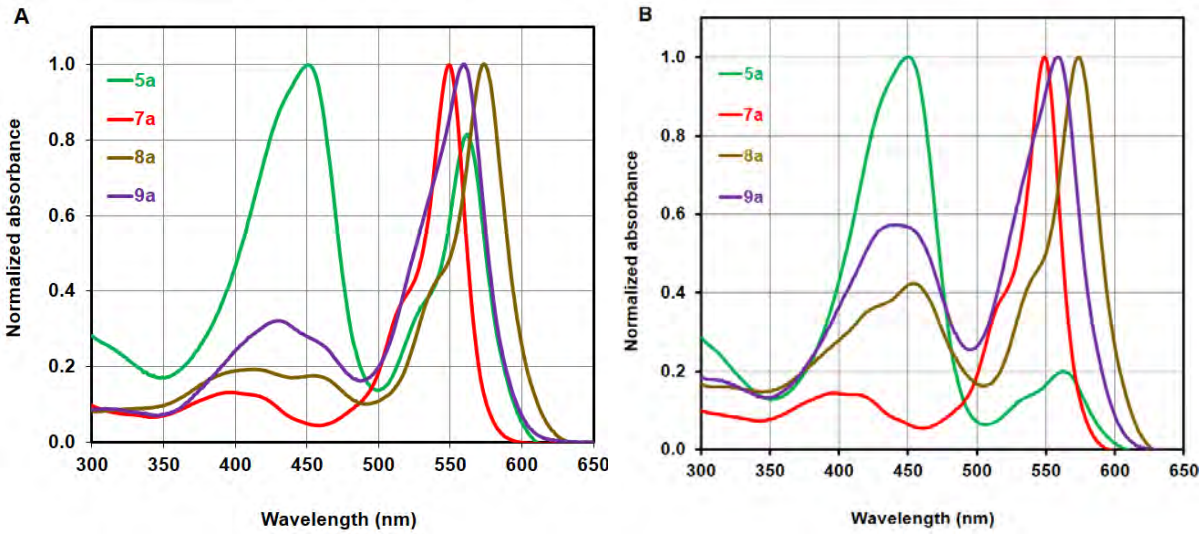

Figure 5.5. Normalized absorption spectra of the halogenated pentafluoroBODIPY cores in DMSO after irradiation with a Thorlabs M530L3 LED (110 mW.cm^{-2}) for 60 min; data obtained after storage in the dark for 24 h (A). The main absorption band of **5a** diminishes significantly after storage in the dark for 48 h (B).

After 24 h, the intensity of the main absorption band of **5a** almost disappears while an intense band appears around 450 nm (**Figure 5.5**). This becomes more pronounced after 48h, implying that **5a** rapidly decomposes relative to the other BODIPYs studied, and this may play a role in the low PACT activity observed above (**Figure 5.4**). In a similar manner to the irradiated samples, a significant decomposition of the main absorption band of **5a** was also observed in the absence of irradiation, relative to the other dyes after storage in the dark for 48 h. It is worth noting that although **9a** was also unstable in organic media (**Figure 5.6**), it exhibited favorable PACT activity (**Figure 5.4**). This can be attributed to the significantly high singlet oxygen quantum yield of this dye. For the dyes being studied here, the absorption spectra show that the order of photostability was: **8a** (80%) > **7a** (78%) > **5a** (74 %) > **9a** (71%) (**Figure 5.6**).

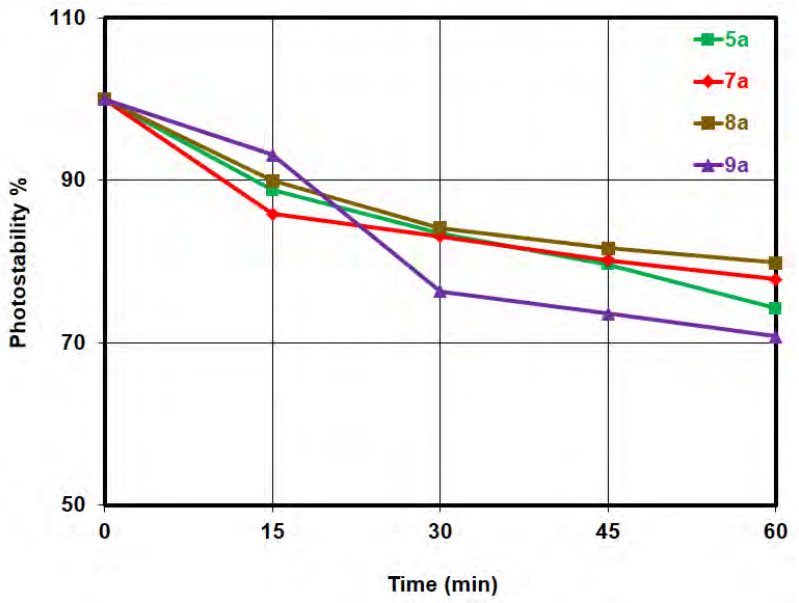

Figure 5.6. Photostability of **5a**, **7a**, **8a** and **9a** in aerated DMSO solutions after irradiation with a Thorlabs M530L3 LED (110 mW.cm^{-2}) for 60 min.

5.2.3. Cellular uptake studies for 5a, 7a, 8a and 9a

To better understand the intracellular accumulation of some of the BODIPYs, the fluorescence profiles of bacterial solutions treated with the dyes were obtained using a spectrofluorometer.[166] Briefly, *Staphylococcus aureus* cells suspended in nutrient broth were treated with each of the BODIPY dyes being studied to a total volume of 6 mL. The cultures were incubated with shaking in an incubator in the dark. After 30, 60, 90, 150 and 270 min, 1 mL aliquots were harvested and centrifuged at 5000 rpm for 5 minutes to remove excess broth. The supernatant was discarded, and the cells were washed three times with 1 mL PBS to remove excess BODIPY dyes. The fluorescence spectra were obtained using 1.5 mL of 2% DMSO-PBS at 540 nm. The increase in fluorescence intensity over time indicates that uptake of each of the dyes increases with time (**Figure 5.7**). BODIPY **8a** exhibited significant fluorescence after 30 min incubation, which correlates with the significant activity observed

during the bacterial inactivation studies (**Figure 5.4**). Contrastingly, there was no significant change in the fluorescence profile of BODIPY **5a** over time (**Figure 5.7**). This is in agreement with the observation of **5a** having the lowest activity against *Staphylococcus aureus* (**Figure 5.4**).

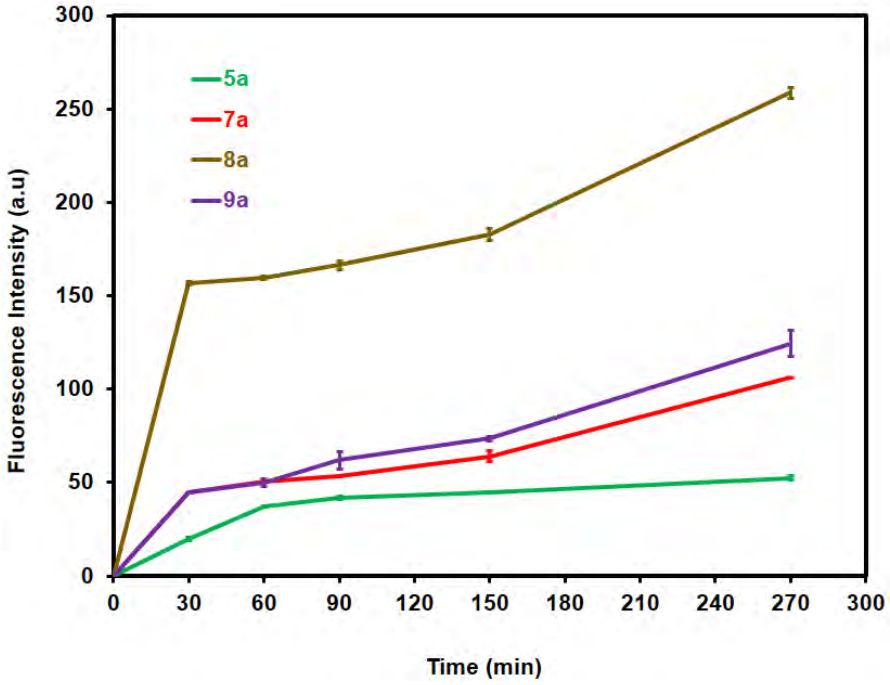

Figure 5.7. Change in fluorescence intensity depicting uptake of **5a**, **7a**, **8a** and **9a**.

5.3. Concluding remarks

All the dyes studied are able to reduce bacterial viability to below 50%. Some of the dyes achieved 0% bacterial viability. These are **6a** (log reduction of 8.4), and **7a**, **7c**, **7g**, **7h**, **7i**, **8a** and **9a**, all with log reductions of 9.6. The main aim of this work was to exploit the structural versatility of the BODIPY core and enhance the photochemical and photosensitizing properties of BODIPYs. This was achieved by using novel and previously synthesized dyes. It can be concluded that the combination of protons at the 1,7-positions and iodines at the 2,6-positions leads to favorable PACT activity, as can be observed for **8a**. Even in the absence of

this combination, each of these still leads to good activity, as observed for **6a** and **9a**. The relatively favorable activity at concentrations of 1 μM can be attributed to the significant singlet oxygen quantum yields as cytotoxic oxygen species are responsible for PACT. It may also be related to the absence of steric strain for **6a** and **8a** as they do not contain methyl or bulky functional groups at the 1,7-positions. This may play a role in enhancing cellular uptake. The effect of steric strain was also evident with **5a**, which contains four bromine atoms at the 1,7-positions and 2,6-positions. This dye also has a relatively low singlet oxygen quantum yield and hence exhibited the lowest PACT activity and poor cellular uptake.

The PACT studies carried out here demonstrate the possible utility of these dyes for this application. Because the PACT properties of BODIPYs have been successfully demonstrated against multiple commercial strains of bacteria, the future outlook relates to the application of further functionlized analogues of these dyes to environmental strains. It is known that bacteria lead to nosocomial infections, and the use of BODIPY dyes in the inactivation of strains responsible for these infections is the next potential line of research. These nosocomial or healthcare-associated infections (HCAIs) are a global challenge and can have devastating effects. Hence viable alternatives to antibiotics are necessary.[167,168]

Chapter 6:

Molecular modelling

This chapter details the optical properties of BODIPY dyes that are predicted using theoretical calculations, also known as molecular modelling. Of interest are the electronic structures and the spectroscopic trends predicted for these dyes. The focus is on the effects of halogenation and π-conjugation on the properties of the dyes used for PACT and NLO studies (**Figure 6.1**). The properties of these selected dyes are discussed in depth below, and these are expected to be similar for the other dyes studied in Chapters 4 and 5.

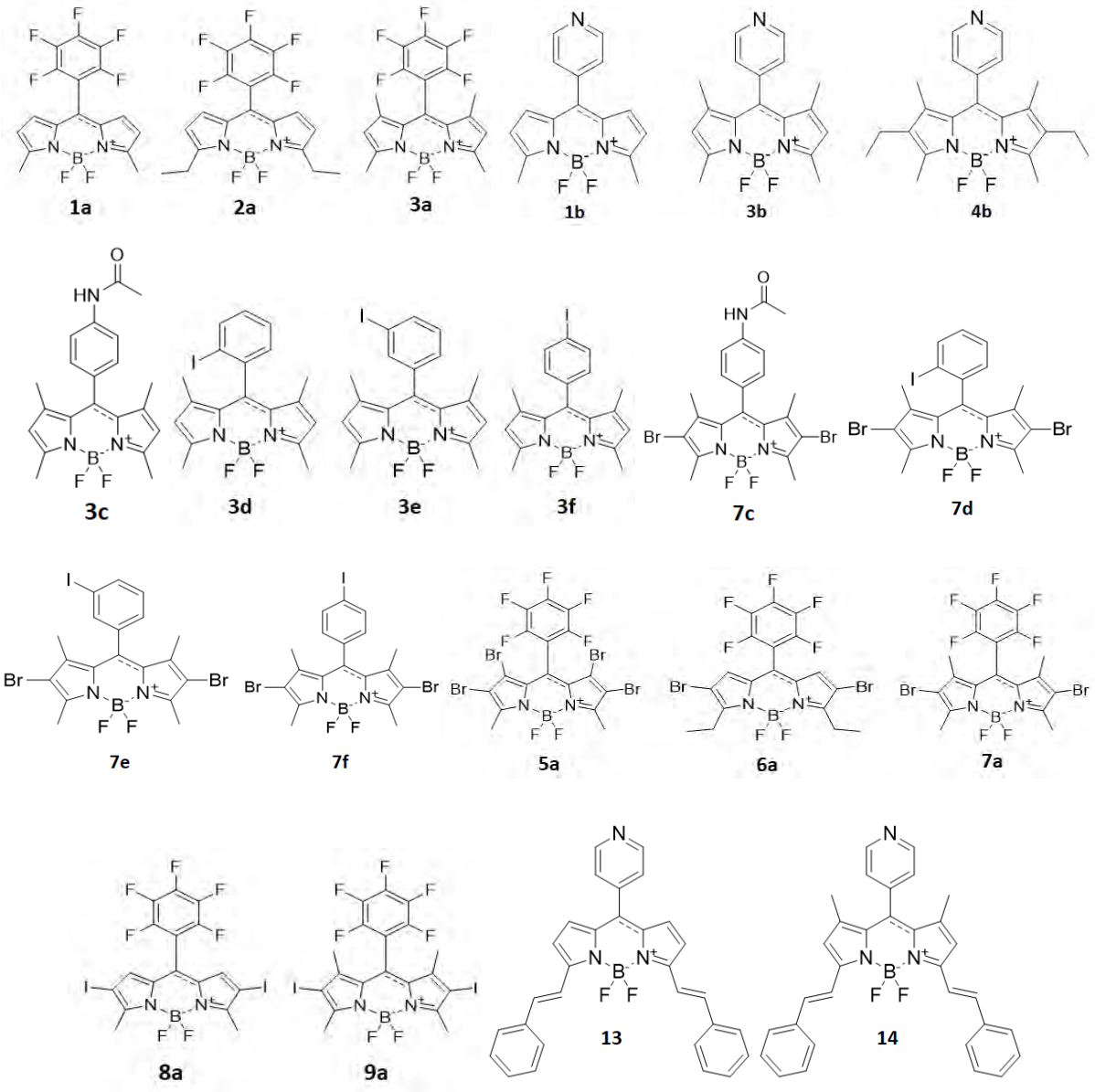

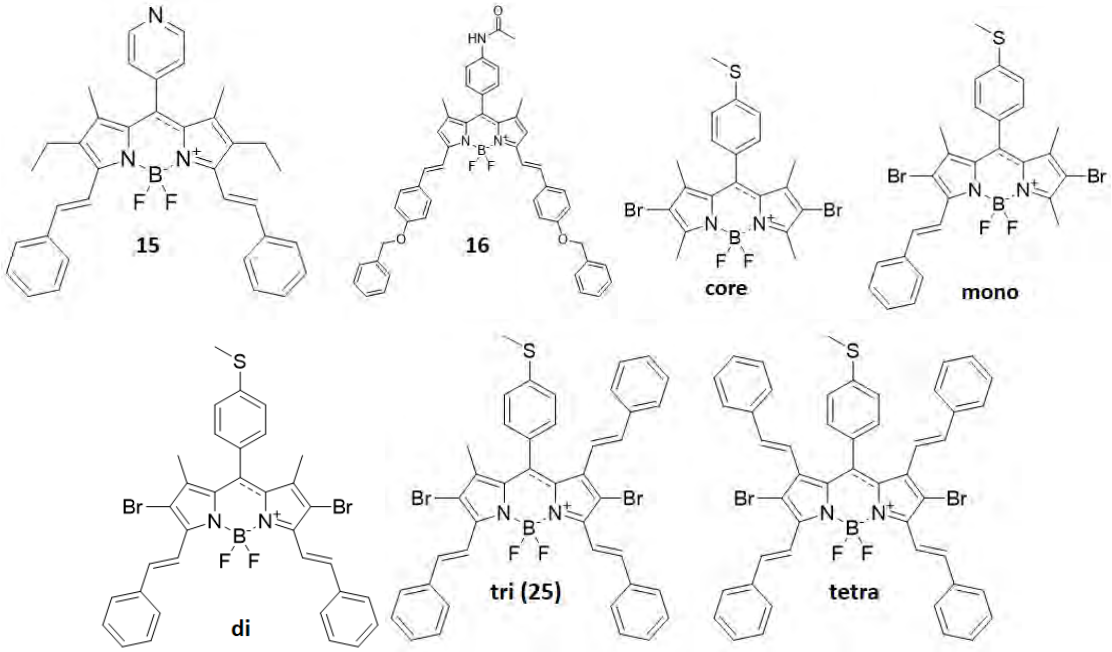

Figure 6.1. Structures used for molecular modelling including both synthesized dyes and a series of model structures (**core**, **mono**, **di** and **tetra**) to examine the effect of styrylation on a series of structural analogues of tristyrylBODIPY **25**.

The calculations were performed with the Gaussian09 software package by first calculating the optimized geometries using the Beck, three-Parameter, Lee-Yang-Parr (B3LYP) functional, with the default Gaussian09 SDD basis set.[118] Subsequently, UV-visible absorption properties were predicted from TD-DFT calculations performed using the Coulomb-attenuated B3LYP (CAM-B3LYP) functional, also with SDD basis sets. The SDD basis set was used in the calculations because it can reasonably predict trends for heavy-atom containing BODIPYs. The CAM-B3LYP functional was used because the B3LYP functional tends to underestimate the energies of excitation with significant charge transfer character that are typically found in styrylated BODIPY dyes.[169,170] The CAM-B3LYP functional, on the other hand, incorporates increasing fractions of semi-empirical Hartree-Fock (HF) exchange parameters to provide a long-range correction.[170]

6.1. Effect of halogenation on spectroscopic properties for photosensitizer applications

This section describes the spectroscopic properties observed for the BODIPYs studied for application in PACT in Chapter 5. The focus is on the spectroscopic changes observed because of the presence of ethyl groups at the 3,5-positions of **2a**, the introduction of bromine or iodine heavy atoms at the 2,6-positions of all the dyes synthesized and studied in this work, and at the 1,7-positions for **5a**.

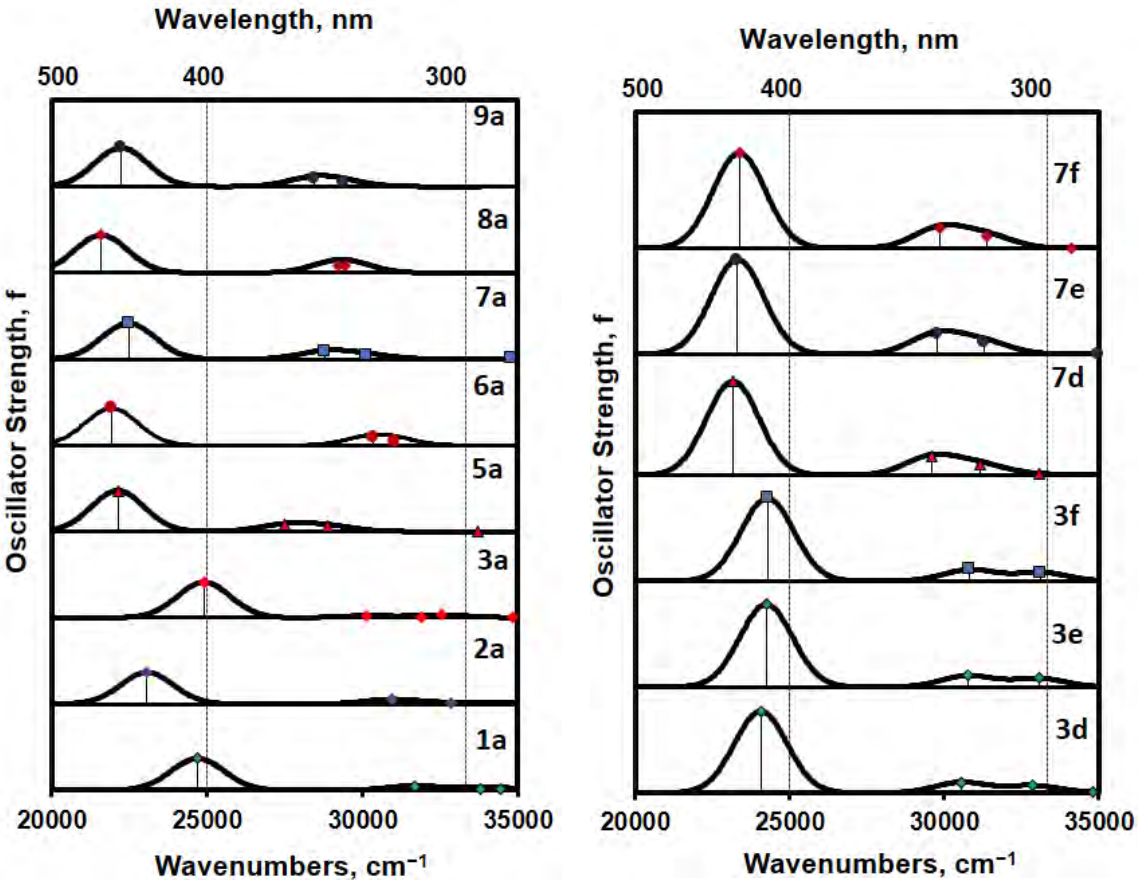

Figure 6.2. Calculated TD-DFT spectra of the optimized geometries of the core and halogenated BODIPY dyes at the CAM-B3LYP/SDD level of theory. The simulated spectra were calculated using the Chemcraft program by using bandwidths of 2000 cm^{-1}.[171]

The TD-DFT calculations show that the main spectral bands of all the core and halogenated BODIPY dyes are due to a one-electron transition from the highest occupied molecular orbital (HOMO) to the lowest unoccupied molecular orbital (LUMO) (**Figure 6.2** and **Table 6.1**). All these $S_0 \rightarrow S_1$ transitions responsible for the main absorption bands are strongly allowed transitions ($f \geq 0.55$) (**Table 6.1**). It is worth noting that although weak bands associated with other orbitals are observed in the 300–450 nm region as it is typically observed for BODIPY dyes,[3,13] these are weak bands due to the small oscillator strengths predicted ($f \leq 0.15$) (**Figure 6.2** and **Table 6.1**). These weak bands are also observed in the experimental spectra discussed in Chapter 3.

Table 6.1. Electronic properties predicted using TD-DFT calculations at the CAM-B3LYP/SDD level of theory for core and halogenated BODIPY dyes.

BODIPY	#[a]	E (ev)[b]	λ_{calc} (nm)[c]	λ_{exp} (nm)[d]	f[e]	Wavefunction[f]
	1	3.06	405	525	0.55	96% H → L; …
1a	2	3.93	316	-	0.08	93% H-1 → L; …
	3	4.19	296	-	0.03	98% H-2 → L; …
	1	2.86	433	527	0.55	96% H → L; …
2a	2	3.84	323	-	0.08	96% H-1 → L; …
	3	4.07	304	-	0.02	98% H-2 → L; …
3a	1	3.09	402	517	0.62	98% H → L; …

	2	3.73	332	-	0.04	97% H-1 → L; …
	1	2.74	452	561	0.71	97% H → L; …
5a	2	3.41	364	-	0.11	96% H-1 → L; …
	3	3.58	346	-	0.10	94% H-2 → L; …
	1	2.72	456	562	0.64	97% H → L; …
6a	2	3.76	330	-	0.15	95% H-2 → L; …
	3	3.85	322	-	0.06	90% H-1 → L; …
	1	2.79	445	549	0.62	97% H → L; …
7a	2	3.57	347	-	0.13	95% H-1 → L; …
	3	3.74	332	-	0.07	93% H-2 → L; …
	1	2.68	463	573	0.65	97% H → L; …
8a	2	3.62	342	-	0.12	48% H-1 → L; 43% H-2 → L; …
	3	3.65	340	-	0.11	49% H-2 → L; 42% H-1 → L; …
	1	2.76	450	558	0.67	97% H → L; …
9a	2	3.53	352	-	0.15	94% H-2 → L; …
	3	3.64	340	-	0.07	90% H-1 → L; …
3d	1	2.98	416	521	0.54	97% H → L; …

	2	3.79	327	-	0.07	90% H-1 → L; …
	3	4.07	305	-	0.05	98% H-3 → L; …
	1	3.01	413	517	0.55	96% H → L; …
3e	2	3.81	325	-	0.07	79% H-1 → L; 16% H-2 → L; …
	3	4.10	302	-	0.06	98% H-3 → L; …
	1	3.01	412	516	0.55	97% H → L; …
3f	2	3.82	324	-	0.07	96% H-1 → L; …
	3	4.11	302	-	0.06	98% H-3 → L; …
	1	2.87	432	536	0.68	97% H → L; …
7d	2	3.67	338	-	0.12	93% H-1 → L; …
	3	3.86	321	-	0.07	92% H-2 → L; …
	1	2.89	429	531	0.62	97% H → L; …
7e	2	3.69	336	-	0.13	90% H-1 → L; …
	3	3.88	320	-	0.08	92% H-2 → L; …
	1	2.90	428	530	0.63	97% H → L; …
7f	2	3.70	335	-	0.13	95% H-1 → L; …
	3	3.89	319	-	0.08	91% H-3 → L; …

[a] - Excited state number in ascending energy. [b] - Calculated band energies in eV. [c] - Calculated wavelengths in nm. [d] - Experimental wavelengths in DMSO. [e] - Calculated oscillator strengths. [f] - Wavefunctions of the transitions based on eigenvectors predicted by TD-DFT. H and L refer to the HOMO and LUMO, respectively.

The BODIPYs synthesized and studied in this thesis are largely analogous with specific structural differences introduced to demonstrate structure-property relationships. For the dyes used as photosensitizers, the starting point is comparing the predicted optical properties of cores **1a**, **2a** and **3a**. These are some of the dyes used as precursors for some of the photosensitizers. BODIPYs **1a** and **2a** do not contain methyl groups at the 1,7-positions, while **3a** does. The effect of this is a relatively narrow HOMO–LUMO gap for **1a** and **2a**, and this is much more significant for **2a** (**Figure 6.3A**). The red-shifted main bands experimentally observed for **1a** and **2a** relative to the typical wavelength of *ca.* 500 nm for BODIPY core dyes, as shown and discussed in Chapter 3, can be attributed to this narrow HOMO–LUMO gap. These differences arise from the absence of steric hindrance in the structures of **1a** and **2a**, which is introduced by the 1,7-methyl groups of **3a**. This steric hindrance causes the *meso*-aryl ring to lie orthogonal to the plane of the BODIPY core for BODIPYs with 1,7-methyl groups, as observed in the optimized geometries (**Figure 6.4**). In the absence of this steric hindrance, the *meso*-aryl ring can rotate relatively freely. The second set of analogous photosensitizers used for PACT were synthesized from the analogous **3d**, **3e** and **3f**. Of these three core dyes, **3d** has a relatively narrow HOMO–LUMO gap. Hence both the calculated and experimental absorption maxima are red-shifted relative to **3e** and **3f** (**Figure 6.3** and **Table 6.1**).

The photosensitizers used for the PACT studies in Chapter 5 were synthesized by introducing heavy atoms onto the BODIPY core. This introduction of bromine and iodine heavy atoms results in a greater destabilization of the HOMO relative to the LUMO as the HOMO possesses a larger MO coefficient at the 2,6-positions for all the dyes (**Figure 6.4**). The result is a narrowing of the HOMO–LUMO gap and a significant red-shift of the main spectral bands (**Figure 6.2** and **Table 6.1**). These changes are more pronounced for **5a**, which contains four bromine atoms at the 1-, 2-, 6- and 7-positions of the BODIPY core, and for the 2,6-diiodo **8a** and **9a** dyes (**Figure 6.4**). For **5a**, this is because of the presence of multiple bromine heavy atoms on the BODIPY core, as it is known that BODIPY absorption maxima tend to red-shift further as the number of bromine atoms increases.[172]

On the other hand, for the iodine-containing **8a**, this is because of the absence of methyl groups at the 1,7-positions and the presence of iodine. The absence of methyl groups eliminates steric hindrance, and as a result, the *meso*-aryl ring does not lie orthogonal to the plane of the BODIPY core. Hence, the *meso*-aryl ring plays a significant role in red-shifting the main band as discussed above for **1a** and **2a**. The presence of the heavier iodine atoms on the structure of **9a** also plays a role similar to that observed for **8a**. The role of iodine becomes clearer in this case. Compared with the experimental main absorption band of **7a**, there is a red-shift of *ca*. 17 nm, while the main absorption band of the analogous **9a** is red-shifted by *ca*. 41 nm (**Table 6.1**). The TD-DFT calculations also predicted this trend, with red shifts of *ca*. 43 and 48 nm for **7a** and **9a** (**Table 6.1**), respectively.

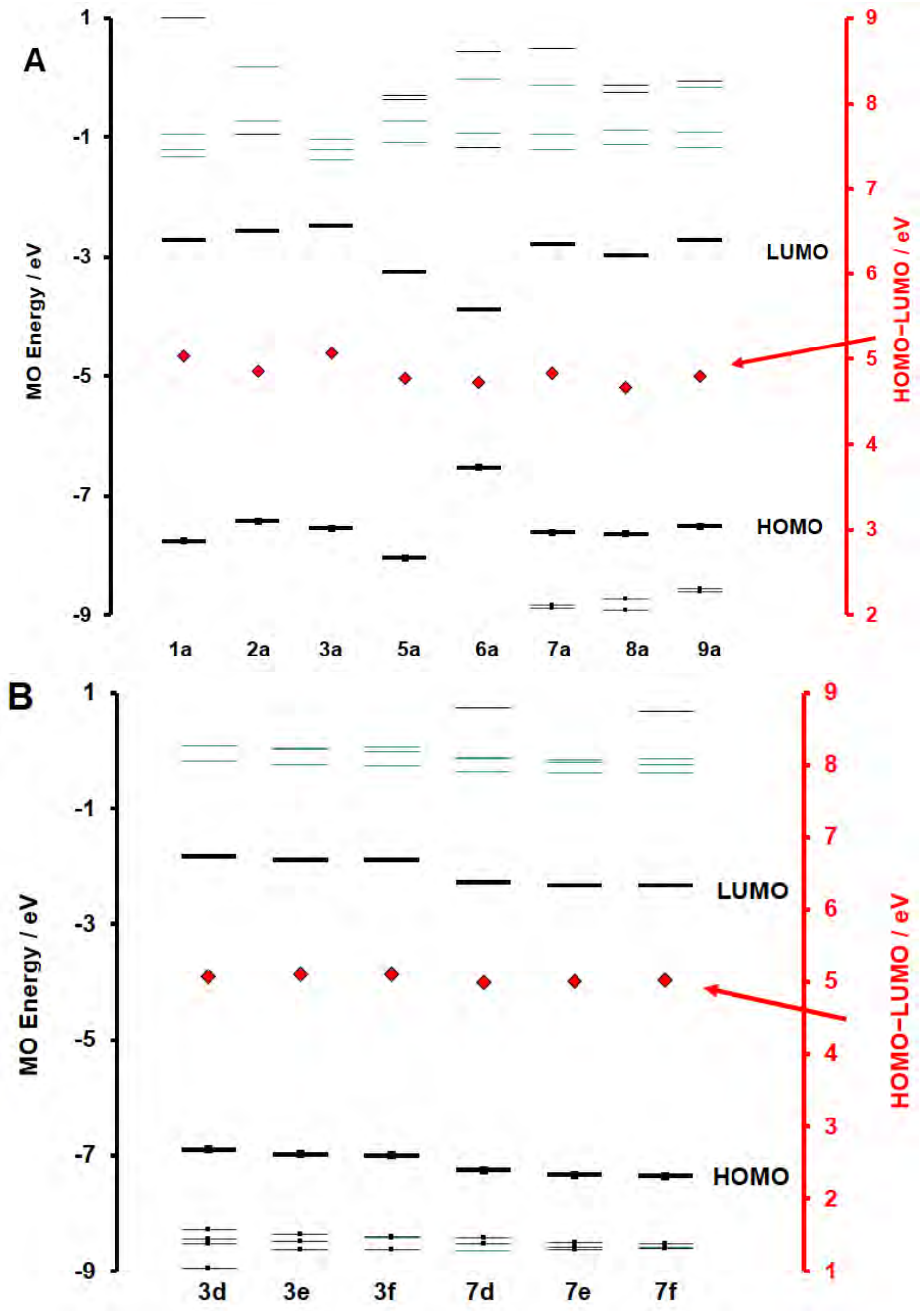

Figure 6.3. Frontier MO energies and HOMO–LUMO gaps of the core and halogenated BODIPYs at the CAM-B3LYP/SDD level of theory. Blue and green lines denote the primary localization of MOs on the styryl and phenyl moieties, respectively. The HOMO–LUMO band gaps are plotted against a secondary axis and are denoted by large red diamonds. The occupied MOs are highlighted with small black squares.

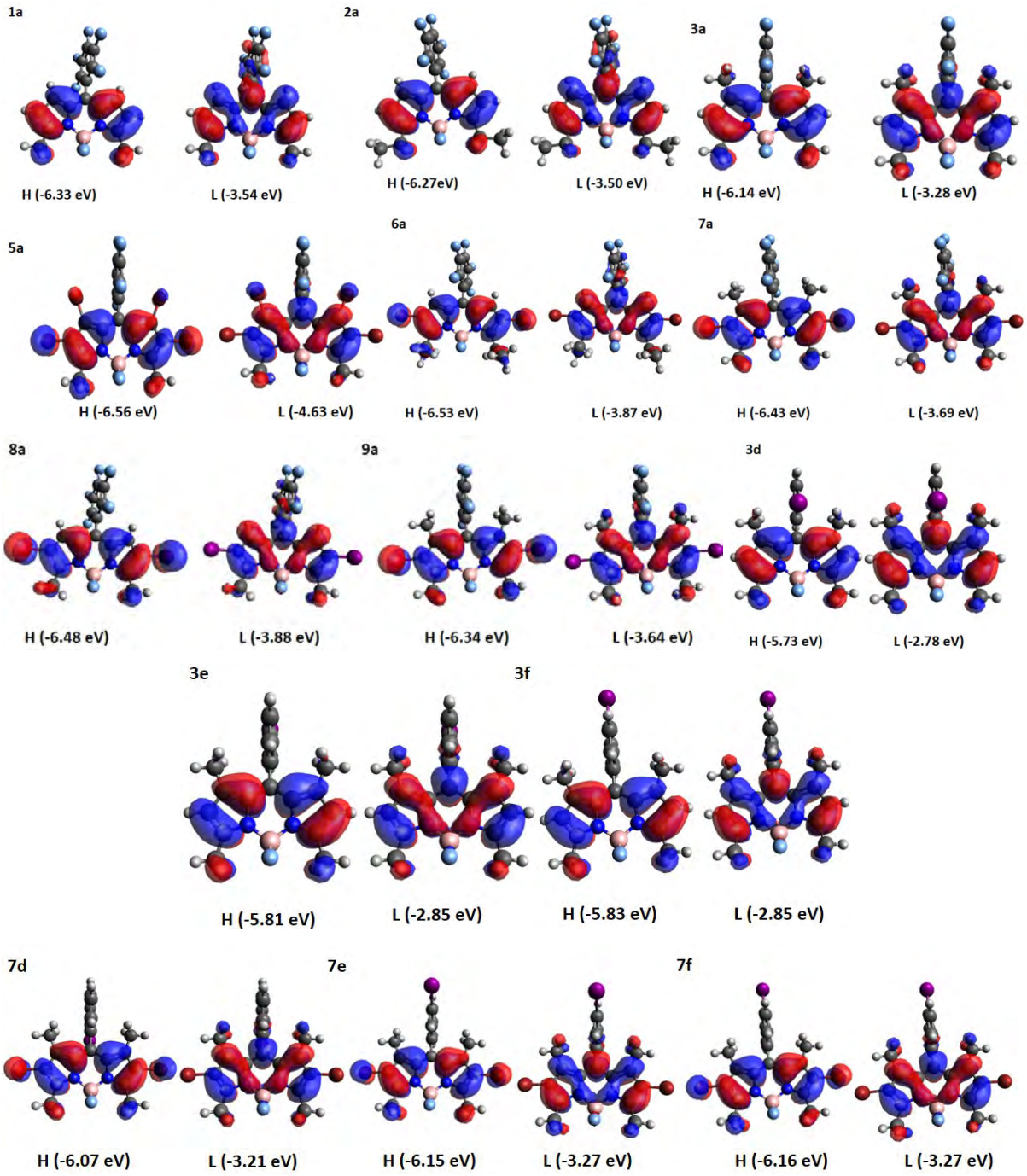

Figure 6.4. Angular nodal patterns and MO energies of the core and halogenated BODIPY dyes for the HOMO and LUMO. H and L denote the HOMO and LUMO.

6.2. StyrylBODIPY dyes for the fabrication of OL materials: effect of π-extension on absorption in the visible region and at 532 nm

Herein, the predicted spectroscopic properties of the BODIPY dyes designed for NLO studies are detailed. The BODIPY dyes used for the TD-DFT studies are **13**, **14** and **15**, and similar trends are expected with other styrylBODIPY dyes. These styrylBODIPY dyes were synthesized from precursor BODIPY core dyes **1b**, **3b** and **4b**, as detailed in Chapters 2 and 3. In a similar manner to the dyes used as photosensitizers, the main spectral bands of all the core dyes are due to the one-electron HOMO–LUMO transition (**Figure 6.5** and **Table 6.2**). These $S_0 \rightarrow S_1$ transitions are also allowed transitions ($f \geq 0.49$) (**Table 6.2**).

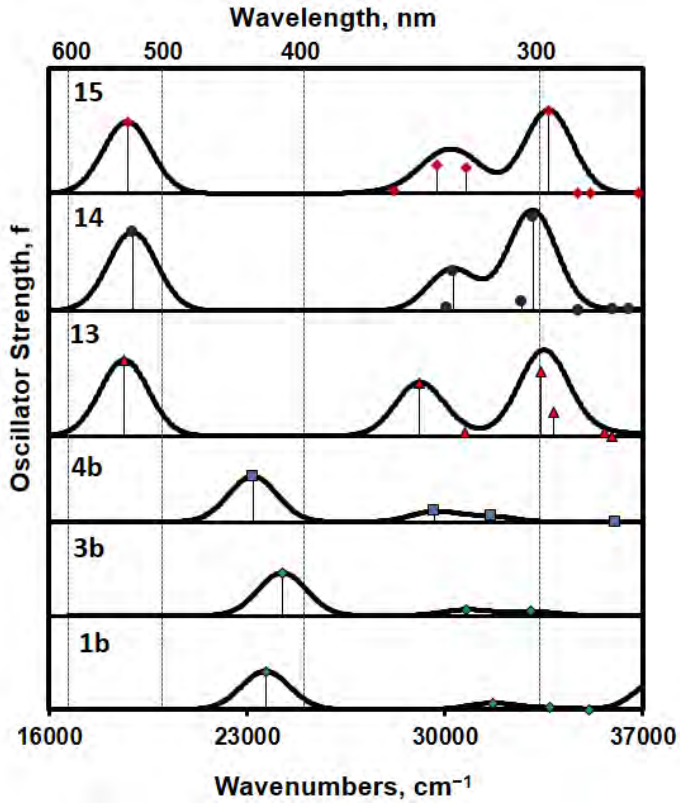

Figure 6.5. Calculated TD-DFT spectra of the optimized geometries of the core and styrylBODIPY dyes at the CAM-B3LYP/SDD level of theory. The simulated spectra were calculated using the Chemcraft program by using bandwidths of 2000 cm^{-1}.[171]

Table 6.2. Electronic properties predicted using TD-DFT calculations at the CAM-B3LYP/SDD level of theory for core and styrylBODIPY dyes.

BODIPY	#[a]	E (ev)[b]	λ_{calc} (nm)[c]	λ_{exp} (nm)[d]	f[e]	Wavefunction[f]
	1	2.93	423	518	0.49	96% H → L; …
1b	2	3.92	316	-	0.08	90% H-1 → L; …
	3	4.18	297	-	0.02	95% H-3 → L; …
	1	3.01	412	505	0.55	96% H → L; …
3b	2	3.81	325	-	0.08	96% H-1 → L; …
	3	4.10	303	-	0.06	98% H-2 → L; …
	1	2.88	431	528	0.58	96% H → L; …
4b	2	3.68	337	-	0.13	96% H-1 → L; …
	3	3.92	316	-	0.07	97% H-2 → L; …
	1	2.31	536	648	0.97	97% H → L; …
	2	3.61	344	-	0.68	93% H-1 → L; …
13	3	3.81	326	-	0.04	61% H-5 → L; 33% H-2 → L; …
	4	4.14	300	357	0.82	88% H → L+1; …
	5	4.20	295	-	0.31	91% H-6 → L; …

	1	2.35	528	634	1.01	97% H → L; …
	2	3.73	333	-	0.03	61% H-3 → L; 34% H-2 → L; …
14	3	3.75	330	-	0.50	89% H-1 → L; …
	4	4.05	306	-	0.10	92% H-6 → L; …
	5	4.11	302	351	1.20	90% H → L+1; …
	1	2.33	533	643	0.92	97% H → L; …
	2	3.49	355	-	0.03	88% H-2 → L; …
15	3	3.69	336	-	0.36	74% H-1 → L; 21% H-4 → L; …
	4	3.81	325	-	0.32	76% H-4 → L; 20% H-1 → L; …
	5	4.17	297	350	1.07	92% H → L+1; …

[a] - Excited state number in ascending energy. [b] - Calculated band energies in eV. [c] - Calculated wavelengths in nm. [d] - Experimental wavelengths in DMSO. [e] - Calculated oscillator strengths. [f] - Wavefunctions of the transitions based on eigenvectors predicted by TD-DFT. H and L refer to the HOMO and LUMO, respectively.

BODIPY **1b**, in a similar manner to **1a**, does not contain methyl groups at the 1,7-positions, while **3b** and **4b** do. BODIPY **4b** also contains ethyl groups at the 2,6-positions. The effect of this structural modification is a relatively narrow HOMO–LUMO gap for **1b** and **4b** relative to **3b** (**Figure 6.6**). As expected, this also results in significantly red-shifted main bands, with that of **4b** being the most red-shifted (**Figure 6.5** and **Table 6.2**). For **1a**, this is due to the absence

of steric hindrance introduced by the 1,7-methyl groups of **3b** and **4b**, similar to what was explained for **1a** above. The presence of 2,6-ethyl groups on **4b** results in a calculated red-shift of *ca*. 19 nm and an experimental red-shift of *ca*. 23 nm relative to **3b**, in a similar manner to the 2,6-dihalogenated BODIPYs discussed above. Because of the presence of large MO coefficients at the 3,5-positions on the HOMO and LUMO, albeit more for the HOMO relative to the LUMO of the three BODIPY core dyes (**Figure 6.7**), the introduction of styryl groups at these positions narrows the HOMO–LUMO gap (**Figure 6.6**). This leads to calculated red-shifts of between 102–116 nm, which were observed experimentally to be *ca*. 115–130 nm (**Table 6.2**).

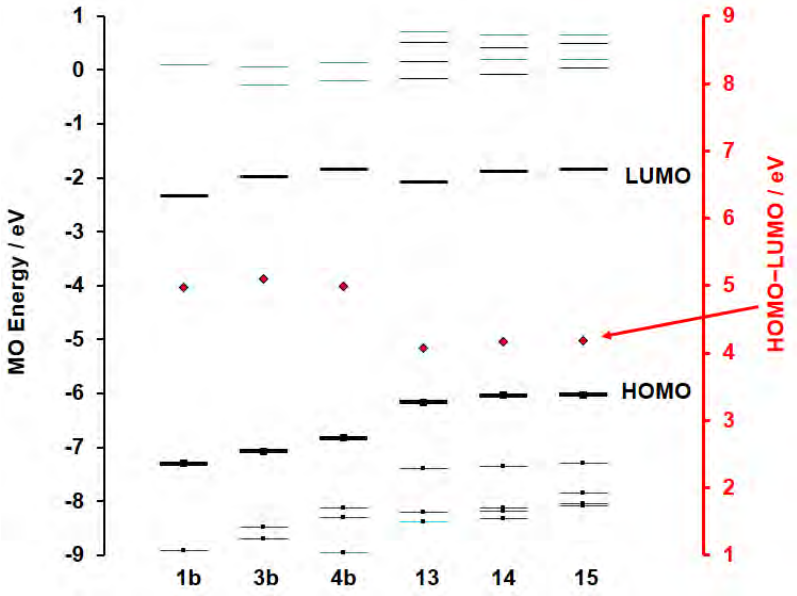

Figure 6.6. Frontier MO energies of the *meso*-pyridyl-substituted core and styrylBODIPY dyes at the CAM-B3LYP/SDD level of theory. Blue and green lines denote the primary localization of MOs on the styryl and phenyl moieties, respectively. The HOMO and LUMO are highlighted with thicker black lines, while small black squares denote occupied MOs. Red diamonds denote the HOMO–LUMO gap values and are plotted against a secondary axis.

In a similar manner to the calculations for the core and halogenated core dyes, the main absorption band is predicted to be due to the HOMO–LUMO one-electron transitions. Additional transitions involving other MOs are also predicted. The most significant of these is the HOMO–LUMO+1 transition with large oscillator strengths ($f \geq 0.82$), which are similar to the oscillator strengths of the main bands. These strong absorption bands were also observed experimentally (**Table 6.2**). Because the BODIPYs were designed to be studied as potential OL materials using the second harmonic of the Nd:YAG laser at 532 nm, the dyes must exhibit minimal absorbance at this wavelength and across most of the visible region. This was demonstrated with the experimental spectra in Chapters 3 and 4, which showed relatively weak absorption at 532 nm and most of the visible region (**Figure 6.5**).

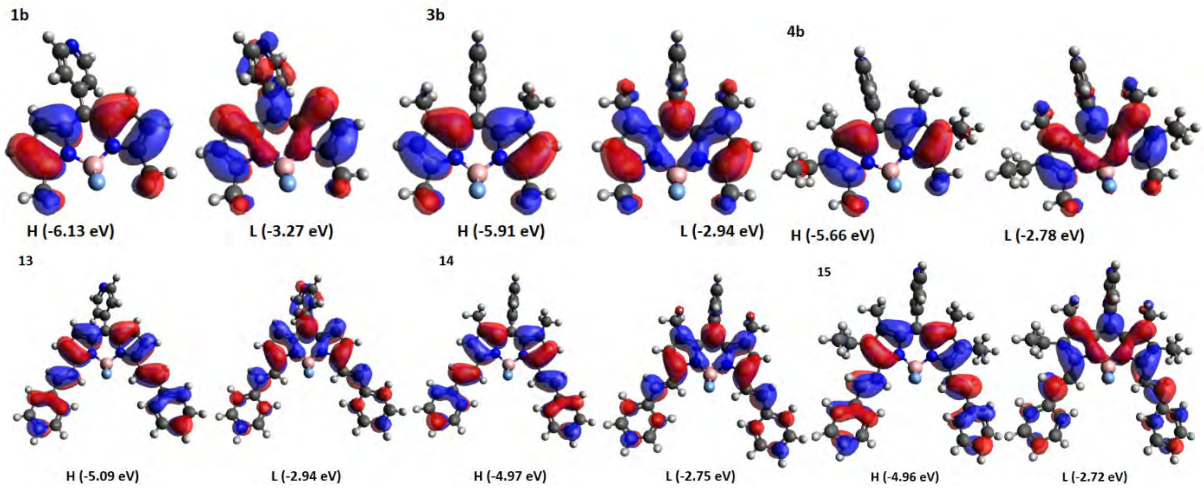

Figure 6.7. Angular nodal patterns and MO energies of the core and styrylBODIPY dyes for the HOMO and LUMO at an isosurface of 0.02 a.u. H and L denote the HOMO and LUMO.

6.3. Comparison of the effects of halogenation and π-extension

In this section, the spectroscopic properties observed for BODIPYs **3c**, **7c** and **16** are discussed. TD-DFT calculations are used to demonstrate the reasons for the spectral changes observed

after introducing bromines at the 2,6-positions to form **7c** and after the introduction of benzyloxy groups at the 3,5-positions to form **16**. In Chapter 4, **16** synthesized from BODIPY core dye **3c** was used to demonstrate the mechanism responsible for the NLO response observed for nonhalogenated BODIPY dyes. **7c** also synthesized from **3c** was used as a photosensitizer in the PACT studies detailed in Chapter 5. In a similar manner to the dyes discussed above, the main spectral bands of **3c**, **7c** and **16** are also due to the one-electron HOMO–LUMO transition (**Figure 6.8** and **Table 6.3**). For **3c** and **7c**, these are allowed transitions ($f \geq 0.54$), whereas for **16** it is a strongly allowed transition ($f = 1.12$) (**Table 6.3**).

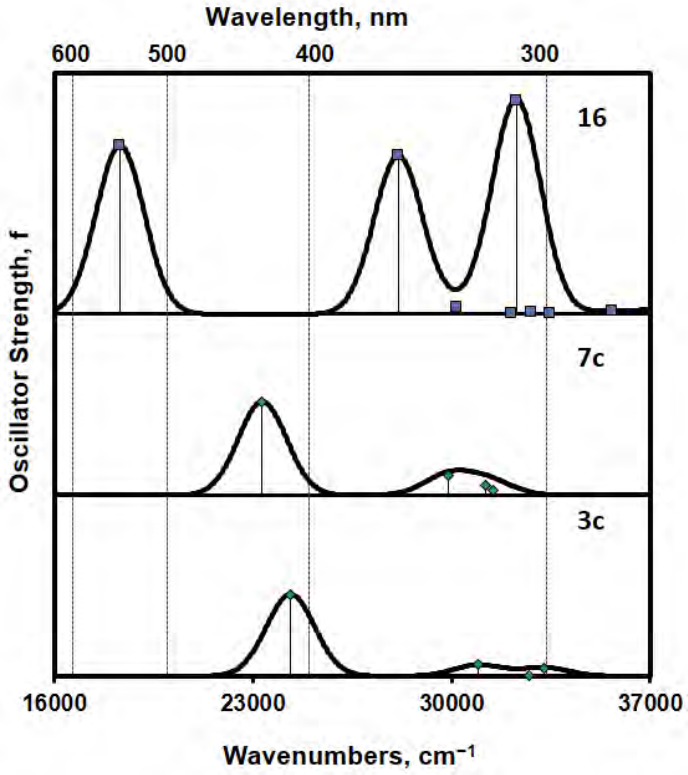

Figure 6.8. Calculated TD-DFT spectra of the optimized geometries of **3c**, **7c** and **16** at the CAM-B3LYP/SDD level of theory. The simulated spectra were calculated using the Chemcraft program by using bandwidths of 2000 cm^{-1}.[171]

Table 6.3. Electronic properties predicted using TD-DFT calculations at the CAM-B3LYP/SDD level of theory for **3c**, **7c** and **16**.

BODIPY	#[a]	E (ev)[b]	λ_{calc} (nm)[c]	λ_{exp} (nm)[d]	f[e]	Wavefunction[f]
3c	1	3.01	411	501	0.54	96% H → L; …
	2	3.83	323	-	0.07	96% H-2 → L; …
	3	4.06	305	-	0.0	94% H-1 → L; …
	4	4.12	301	-	0.06	98% H-3 → L; …
7c	1	2.89	428	527	0.62	97% H → L; …
	2	3.70	335	-	0.13	96% H-2 → L; …
	3	3.87	320	-	0.06	73% H-1 → L; 19% H-3 → L; …
16	1	2.27	546	647	1.12	96% H → L; …
	2	3.49	356	597	1.05	94% H-1 → L; …
	3	3.74	331	-	0.04	91% H-6 → L; …
	4	3.98	311	-	0.0	92% H-3 → L; …
	5	4.00	310	372	1.41	89% H → L+1; …

[a] - Excited state number in ascending energy. [b] - Calculated band energies in eV. [c] - Calculated wavelengths in nm. [d] - Experimental wavelengths in DMSO. [e] - Calculated oscillator

strengths. [f] - Wavefunctions of the transitions based on eigenvectors predicted by TD-DFT. H and L refer to the HOMO and LUMO, respectively.

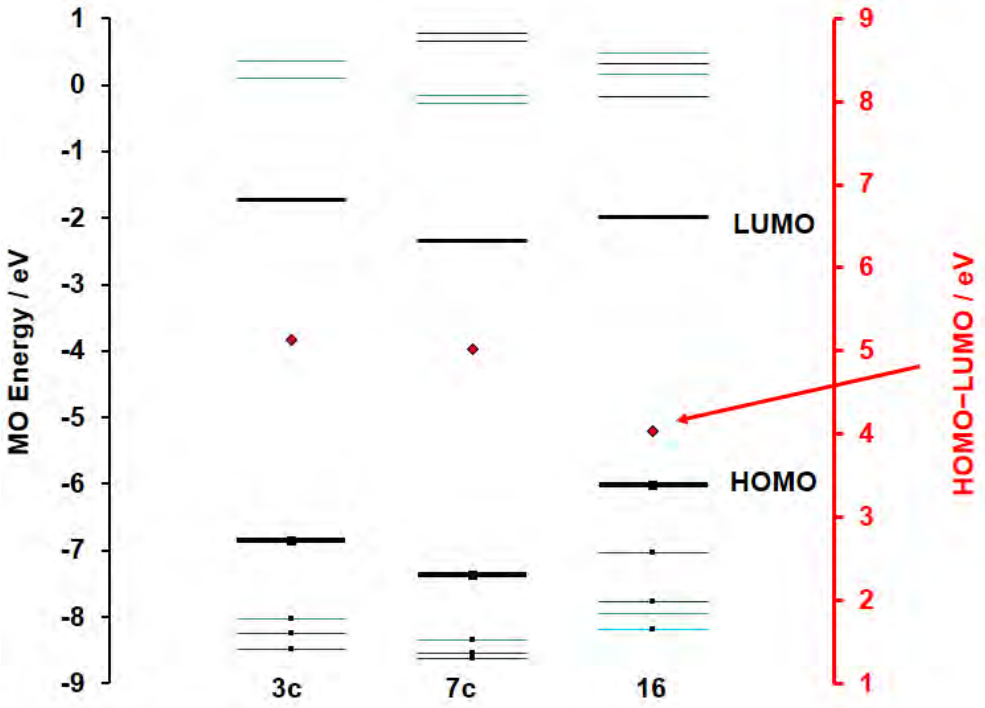

Figure 6.9. Frontier MO energies of **3c**, **7c** and **16** at the CAM-B3LYP/SDD level of theory. Blue and green lines denote the primary localization of MOs on the styryl and phenyl moieties, respectively. The HOMO and LUMO are highlighted with thicker black lines, while small black squares denote occupied MOs. Red diamonds denote the HOMO–LUMO gap values and are plotted against a secondary axis.

The introduction of bromine atoms at the 2,6-positions of **3c** to form **7c** leads to a destabilisation of both the HOMO and LUMO, leading to the narrowing of the HOMO–LUMO gap (**Figure 6.9**). This narrowing of the HOMO–LUMO gap results in a calculated red-shift of *ca*. 17 nm and an experimental red-shift of *ca*. 26 nm (**Table 6.3**). As mentioned above, styryl

groups were introduced at the 3,5-positions of **3c** to form **16**. These 3,5-positions possess large MO coefficients on the HOMO and LUMO (**Figure 6.10**). Hence the introduction of styryl groups at these positions leads to a calculated red-shift of *ca*. 135 nm, which was experimentally observed to be *ca*. 146 nm (**Table 6.3**).

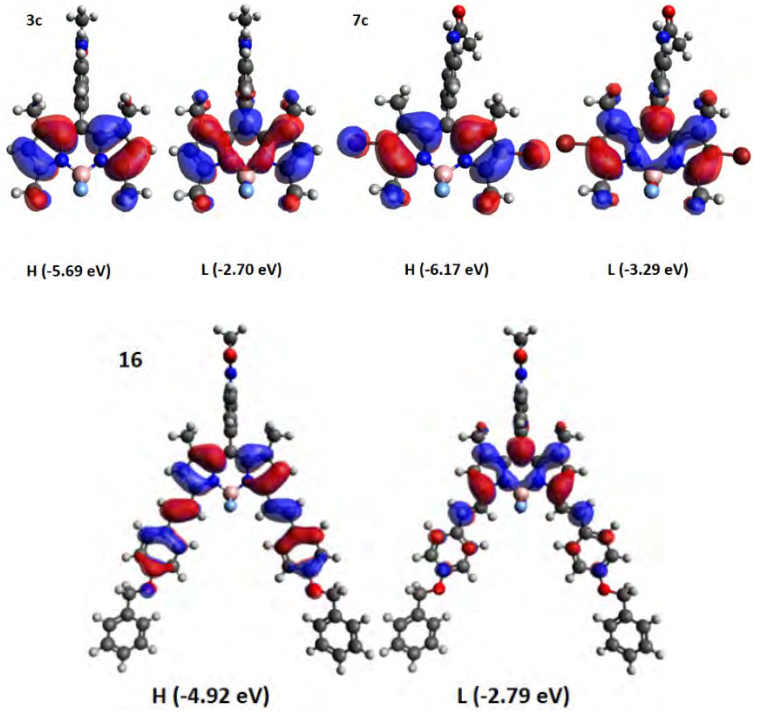

Figure 6.10. Angular nodal patterns and MO energies of **3c**, **7c** and **16** for the HOMO and LUMO at an isosurface of 0.02 a.u. H and L denote the HOMO and LUMO

In a similar manner to the other styrylBODIPY dyes discussed above, additional transitions involving other MOs are also predicted. The two strongly allowed transitions involved are a HOMO–LUMO+1 transition (f = 1.41) and a HOMO-1–LUMO transition (f = 1.05) (**Table 6.3**). The TD-DFT calculations predict these bands to be at 310 and 356 nm, in addition to the main band at 546 nm. In the experimental ground state absorption spectrum, they are respectively observed at 372 and 597 nm, with the main band observed at 647 nm (**Table 6.3**). It is worth noting that from the transient absorption spectrum discussed in Chapter 4, these three bands

appear as intense ground state depletion peaks at 371, 596 and 645 nm. As mentioned above, for a BODIPY dye to be suitable for study as a potential OL material using the second harmonic of the Nd:YAG laser at 532 nm, there must be minimal absorbance at this wavelength and across most of the visible region. BODIPY **16** does possess this property, as it was observed in the experimental spectrum in Chapter 4. This holds even with the TD-DFT spectrum (**Figure 6.8**).

6.4. Partial atomic charge visualization and dipole moments on optimized geometries of styrylBODIPY dyes used in NLO studies

In this section, the partial atomic charges of the optimized geometries are discussed briefly, and the direction of the predicted dipole moments of some of the dyes studied for NLO are shown (**Figure 6.11**). The values of the predicted Mulliken atomic charges are included for some of the dyes (**Table 6.4**). Because Mulliken charges obtained from DFT calculations are known to be dependent on the basis set used, the results will be limited to a qualitative analysis.[173–175] The precursor BODIPY core dyes are also included. The arrow displayed on the structures shows the ground state dipole (**Figure 6.11**). This is influenced by the nature of the atoms on the substituents present on the functional groups attached to the BODIPY core at different positions. Using the scale shown at the bottom, the direction and magnitude of the charge on each atom can be deduced from the color of the atom (**Figure 6.11**).

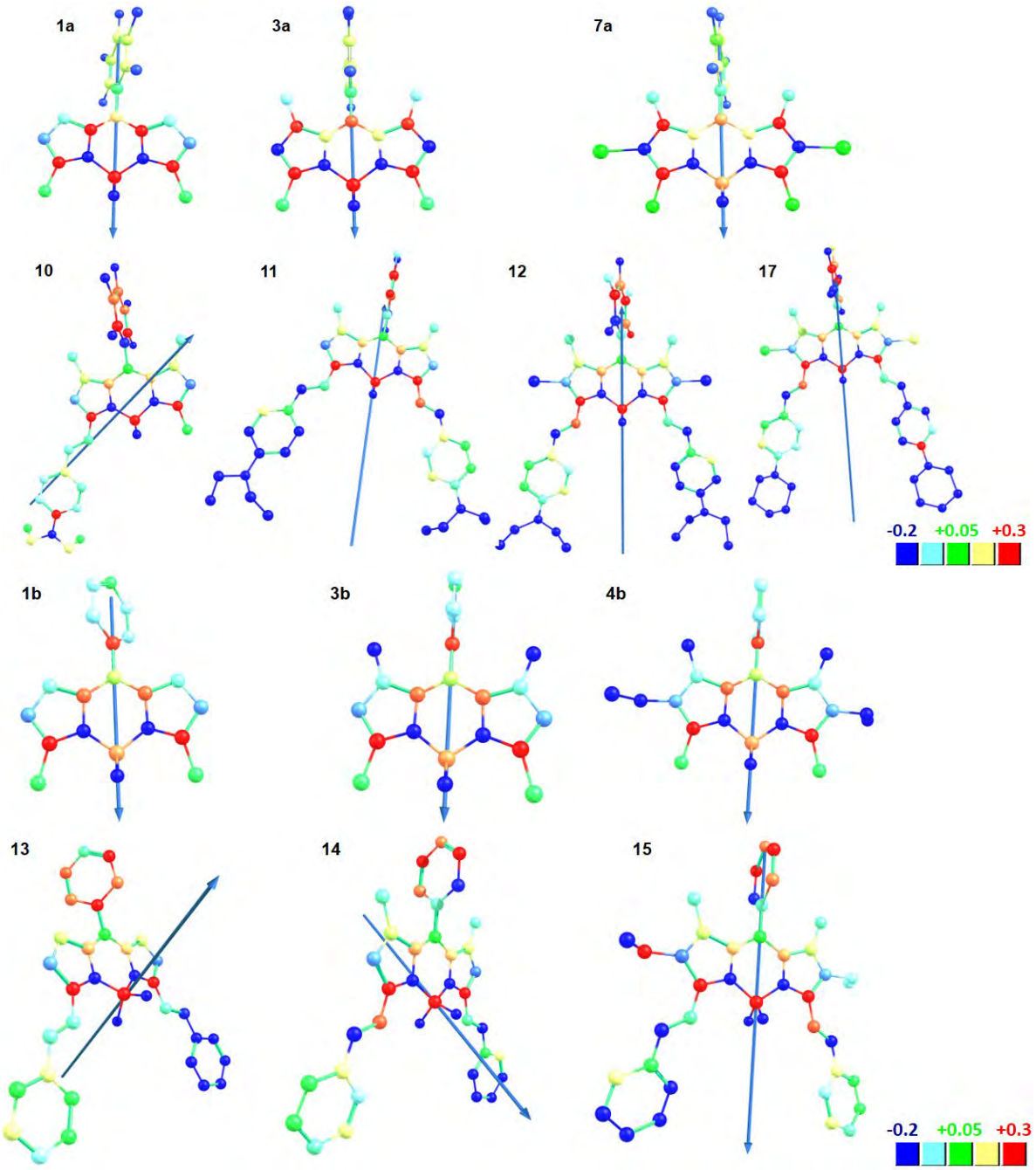

Figure 6.11. Partial atomic charge visualization on the optimized structures. Atoms are colored according to the degree of partial charge, and hydrogen atoms are hidden. The range and index at the bottom relate the magnitude of the partial charge to color, with blue and red representing the most negatively and positively charged atoms, respectively. The visualizations were created using the Chemcraft program.[171]

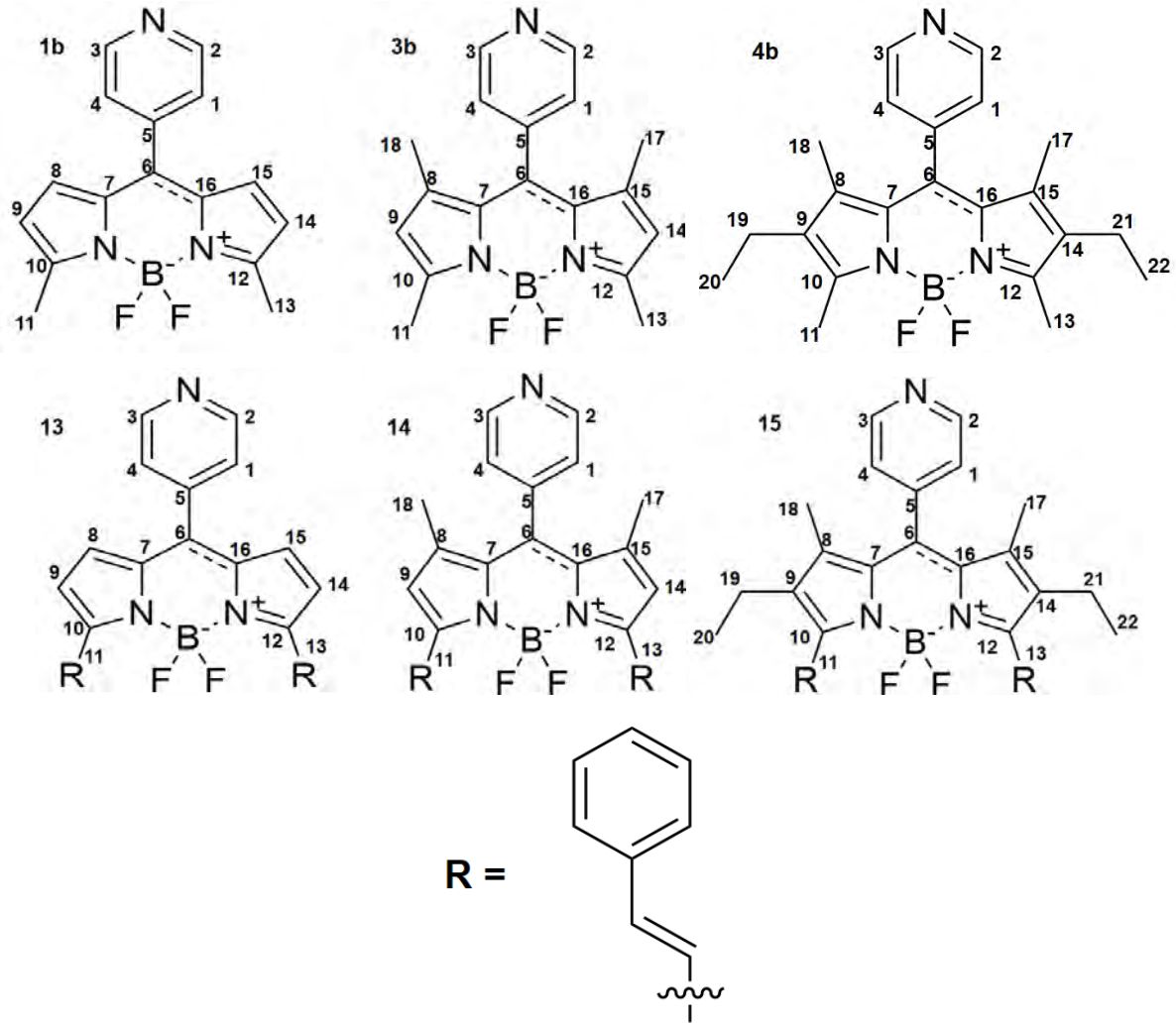

Figure 6.12. Atom number labels on the carbon atoms of **1b**, **3b**, **4b**, **13**, **14** and **15**. The numbering of the atoms corresponds to **Table 6.4**.

The predicted Mulliken atomic charges for the *meso*-pyridyl-substituted BODIPY dyes are shown below (**Table 6.4**). The atoms are numbered as shown in **Fig.6.12**. The charges on identical atoms on all the core and styryl BODIPY dyes are approximately the same except in the instances highlighted in bold (**Table 6.4**). Using **1b** as the starting point, the differences observed can be attributed to the introduction of methyl, ethyl and styryl groups at the 1,7-, 2,6- and 3,5-positions of the BODIPY core, respectively (**Figure 6.12**). The presence of methyl groups affects the charges on carbons 7–9 and 14–16 (**Table 6.4**). The charges on the carbons

at the 1,7-positions (carbons 8 and 15) of **3b**, **4b**, **14** and **15** are inverted relative to **1b** and **13**, and these are the carbons which form C–C bonds as the methyl groups are directly attached to them (**Figure 6.12**). A similar observation can be made at the 2,6-positions (carbons 9 and 14) of **4b** and **15**, where the ethyl groups are directly attached. The introduction of styryl groups at the 3,5-positions (carbons 10 and 12) does not change the direction of the charge on these carbon atoms, but there are changes in the magnitude of the charge on these atoms.

Table 6.4. Mulliken atomic charges for the *meso*-pyridyl-substituted BODIPY dyes. Atoms whose charges change significantly (in magnitude and/or direction) upon introducing methyl, ethyl or styryl groups are highlighted in bold.

Carbon atom number	**1b**	**3b**	**4b**	**13**	**14**	**15**
1	-0.023	-0.015	-0.030	-0.011	-0.008	-0.015
2	-0.030	-0.030	-0.005	**0.208**	**0.206**	**0.208**
3	-0.092	-0.104	-0.105	**0.204**	**0.209**	**0.204**
4	-0.148	-0.135	-0.120	-0.003	-0.015	-0.008
5	0.262	0.252	0.230	**0.050**	**0.053**	**0.054**
6	0.129	0.116	0.103	**-0.060**	**-0.047**	**-0.041**
7	0.251	0.164	0.191	0.276	0.242	0.230
8	-0.024	**0.318**	**0.161**	-0.023	**0.121**	**0.087**
9	-0.080	-0.237	**0.132**	-0.070	-0.127	**0.010**
10	0.356	0.382	0.252	0.373	0.369	**0.336**
11	0.004	-0.001	-0.053	0.013	0.013	0.015

12	0.431	0.437	0.213	**0.375**	**0.369**	**0.334**
13	-0.043	-0.042	-0.031	0.013	0.013	0.016
14	-0.189	-0.264	**0.130**	-0.088	-0.127	**0.011**
15	-0.135	**0.202**	**0.089**	-0.003	**0.121**	**0.087**
16	0.319	**0.143**	**0.154**	0.275	**0.242**	**0.231**
17	-	-0.090	-0.074	-	-0.032	-0.038
18	-	-0.089	-0.072	-	-0.032	-0.039
19	-	-	-0.013	-	-	-0.047
20	-	-	-0.032	-	-	0.023
21	-	-	-0.015	-	-	-0.046
22	-	-	-0.064	-	-	0.022

6.5. Molecular Electrostatic Potential maps for the distyrylBODIPY dyes studied for application in NLO

This section describes the charge distributions of the distyrylBODIPY dyes studied for application in NLO in Chapter 4. Different surface charges across the BODIPY structure can be visualized using electrostatic potential maps (**Figure 6.13**).[176,177] For the purposes of this study, charge distributions can be useful in enhancing the understanding of the dipole moments discussed above. Because large dipoles of organic molecules are known to enhance hyperpolarizability in the context of NLO studies, visualizing charge distribution is important. On the maps, the red area corresponds to the negative region of the ESP map where electron-rich portions of the structure attract a point positive charge, whereas the blue area

corresponds to the positive region where electron-deficient portions of the structure repel a point positive charge (**Figure 6.13**).

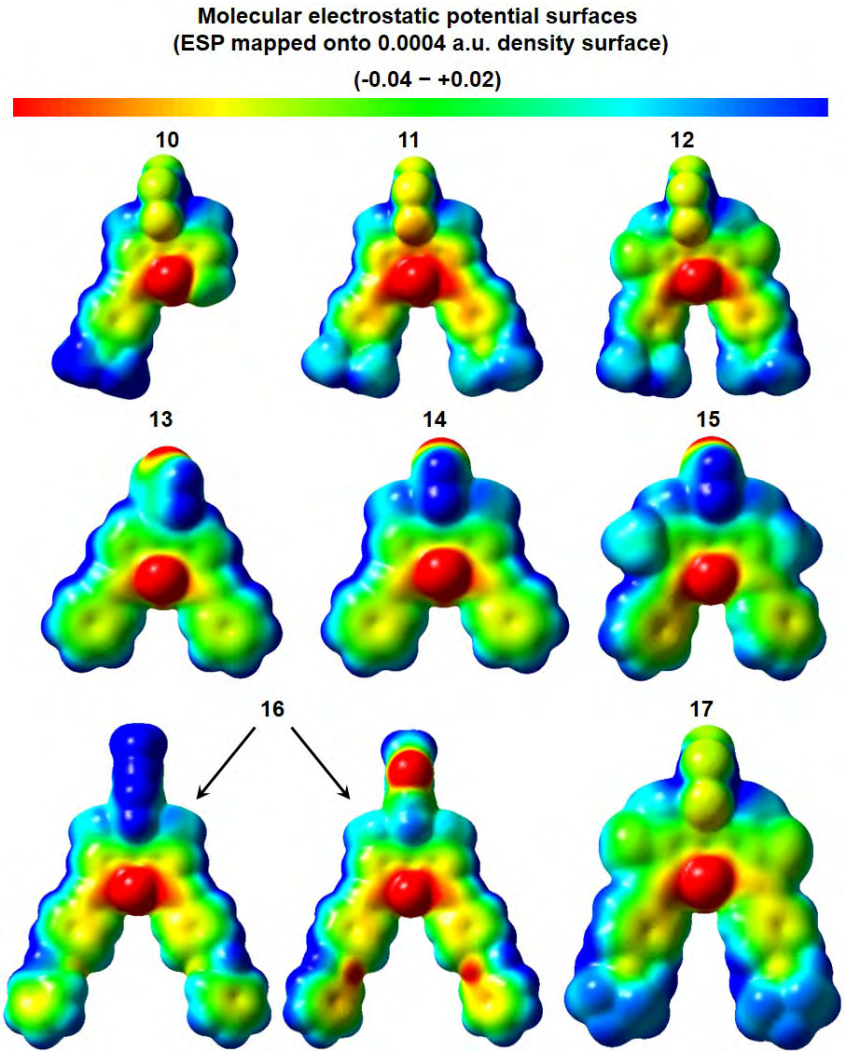

Figure 6.13. Molecular electrostatic potential maps for the distyrylBODIPY dyes studied for NLO applications. The mapping was performed using GaussView and corresponds to the attractive and repulsive force exerted on a point positive charge. A red surface color corresponds to the negative region of the electrostatic potential where electron-rich portions of the structure attract the point positive charge. In contrast, the blue surfaces correspond to the positive regions where electron-deficient portions of the structure repel the point positive charge.

The substituents at the *meso*- and 3,5-positions of **10**, **11**, **12** and **17** were selected to form D–π–A type dyes. The alkyl groups on the electronegative nitrogen atoms are electron-deficient and hence positively charged (blue color), while the electron-donating properties of the $–NR_2$ group increase electron density charge across the BODIPY π-system structure (**Figure 6.13**). For **13**, **14** and **15**, the nitrogen atoms on the pyridine group at the *meso*-position are more electronegative than the carbon atoms. Hence the nitrogen atoms possess an intense red color while the blue color on the carbon atoms of the *meso*-phenyl ring indicates that they become electron-deficient (**Figure 6.13**). For **16**, the most electronegative atom on the *meso*-phenyl ring is the oxygen atom, and the intense red color is consistent with this, and is supported by an intense blue color on the rest of the *meso*-phenyl ring (**Figure 6.13**). The intense red color on the oxygen atoms of the benzyloxy rings of the styryl groups at the 3,5-positions also highlights the electronegative nature of the oxygen atoms, which increases the negative charge centered on these atoms. For all the BODIPYs, the BF_2 center contains an intense red color consistent with the electron-withdrawing nature of the fluorine atoms.

6.6. Comparison of the spectroscopic and electronic properties of mono-, di-, tri-, and tetrastyrylBODIPY dyes

In this section, the properties predicted for the 1,3,5-tristyrylBODIPY dye, **25**, and a series of model compounds from the corresponding core dye to its 1,3,5,7-tetrastyryl analogue are discussed. For the purposes of this thesis, only the theoretical calculations are carried out for the analogues, and the results are used to assess which of the styrylBODIPY analogues amongst the monostyrylBODIPY, distyrylBODIPY, tristyrylBODIPY and tetrastyrylBODIPY

would be more suitable for study in NLO applications. Having studied the NLO properties of a monostyrylBODIPY, distyrylBODIPYs and a tristyrylBODIPY in this thesis, the TD-DFT results discussed here provide additional information on the trends observed in relation to spectroscopic properties of styrylBODIPY dyes and helped guide the decision to not further pursue the OL properties of tristyryl and tetrastyryl dyes. These spectroscopic properties help shape the NLO responses obtained in the visible region at 532 nm with the second harmonic of the Nd:YAG laser.

As demonstrated above with the *meso*-pyridyl-substituted BODIPY dye series and **3c**, **7c** and **16**, the 3,5-positions are known to have significant MO coefficients at the HOMO and LUMO relative to the 1,7-positions. Therefore, this means that introducing styryl groups at the 3,5-positions is expected to narrow the HOMO–LUMO gap and significantly red-shift the absorption bands relative to when the styryl groups are at the 1,7-positions (**Figure 6.14**). The TD-DFT calculations performed for **25** and analogues clearly show this. The introduction of styryl groups at the 3,5-positions of the core to form the mono- and distyrylBODIPY dyes results in successive large red-shifts of the main spectral band of 47 and 56 nm, respectively (**Figure 6.15** and **Table 6.5**). In contrast, introducing styryl groups at the 1,7-positions to form the tri- and tetrastyrylBODIPY dyes results in much smaller red shifts. The addition of a third styryl group results in a red-shift of 16 nm, whereas the addition of a fourth styryl group results in a red shift of 20 nm (**Figure 6.15** and **Table 6.5**). This clearly demonstrates that additional styryl groups at the 1,7-positions do not alter the spectroscopic properties of distyrylBODIPY dyes significantly enough in the context of the main spectral band and hence are unlikely to eliminate the issue of having significant absorbance at the red end of the visible.

Additionally, in the context of NLO applications related to the protection of optically sensitive materials such as the human eye, a significant disadvantage is introduced by styrylation at the 1,7-positions. This is the appearance of additional absorption bands in the visible region, which can be seen in the TD-DFT spectra of the tri- and tetrastyrylBODIPY dyes (**Figure 6.15**). These bands are predicted to be at 411 and 413 nm, and arise from weak transitions (f = 0.21 and 0.19) (**Table 6.5**). In a similar manner to the spectra of the distyrylBODIPY dyes **13**, **14**, **15** and **16** discussed above, the presence of relatively weak absorption across the visible region makes BODIPY dyes less suitable for study as potential OL materials that can be used in the protection of optically sensitive materials such as the human eye.

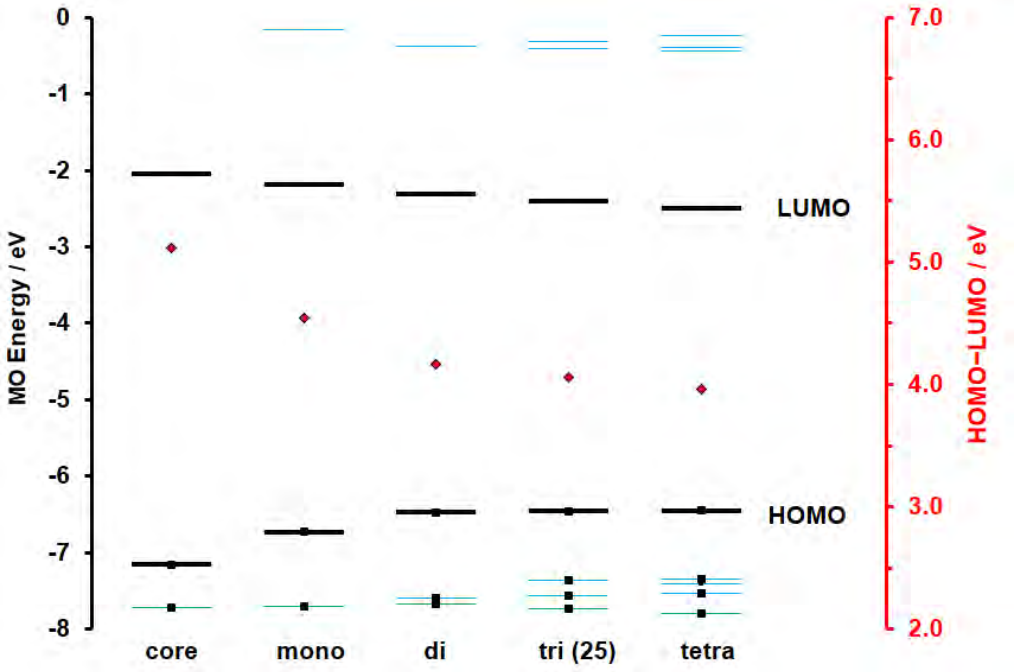

Figure 6.14. Frontier MO energies of **25** and analogues at the CAM-B3LYP/SDD level of theory. Blue and green lines denote the primary localization of MOs on the styryl and phenyl moieties, respectively. The HOMO and LUMO are highlighted with thicker black lines, while small black squares denote occupied MOs. Red diamonds denote the HOMO–LUMO gap values and are plotted against a secondary axis

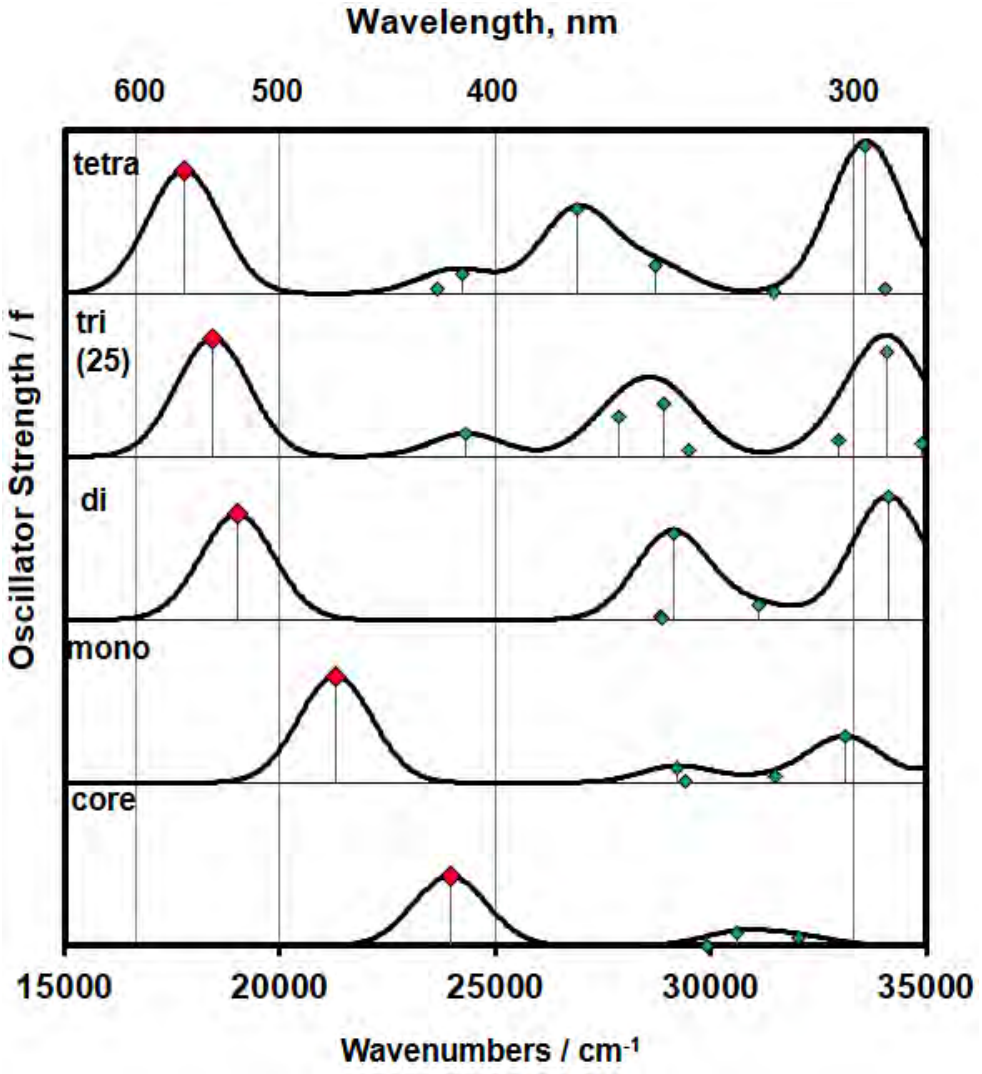

Figure 6.15. Calculated TD-DFT spectra of the optimized geometries of **25** and analogues at the CAM-B3LYP/SDD level of theory. The main spectral bands are highlighted with red diamonds. The simulated spectra were calculated using the Chemcraft program by using bandwidths of 2000 cm^{-1}.[171]

Table 6.5. Electronic properties predicted using TD-DFT calculations at the CAM-B3LYP/SDD level of theory for **25** and analogues.

BODIPY	#[a]	E (ev)[b]	λ_{calc} (nm)[c]	λ_{exp} (nm)[d]	f[e]	Wavefunction[f]
core	1	2.97	423	528	0.64	97% H → L; …
	2	3.71	334	-	0.00	91% H-1 → L; …
	3	3.79	327	-	0.12	96% H-2 → L; …
	4	3.97	312	-	0.08	93% H-3 → L; …
mono	1	2.64	470	-	0.98	96% H → L; …
	2	3.62	342	-	0.14	36% H-1 → L; 28% H-2 → L; 28% H-3 → L; …
	3	3.65	340	-	0.02	54% H-1 → L; 19% H-3 → L; 18% H-2 → L; …
	4	3.91	317	-	0.05	93% H-4 → L; …
	5	4.11	302	-	0.42	48% H-3 → L; 46% H-2 → L; …
di	1	2.36	526	-	0.97	97% H → L; …
	2	3.57	347	-	0.02	70% H-3 → L; 16% H-2 → L; …
	3	3.58	346	-	0.01	75% H-2 → L; 14% H-3 → L; …
	4	3.61	343	-	0.79	94% H-1 → L; …
	5	3.86	321	-	0.14	93% H-4 → L; …

	6	4.23	293	-	1.13	93% H → L+1; …
	7	4.36	285	-	0.01	49% H-5 → L; 34% H-7 → L; 10% H-3 → L; …
tri (25)	1	2.29	542	647	1.09	97% H → L; …
	2	3.02	411	-	0.21	89% H-1 → L; …
	3	3.46	359	-	0.36	64% H-2 → L; 27% H-3 → L; …
	4	3.58	346	-	0.48	58% H-3 → L; 29% H-2 → L; …
	5	3.66	339	-	0.06	60% H-4 → L; 28% H-5 → L; …
	6	4.09	303	-	0.16	40% H-5 → L; 25% H → L+1; 14% H-4 → L; …
	7	4.23	293	-	0.97	56% H → L+1; 13% H-5 → L; 11% H → L+2; …
	8	4.33	286	-	0.13	76% H → L+2; 5% H → L+1; …
tetra	1	2.21	562	-	1.13	97% H → L; …
	2	2.93	423	-	0.05	71% H-1 → L; 19% H-2 → L; …
	3	3.00	413	-	0.19	72% H-2 → L; 20% H-1 → L; …
	4	3.34	372	-	0.78	78% H-3 → L; 14% H-4 → L; …
	5	3.56	348	-	0.26	74% H-4 → L; 15% H-3 → L; …
	6	3.90	318	-	0.01	74% H-5 → L; 6% H → L+2; …
	7	4.17	298	-	1.36	72% H → L+2; 7% H → L+3; …
	8	4.22	294	-	0.05	73% H → L+2; 8% H-5 → L; …

[a] - Excited state number in ascending energy. [b] - Calculated band energies in eV. [c] - Calculated wavelengths in nm. [d] - Experimental wavelengths in DMSO. [e] - Calculated oscillator strengths. [f] - Wavefunctions of the transitions based on eigenvectors predicted by TD-DFT. H and L refer to the HOMO and LUMO, respectively.

In addition to the spectroscopic properties discussed above for **25** and its series of styrylated analogs, the charge distributions can be studied using electrostatic potential maps. In a similar manner to distyrylBODIPY dyes **10**-**17**, the visualization of different charges across the BODIPY structure using color provides information on how different substituents influence the distribution of electrons across the BODIPY structure. Based on the understanding that the red area on the maps corresponds to the negative region of the electrostatic potential, whereas the blue area corresponds to the positive region (**Figure 6.16**), the effect of the presence of additional styryl groups at the 1,7-positions on electron distribution can be studied.

From the ESP maps, it is clear that the presence of additional styryl groups does not significantly alter the distribution of electrons across the BODIPY structure. This is demonstrated by different moieties on the structures maintaining a similar color upon the successive introduction of styryl groups at the 1- and 7-positions in addition to the 3,5-positions (**Figure 6.16**). However, it is worth noting that the electron-deficiency of the *meso*-phenyl ring is altered by the presence of styryl groups at the 1,7-positions. This is demonstrated by the weaker blue color for the *meso*-phenyl rings of the tri- and tetrastyrylBODIPY dyes after introducing the benzene rings, which form part of the 1,7-styryl

groups (**Figure 6.16**). This can be expected to decrease the magnitude of the dipole moment across the BODIPY structure, and hence may result in less favorable OL properties.

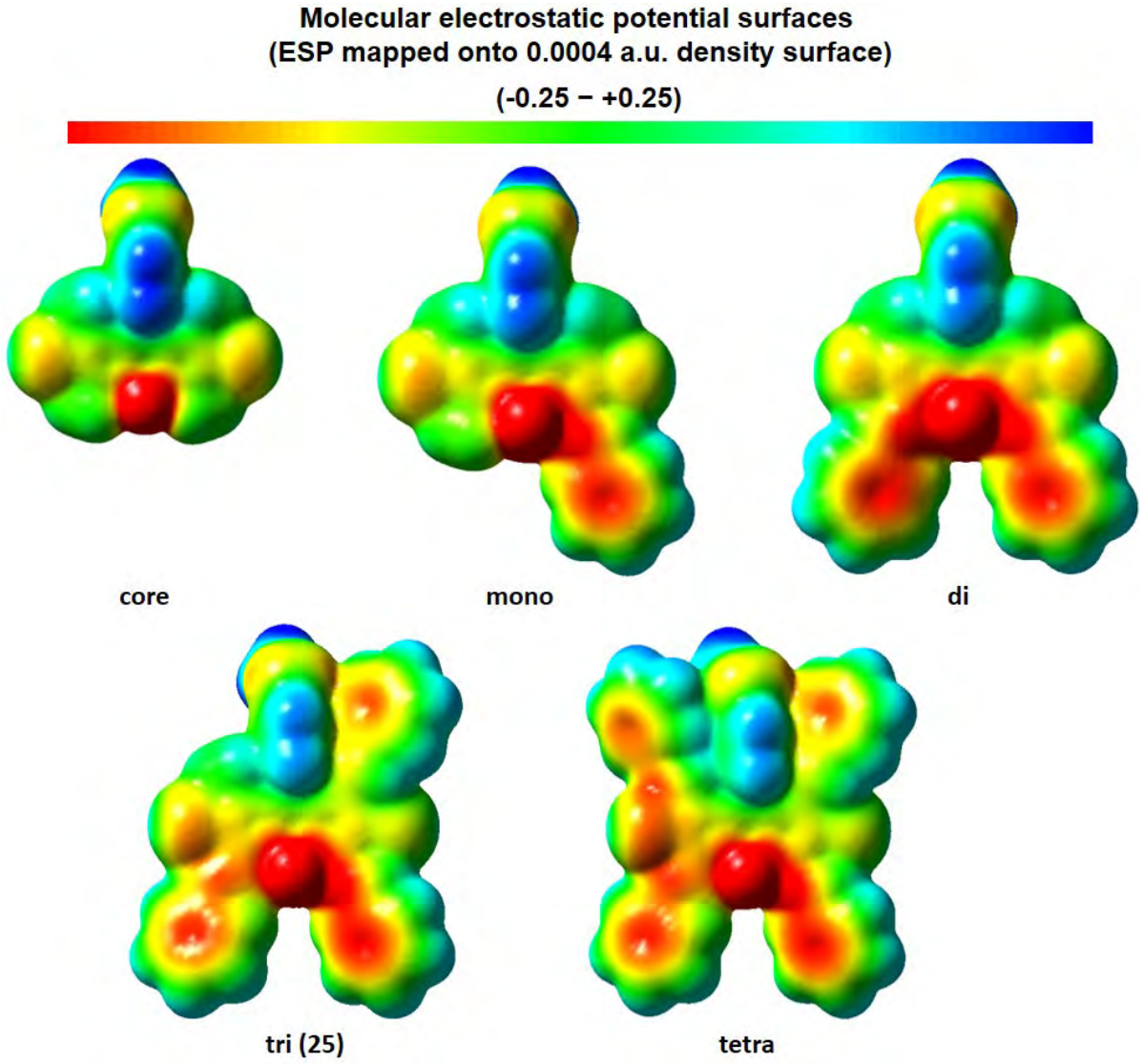

Figure 6.16. Molecular electrostatic potential maps for **25** and analogues. The mapping was performed using GaussView and corresponds to the attractive and repulsive force exerted on a point positive charge. A red surface color corresponds to the negative region of the electrostatic potential where electron-rich portions of the structure attract the point positive charge, whereas the blue area corresponds to the positive region where electron-deficient portions of the structure repel the point positive charge.

6.7. Concluding remarks

A series of novel and previously synthesized BODIPY dyes were studied in this thesis, and in this chapter, their optimized geometries and spectroscopic properties were successfully calculated and analyzed in detail. The optimized geometries were obtained using the B3LYP functional, while the optical properties were predicted using TD-DFT calculations using the CAM-B3LYP functional. For both the geometry optimization and TD-DFT calculations, the default Gaussian 09 SDD basis sets were used. From the results discussed above, the presence of bromine, iodine, ethyl and styryl groups at all positions of the BODIPY core leads to a narrowing of the HOMO–LUMO band gap. This led in each case to a red-shift of the main spectral band of differing magnitudes due to their differing mesomeric effects, as is often the case for BODIPY dyes.[3,178] The trend in the magnitude of the red-shift is styryl > iodine > bromine > ethyl.

While the introduction of styryl groups at the 3,5-positions significantly red-shifts the main absorption band of BODIPY dyes and minimizes the absorption at the 532 nm wavelength used for NLO studies, there is still an envelope of relatively weak absorption across the visible region. This minimal absorption differs in magnitude, with BODIPY **16** having significantly weaker absorption at 532 nm than the other dyes. This was observed with both the predicted and experimental spectra, posing a challenge in the application of BODIPY dyes as OL materials, especially in the fabrication of materials that can protect the human eye from light sources such as laser irradiation. Tri- and tetrastyrylBODIPY dyes have extra bands in the 400−600 nm region in addition to what is typically observed for 3,5-distyrylBODIPY dyes, tri- and tetrastyrylBODIPY dyes are less suitable for OL applications related to the protection of the human eye since they are less likely to transmit visible region photons under ambient light

conditions. While organic molecular dyes such as porphyrins and phthalocyanines, and recently BODIPYs have been extensively studied for the fabrication of potential OL materials, issues related to significant absorbance across the visible region under ambient light conditions introduces a need for alternatives. The optically transparent thin films discussed in Chapter 4 may provide a solution to this as the disilane-bridged architectures may serve as a starting point towards researching alternatives.

Partial atomic charges have been calculated for some of the styrylBODIPY dyes studied for application in NLO. Structural changes which change the nature of the bonds on the carbon atoms of the BODIPY core modify the distribution of electrons on these atoms. The structural changes observed here are the formation of C–C bonds at the 1,7-, 2,6- and 3,5-positions of the BODIPY core. These lead to changes in the magnitude of the atomic charges on the carbons at these positions, and the charges on the carbons at the 1,7- and 2,6-positions become positive. The charge distributions of the distyrylBODIPY dyes studied for application in NLO in Chapter 4 have been studied by using electrostatic potential energy maps. The differences in the electronegativities of the atoms present on the different substituents on the BODIPY structure are responsible for the charge distributions. Worth noting in the context of NLO and the related hyperpolarizability is the push-pull system formed by the charge distributions obtained for **10**, **11**, **12** and **17**. These D–π–A type dyes are a clear example of the effect of electronegativity on charge distribution, as they possess distinct positive charges on the nitrogen atoms at the 3,5-position styryl groups (blue color) and distinct negative charges on the nitrogen atoms at the *meso*-position which contains fluorine atoms (slightly red color). For all the BODIPYs studied, the electronegativities of the atoms modulate charge distribution on the BODIPY structure.

Chapter 7:

Conclusions and future recommendations

7.1. General conclusions

In this thesis, a series of structurally diverse BODIPY dyes have been synthesized, characterized and their suitability for use as photosensitizers in PACT and as optical limiters in NLO assessed. From the synthesized BODIPY core dyes, **1a**, **1b**, **1k**, **3d** and **3e** are novel, while the rest of the core dyes have been previously synthesized,[123–126,129,130] and all the styrylBODIPY dyes synthesized were novel. The BODIPY core dyes were synthesized using the classic "one-pot three-step" acid-catalyzed condensation reaction, whereas the styrylBODIPY dyes were synthesized using a modified Knoevenagel condensation reaction.[1,3] Challenges were encountered when D-π-A type BODIPY dyes analogues of BODIPYs **10**-**13** and **17** were synthesized using electron-deficient aldehydes as substituents at the 3,5-positions. This strategy of using aldehydes containing electron-withdrawing groups was used to target novel styrylBODIPY dyes using an approach that would normally not yield the target structures, since electron-deficient aldehydes are known to be unreactive during Knoevenagel condensation reactions.[5,15,16]

BODIPY core dyes **1a**, **2a** and **3a**, are structural analogues. The difference between them arises from using 2-methylpyrrole, 2-ethylpyrrole and 2,4-dimethylpyrrole as the starting pyrroles, respectively. BODIPY core dyes **1b**, **3b** and **4b** are also analogues, and the difference, in this case, is the use of 2-methylpyrrole, 2,4-dimethylpyrrole and 3-ethyl-2,4-dimethylpyrrole as the starting pyrroles, respectively. For BODIPY core dyes **1c** and **3c**, 2-methylpyrrole and 2,4-dimethylpyrrole were used as the starting pyrroles, respectively. The other set of BODIPY core dye analogues is **3d**, **3e** and **3f**, synthesized from 2-iodobenzaldehyde, 3-iodobenzaldehyde or 4-iodobenzaldehyde, respectively. After synthesizing the BODIPY core dyes, halogen heavy atoms (bromine or iodine) were introduced at the 2,6-positions of BODIPYs **1a**, **2a**, **3a**, **3c**–**i** to

form **5a**, **6a**, **7a**, **7c**-**i**, **8a** and **9a**, as described in Chapters 2 and 3. The reaction of **1a** with NBS gave **5a**, which contains bromine heavy atoms at the 1,7- and 2,6-positions. In contrast, the reaction of **1a** with an equivalent amount of NIS gave **8a**, which does not contain iodine heavy atoms at the 1,7-positions. The halogenated BODIPY core dyes were obtained in small yields in some instances, as reported in Chapter 2. The substituents at the *meso* position can also be halogenated and this leads to side products which were isolated during column chromatography, especially for the dyes containing phenyl substituents. During the synthesis of **5a**, **6a** and **8a**, the yields of the side products increased due to the absence of methyl substituents at the 1,7-positions. The introduction of heavy atoms onto the BODIPY core dyes was carried out firstly to red-shift the main absorption bands of the dyes and secondly to enhance the generation of singlet oxygen upon photoexcitation. Red-shifted spectral bands were observed experimentally, as discussed in Chapter 3, and the reasons for this are discussed in depth in the context of the TD-DFT calculations discussed in Chapter 6. The halogenated BODIPY core dyes have moderately high singlet oxygen quantum yields in DMSO with the sole exception of **5a**. This makes the halogenated core dyes suitable for study as photosensitizers in PACT. The low singlet oxygen quantum yield for **5a** was attributed to poor photostability, making the dye a poor candidate for photosensitizer applications, as detailed in Chapter 5.

The PACT studies carried out in Chapter 5 using the neutral halogenated BODIPY core dyes were aimed primarily at identifying structure-property relationships that determine the suitability of BODIPYs for use as photosensitizer dyes in this context. Because neutral BODIPY dyes are known to be active against the Gram-positive *Staphylococcus aureus*,[160,161] this was the bacteria selected in this work. The structure-property relationships were assessed

primarily by using two different series of BODIPY analogues. The PACT activities of other novel and previously synthesized halogenated BODIPYs against *Staphylococcus aureus* were also analyzed where appropriate. The first set of BODIPY analogues is **5a**, **6a**, **7a**, **8a** and **9a**, which exhibit minor differences on the BODIPY core related to the absence and presence of methyl groups at the 1,7-positions, the presence of ethyl or methyl groups at the 3,5-positions, and the presence of bromine or iodine heavy atoms at the 2,6-positions. The other set of dye analogues are **7d**, **7e** and **7f**, which contain an iodine heavy atom at different positions of the *meso*-aryl ring.

All the dyes studied reduced bacterial viability to below 50%, and there was no significant difference in the number of viable colonies remaining after the bacterial cells were treated with **7d**, **7e** and **7f**. For the bacterial cells treated with **5a**, **6a**, **7a**, **8a** and **9a**, no viable colonies remained after treatment with the BODIPYs containing protons at the 1,7-positions or iodines at the 2,6-positions, except for **5a** which has a significantly low singlet oxygen quantum yield. Hence, it can be concluded that the presence of protons at the 1,7-positions and iodines at the 2,6-positions leads to more favorable PACT activity, especially when combined, as is the case with the structure of **8a**. This dye was the best performing dye in this set of analogues. Even in the absence of this combination, each of these dyes still exhibits favorable PACT activity, as observed for **6a** and **9a**, which exclusively contain protons at the 1,7-positions and iodines at the 2,6-positions, respectively.

Using a modified Knoevenagel condensation reaction, the styrylBODIPY dyes studied in this thesis were synthesized from the core dyes. BODIPYs **1a**, **2a** and **7a** were used to synthesize **10**, **11** and **12**, respectively. BODIPY **17** was also synthesized from **7a**. These dyes were rationally designed to contain electron-donating groups at the 3,5-positions and electron-

withdrawing groups at the *meso* position. This creates a D–π–A or push-pull system which typically enhances the NLO properties of BODIPYs and other organic compounds.[19,20,98–100] BODIPYs **13**, **14** and **15** were synthesized from **1b**, **3b** and **4b**, whereas **16** was synthesized from **3c**. BODIPYs **13**, **14** and **15** contain a pyridine group at the *meso*-position and benzene rings on the styryl groups at the 3,5-positions and differ structurally by the type of substituent present at the 1,7- and 2,6-positions. BODIPY **16** contains an acetamido moiety at the *meso* position and benzyloxy moieties on the styryl groups at the 3,5-positions. These nonhalogenated styrylBODIPY dyes were selected to study the effect of substituents other than heavy atoms on the BODIPY core on the NLO properties. BODIPY **16** was specifically used to better understand the mechanism responsible for the typically favorable NLO responses observed for nonhalogenated BODIPY dyes.[37] The NLO studies were carried out with organic solutions of all the styrylBODIPY dyes at concentrations that lie in the linear range of Beer-Lambert plots using the Z-scan setup described in Chapter 2 with 7 or 10 ns laser pulses at an input intensity of *ca.* 35 μJ. The second harmonic of the Nd:YAG laser at 532 nm was used to provide the beam, since this lies in the portion of the visible region where the human eye is most sensitive.

During the z-scan measurements, all the BODIPYs exhibited favorable reverse saturable absorption responses characterized by a significant decrease in transmittance at high laser light intensity. Research into the suitability of BODIPY dyes as optical limiters at 532 nm is not a widely researched area. On the basis of the work conducted in this thesis and recently published research articles,[19,93,95,132,179,180] the following conclusions on the suitability of BODIPY dyes as optical limiters can be drawn:

- Slightly enhanced OL parameters, especially hyperpolarizability, are observed for styrylBODIPY dyes with no methyl groups at the 1,7-positions relative to other analogue structures.[100] This is thought to be due to the absence of steric hindrance introduced by the methyl groups. In the absence of this, the *meso*-aryl ring lies closer to the π-system of the BODIPY core and leads to enhanced D-π-A properties and the overall improvement of the NLO properties.
- Comparing the OL properties obtained for the **11** and **12** analogue dyes leads to the conclusion that there is no evidence that the introduction of heavy atoms onto the structure of BODIPY dyes significantly enhances OL properties,[100] as has been observed in other organic dyes. This observation has been made previously using another pair of BODIPY analogue dyes.[93]
- Using the **14** and **15** analogue dyes, the effect of the presence of ethyl groups at the 2,6-positions on the NLO properties of a distyrylBODIPY dye has been assessed for the first time by using the latter. From the results obtained in this thesis, incorporating alkyl substituents onto the BODIPY core does not significantly enhance the OL properties of styrylBODIPY dyes.
- Because it was established that the presence of heavy atoms on the BODIPY core does not significantly enhance BODIPY OL properties relative to the nonhalogenated analogue dyes, **16** was used to study the mechanism responsible for the NLO responses observed for nonhalogenated styrylBODIPY dyes.[37] The mechanism was established by combining an analysis of the z-scan data obtained with a transient absorption spectroscopy study with a femtosecond laser system, which identified a broad peak attributable to ESA. This ESA was postulated to be strictly from the S_1 since **16** contains no heavy atoms to

promote intersystem crossing into the triplet state. To confirm this, triplet decay curves were measured on the microsecond timescale for **16**, and no signal was observed. This led to the conclusion that the mechanism is one-photon absorption from the ground state followed by ESA in the singlet manifold.

- Having studied the NLO properties of a monostyrylBODIPY dye and distyrylBODIPY dyes, the properties of a 1,3,5-tristyrylBODIPY dye, **25** were assessed.[142] The NLO properties and calculated OL parameters obtained at 532 nm were found not to be significantly different to those of other styrylBODIPY dyes obtained under similar conditions.[95] From the diverse structures studied, monostyrylBODIPY, distyrylBODIPY, and tristyrylBODIPY dyes all possess OL parameters with values similar in magnitude to those of other organic dyes that are viewed as suitable for this application.[79,144,156]

In addition to assessing the NLO properties of BODIPY dyes, the properties of scandium phthalocyanines were assessed for the first time. This was achieved using a monomeric $Sc^{III}Pc$ and both the green and blue forms of a dimeric $Sc^{III}Pc_2$.[141] The properties of the latter were found to be similar in magnitude to what has been reported for other dimeric phthalocyanines. Therefore, it can be concluded that the introduction of a scandium ion as a first-row transition metal does not significantly enhance OL properties relative to those observed for other metallophthalocyanines, such as rare earth dimeric phthalocyanine complexes. Because there is a requirement for minimal to no absorption in the visible region by materials used to fabricate protective OL materials, especially for the human eye, challenges arise regarding BODIPYs and phthalocyanines. Both BODIPYs and phthalocyanines tend to absorb significantly in the visible region, as is evident from the dyes studied in this work. This may be circumvented by designing OL materials that remain transparent under

ambient light conditions.[140] As flexible as the BODIPY structure is from a synthetic standpoint, shifting the main spectral band into the NIR region does not eliminate absorption across the visible region under ambient light conditions. This holds for phthalocyanines too.

7.2. Future recommendations

The structure-property relationships of interest in the PACT studies carried out in this thesis demonstrated that the absence of methyls at the 1,7-positions and the presence of iodines at the 2,6-positions of neutral BODIPYs leads to favorable PACT activity against a commercial strain of the gram-positive *Staphylococcus aureus*. Once this is combined with the established research on the activity of cationic BODIPYs against commercial strains of gram-negative bacteria such as *Escherichia coli*,[49,72,181,182] BODIPYs can be structurally designed in this manner to target environmental strains. One environment of interest is healthcare centers that possess various strains of bacteria, which lead to nosocomial or healthcare-associated infections (HCAIs).[167,166,183,184] We, therefore, propose the use of BODIPY dyes in the inactivation of strains responsible for these infections as the next potential line of research to create viable alternatives to antibiotics.

Because of the challenge posed by the absorbance of photons in the visible region by phthalocyanines and BODIPYs under ambient light conditions, the future development of protective OL materials designed specifically to protect the human eye as opposed to sensitive optical equipment may lie in compounds with minimal ground state absorption in the visible region. One such set of compounds is the σ-bridged molecules connected *via* disilane linkers synthesized at Hangzhou Normal University, whose optical limiting properties were studied at Rhodes University during this work.[140] These optically transparent disilane-

bridged compounds do not absorb significantly in the visible region, i.e. *ca.* 400–700 nm, and their PBC polymer thin films exhibit an excellent RSA response. The high I_{lim} values obtained for these transparent thin films (above 0.95 J.cm^{-2}) could be further lowered by using higher concentrations of the dyes during thin film preparation.

References

(1) Atilgan, S.; Ekmekci, Z.; Dogan, A. L.; Guc, D.; Akkaya, E. U. Water Soluble Distyryl-Boradiazaindacenes as Efficient Photosensitizers for Photodynamic Therapy. *Chem. Commun.* **2006**, *43* (42), 4398–4400.

(2) Dost, Z.; Atilgan, S.; Akkaya, E. U. Distyryl-Boradiazaindacenes: Facile Synthesis of Novel near IR Emitting Fluorophores. *Tetrahedron* **2006**, *62* (36), 8484–8488.

(3) Lu, H.; Mack, J.; Yang, Y.; Shen, Z. Structural Modification Strategies for the Rational Design of Red/NIR Region BODIPYs. *Chem. Soc. Rev.* **2014**, *43* (13), 4778–4823.

(4) Schmitt, A.; Hinkeldey, B.; Wild, M.; Jung, G. Synthesis of the Core Compound of the BODIPY Dye Class: 4,4'-Difluoro-4-Bora-(3a,4a)-Diaza-*s*-Indacene. *J. Fluoresc.* **2009**, *19* (4), 755–758.

(5) Leen, V. Synthesis and Application of Reactive BODIPY Dyes, PhD thesis, Katholieke Universiteit Leuven, Leuven, Belgium, 2010.

(6) Treibs, A.; Kreuzer, F. . Difluorboryl-Komplexe von Di Und Tripyrrylmethenen. *Justus Liebigs Ann. Chem.* **1968**, *718*, 208–223.

(7) Ulrich, G.; Goze, C.; Guardigli, M.; Roda, A.; Ziessel, R. Pyrromethene Dialkynyl Borane Complexes for "Cascatelle" Energy Transfer and Protein Labeling. *Angew. Chem Int. Ed.* **2005**, *44* (24), 3694–3698.

(8) Nguyen, A. L. Boron Functionalization of BODIPY Dyes, and Their Evaluation as Bioimaging Agents, PhD thesis, Louisiana State University and Agricultural and Mechanical College, Baton Rouge, United States, 2015.

(9) Li, L.; Nguyen, B.; Burgess, K. Functionalization of the 4,4-Difluoro-4-Bora-3a,4a-Diaza-*s*-Indacene (BODIPY) Core. *Bioorg. Med. Chem. Lett.* **2008**, *18* (10), 3112–3116.

(10) Jagtap, K. K.; Shivran, N.; Mula, S.; Naik, D. B.; Sarkar, S. K.; Mukherjee, T.; Maity, D. K.; Ray, A. K. Change of Boron Substitution Improves the Lasing Performance of BODIPY Dyes: A Mechanistic Rationalisation. *Chem. Eur. J.* **2013**, *19* (2), 702–708.

(11) Ulrich, G.; Ziessel, R.; Harriman, A. The Chemistry of Fluorescent BODIPY Dyes: Versatility Unsurpassed. *Angew. Chem Int. Ed.* **2008**, *47* (7), 1184–1201.

(12) Clarke, R. G.; Hall, M. J. Recent Developments in the Synthesis of the BODIPY Dyes. In *Advances in Heterocyclic Chemistry Vol. 128*, Scriven, E. F. V.; Ramsden, C. A., Eds; Elsevier: Amsterdam, 2019; pp 181–261.

(13) Loudet, A.; Burgess, K. BODIPY Dyes and Their Derivatives: Syntheses and Spectroscopic Properties. *Chem. Rev.* **2007**, *107* (11), 4891–4932.

(14) Saki, N.; Dinc, T.; Akkaya, E. U. Excimer Emission and Energy Transfer in Cofacial Boradiazaindacene (BODIPY) Dimers Built on a Xanthene Scaffold. *Tetrahedron* **2006**, *62* (11), 2721–2725.

(15) Galangau, O.; Dumas-Verdes, C.; Méallet-Renault, R.; Clavier, G. Rational Design of Visible and NIR Distyryl-BODIPY Dyes from a Novel Fluorinated Platform. *Org. Biomol. Chem.* **2010**, *8* (20), 4546–4553.

(16) Hayes, J. S. Synthesis, Characterization, and Evaluation of Novel BODIPY Dyes With Theranostic Applications, PhD thesis, Louisiana State University and Agricultural and

Mechanical College, Baton Rouge, United States, 2014.

(17) Chen, J.; Burghart, A.; Derecskei-Kovacs, A.; Burgess, K. 4,4-Difluoro-4-Bora-3a,4a-Diaza-*s*-Indacene (BODIPY) Dyes Modified for Extended Conjugation and Restricted Bond Rotations. *J. Org. Chem.* **2000**, *65* (10), 2900–2906.

(18) Mafukidze, D. M.; Nyokong, T. Photodynamic Antimicrobial Chemotherapy of a Dimethylamino-Functionalized Asymmetric Zinc(II) Phthalocyanine and Its Quaternized Derivative against Staphylococcus Aureus When Supported on Asymmetric Polystyrene Polymer Membranes. *React. Funct. Polym.* **2020**, *154* (2020), 104634.

(19) Harris, J.; Gai, L.; Kubheka, G.; Mack, J.; Nyokong, T.; Shen, Z. Optical Limiting Properties of 3,5-Dithienylenevinylene BODIPY Dyes at 532 nm. *Chem. Eur. J.* **2017**, *23* (58), 14507–14514.

(20) Sutherland, R. L. *Handbook of Nonlinear Optics*, 2nd ed.; CRC Press: New York, 2003.

(21) Kasha, M. Characterization of Electronic Transitions in Complex Molecules. *Discuss. Faraday Soc.* **1950**, *9*, 14–19.

(22) López Arbeloa, F.; Bañuelos, J.; Martínez, V.; Arbeloa, T.; López Arbeloa, I. Structural, Photophysical and Lasing Properties of Pyrromethene Dyes. *Int. Rev. Phys. Chem.* **2005**, *24* (2), 339–374.

(23) Awuah, S. G.; Polreis, J.; Biradar, V.; You, Y. Singlet Oxygen Generation by Novel NIR BODIPY Dyes. *Org. Lett.* **2011**, *13* (15), 3884–3887.

(24) Yang, Y.; Guo, Q.; Chen, H.; Zhou, Z.; Guo, Z.; Shen, Z. Thienopyrrole-Expanded BODIPY as a Potential NIR Photosensitizer for Photodynamic Therapy. *Chem. Commun.* **2013**, *49* (38), 3940–3942.

(25) Yogo, T.; Urano, Y.; Ishitsuka, Y.; Maniwa, F.; Nagano, T. Highly Efficient and

Photostable Photosensitizer Based on BODIPY Chromophore. *J. Am. Chem. Soc.* **2005**, *127* (35), 12162–12163.

(26) Wang, Y. W.; Descalzo, A. B.; Shen, Z.; You, X. Z.; Rurack, K. Dihydronaphthalene-Fused Boron-Dipyrromethene (BODIPY) Dyes: Insight into the Electronic and Conformational Tuning Modes of BODIPY Fluorophores. *Chem. Eur. J.* **2010**, *16* (9), 2887–2903.

(27) López Arbeloa, F.; López Arbeloa, T.; López Arbeloa, I.; García-Moreno, I.; Costela, A.; Sastre, R.; Amat-Guerri, F. Photophysical and Lasing Properties of Pyrromethene 567 Dye in Liquid Solution. Environment Effects. *Chem. Phys.* **1998**, *236* (1–3), 331–341.

(28) Fery-Forgues, S.; Lavabre, D. Are Fluorescence Quantum Yields So Tricky to Measure? A Demonstration Using Familiar Stationery Products. *J. Chem. Educ.* **1999**, *76* (9), 1260–1264.

(29) Fletcher, A.; Kubin, R. F. Fluorescence Quantum Yields of Some Rhodamine Dyes. *J. Lumin.* **1982**, *27*, 455–462.

(30) Ogunsipe, A.; Chen, J.; Nyokong, T. Photophysical and Photochemical Studies of Zinc(II) Phthalocyanine Derivatives-Effects of Substituents and Solvents. *New J. Chem.* **2004**, *28*, 822–827.

(31) Rurack, K.; Kollmannsberger, M.; Daub, J. A Highly Efficient Sensor Molecule Emitting in the near Infrared (NIR): 3,5-Distyryl-8-(*p*-Dimethylaminophenyl)Difluoroboradiaza-*s*-Indacene. *New J. Chem.* **2001**, *25* (2), 289–292.

(32) Wu, W.; Guo, H.; Wu, W.; Ji, S.; Zhao, J. Organic Triplet Sensitizer Library Derived from a Single Chromophore (BODIPY) with Long-Lived Triplet Excited State for Triplet-Triplet Annihilation Based Upconversion. *J. Org. Chem.* **2011**, *76* (17), 7056–7064.

(33) Luo, G.-G.; Lu, H.; Zhang, X.-L.; Dai, J.-C.; Wu, J.-H.; Wu, J.-J. The Relationship between

the Boron Dipyrromethene (BODIPY) Structure and the Effectiveness of Homogeneous and Heterogeneous Solar Hydrogen-Generating Systems as Well as DSSCs. *Phys. Chem. Chem. Phys.* **2015**, *17* (15), 9716–9729.

(34) Seotsanyana-Mokhosi, I.; Nyokong, T. Synthesis and Photochemical Studies of Substituted Adjacent Binaphthalophthalocyanines. *J. Porphyrins Phthalocyanines* **2004**, *08* (10), 1214–1221.

(35) Ogunsipe, A.; Nyokong, T. Effects of Central Metal on the Photophysical and Photochemical Properties of Non-Transition Metal Sulfophthalocyanine. *J. Porphyrins Phthalocyanines* **2005**, *9* (2), 121–129.

(36) Deniz, E.; Isbasar, G. C.; Bozdemir, Ö. A.; Yildirim, L. T.; Siemiarczuk, A.; Akkaya, E. U. Bidirectional Switching of near IR Emitting Boradiazaindacene Fluorophores. *Org. Lett.* **2008**, *10* (16), 3401–3403.

(37) Ngoy, B. P.; May, A. K.; Mack, J.; Nyokong, T. Optical Limiting and Femtosecond Pump-Probe Transient Absorbance Properties of a 3,5-DistyrylBODIPY Dye. *Front. Chem.* **2019**, *7*, 1–9.

(38) Coskun, A.; Akkaya, E. Ion Sensing Coupled to Resonance Energy Transfer: A Highly Selective and Sensitive Ratiometric Fluorescent Chemosensor for Ag (I) by a Modular Approach. *J. Am. Chem. Soc.* **2005**, *127*, 10464–10465.

(39) Li, F.; Yang, S. I.; Ciringh, Y.; Seth, J.; Martin, C. H.; Singh, D. L.; Kim, D.; Birge, R. R.; Bocian, D. F.; Holten, D.; Lindsey, J. S. Design, Synthesis, and Photodynamics of Light-Harvesting Arrays Comprised of a Porphyrin and One, Two, or Eight Boron-Dipyrrin Accessory Pigments. *J. Am. Chem. Soc.* **1998**, *120* (39), 10001–10017.

(40) Yee, M. C.; Fas, S. C.; Stohlmeyer, M. M.; Wandless, T. J.; Cimprich, K. A. A Cell-

Permeable, Activity-Based Probe for Protein and Lipid Kinases. *J. Biol. Chem.* **2005**, *280* (32), 29053–29059.

(41) Bañuelos, J.; Martín, V.; Gómez-Durán, C. F. A.; Córdoba, I. J. A.; Peña-Cabrera, E.; García-Moreno, I.; Costela, Á.; Pérez-Ojeda, M. E.; Arbeloa, T.; Arbeloa, Í. L. New 8-Amino-BODIPY Derivatives: Surpassing Laser Dyes at Blue-Edge Wavelengths. *Chem. Eur. J.* **2011**, *17* (26), 7261–7270.

(42) Niu, S. L.; Massif, C.; Ulrich, G.; Renard, P. Y.; Romieu, A.; Ziessel, R. Water-Soluble Red-Emitting Distyryl-Borondipyrromethene (BODIPY) Dyes for Biolabeling. *Chem. Eur. J.* **2012**, *18* (23), 7229–7242.

(43) He, H.; Lo, P.-C.; Yeung, S.-L.; Fong, W.-P.; Ng, D. K. P. Preparation of Unsymmetrical Distyryl BODIPY Derivatives and Effects of the Styryl Substituents on Their in Vitro Photodynamic Properties. *Chem. Commun.* **2011**, *47* (16), 4748–4750.

(44) Benniston, A. C.; Copley, G. Lighting the Way Ahead with Boron Dipyrromethene (Bodipy) Dyes. *Phys. Chem. Chem. Phys.* **2009**, *11* (21), 4124.

(45) Buyukcakir, O.; Bozdemir, O. A.; Kolemen, S.; Erbas, S.; Akkaya, E. U. Tetrastyryl-Bodipy Dyes: Convenient Synthesis and Characterization of Elusive near IR Fluorophores. *Org. Lett.* **2009**, *11* (20), 4644–4647.

(46) Monsma, F. J.; Barton, C.; Kang, H. C.; Brassard, D. L.; Haugland, R. P.; Sibley, D. R. Characterization of Novel Fluorescent Ligands with High Affinity for D_1 and D_2 Dopaminergic Receptors. *J. Neurochem.* **1989**, *52 (5)*, 1641–1644.

(47) Huang, X.; El-Sayed, M. A. Plasmonic Photo-Thermal Therapy (PPTT). *Alexandria J. Med.* **2011**, *47* (1), 1–9.

(48) Dickerson, E. B.; Dreaden, E. C.; Huang, X.; El-Sayed, I. H.; Chu, H.; Pushpanketh, S.;

McDonald, J. F.; El-Sayed, M. A. Gold Nanorod Assisted Near-Infrared Plasmonic Photothermal Therapy (PPTT) of Squamous Cell Carcinoma in Mice. *Cancer Lett.* **2008**, *269* (1), 57–66.

(49) Awuah, S. G.; You, Y. Boron Dipyrromethene (BODIPY)-Based Photosensitizers for Photodynamic Therapy. *RSC Adv.* **2012**, *2* (30), 11169–11183.

(50) Agostinis, P.; Berg, K.; Cengel, K. A.; Foster, T. H.; Girotti, A. W.; Gollnick, S. O.; Hahn, S. M.; Hamblin, M. R.; Juzeniene, A.; Kessel, D.; Korbelik, D.; Moan, J.; Mroz, P.; Nowis, D.; Piette, J.; Wilson, B. C.; Golab, J. Photodynamic Therapy of Cancer : An Update. *Am. Cancer Soc.* **2011**, *61*, 250–281.

(51) Gallardo-Villagrán, M.; Leger, D. Y.; Liagre, B.; Therrien, B. Photosensitizers Used in the Photodynamic Therapy of Rheumatoid Arthritis. *Int. J. Mol. Sci.* **2019**, *20* (13), 3339.

(52) Kamkaew, A.; Lim, S. H.; Lee, H. B.; Kiew, L. V.; Chung, L. Y.; Burgess, K. BODIPY Dyes in Photodynamic Therapy. *Chem. Soc. Rev.* **2013**, *42* (1), 77–88.

(53) Wainwright, M.; Byrne, M. N.; Gattrell, M. A. Phenothiazinium-Based Photobactericidal Materials. *J. Photochem. Photobiol. B* **2006**, *84* (3), 227–230.

(54) O'Connor, A. E.; Gallagher, W. M.; Byrne, A. T. Porphyrin and Nonporphyrin Photosensitizers in Oncology: Preclinical and Clinical Advances in Photodynamic Therapy. *Photochem. Photobiol. B* **2009**, *85* (5), 1053–1074.

(55) Dai, T.; Fuchs, B. B.; Coleman, J. J.; Prates, R. A.; Astrakas, C.; St. Denis, T. G.; Ribeiro, M. S.; Mylonakis, E.; Hamblin, M. R.; Tegos, G. P. Concepts and Principles of Photodynamic Therapy as an Alternative Antifungal Discovery Platform. *Front. Microbiol.* **2012**, *3*, 1–16.

(56) Alberto, M. E.; De Simone, B. C.; Russo, N.; Sicilia, E.; Toscano, M. Can BODIPY Dimers

Act as Photosensitizers in Photodynamic Therapy? A Theoretical Prediction. *Front. Phys.* **2018**, *6*, 143.

(57) Molupe, N.; Babu, B.; Oluwole, D. O.; Prinsloo, E.; Gai, L.; Shen, Z.; MacK, J.; Nyokong, T. Photodynamic Activity of 2,6-Diiodo-3,5-DithienylvinyleneBODIPYs and Their Folate-Functionalized Chitosan-Coated Pluronic® F-127 Micelles on MCF-7 Breast Cancer Cells. *J. Porphyrins Phthalocyanines* **2020**, 24 (05n07), 973–984.

(58) Green, B. N.; Johnson, C. D.; Egan, J. T.; Rosenthal, M.; Griffith, E. A.; Evans, M. W. Methicillin-Resistant Staphylococcus Aureus: An Overview for Manual Therapists. *J. Chiropr. Med.* **2012**, *11* (1), 64–76.

(59) Phoenix, D. A.; Harris, F.; Dennison, S. R. Photodynamic Antimicrobial Chemotherapy. In *Novel Antimicrobial Agents and Strategies*; Phoenix, D. A., Harris, F., Dennison, S. R., Eds; Wiley-VCH: Weinheim, Germany, 2014; pp 295–330.

(60) Wainwright, M. Photodynamic Antimicrobial Chemotherapy (PACT). *J. Antimicrob. Chemother.* **1998**, *42* (1), 13–28.

(61) Mafukidze, D. M.; Sindelo, A.; Nyokong, T. Spectroscopic Characterization and Photodynamic Antimicrobial Chemotherapy of Phthalocyanine-Silver Triangular Nanoprism Conjugates When Supported on Asymmetric Polymer Membranes. *Spectrochim. Acta A* **2019**, *219*, 333–345.

(62) Sindelo, A.; Kobayashi, N.; Kimura, M.; Nyokong, T. Physicochemical and Photodynamic Antimicrobial Chemotherapy Activity of Morpholine-Substituted Phthalocyanines: Effect of Point of Substitution and Central Metal. *J. Photochem. Photobiol. A* **2019**, *374*, 58–67.

(63) Chen, J.; Chen, Z.; Zheng, Y.; Zhou, S.; Wang, J.; Chen, N.; Huang, J.; Yan, F.; Huang, M.

Substituted Zinc Phthalocyanine as an Antimicrobial Photosensitizer for Periodontitis Treatment. *J. Porphyrins Phthalocyanines* **2011**, *15* (4), 293–299.

(64) Wainwright, M. Photoinactivation of Viruses. *Photochem. Photobiol. Sci.* **2004**, *3* (5), 406–411.

(65) Harris, F.; Dennison, S. R.; Phoenix, D. A. The Antimicrobial Effects of Ultrasound. In *Novel Antimicrobial Agents and Strategies*; Phoenix, D. A., Harris, F., Dennison, S. R., Eds; Wiley-VCH: Weinheim, Germany, 2014; pp 331–355.

(66) Diffen.com, https://www.diffen.com/difference/Gram-negative_Bacteria_vs_Gram-positive_Bacteria (accessed May 20, 2020).

(67) Jori, G.; Brown, S. B. Photosensitized Inactivation of Microorganisms. *Photochem. Photobiol. Sci.* **2004**, *3* (5), 403–405.

(68) Magadla, A.; Oluwole, D. O.; Managa, M.; Nyokong, T. Physicochemical and Antimicrobial Photodynamic Chemotherapy (against E. Coli) by Indium Phthalocyanines in the Presence of Silver–Iron Bimetallic Nanoparticles. *Polyhedron* **2019**, *162*, 30–38.

(69) Minnock, A.; Vernon, D. I.; Schofield, J.; Griffiths, J.; Parish, J. H.; Brown, S. B. Mechanism of Uptake of a Cationic Water-Soluble Pyridinium Zinc Phthalocyanine across the Outer Membrane of Escherichia Coli. *Antimicrob. Agents Chemother.* **2000**, *44* (3), 522–527.

(70) Minnock, A.; Vernon, D. I.; Schofield, J.; Griffiths, J.; Parish, J. H.; Brown, S. B. Photoinactivation of Bacteria. Use of a Cationic Water-Soluble Zinc Phthalocyanine to Photoinactivate Both Gram-Negative and Gram-Positive Bacteria. *J. Photochem. Photobiol. B* **1996**, *32* (3), 159–164.

(71) Turksoy, A.; Yildiz, D.; Akkaya, E. U. Photosensitization and Controlled Photosensitization with BODIPY Dyes. *Coord. Chem. Rev.* **2019**, *379*, 47–64.

(72) Caruso, E.; Banfi, S.; Barbieri, P.; Leva, B.; Orlandi, V. T. Synthesis and Antibacterial Activity of Novel Cationic BODIPY Photosensitizers. *J. Photochem. Photobiol. B* **2012**, *114*, 44–51.

(73) Gadhwal, R.; Devi, A. A Review on the Development of Optical Limiters from Homogeneous to Reflective 1-D Photonic Crystal Structures. *Opt. Laser Technol.* **2021**, *141*, 107144.

(74) Karpo, A. B.; Pushkarev, V. E.; Krasovskii, V. I.; Tomilova, L. G. Z-Scan Study of Nonlinear Absorption in Novel Lanthanide Bis-Phthalocyanines. *Chem. Phys. Lett.* **2012**, *554*, 155–158.

(75) Sheik-Bahae, M. and Van Stryland, E.W. Z-scan Measurements of Optical Nonlinearities. In *Characterization Techniques and Tabulations for Organic Nonlinear Materials*, Kuzyk, M. G. and Dirk, C.W., Eds; Marcel Dekker: New York, 1998; pp 655–692.

(76) de la Torre, G.; Vazquez, P.; Agullo-Lopez, F.; Torres, T. Role of Structural Factors in the Nonlinear Optical Properties of Phthalocyanines and Related Compounds. *Chem. Rev.* **2004**, *104* (9), 3723–3750.

(77) Zhu, M.; Jiang, L.; Yuan, M.; Liu, X.; Ouyang, C.; Zheng, H.; Yin, X.; Zuo, Z.; Liu, H.; Li, Y. Efficient Tuning Nonlinear Optical Properties: Synthesis and Characterization of a Series of Novel Poly(Aryleneethynylene)s Co-Containing BODIPY. *J. Polym. Sci. A* **2008**, *46 (22)*, 7401–7410.

(78) Barkana, Y.; Belkin, M. Laser Eye Injuries. *Surv. Ophthalmol.* **2000**, *44* (6), 459–478.

(79) Chen, Y.; Hanack, M.; Araki, Y.; Ito, O. Axially Modified Gallium Phthalocyanines and Naphthalocyanines for Optical Limiting. *Chem. Soc. Rev.* **2005**, *34* (6), 517–529.

(80) Dini, D.; Barthel, M.; Hanack, M. Phthalocyanines as Active Materials for Optical Limiting. *Eur. J. Org. Chem.* **2001**, *2001* (20), 3759–3769.

(81) defenceWeb, https://www.defenceweb.co.za/aerospace/aerospace-aerospace/sacaa-launching-laser-pointer-awareness-campaign/ (accessed May 21, 2020).

(82) Kubheka, G.; Achadu, O.; Mack, J.; Nyokong, T. Optical Limiting Properties of 3,5-Diphenyldibenzo-AzaBODIPY at 532 nm. *New J. Chem.* **2017**, *41* (20), 12319–12325.

(83) LaserPointerSafety.com, https://www.laserpointersafety.com/news/news/nonaviation-incidents_files/375a3337d0faaf1d4ca4ba79a97e7f2b-399.php#on (accessed May 21, 2020).

(84) Senge, M. O.; Fazekas, M.; Notaras, E. G. A.; Blau, W. J.; Zawadzka, M.; Locos, O. B.; Mhuircheartaigh, E. M. N. Nonlinear Optical Properties of Porphyrins. *Adv. Mater.* **2007**, *19* (19), 2737–2774.

(85) de la Torre, G.; Vazquez, P.; Agullo-Lopez, F.; Torres, T. Phthalocyanines and Related Compounds: Organic Targets for Nonlinear Optical Applications. *J. Mater. Chem.* **1998**, *8* (8), 1671–1683.

(86) Zhou, G.; Wang, X.; Wang, D.; Wang, C.; Shao, Z.; Fang, Q.; Jiang, M. Two-Photon Absorption and Nonlinear Optical Properties of a New Organic Dye PSPI. *Opt. Commun.* **2001**, *190* (1–6), 345–349.

(87) Kandasamy, K.; Shetty, S. J.; Puntambekar, P. N.; Srivastava, T. S.; Kundu, T.; Singh, B. P. Non-Resonant Third-Order Optical Non-Linearity of Porphyrin Derivatives. *Chem. Commun.* **1997**, *33* (13), 1159–1160.

(88) Ogawa, K.; Zhang, T.; Yoshihara, K.; Kobuke, Y. Large Third-Order Optical Nonlinearity of Self-Assembled Porphyrin Oligomers. *J. Am. Chem. Soc.* **2002**, *124* (1), 22–23.

(89) Bankole, O. M.; Nyokong, T. Mercaptopyridine-Substituted Indium, Zinc, and Metal-Free Phthalocyanines: Nonlinear Optical Studies in Solution and on Polymer Matrices. *J. Coord. Chem.* **2015**, *68* (20), 3727–3740.

(90) Piechocki, C.; Simon, J.; André, J. J.; Guillon, D.; Petit, P.; Skoulios, A.; Weber, P. Synthesis and Physico-Chemical Studies of Neutral and Chemically Oxidized Forms of Bis(Octaalkyloxyphthalocyaninato) Lutetium. *Chem. Phys. Lett.* **1985**, *122* (1–2), 124–128.

(91) Sanusi, K.; Antunes, E.; Nyokong, T. Optical Nonlinearities in Non-Peripherally Substituted Pyridyloxy Phthalocyanines: A Combined Effect of Symmetry, Ring-Strain and Demetallation. *Dalton Trans.* **2014**, *43* (3), 999–1010.

(92) May, A. K.; Stone, J.; Ngoy, B. P.; Mack, J.; Nyokong, T.; Kimura, M.; Kobayashi, N. Photophysical and Optical Limiting Properties of a Novel Distyryl-BODIPY with Fused Crown Ether Moieties. *J. Porphyrins Phthalocyanines* **2017**, *21* (12), 832–843.

(93) Ngoy, B. P.; May, A. K.; Mack, J.; Nyokong, T. Effect of Bromination on the Optical Limiting Properties at 532 nm of BODIPY Dyes with P-Benzyloxystyryl Groups at the 3,5-Positions. *J. Mol. Struct.* **2019**, *1175*, 745–753.

(94) Sheik-Bahae, M.; Said, A. A.; Wei, T.-H.; Hagan, D. J.; Van Stryland, E. W. Sensitive Measurement of Optical Nonlinearities Using a Single Beam. *Quantum Electron. IEEE J.* **1990**, *26* (4), 760–769.

(95) Ndebele, N.; Hlatshwayo, Z.; Ngoy, B. P.; Kubheka, G.; Mack, J.; Nyokong, T. Optical Limiting Properties of BODIPY Dyes Substituted with Styryl or Vinylene Groups on the

Nanosecond Timescale. *J. Porphyrins Phthalocyanines* **2019**, *23 (07n08)*, 701–717.

(96) Matthes, R. I. Commission on non-ionizing radiation protection. Revision of Guidelines on Limits of Exposure to Laser Radiation of Wavelengths between 400 nm and 1.4 μm. *Health Phys.* **2000**, *79* (4), 431–440.

(97) Hollins, R. C. Materials for Optical Limiters. *Curr. Opin. Solid State Mater. Sci.* **1999**, *4* (2), 189–196.

(98) Misra, R.; Kumar, R.; PrabhuRaja, V.; Chandrashekar, T. K. Modified Push-Pull Expanded Corroles: Syntheses, Structure and Nonlinear Optical Properties. *J. Photochem. Photobiol. A* **2005**, *175* (2–3), 108–117.

(99) Marder, S. R.; Perry, J. W. Molecular Materials for Second-Order Nonlinear Optical Applications. *Adv. Mater.* **1993**, *5* (11), 804–815.

(100) May, A.; Mack, J.; Nyokong, T. Optical Limiting Properties of D-π-A BODIPY Dyes in the Presence and Absence of Methyl Groups at the 1,7-Positions. *J. Porphyrins Phthalocyanines* **2020**, 1129–1137.

(101) Zhang, Y. P.; Xue, K. C.; Zhang, W. P.; Song, C.; Zhang, R. L.; Zhao, J. S. Synthesis and Catalytic Performance of MCM-41 Modified with Tetracarboxylphthalocyanine. *Chem. Papers* **2013**, *67* (4), 372–379.

(102) Sakamoto, K.; Ohno-Okumura, E. Syntheses and Functional Properties of Phthalocyanines. *Materials* **2009**, *2* (3), 1127–1179.

(103) Nemykina, V. N.; Lukyanets, E. A. Synthesis of Substituted Phthalocyanines. *Arkivoc* **2010**, *2010* (1), 136–208.

(104) Mack, J.; Kobayashi, N. Low Symmetry Phthalocyanines and Their Analogues. *Chem. Rev.* **2011**, *111* (2), 281–321.

(105) Kharisov, B. I.; Ortiz Mendez, U.; Almaraz Garza, J. L.; Almageur Rodriguez, J. R. Synthesis of Non-Substituted Phthalocyanines by Standard and Non-Standard Techniques. Influence of Solvent Nature in Phthalocyanine Preparation at Low Temperature by UV-Treatment of the Reaction System. *New J. Chem.* **2005**, *29*, 686–692.

(106) Lapkina, L. A.; Sakharov, S. G.; Konstantinov, N. Y.; Larchenko, V. E.; Gorbunova, Y. G.; Tsivadze, A. Y. Crown-Substituted Sc(III) Phthalocyaninates: Synthesis and Spectral Properties. *Russ. J. Inorg. Chem.* **2007**, *52* (11), 1758–1768.

(107) Martynov, A. G.; Gorbunova, Y. G. Heteroleptic Phthalocyaninato-[Tetra(15-Crown-5)Phthalocyaninato] Lanthanides(III) Double-Deckers: Synthesis and Cation-Induced Supramolecular Dimerisation. *Inorg. Chim. Acta* **2007**, *360* (1), 122–130.

(108) Rio, Y.; Rodríguez-Morgade, M. S.; Torres, T. Modulating the Electronic Properties of Porphyrinoids: A Voyage from the Violet to the Infrared Regions of the Electromagnetic Spectrum. *Org. Biomol. Chem.* **2008**, *6* (11), 1877–1894.

(109) Sekhosana, K. E.; Nkhahle, R.; Nyokong, T. The Primary Demonstration of Exciton Coupling Effects on Optical Limiting Properties of Blue Double-Decker Lanthanide Phthalocyanine Salts. *ChemistrySelect* **2018**, *3* (23), 6671–6682.

(110) Karpo, A. B.; Zasedatelev, A. V.; Pushkarev, V. E.; Krasovskii, V. I.; Tomilova, L. G. Influence of Blue Valence Absorption Band on Nonlinear Absorption in Dysprosium Bisphthalocyanine Studied by Open Aperture Z-Scan. *Chem. Phys. Lett.* **2013**, *585*, 153–156.

(111) Sekhosana, K. E.; Nyokong, T. Nonlinear Optical Behavior of n-Tuple Decker Phthalocyanines at the Nanosecond Regime: Investigation of Change in Mechanisms.

RSC Adv. **2019**, *9* (28), 16223–16234.

(112) Orti, E.; Brédas, J. L.; Clarisse, C. Electronic Structure of Phthalocyanines: Theoretical Investigation of the Optical Properties of Phthalocyanine Monomers, Dimers, and Crystals. *J. Chem. Phys.* **1990**, *92* (2), 1228–1235.

(113) Sekhosana, K. E. Nonlinear Optical Behavior of Lanthanide Phthalocyanines and Their Conjugates with a Selection of Nanomaterials, PhD thesis, Rhodes University, Grahamstown, South Africa, 2016.

(114) Keizer, S. P.; Mack, J.; Bench, B. A.; Gorun, S. M.; Stillman, M. J. Spectroscopy and Electronic Structure of Electron Deficient Zinc Phthalocyanines. *J. Am. Chem. Soc.* **2003**, *125* (23), 7067–7085.

(115) Mack, J.; Stillman, M. J. Assignment of the Optical Spectrum of Metal Porphyrin and Phthalocyanine Radical Anions. *J. Porphyrins Phthalocyanines* **2001**, *5* (1), 67–76.

(116) Mack, J.; Stillman, M. J. Assignment of the Optical Spectra of Metal Phthalocyanines through Spectral Band Deconvolution Analysis and ZINDO Calculations. *Coord. Chem. Rev.* **2001**, *219–221*, 993–1032.

(117) Klíčová, Ĺ.; Šebej, P.; Šolomek, T.; Hellrung, B.; Slavíček, P.; Klán, P.; Heger, D.; Wirz, J. Adiabatic Triplet State Tautomerization of *p*-Hydroxyacetophenone in Aqueous Solution. *J. Phys. Chem. A* **2012**, *116* (11), 2935–2944.

(118) Frisch, M. J.; Trucks, G. W.; Schlegel, H. B.; Scuseria, G. E.; Robb, M. A.; Cheeseman, J. R.; Scalmani, G.; Barone, V.; Petersson, G. A.; Nakatsuji, H.; Li, X.; Caricato, M.; Marenich, M.; Bloino, J.; Janesko, B. G.; Gomperts, R.; Mennuci, B.; Hratachian, H. P.; Oritiz, J. V.; Izmoylov, A. F.; Sonnenberg, J. L.; Williams-Young, D.; Ding, F.; Lipparini, F.; Egidi, F.; Goings, J.; Peng, B.; Petrone, A.; Henderson, T.; Ranasinghe, D.; Zakrzewski, V.

G.; Gao, J.; Rega, N.; Zheng, G.; Liang, W.; Hada, M.; Ehara, M.; Toyota, K.; Fukuda, R.; Hasegawa, J.; Ishida, M.; Nakajima, T.; Honda, Y.; Kitao, O.; Nakai, H.; Vreven, T.; Throssell, K.; Montgomery, J. A.; Peralta, J. E.; Ogliaro, F.; Bearpark, M.; Heyd, J. J.; Brothers, E.; Kudin, K. N.; Staroverov, V. N.; Keith, T.; Kobayashi, R.; Normand, J.; Raghavachari, K.; Rendell, A.; Burant, J. C.; Iyengar, S. S.; Tomasi, J.; Cossi, M.; Millam, J. M.; Klene, M.; Adamo, C.; Cammi, R.; Ochterski, J. W.; Martin, R. L.; Morokuma, K.; Farkas, O.; Foresman, J. B.; Fox, D. J. Gaussian 09, Revision D.01. Gaussian, Inc.: Wallingford CT 2016.

(119) Hanwell, M. D.; Curtis, D. E.; Lonie, D. C.; Vandermeersch, T.; Zurek, E.; Hutchison, G. R. Avogadro: An Advanced Semantic Chemical Editor, Visualization, and Analysis Platform. *J. Cheminform.* **2012**, *4* (8), 1–17.

(120) Qin, W.; Baruah, M.; Van Der Auweraer, M.; De Schryver, F. C.; Boens, N. Photophysical Properties of Borondipyrromethene Analogues in Solution. *J. Phys. Chem. A* **2005**, *109* (33), 7371–7384.

(121) de J. Gómez-Infante, A.; Bañuelos, J.; Valois-Escamilla, I.; Cruz-Cruz, D.; Prieto-Montero, R.; López-Arbeloa, I.; Arbeloa, T.; Peña-Cabrera, E. Synthesis, Properties, and Functionalization of Nonsymmetric 8-MethylthioBODIPYs. *Eur. J. Org. Chem.* **2016**, *2016* (29), 5009–5023.

(122) Lintao, Z.; Junchao, X.; Jiayu, C.; Liang, W.; Qiusheng, W. Novel BODIPY Flourescent Dye with Adjustable Emission Wavelength and Preparation Method Thereof. Chinese Patent, CN103194085A, 2013.

(123) Machado, L. A.; de Souza, M. C.; da Silva, C. M.; Yoneda, J.; de Rezende, L. C. D.; Emery, F. S.; de Simone, C. A.; da Silva Júnior, E. N.; Pedrosa, L. F. On the Synthesis, Optical and

Computational Studies of Novel BODIPY-Based Phosphoramidate Fluorescent Dyes. *J. Fluor. Chem.* **2019**, *220* (2019), 9–15.

(124) Lamaster, D. J.; Kaufman, N. E. M.; Bruner, A. S.; Vicente, M. G. H. Structure Based Modulation of Electron Dynamics in *meso*-(4-Pyridyl)-BODIPYs: A Computational and Synthetic Approach. *J. Phys. Chem. A* **2018**, *122* (31), 6372–6380.

(125) Quan, L.; Lin, W.; Sun, T.; Xie, Z.; Huang, Y.; Jing, X. Green Photocatalysis with Oxygen Sensitive BODIPYs under Visible Light. *Catal. Lett.* **2014**, *144* (2), 308–313.

(126) Osati, S.; Ali, H.; Guerin, B.; van Lier, J. E. Synthesis and Spectral Properties of Estrogen- and Androgen-BODIPY Conjugates. *Steroids* **2017**, *123* (2017), 27–36.

(127) Liu, W.; Tang, A.; Chen, J.; Wu, Y.; Zhan, C.; Yao, J. Photocurrent Enhancement of BODIPY-Based Solution-Processed Small-Molecule Solar Cells by Dimerization via the Meso Position. *ACS Appl. Mater. Interfaces* **2014**, *6* (24), 22496–22505.

(128) Zhang, S.; Wu, T.; Fan, J.; Li, Z.; Jiang, N.; Wang, J.; Dou, B.; Sun, S.; Song, F.; Peng, X. A BODIPY-Based Fluorescent Dye for Mitochondria in Living Cells, with Low Cytotoxicity and High Photostability. *Org. Biomol. Chem.* **2013**, *11* (4), 555–558.

(129) Xiong, H.; Zhou, K.; Yan, Y.; Miller, J. B.; Siegwart, D. J. Tumor-Activated Water-Soluble Photosensitizers for Near-Infrared Photodynamic Cancer Therapy. *ACS Appl. Mater. Interfaces* **2018**, *10* (19), 16335–16343.

(130) Banfi, S.; Nasini, G.; Zaza, S.; Caruso, E. Synthesis and Photo-Physical Properties of a Series of BODIPY Dyes. *Tetrahedron* **2013**, *69* (24), 4845–4856.

(131) Martínez, S. R.; Palacios, Y. B.; Heredia, D. A.; Agazzi, M. L.; Durantini, A. M. Phenotypic Resistance in Photodynamic Inactivation Unravelled at the Single Bacterium Level. *ACS Infect. Dis.* **2019**, *5* (9), 1624–1633.

(132) Ngoy, B. P.; Hlatshwayo, Z.; Nwaji, N.; Fomo, G.; Mack, J.; Nyokong, T. Photophysical and Optical Limiting Properties at 532 Nm of BODIPY Dyes with *p*-Benzyloxystyryl Groups at the 3,5-Positions . *J. Porphyrins Phthalocyanines* **2018**, *22* (05), 413–422.

(133) Harris, J. BODIPY Dyes for Singlet Oxygen and Optical Limiting Applications, MSc thesis, Rhodes University, Grahamstown, South Africa, 2017.

(134) Wood, T. E.; Thompson, A. Advances in the Chemistry of Dipyrrins and Their Complexes. *Chem. Rev.* **2007**, *107* (5), 1831–1861.

(135) Saino, S.; Saikawa, M.; Nakamura, T.; Yamamura, M.; Nabeshima, T. Remarkable Red-Shift in Absorption and Emission of Linear BODIPY Oligomers Containing Thiophene Linkers. *Tetrahedron Lett.* **2016**, *57* (14), 1629–1634.

(136) Baruah, M.; Qin, W.; Vallée, R. A. L.; Beljonne, D.; Rohand, T.; Dehaen, W.; Boens, N. A Highly Potassium-Selective Ratiometric Fluorescent Indicator Based on BODIPY Azacrown Ether Excitable with Visible Light. *Org. Lett.* **2005**, *7* (20), 4377–4380.

(137) Bañuelos, J. BODIPY Dye, the Most Versatile Fluorophore Ever? *Chem. Rec.* **2016**, *16* (1), 335–348.

(138) Zhang, S.; Liu, J.; Chen, Y.; Xiong, S.; Wang, G.; Chen, J.; Yang, G. A Novel Strategy for MALDI-TOF MS Analysis of Small Molecules. *J. Am. Soc. Mass Spectrom.* **2010**, *21* (1), 154–160.

(139) Amiri, R.; Farrokhpour, H.; Tabrizchi, M. Sodium Salts Effect on the Time of Flight Mass Spectra of Some Amino Acids in the Direct-Laser Desorption Ionization and Matrix-Assisted Laser Desorption/Ionization. *J. Chin. Chem. Soc.* **2021**, *68* (7), 1263–1270.

(140) Feng, H.; Zhou, Z.; May, A. K.; Chen, J.; Mack, J.; Nyokong, T.; Gai, L.; Lu, H. Disilane-Bridged Architectures with High Optical Transparency for Optical Limiting. *J. Mater.*

Chem. C **2021**, *9* (20), 6470–6476.

(141) May, A.; Majumdar, P.; Martynov, A. G.; Lapkina, L. A.; Troyanov, S. I.; Gorbunova, Y. G.; Tsivadze, A. Y.; Mack, J.; Nyokong, T. Optical Limiting Properties, Structure and Simplified TD-DFT Calculations of Scandium Tetra-15-Crown-5 Phthalocyaninates. *J. Porphyrins Phthalocyanines* **2020**, *24* (4), 589–601.

(142) Harris, J.; May, A. K.; Ngoy, B. P.; Mack, J.; Nyokong, T. An Analysis of the Photophysical and Optical Limiting Properties of a Novel 1,3,5-TristyrylBODIPY Dye. *J. Porphyrins Phthalocyanines* **2019**, *23* (01n02), 63–75.

(143) Saleh, B. E. A.; Teich, M. C. *Fundamentals of Photonics*; Wiley: New York, 1991.

(144) Chauke, V.; Durmus, M.; Nyokong, T. Photochemistry, Photophysics and Nonlinear Optical Parameters of Phenoxy and Tert-Butylphenoxy Substituted Indium(III) Phthalocyanines. *J. Photochem. Photobiol. A* **2007**, *192* (2–3), 179–187.

(145) Mkhize, C.; Britton, J.; Nyokong, T. Enhanced Nonlinear Optical Properties of Octa-Substituted Lead and Cadmium Phthalocyanines When Embedded in Poly(Bisphenol A Carbonate) as Thin Films. *Polyhedron* **2014**, *81*, 607–613.

(146) Prem Kiran, P.; Naga Srinivas, N. K. M.; Raghunath Reddy, D.; Maiya, B. G.; Dharmadhikari, A.; Sandhu, A. S.; Ravindra Kumar, G.; Narayana Rao, D. Heavy Atom Effect on Nonlinear Absorption and Optical Limiting Characteristics of 5,10,15,20-(Tetratolyl) Porphyrinato Phosphorus (V) Dichloride. *Opt. Commun.* **2002**, *202* (4–6), 347–352.

(147) Bankole, O. M.; Nyokong, T. Nonlinear Optical Response of a Low Symmetry Phthalocyanine in the Presence of Gold Nanoparticles When in Solution or Embedded in Poly Acrylic Acid Polymer Thin Films. *J. Photochem. Photobiol. A* **2016**, *319–320*, 8–

17.

(148) Sheng, N.; Gu, B.; Ren, B.; Wang, Y.; Han, L.; Wang, J.; Cao, H.; Guan, M.; Zhai, X.; Sha, J. Strong Two-Photon Absorptions in Heteroleptic Bis(Phthalocyaninato) Rare Earth Sandwich Complexes. *Dyes Pigments* **2017**, *136*, 553–558.

(149) Wang, H.; Qi, D.; Xie, Z.; Cao, W.; Wang, K.; Shang, H.; Jiang, J. A Sandwich-Type Phthalocyaninato Metal Sextuple-Decker Complex: Synthesis and NLO Properties. *Chem. Commun.* **2013**, *49* (9), 889–891.

(150) Sheng, N.; Liu, D.; Gu, B.; He, J.; Cui, Y. A Series of Homoleptic Bis(Phthalocyaninato) Rare Earth Sandwich Complexes with Large Two-Photon Absorption Cross-Section. *Dyes Pigments* **2015**, *122*, 346–350.

(151) Huang, C.; Wang, K.; Sun, J.; Jiang, J. Planar Binuclear Phthalocyanine-Containing Sandwich-Type Rare-Earth Complexes: Synthesis, Spectroscopy, Electrochemistry, and NLO Properties. *Eur. J. Inorg. Chem.* **2014**, No. 9, 1546–1551.

(152) Ganga-Sah, Y.; Tajbakhsh, E.; Platel, R. H.; Zhou, W.; Leznoff, D. B. Synthesis, Structures and Reduction Chemistry of Monophthalocyanine Scandium Hydroxides. *J. Porphyrins Phthalocyanines* **2019**, *23* (11n12), 1592–1602.

(153) Platel, R. H.; Teixeira Tasso, T.; Zhou, W.; Furuyama, T.; Kobayashi, N.; Leznoff, D. B. Metallophthalocyanin-Ocenes: Scandium Phthalocyanines with an η^5-Bound Cp Ring. *Chem. Commun.* **2015**, *51* (27), 5986–5989.

(154) Nwaji, N.; Mack, J.; Britton, J.; Nyokong, T. Synthesis, Photophysical and Nonlinear Optical Properties of a Series of Ball-Type Phthalocyanines in Solution and Thin Films. *New J. Chem.* **2017**, *41* (5), 2020–2028.

(155) Slodek, A.; Wöhrle, D.; Doyle, J. J.; Blau, W. Metal Complexes of Phthalocyanines in

Polymers as Suitable-Materials for Optical Limiting. *Macromol. Symp.* **2006**, *235*, 9–18.

(156) Sekhosana, K. E.; Amuhaya, E.; Nyokong, T. Nanosecond Nonlinear Optical Limiting Properties of New Trinuclear Lanthanide Phthalocyanines in Solution and as Thin Films. *Polyhedron* **2015**, *85*, 347–354.

(157) Britton, J.; Durmuş, M.; Khene, S.; Chauke, V.; Nyokong, T. Third Order Nonlinear Optical Properties of Phthalocyanines in the Presence Nanomaterials and in Polymer Thin Films. *J. Porphyrins Phthalocyanines* **2013**, *17* (08n09), 691–702.

(158) Nishijima, S.; Namura, S.; Mitsuya, K.; Asada, Y. The Incidence of Isolation of Methicillin-resistant Staphylococcus Aureus (MRSA) Strains from Skin Infections during the Past Three Years (1989-1991). *J. Dermatol.* **1993**, *20* (4), 193–197.

(159) Sharman, W. M.; Allen, C. M.; Van Lier, J. E. Photodynamic Therapeutics: Basic Principles and Clinical Applications. *Drug Discov. Today* **1999**, *4* (11), 507–517.

(160) Bomanda, B. T.; Waudo, W.; Ngoy, B. P.; Muya, J. T.; Mpiana, P. T.; Mbala, M.; Openda, I.; Mack, J.; Nyokong, T. Photophysical and in Vitro Antibacterial Studies of 2,6-Dibromo-BODIPY Dye Substituted with Dithienylenevinylene at 3,5-Positions. *Macroheterocycles* **2018**, *11* (4), 429–437.

(161) Lebechi, K. A.; Ngoy, B. P.; Mack, J.; Nyokong, T. 2,6-Dibrominated 3,5-DistyryLBODIPYs as Photosensitizer Dyes for Photodynamic Antimicrobial Chemotherapy. *Macroheterocycles* **2019**, *12* (3), 292–299.

(162) Sindelo, A.; Osifeko, O. L.; Nyokong, T. Synthesis, Photophysicochemical and Photodynamic Antimicrobial Chemotherapy Studies of Indium Pyridyl Phthalocyanines: Charge versus Bridging Atom. *Inorg. Chim. Acta* **2018**, *476*, 68–76.

(163) Osifeko, O. L.; Uddin, I.; Mashazi, P. N.; Nyokong, T. Physicochemical and Antimicrobial

Photodynamic Chemotherapy of Unsymmetrical Indium Phthalocyanines Alone or in the Presence of Magnetic Nanoparticles. *New J. Chem.* **2016**, *40* (3), 2710–2721.

(164) Prieto-Montero, R.; Prieto-Castañeda, A.; Sola-Llano, R.; Agarrabeitia, A. R.; García-Fresnadillo, D.; López-Arbeloa, I.; Villanueva, A.; Ortiz, M. J.; de la Moya, S.; Martínez-Martínez, V. Exploring BODIPY Derivatives as Singlet Oxygen Photosensitizers for PDT. *Photochem. Photobiol.* **2020**, *96* (3), 458–477.

(165) Babu, B.; Sindelo, A.; Mack, J.; Nyokong, T. Thien-2-Yl Substituted Chlorins as Photosensitizers for Photodynamic Therapy and Photodynamic Antimicrobial Chemotherapy. *Dyes Pigments* **2021**, *185*, 108886.

(166) Soman, R.; Raghav, D.; Sujatha, S.; Rathinasamy, K.; Arunkumar, C. Axial Ligand Modified High Valent Tin(IV) Porphyrins: Synthesis, Structure, Photophysical Studies and Photodynamic Antimicrobial Activities on Candida Albicans. *RSC Adv.* **2015**, *5* (75), 61103–61117.

(167) Nair, A.; Steinberg, W. J.; Habib, T.; Saeed, H.; Raubenheimer, J. E. Prevalence of Healthcare-Associated Infection at a Tertiary Hospital in the Northern Cape Province, South Africa. *S. Afr. Fam. Pract.* **2018**, *60* (5), 162–167.

(168) Rothe, C.; Schlaich, C.; Thompson, S. Healthcare-Associated Infections in Sub-Saharan Africa. *J. Hosp. Infect.* **2013**, *85* (4), 257–267.

(169) Komatsu, T.; Urano, Y.; Fujikawa, Y.; Kobayashi, T.; Kojima, H.; Terai, T.; Hanaoka, K.; Nagano, T. Development of 2,6-Carboxy-Substituted Boron Dipyrromethene (BODIPY) as a Novel Scaffold of Ratiometric Fluorescent Probes for Live Cell Imaging. *Chem. Commun.* **2009**, *46* (45), 7015–7017.

(170) Yanai, T.; Tew, D. P.; Handy, N. C. A New Hybrid Exchange-Correlation Functional Using

the Coulomb-Attenuating Method (CAM-B3LYP). *Chem. Phys. Lett.* **2004**, *393* (1–3), 51–57.

(171) Andrienko, G. A, http://www.chemcraftprog.com/ (accessed Feb 24, 2021).

(172) Jiao, L.; Pang, W.; Zhou, J.; Wei, Y.; Mu, X.; Bai, G.; Hao, E. Regioselective Stepwise Bromination of Boron Dipyrromethene (BODIPY) Dyes. *J. Org. Chem.* **2011**, *76* (24), 9988–9996.

(173) Nevidimov, A. V. Quantum Chemical Modeling of the Spectral Properties of a BODIPY Dye with Different Substituents. *Russ. J. Phys. Chem.* **2020**, *94* (5), 951–955.

(174) Marahatta, A.; Marahatta, A. B. A DFT Analysis for the Electronic Structure, Mulliken Charges Distribution and Frontier Molecular Orbitals of Monolayer Graphene Sheet. *Int. J. Prog. Sci. Tech.* **2019**, *16* (1), 51–65.

(175) Mao, J. X. Atomic Charges in Molecules: A Classical Concept in Modern Computational Chemistry. *Postdoc J.* **2014**, *2* (2).

(176) Wei, Y.; Zheng, M.; Zhou, Q.; Zhou, X.; Liu, S. Application of a Bodipy-C70 Dyad in Triplet-Triplet Annihilation Upconversion of Perylene as a Metal-Free Photosensitizer. *Org. Biomol. Chem.* **2018**, *16* (31), 5598–5608.

(177) Oliden-Sánchez, A.; Sola-Llano, R.; Bañuelos, J.; García-Moreno, I.; Uriel, C.; López, J. C.; Gómez, A. M. Tuning the Photonic Behavior of Symmetrical Bis-BODIPY Architectures: The Key Role of the Spacer Moiety. *Front. Chem.* **2019**, *7*, 1–18.

(178) Gai, L.; Mack, J.; Lu, H.; Yamada, H.; Kuzuhara, D.; Lai, G.; Li, Z.; Shen, Z. New 2,6-Distyryl-Substituted BODIPY Isomers: Synthesis, Photophysical Properties, and Theoretical Calculations. *Chem. Eur. J.* **2014**, *20* (4), 1091–1102.

(179) Kubheka, G.; Mack, J.; Kobayashi, N.; Kimura, M.; Nyokong, T. Optical Limiting

Properties of 2,6-Dibromo-3,5- DistyrylBODIPY Dyes at 532 nm. *J. Porphyrins Phthalocyanines* **2017**, *21* (07n08), 523–531.

(180) Kubheka, G.; Sanusi, K.; Mack, J.; Nyokong, T. Optical Limiting Properties of 3,5-DipyrenylvinyleneBODIPY Dyes at 532 nm. *Spectrochim. Acta A* **2018**, *191*, 357–364.

(181) Agazzi, M. L.; Ballatore, M. B.; Durantini, A. M.; Durantini, E. N.; Tomé, A. C. BODIPYs in Antitumoral and Antimicrobial Photodynamic Therapy: An Integrating Review. *J. Photochem. Photobiol. C* **2019**, *40*, 21–48.

(182) Prasannan, D.; Raghav, D.; Sujatha, S.; Hareendrakrishna kumar, H.; Rathinasamy, K.; Arunkumar, C. Synthesis, Structure, Photophysical, Electrochemical Properties and Antibacterial Activity of Brominated BODIPYs. *RSC Adv.* **2016**, *6* (84), 80808–80824.

(183) Michael J. Smart, R. B. N. O. C. Burden, Spectrum, and Impact of Healthcare-Associated Infection at a South African Children's Hospital. *J. Hosp. Infect.* **2016**, *94*, 364–372.

(184) Rawlinson, S.; Ciric, L.; Cloutman-Green, E. How to Carry out Microbiological Sampling of Healthcare Environment Surfaces? A Review of Current Evidence. *J. Hosp. Infect.* **2019**, *103* (4), 363–374.